Yann Kevin Petit, MSc

Singlet oxygen in metal-air batteries: Origins, consequences and mitigation

DOCTORAL THESIS

to achieve the university degree of

Doktor der technischen Wissenschaften

submitted to

Graz University of Technology

Supervisor

Dipl.-Ing. Dr.sc.ETH Stefan Freunberger

Institut für Chemische Technologie von Materialien

Graz, month and year

AFFIDAVIT

I declare that I have authored this thesis independently, that I have not used other than the declared sources/resources, and that I have explicitly indicated all material which has been quoted either literally or by content from the sources used. The text document uploaded to TUGRAZonline is identical to the present doctoral thesis.

_____   _____

Date   Signature

*There's more to the picture
than meet the eye.*

Neil Young

Acknowledgement

Table of contents

List of Figures

Abbreviation

Abstract

Bonjour je suis un abstract

Oxygen chemistry, a pathway to next generation batteries

What a gift we have been given to be born in an atmosphere with oxygen.
Marina Keegan

Contents

Figures

Introduction

Energy storage ever rising importance in modern society imposes massive and quick technology changes. Lithium-ion battery technology is currently the solution of choice for many applications; New technologies based on sustainable lightweight active and inactive elements with increased electrons exchanged per redox centre are nevertheless inevitable for future energy intensive purpose vehicle electrical drive[1–4]. A proposed battery type to reach these objectives are 'beyond-intercalation chemistries', notably metal–air, abandoning the intercalation paradigm[1,3–5]. Among them, organic Li-air technology has received a particular enthusiasm, sometimes for misaddressed reason, by dint of Li_2O_2 high theoretical capacity (1168 ma·h·g^{-1}[6]) and will be the focus of this introductory chapter.

Li-air batteries are based on a lithium metal anode and a porous matrix filled with electrolyte as cathode where oxygen will react to form lithium peroxide during discharge followed by the inverse process in charge as illustrated in fig 1.1. The exact reaction mechanisms are however complexes and still subject to debate. The consensus tends to a two step reaction during both discharge and charge; The reaction is divided between the formation of superoxide through a one electron exchange and a subsequent one electron process or superoxide disproportionation[7–11]. The mentioned steps are influencde by numerous parameters as the electrolyte, the species in presence or the applied potential[12–14]. The reaction product itself is a wide band gap insulator and consequently the exact reaction interface is still unknown. We will present the current understanding of the different implications of this convoluted reaction mechanism which is the stepping stones for this thesis results.
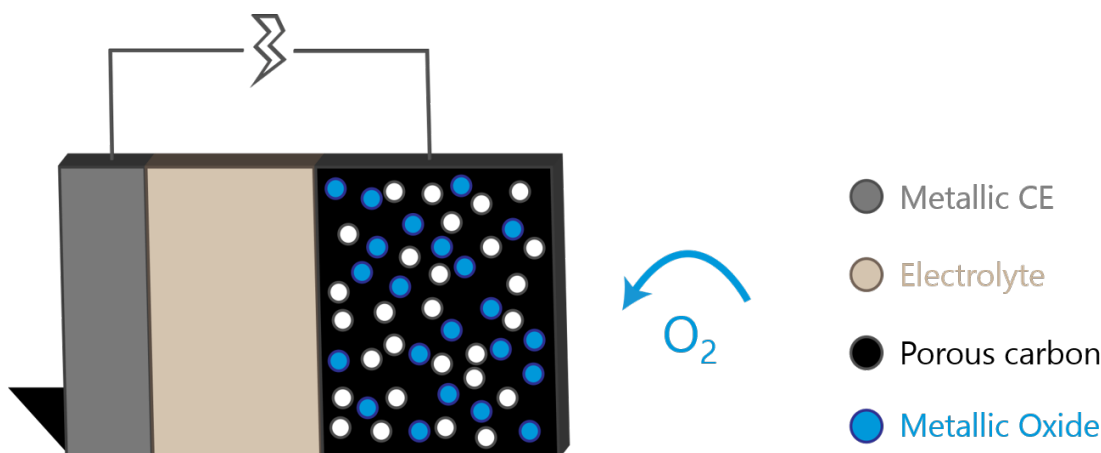
Figure 1.1: **Scheme of the metal–air principle on discharge.**

The li-air battery cathode is a porous matrix that needs to sustain the Li_2O_2 formation and provide electrical contact rather than directly store the charge. The material of choice is carbon due to its lightweight, adaptable and inexpensive nature. We will discuss the stability of carbon electrodes in metal–air chemistry which can be problematic and the proposed replacement materials. Concerning the lithium metal anode, its poor coulombic efficiencies is fairly known especially in metal–air conditions and we will explore the solution offers by contemporary researches. The Li-air electrolyte is also subject to constraining limitation due to the aggressive reduced oxygen species in presence and its roles in reaction mechanism. We will hence resume here the advantages and disadvantages of organic solvent, ionic

liquids and solid electrolytes in Li-air batteries. The main difference between metal-air and intercalation batteries is the formation and disappearance of new products while cycling. We will introduce the consequence on the capacity calculation that it imposes to realistically compare different technologies.

Severe parasitic reactions is the major hurdle to efficient Li-air battery[10,15]. These reactions are known to degrade both the electrolyte and electrodes which in turn provoke high charge voltage, poor reversibly and cell lifetime. Due to the novelty of this chemistry, specific performance metrics have been developed that enclose characterization of the gaseous species in presence. From these analytical methods, side reactivity is often solely attributed to reduced oxygen species owing to their reactivity with common lithium-ion electrolytes. We will, yet, show that the development of adapted cell component does not permit to attributed the crippling parasitic chemistry to lithium superoxide and peroxide, a fact that will be expanded through the rest of this thesis.

1.1 Metal–air batteries: interest, principles and advantages

1.1.1 Beyond intercalation batteries

The technological breakthrough of lithium-ion batteries in the early 21st century has led to a paradigm shift in our habits with the spur of portable electronics, electric vehicle drives or integration to electrical grid [16,17]. With multiplied needs and applications of energy storage, the use of lithium technology has seen a tremendous increase in the past decades. Hence, energy storage came to the forefront of societal changes and research subject [1,16]. Lithium-ion battery technology approaches its theoretical limits and impose new technologies, especially due to the expected expansion of the electrical vehicle market [1–4].

Lithium-ion battery capacities are notably plagued by the important amount of inactive materials. This technology rest on transition metal oxide as cathode and carbon as anode which acts as host materials [2]. Lighter redox active elements, increased number of electron exchanged and lightweight cells are necessary to achieve the high capacity needed for future technologies. Li-rich transition-metal oxide cathodes, featuring higher voltage and capacity are one possible pathway towards new generation batteries but still depends on insertion chemistries [4]. Together with the sustainability demands rise, it motivates "beyond-intercalation chemistry" technologies [1,3–5]. Charge storage in these promising chemistries involves distinctive process compared to the well-known intercalation reaction.

Strategies to avoid this overweight concerns both the anode and the cathode. Alloying materials as Si or alkaline metal direct use are for example proposed to reduce inactive materials at the anode [16,18,19]. Concerning the cathode, principal hinder to high capacity batteries, the main proposition is to reduce the electrode to a electron conductor role; The charge are then stored with the formation a new products by reacting alkaline ions either with O_2 or S [16] [20–24].

1.1.2 Metal–air batteries

Among the proposed technology, the metal–air technology receive a high interest due to its high theoric capacity despite its lower voltage (theoretically 1168 mAh·g^{-1} for Li-O_2 [6]). As every battery, Metal–air cells are comprised of two electrodes separated by an electrolyte. Yet, as part of "beyond intercalation" technology, it replaces the graphite anode by alkaline metal and transition metal compounds by an oxygen cathode. The cathode is composed of a porous electron conductive matrix, usually carbon, filled with liquid non-aqueous alkaline cation electrolyte. The porosity of the cathode allows oxygen to diffuse to its surface where oxygen redox chemistry will act as charge storage. On discharge, oxygen is reduced to form superoxide or peroxide which is oxidized back to alkaline cation and O_2 on charge.

Despite its lower coulombic efficiency and higher overpotential compare to state of the art Na or K cells [22,25], Li-O_2 chemistry is interesting due to its higher energy density; it is the more lightweight metal and react by two electron with oxygen [26]. The chemistry of the O_2/MO_2 (M = Li$_2$, Na, K) redox couple in aprotic media is a rather recent research subject and the still incomplete mechanistic understanding, a barrier for practical realization. By virtue of the similarity between the different metal–air technologies, emphasis will be put on Li-O_2 batteries, focusing on high specific capacity. Li-O_2 cells furthermore present the more complicated reactivity and the mechanisms encountered in lithium chemistry encompass the other alkali cases since Li-O_2 batteries are usually based on peroxide whereas Na and K potassium cells favoured the formation of alkali superoxide [25,27–29]. Due to their more complex chemistry, Li-O_2 cells present as well the highest parasitic degradation through

cycling[30].

1.2 The lithium–air technology state of the art

1.2.1 Reaction mechanism

1.2.1.1 Discharge

The discharge reaction in Li–O_2 batteries is the O_2 reduction in presence of lithium ions to form Li_2O_2 according to an overall 2 e^- reaction (Eq. 1.1). Li_2O_2 formation in aprotic media is complicated and the exact mechanism still not entirely understood. It is commonly accepted that the reaction is divided in two steps. Discharge commences with a 1 e^- O_2 reduction to superoxide (O_2^-) which may combine with Li^+ to form LiO_2 (Eq. 1.2)[7,31,32]. This step is followed by either a second 1 e^- reduction (Eq. 1.3) or disproportionation of the superoxide to forms its peroxide (Eq. 1.4)[7–10]. The second step pathways are governed by the equilibrium between solvated and adsorbed superoxide (Eq. 1.5)[12]. Adsorbed peroxide can undergoes a second reduction at the electrode surface or disproportionate. Solvated [Li^+ O_2] couple is disconnected from the electrode and can only undergoes disproportionation followed by subsequent precipitation. Both lead to an overall two electrons reduction of oxygen, as systematized in Fig. 1.2.

$$O_2 + 2\,e^- + 2\,Li^+ \longrightarrow Li_2O_2 \tag{1.1}$$

$$O_2 + e^- + Li^+ \longrightarrow LiO_2 \tag{1.2}$$

$$LiO_2 + e^- + Li^+ \longrightarrow Li_2O_2 \tag{1.3}$$

$$2\,LiO_2 \longrightarrow Li_2O_2 + O_2 \tag{1.4}$$

$$LiO_2 \rightleftharpoons Li^+_{(sol)} + O_2^-{}_{(sol)} + \text{ion pairs} + \text{higher aggregates} \tag{1.5}$$
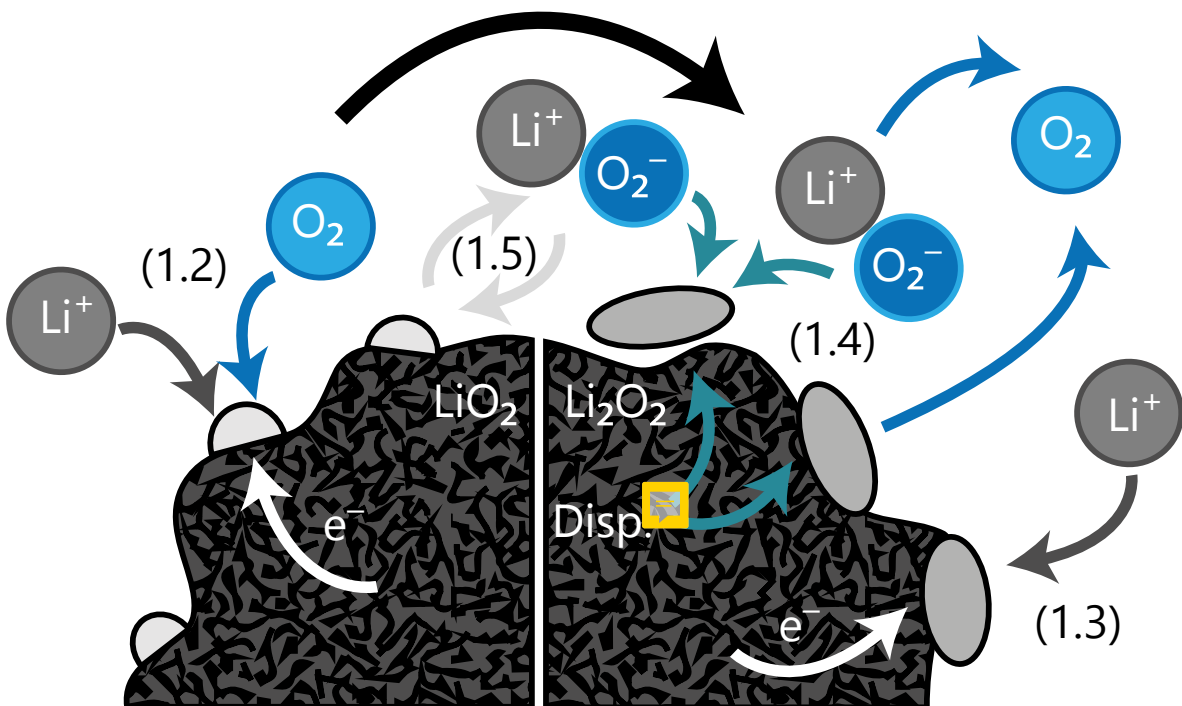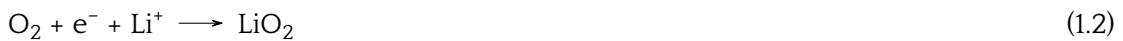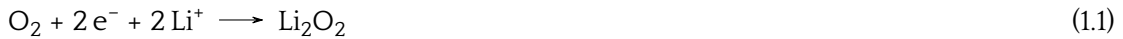
Figure 1.2: **Scheme of the discharge reaction and the equations corresponding to each step.**

The cation solvatation dependents on the coordination strength with the solvent characterised by its Lewis basicity, measured with the Guttman donor number (DN)[8,12,33,34]; Superoxide solvation correlates reciprocally with the Lewis acidity characterized by the acceptor number (AN), even though its influence is lower[33]. Common organic solvent covers an extensive range of DN. Among them are the nitriles and sulfones (DN=14–16), glymes (DN=20–24), amides (DN $\approx$ 26), and sulfoxide (DN $\approx$ 30)[12,34]. A high DN solvent leads then to a higher solvation of the lithium superoxide and disproportionation proportion. Current solvent abilities to disolve LiO_2 is given in fig. 1.3. An alternative explanation concerning the reaction pathway control by the electrolyte is the solvent effective polarity[35]. Additives addition tuning the solvent polarity changed the second reduction activation barrier, effect not explainable by the previous theory.
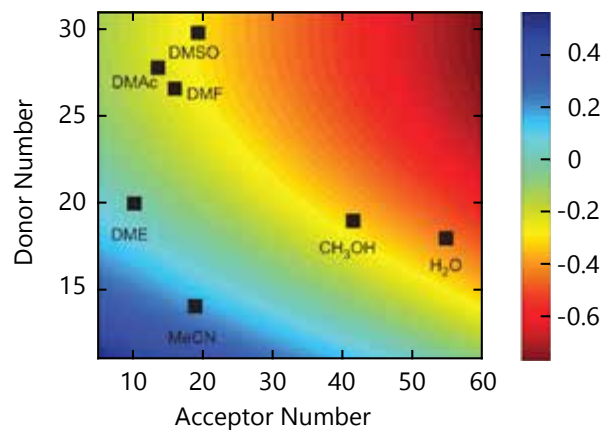
Figure 1.3: **Free energy of LiO dissolution of different solvents in function of the solvent Acceptor Number and Donor Number, adapted from [36].** The energy value are relative to Dimetoxyethane.

Solvating properties of the electrolyte are further influenced by additives. Strongly Li^+ coordinating salt anions like NO_3^-, associated with poor dissociation, increase solubilized superoxide but at the cost of the electrolyte conductivity[13,37–39]. Other examples are Lewis or Brønsted acids used to improve the surperoxide solvatation as as water, alcohols, onium cations, or other alkali ions despite increased side reactivities[36,40,41,41–43]. Favouring solution growth through additives has grown more importortant since high Lewis basicity solvent are also more susceptible to nucleophilic attack by O_2^- [44].

Given the O_2/Li_2O_2 and O_2/O_2^- standard potential respectively 2.96 and 2.68 V_{Li/Li^+}, the higher stability of peroxide versus superoxide in presence of Li^+ drives disproportionation[45]. The second reduction has also at all discharge potentials a strong driving force, the O_2^-/Li_2O_2 standard potential of being 3.3 V_{Li/Li^+} [12]. Due to kinetics, the disproportionation reactions appears to be the most favoured reaction at low overpotentials[12,14,46,47]. Higher overpotential increases the second reduction rate at the disproportionation expense and favour surface growth.

The Li_2O_2 pathway growth holds a major importance on the discharge capacity. Electrolytes such as CH_3CN and dimethoxyethane (DME) solvate LiO_2 poorly and leads to a conformal coating of the electrode by peroxide, as illustrated in fig. 1.4(a). The potential curves are characterized by a very quick decay associated with the passivation of the electrode. The reaction seats at the Li_2O_2/electrolyte interface, the reaction being more facile on the peroxide than at the electrode interface[10,48–50]. Beyond a layer thickness of only 5 to 10

nm discharge, charge transport resistance increases due to ~~the~~ peroxide poor conductivity; Discharge ceases when electrons are not transported through the layer, corresponding to low capacity[46,49,51,52]. A higher current density is associated, moreover, with a higher nucleation rate, ~~leading to a more~~ conformal deposition and a quicker death of the electrode[46].

A solution mechanism delays the ~~apparition~~ of a Li_2O_2 layer and allows for higher capacity. Fig. 1.4(c) shows higher capacity with higher donor number electrolyte. Due to the lower driving force, particles grow as large micrometre-sized toroidal particles composed of lamellaes[12,36], as illustrated in fig. 1.4(b). Superoxide like ~~structure~~ has been found on the surface of such structure[53]. The local overpotential increase with the ~~re~~covering of the matrix by the toroidal structure changing to a surface control growth. This leads to the formation of smaller and flatter particles as the discharge progress[54]. Surface blocking finally leads to the end of discharge. Impedance spectroscopy showed a similar blocking for either pathway due to increased charge transfer resistance[52].
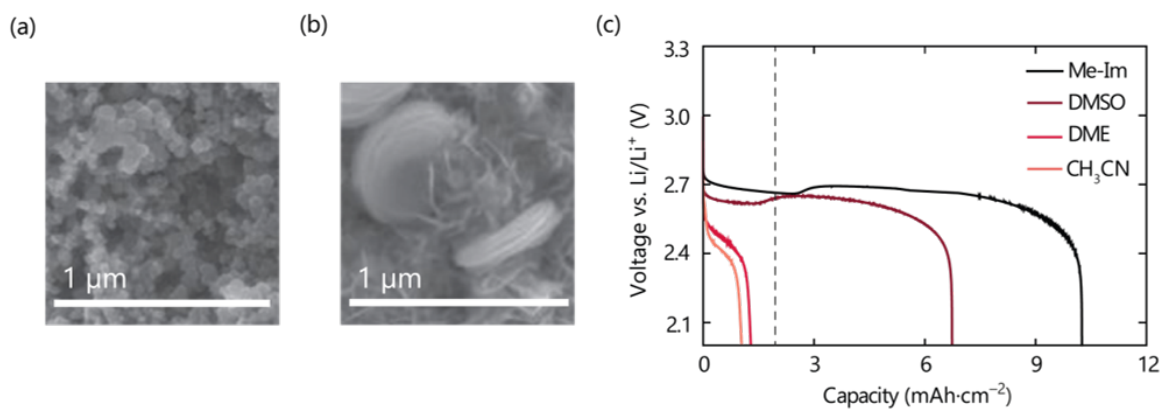
Figure 1.4: **Reaction pathway influence on discharge.** (a) SEM ~~picture~~ of Li_2O_2 ~~layer~~ obtained ~~by surface mechanism~~, adapted form[36], (b) SEM ~~picture~~ of Li_2O_2 toroid ~~from~~ solution mechanism, adapted from[36]. (c) Dependence of galvanostatic discharge with solvent donor number (0.1 M LiClO4), adapted from[12]. The dashed line represent the 7 nm Li_2O_2 thickness, limit ~~of the~~ achievable ~~capacity~~ by pure surface mechanism.

1.2.1.2 Charge

The Li_2O_2 oxidation mechanism is less ~~defined~~ than the discharge mechanism. Several points are still determined. First, the oxidation proceeds incipiently at low overpotential with oxygen evolution at potential as low as 3 V_{Li/Li^+}; the thermodynamic potential being 2.96 V_{Li^+}[10,55,56]. Second, voltage rise correlates with side products formation from the charge onset, accelerated ~~with~~ growing potential, ~~which~~ are harder to oxidized than Li_2O_2[10,57,58]. Third, overpotential arises to a lesser extent by increasingly difficult electron transfer as Li_2O_2 recede[59].

With these considerations in mind, three different mechanistic models were discussed, each backed ~~up~~ by experiments and calculation. First, a direct two-electron oxidation, due to the absence of LiO_2 in acetonitrile, as shown by in situ surface-enhanced Raman spectroscopy[7]. Second, a topotactic delithiation forming a metastable $Li_{2-x}O_2$ comprising Li_2O_2 and LiO_2 domains, based on DFT calculations and X-ray diffraction experiments[45,60]. Third, ~~a~~ formation of a LiO_2 surface layer at low overpotential and a direct two-electrons oxidation at high overpotential, based on electrochemical experiments[61]. LiO_2 formation and consequent disproportionation was supported by TEM analysis[62]. DFT calulation shown

possible lithium extraction at low overpotential with ~~the~~ progressive dilatation of the Li_2O_2, while O_2 evolution is responsible for the high overpotential, being the more ~~defavourbale~~ step.[45,63,64].

A unified model governed by the solvent DN, in a similar fashion ~~than~~ discharge, was recently proposed[11]. Using thin–film RRDE, dissolved LiO_2 ~~is reduced~~ at the ring with high DN solvent (DMSO) while absent in a lower DN solvent (TEGDME), as shown in fig. 1.5. Similarly, XANES experiments showed the formation of LiO_2 at the surface upon charging only in high DN solvent.
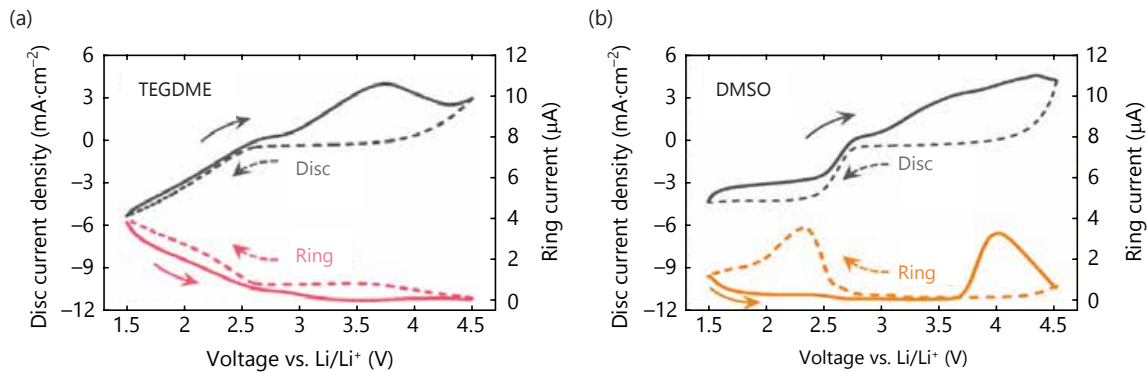
Figure 1.5: **Thin-Film RRDE Cyclic voltametry in presence of oxygen in different electrolyte (0.2 M LiTFSI) at 50 mV.s-1 and a rotating speed of 900 rpm, adapted from**[11]. The Au ring potential was 4.0 V vs Li/Li+, sufficient for superoxide oxidation. (a) in TEGDME, (b) in DMSO.

As for discharge, the solvent influence the Li_2O_2 decomposition pathway, either via solvat~~at~~ed superoxides or topotactic surface delithiation. A higher ~~kinetic~~ applied by ~~the~~ overpotential favours the surface route as for discharge. The overall 2e- oxidation ~~is composed of~~ two step~~s~~ charge mechanism (Eq. 1.6); it commences with a first delithiation forming superoxide like species. The second step, as for discharge, is either a second oxidation (Eq. 1.7) or disproportionation (Eq. 1.8). In high DN solvents, $Li_{2-x}O_2$ is partly dissolve to $LiO_{2\,(sol)}$ ~~that~~ can disproportionate. ~~It~~ explains the absence of solubilized LiO_2 detection in acetonitrile[7]. The reaction scheme ~~can be found~~ in fig. 1.6.

$$Li_2O_2 \longrightarrow Li_{2-x}O_2 + xLi^+ + xe^- \tag{1.6}$$

$$Li_{2-x}O_2 \longrightarrow O_2 + (2-x)\,Li^+ + (2-x)\,e- \tag{1.7}$$

$$2\,LiO_{2\,(sol)} \longrightarrow Li_2O_2 + O_2 \tag{1.8}$$
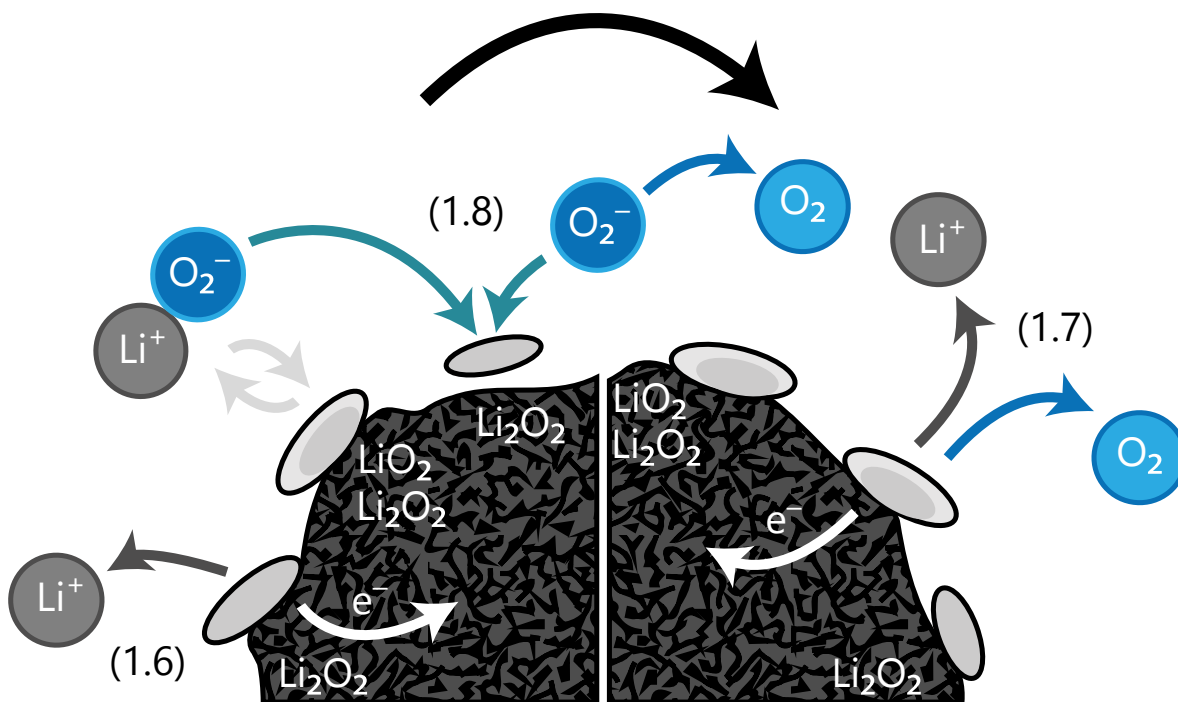
Figure 1.6: **Scheme of the charge reaction (simplified to x = 1) and the equations corresponding to each steps.**

It remains elusive if the adsorbed LiO_2 after initial delithiation will undergo disproportionation or only direct reduction. Evidence seems to indicate disproportionation of absorbed LiO_2 during charge [62,65]. In any case, the disproportionation in charge is beyond doubt in high DN solvent. Chemically synthesized Li_2O_2 is converted into lamellar morphology due to disproportionation after being partly oxidized, as illustrated by fig. 1.7; is accompanied by the formation of nanocrystalline Li_2O_2 detected by XANES.
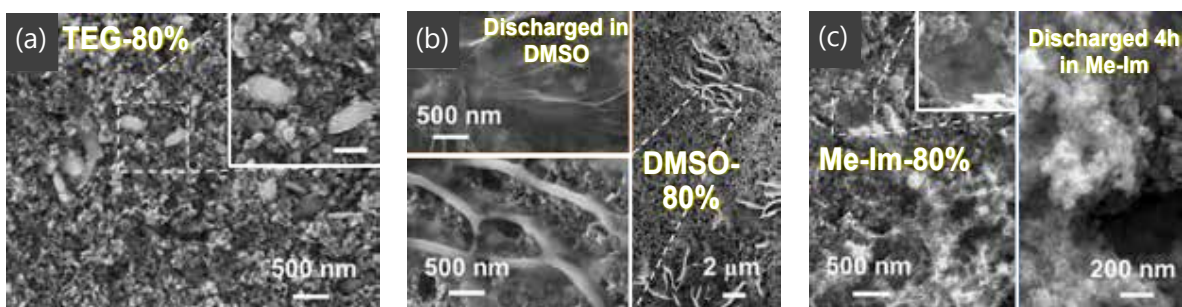
Figure 1.7: **SEM at 80 % of the charge in different electrolytes (1 M LiTSFI), adapted form** [11]. (a) in TEGDME, (b) in DMSO and (c) in Me-IM. The insert mentioning discharge are here for comparison with solution mechanism during discharge. If not mentioned, the scale bars represent 200 nm

1.2.1.3 Discharge product

Li-O2 cells, being a "beyond intercalation" technology, heavily rely on the discharge products properties and notably mass/charge transport in Li_2O_2. Crystallinity, defects and applied voltage govern charge transport properties of the peroxide. The deposition driving force imposed two distinct morphologies as described in part **??**. The formation of a well-contacted amorphous Li_2O_2 layer, through the surface pathway, results in lower oxidation potential [11,60,66,67].

The reaction is facilitated by defect-rich peroxide; Defects result in two orders of magnitude lower transport resistance compared to crystallites formed by disproportion as illustated by fig. 1.8[66,68,69]. Li_2O_2 disproportionation morphologies, despite driving higher discharge capacities, leads to higher overpotential in charge and hence more side products.
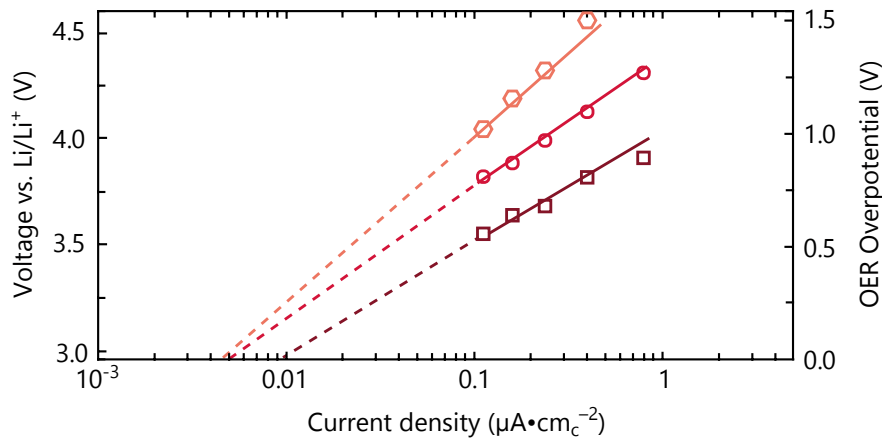
Figure 1.8: **Charging voltage Tafel slope dependence on Li_2O_2 crystallographic structure, adapted from[66].** Pink hexagonal correspond to commercial crystalline Li_2O_2, red circle to annealed Li_2O_2 and dark red square to amorphous Li_2O_2

Li_2O_2 electronic conductivity present a particular dependence on the applied voltage. Lower potential is implied to result in reduced tunnelling barriers and easier charge transport in Li-deficient phases, notably by lithium vacancy formation as seen in fig. **??**; The reduced charge conductivity during charge corroborate with the low discharge capacity and low overpotential at the charge start point. Different morphologies presence would lead to several charge plateau for Li_2O_2 oxidation, due to different transfer resistance.
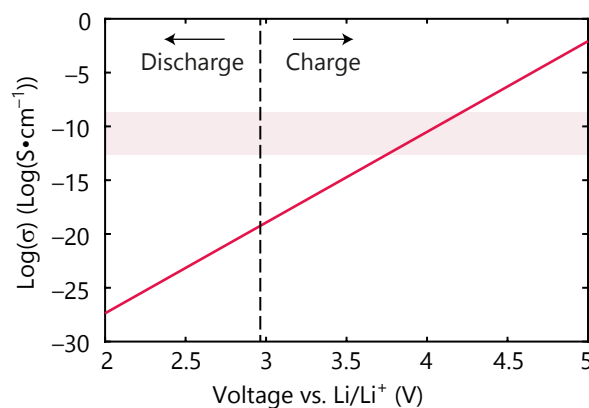
Figure 1.9: **Lithium peroxide electronic conductivity versus the cell potential, adapted from[59].** The light pink region represents a IR drop lower than 0.1 V for a 6 nm thick Li2O2 film. O2/Li2O2 thermodynamic potential correspond to the dashed line.

The charge transport importance lies in the reaction interface. The reaction could proceed either at the cathode/Li_2O_2 or the Li_2O_2/electrolyte interface. The electrolyte/Li_2O_2 interface is generally accepted as reaction site during discharge[48–50,70], in spite of contradictory results[71]. The reaction interface is more disputed during the charge and leads to different interpretations of the overpotential rise. Considering a Li_2O_2/electrolyte interface, Li_2O_2 poor conductivity will be limiting at all step of the charge[70,72,73]. For a cathode/Li_2O_2

interface, the depletion will proceeds preferentially at the electrode surface, reducing contact interface between the discharge products and the electrode, contributing to reduced electron path and increasing overpotential[48–50,71,74]. In the first stage of charge, mass transport of O_2 and Li^+ through the layer will be limiting. As experiments supporte both assumptions, more thorough experimentations are needed to unravel completely the reaction interface as its position appears related to the reaction pathway during discharge as well as the charge applied rate[70]. The charge potential rise cannot, however, be fully accounted by an increased impedance of the cell. The rise was mostly assigned to the formation of side products as lithium carbonates[10,15,75,76].
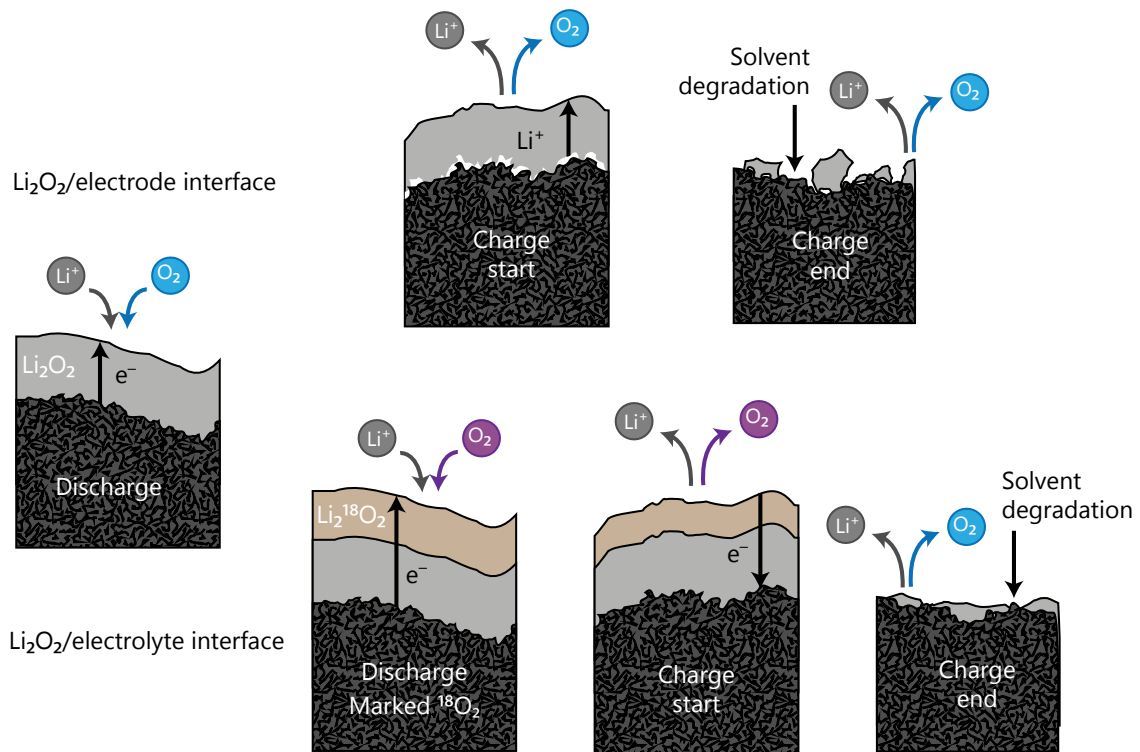
Figure 1.10: **Scheme of the reaction interface and the subsequent implication.** The Li_2O_2/electrode interface case is adapted from impedance spectrosopy results[48]. The Li_2O_2/electrolyte interface case is adapted from mass spectrometry results[70].

1.2.2   Electrodes

1.2.2.1   Cathode

$Li-O_2$ cells repose on the formation/decomposition of lithium peroxide. This reaction needs to proceed on a conductive matrix that can accommodate Li_2O_2. Peroxide will grow inside and fill the matrix pores; Electrode material with sufficient porosity is necessary to allow important Li_2O_2 formation, hence high capacity. Owing to its low cost, good conductivity and adaptable surface geometry, carbon is the materials of choice for $Li-O_2$ battery electrodes.

Carbon stability in $Li-O_2$ chemistry is however not perfect and was found to promote the amount of side reactions[58,75,77,78]. By ^1_3C labelled carbon electrode and mass spectroscopy in situ analysis, CO_2 evolution from deteriorated electrode was detected which is a common decomposition products. Contact with Li_2O_2 and discharge release no notable CO_2 amount form the electrode[58]. Side products formation must hence arise entirely from electrolyte degradation during discharge. Electrode degradation commence with charge and accelerate

~~with~~ the overpotential rise, forming Li_2CO_3, as shown in fig. 1.11[58,75,77]. An aggravating factor ~~concerning~~ is the presence of defect and hydrophilic moieties at the carbon surface, promoting ~~the~~ electrode and electrolyte decomposition, as ~~dpecited~~ in fig. 1.11[58] [78]. Another carbon cathode issue arise from polymer binders. Commonly used lithium ion battery binders, as PVDF, are unfortunately not stable in $Li–O_2$ cells[79–82]. Nowadays, Nafion or PTFE are the binders of choice but their stability remains to be tested thoroughly towards aggressive chemicals formed in $Li–O_2$ cells[81–83].
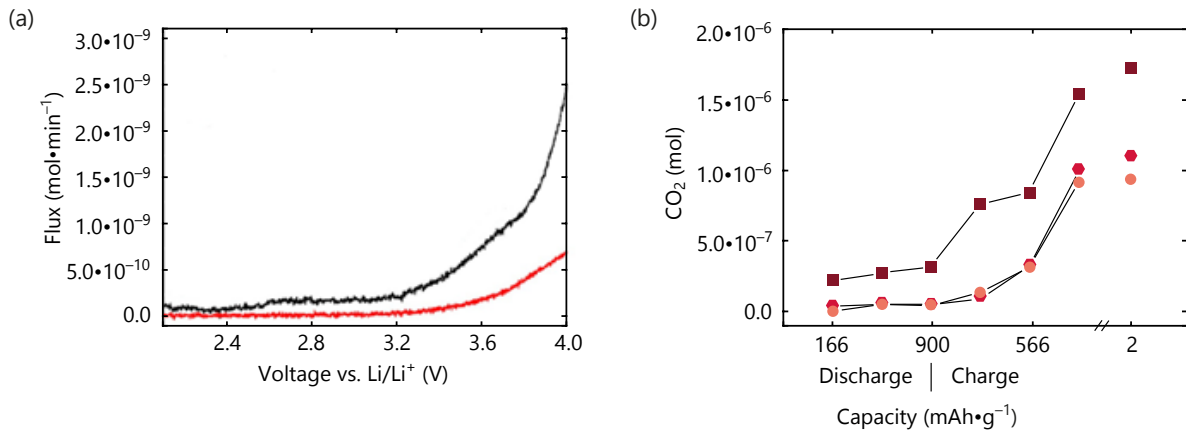
Figure 1.11: **Carbon electrode stability.** (a) In situ CO_2 mass spectroscopy during $Li–O_2$ cell charge, adapted from[58]. In red, $^{13}CO_2$ characterizing side reaction form the electrode, and in black $^{12}CO_2$ side reaction ~~form~~ the electrolyte. The results where obtain by DEMS with a DMSO electrolyte after a prior discharge ~~up~~ to 2 V_{Li/Li^+}. (b) CO_2 ~~evolution from~~ Li_2CO_3 ~~decomposition formed by electrode decomposition in DMSO electrolyte~~, adapted from[58]. The pink circles represent ~~H~~ydrophobic carbon, the red hexagons commercial carbon, the dark red square hydrophilic carbon.

As a result of carbon instability, more stable materials have been tested as electrode materials. To ~~stay~~ competitive, these materials should not catalyse electrolyte decomposition as well as keep a high porosity, a low density and price. Among the materials tested, Ti ceramics and nanoporous Au showed, for example, an improve cyclability and reduced side reactivity[20] [83,84]. If gold is naturally protected in $Li–O_2$ cells conditions, Ti materials as TiC or metallic Magnéli phase Ti_4O_7 needs a passivation layer[83–85]. This layer is formed likely by oxygen–deficient titanium oxide (TiO_{2-x}), enhancing the corrosion resistance and the conductivity of Ti materials. A similar ad–hoc passivation layer of ZnO or Au deposited carbon increased its corrosion resistance. This method face nevertheless passivation layer breaking after some cycling due to the deposition of Li_2O_2 below the passivation layer[86,87]. The materials higher density compared to carbon ~~imposed~~ a higher ~~surface area~~ to convey an interesting capacity. Unfortunately, these alternative cathodes cannot compete yet with carbon porosity.
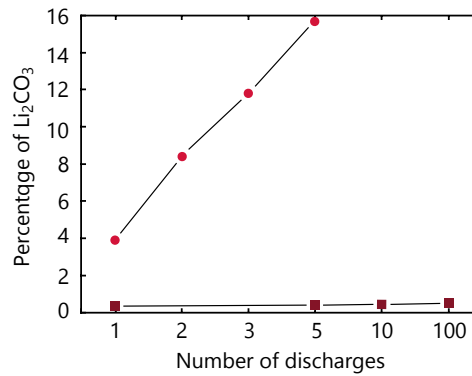
Figure 1.12: **Materials dependency of CO$_2$ evolution from Li$_2$CO$_3$ decomposition formed by electrolyte decomposition in DMSO electrolyte, adapted from[84].** The red hexagons represents carbon cathode, the dark red square TiC cathode.

Considering the porosity, the influence of the electrode pore size have been investigated[88,89]. Several geometries and their impacts are tested as mesostructure carbon, carbon aerogels, graphene–based electrodes[89][90–92]. Modelling use allows verifying the porosity importance[93]. The pathway to these pores, especially with nanomaterials, should not be neglected. At high current density, mass transport is limiting[92]. Li$_2$O$_2$ and side products formation could provoke clogging of the small matrix pore. Higher pore size appears to enhance the lifetime of similarly constituted electrodes, as demonstrated in fig. 1.13[88,89]. In a similar fashion, bigger molecules as additives also require access to the pore and a nano–grid electrode was proposed to facilitate their diffusion[94].
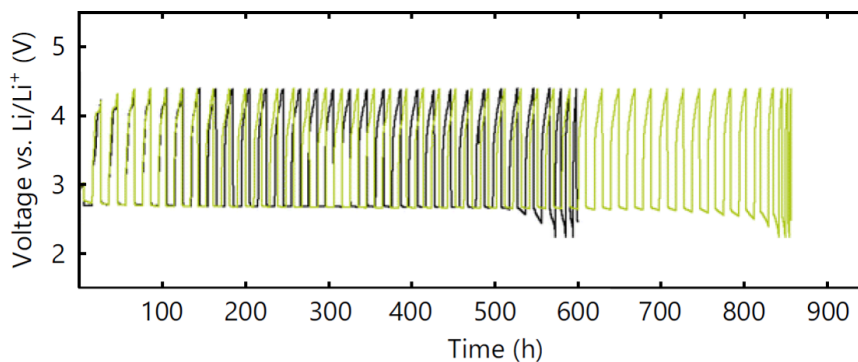
Figure 1.13: **Porosity size influence on Li–O$_2$ cells, adapted from[89].** In green cycling of large pore size carbon and in black, small pore size. The discharge capacity are limited to 1.0 mA·h·cm^{-2} and current fixed to 0.1 mA·cm^{-2}.

1.2.2.2 Anode

Cathode limits mostly the capacities with current Lithium–ion technology. High capacity anode rises, however, as problematic to follow the increased cathode capacity. Anode technology with similar capacity to O$_2$ cathodes requires "beyond intercalation" approach. Lithium metal has a very good specific energy, a low density and the lowest electrochemical potential. Lithium metal anode is however still not ready, despite in–depth mechanistic study[95][96].

The anode lose quickly coulombic efficiency with the formation of a so-called surface electrolyte interphase (SEI). The SEI is formed by decomposition side products as Li car–

bonates, LiOH or LiF[97–99]. These reaction can be due to decomposition of counter ions (PF_6^-, $TFSI^-$), impurities present in the electrolyte (H_2O, H^+) or the decomposition of the electrolyte itself (O_2, carbonate, CO_2). The lithium passivation layer presents a different resistance and tensile strength depending on its composition, generally composed of an inorganic compounds core and an outer layer of organic chemicals, as schemed in fig. 1.14[98].
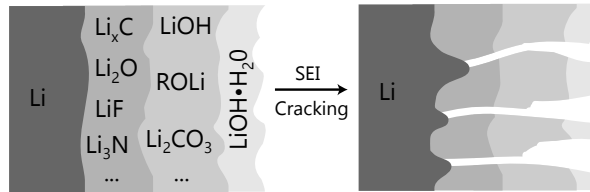
Figure 1.14: **SEI composition and formation of preferentiel deposition pathway, adapted from [98].**

In addition, lithium preferably grows as dendrites that lead to short circuits after some cycles, hazardous due to flammable organic electrolytes. Due to non-homogeneity, breaking of the SEI forms preferential deposition pathways, enhancing the tendency to produce dendrites[100]. This newly formed dendrites growth is favoured by non-uniform field distribution, accelerating deposition at the tip of the dendrites[101]. The pristine lithium surface of the dendrites is also subject to SEI reformation, increasing the side reactions. Lithium dendrites can disconnect from the anode due to side reactivity, synonym of dead weight and capacity loss[102]. Considering solid–state electrolyte, mossy or diacritics deposition reduce electrode/electrolyte contact, increasing cell resistance and leading to quick death[103].
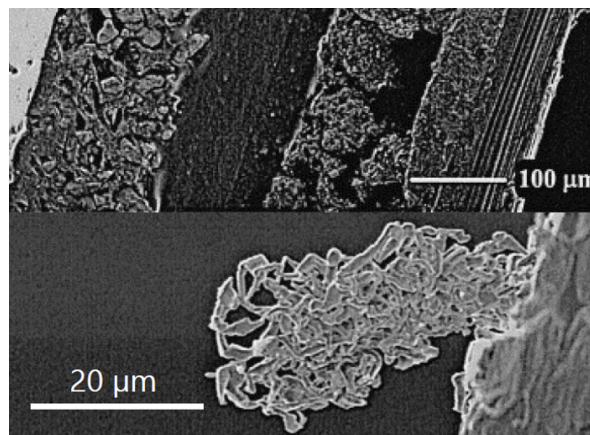
Figure 1.15: **SEM image of mossy (top) and dendritic (bottom) deposition.** Top picture represent the 14th at 0.45 mA·cm^{-2} and bottom picture after first charge at 2.2 mA·cm^{-2}

Since SEI formation appears inevitable, the formation of a compact and uniform layer, with good mechanical and electrical properties is required to successfully use Li metal anodes. The presence of O_2 impose specific stability requirements[95]. Even though lithium metal would require a separation from moisture and oxygenated species produce at the cathodes[104], a strong SEI remains a must–have to ensure long term cycling. The electrolyte constitution holds a strong influence on the SEI composition. As the solvent itself is not completely stable, it will change the composition of the SEI. Carbonates usually lead to good stability but are not useable in Li–O_2 batteries[105]. The salts are neither stable, especially in contact with water impurities in the solvent, and can form LiF in case of PF_6^- or $TFSI^-$ cations[99,105]. LiF is actually a compact layer with good uniformity and strength improving

stability but brings a lower conductivity. Nitrate/azide based lithium salt are also employed to produce a stable SEI and have been tested in Li–O$_2$ cells conditions, as show in in fig. 1.16(a)[106–109]. NO$_3^-$ enhances furthermore solution pathway at the cathode and gets reduced at the Li to generate NO$_2^-$ ~~that~~ facilitate Li$_2$O$_2$ oxidation by oxidation mediator effect[37][39]. Azides are known to quench reactive species formed in Li–O$_2$ batteries as discussed in **quencher**[110]. Yet, nitrate ~~salt~~ suffers from lower conductivities compared to TFSI$^-$ ~~ions~~ and should be used as additives. Other additives commonly used for lithium metal, as CO$_2$ or organic additives for example, are not applicable ~~to~~ Li–O$_2$ cells ~~for~~ cathode stability issue.
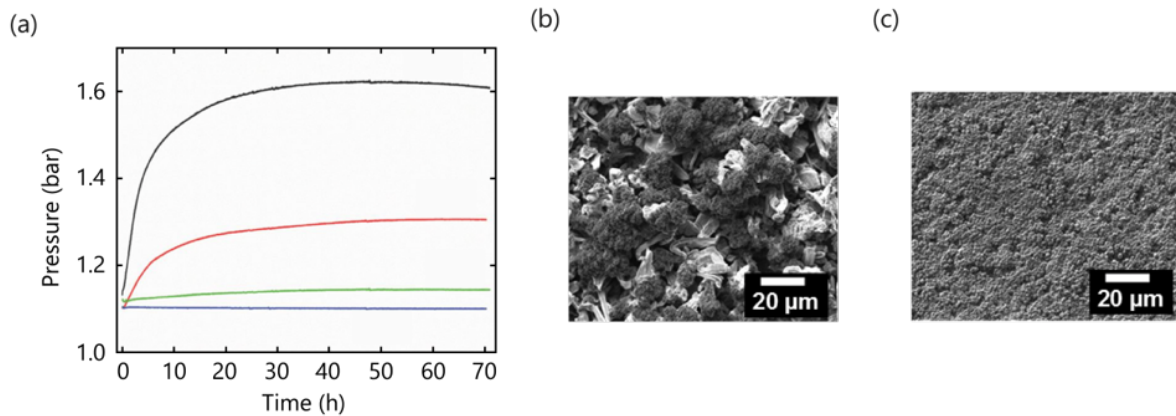
Figure 1.16: **Formation of a stable SEI.** (a) Pressure evolution at OCV in a closed symmetric Li/Li cell, adapted from[106]. Pressure evolution ~~denotes a~~ side reaction of the electrolyte with lithium metal. In black, evolution of cells with a N,N–Dimethylacetamide electrolyte and LiTFSI salt under argon; In red, the same electrolyte under oxygen atmosphere. In green, evolution of cells with a N,N–Dimethylacetamide electrolyte and LiTFSI/LiNO$_3$ salt under argon; In blue, the same electrolyte under oxygen atmosphere. (b) SEM image of Li anode after 10$_{th}$ deposition at 0.1 mA·cm^{-2} with a 1 M LiPF$_6$ in propylene carbonate electrolyte, adapted from[111]. (c) SEM image of Li anode after 10$_{th}$ deposition at 0.1 mA·cm^{-2} with a 1 M LiPF$_6$ and 0.05 M CsPF$_6$ in propylene carbonate electrolyte, adapted from[111].

A proposed solution is to preform a SEI by plunging the lithium in a fluorinated solvent[112]. After this treatment, lithium metal was able to cycle in acetonitrile, a common solvent Li–O$_2$ chemistry. Another fashion to produce a SEI is by protecting the anode with a solid state electrolyte as discussed in **intro electrolyte**. More exotic ways to reduce dendrites are investigated as control the lithium deposition rates or formation of self–healing electrostatic shield by incorporating Cs$^+$ or Na$^+$ ions, demonstrated in fig. 1.16(b)–(c)[111][113].

1.2.3   Electrolyte

Difficult criterions are to be met for Li–O$_2$ cells electrolyte, namely sufficient electrochemical window~~s~~, formation of a stable passivation layer ~~with~~ the anode, a high conductivity and ~~be~~ chemically stable. Electrolyte in Li–O$_2$ cells holds , moreover, a major influence on the discharge and charge mechanism. Li–O$_2$ chemistries induce very aggressive species in solution. For this reason, solvents such as ethers (particularly glymes)[114,115], sulfones[116], amides[106,108,117,118], sulfoxides[20] replace carbonates usually used in lithium batteries[119]. Nitriles ~~present~~ likewise a good stability towards reduced oxygen species, its interested is nevertheless reduced due to lithium metal instability and low donor number[120].

High capacity enticed by the solution pathway, as described in 1.2.1.1, favoured high DN solvents use. Solution pathway is nonetheless a double-edge sword, solvating more aggressive species for the electrolyte and increasing superoxide attack, as illustrated in fig. 1.17[44]. A trade-off needs to be found between the longevity and capacity, high DN solvent being more susceptible to nucleophilic attack. To improve stability towards reduced O_2 species, solvents are designed to avoid nucleophilic attack by avoiding any protons in a-position to heteroatoms. Among them, fully methylated glyme[121], hexamethylphosphoramide (HMPA)[122], or the fully methylated methoxy ketone 2,4-dimethoxy-2,4-dimethylpentan-3-one[123] suggest increased stability. Yet, such electrolytes are for the moment impeded by extreme toxicity (HMPA) or instability with a Lithium metal. The choice of the salt equally influence the reaction mechanism and should not only be chosen for their conductivity and stability towards lithium metal/oxygen species, as discussed in ??. The same reasoning goes with additives such as phenol, protic species or mediators.
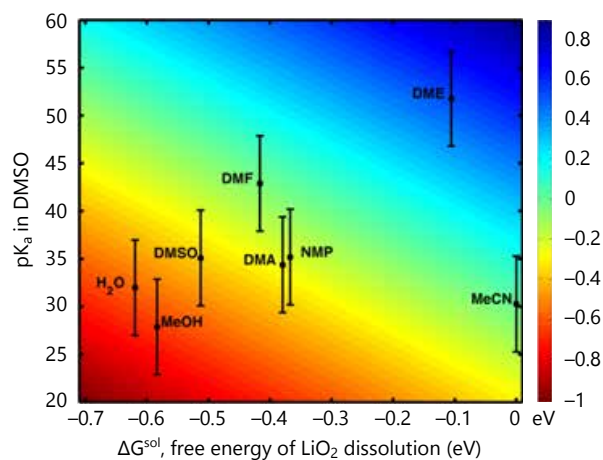
Figure 1.17: **Contour map of nucleophilic attack thermodynamic driving force for different solvents, adapted from[44].** The driving force is given in function of the Gibbs free energy for dissolution with MeCN as reference and the solvent pK_a in DMSO. Low dissolution energy denotes a tendency for the solution mechanism and low pk_a easier hydrogen abstraction

Ionic liquids, in addition to advantages as high electrochemical and chemical stability, present low volatility especially interesting for real application with an airflow[6]. Use of ionic liquids is furthermore motivated by low charge hysteresis. The oxygen reduction mechanism in ionic liquids appears to differ from conventional electrolytes, notably influenced by the weaker Lewis acidity of the ionic liquid cations, favouring superoxide solvation[124,125]. Unfortunately, O_2 solubility and diffusivity are low due to their viscosity[126]. The ionic liquids chemical stability is also problematic for Li-O_2 application, since common imidazolium-based ionic liquids are not stable towards superoxide[127]. Pyrrolidinium or piperidinium based ionic liquids present a better compatibility with superoxide and lithium metal but still insufficient reversibility and tendency to parasitic chemistry[120,128–130]. Among other issues, higher price, possible stability issue towards lithium metal and lower Li-ions solubility also speak in disfavour of ionic liquids[131].

Solid-state electrolytes are promising due to the external protection they offer to lithium metal from O_2 or H_2O. Dendrites growth can also be inhered by applying external pressure on the anode. Solid-state electrolytes comprise ceramic (perovskite, garnet, NASICON) and polymer. Solid-state electrolytes have the detrimental characteristics of lower conductivities[132,133]. Li-air cells would specifically require the arrival of gaseous O_2 at the surface, O_2 transport in solid being low, and volume acclimation with peroxide formation. The solid-

state electronic also prevents the solution pathway, leading to low capacities. The stability of polymer against reduced oxygen species is moreover problematic[132][134]. Ceramic suffers from mechanical degradation due to their brittleness combined with volume changes of both electrodes[133].

A promising use of solid–state electrolytes is separator between the oxygenated species/moisture and the lithium metal, necessary to prevent the anode corrosion. Solid–state electrolytes can separate anodic and cathodic compartment avoiding cross-talk between the two electrodes[104,135]. A separator allows moreover two different electrolytes, a fluorinated carbonate for SEI production at the anode and an ether at the cathode for its stability. Such methods can also permit the use of additives in the cathode compartment that would not be stable in contact with lithium metal, as schematized in fig. 1.18[136]. Solid–state electrolyte is then of major importance for long term cycling but not as direct electrolyte. Work on Li–O$_2$ solid electrolytes are still at the beginning but researches are motivated by the possibility of flexible batteries and potential moisture and air protection of the anode[137,138].
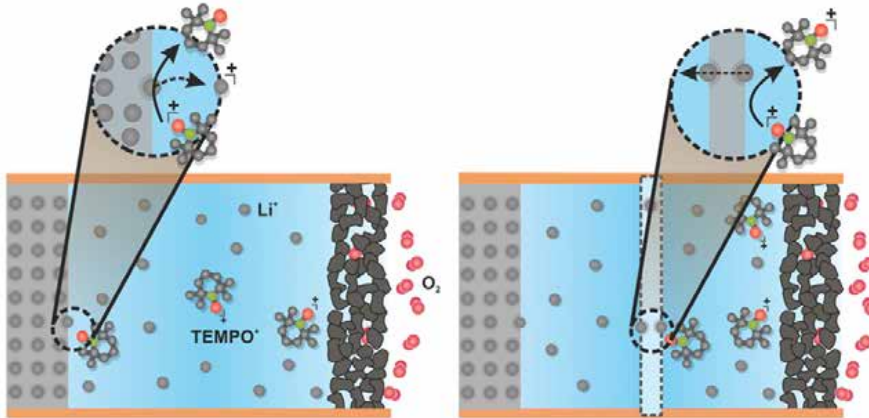
Figure 1.18: **Scheme of solid state electrolyte used as separator taken from[136].** The Tempo additives are confined to the cathode and does not crosstalk to the lithium anode.

1.2.4   Complete stack

Li–O$_2$ batteries main advantage is often described as the Li$_2$O$_2$ theoretical capacity (1168 mAh·g^{-1}[6]). Given the nature of beyond intercalation batteries, achievable capacity is often misgiven as the capacity per gram of porous substrate; Flattering numbers can be obtained, between 1000 and 4000 mAh·g$_{carbon}^{-1}$, compared to $\approx$ 100–500 mAh·g^{-1} for traditional technologies[4][5][139]. Limited capacity discharge, usually around 1000 mAh·g$_{carbon}^{-1}$, limits as well side reactions amounts, improves cyclability and still compare favourably with intercalation materials. The electrode mass is an accurate descriptor of the achievable capacity in intercalation materials; the host material mass and volume are well defined and relatively stable between discharge and charge state[5]. In Li–O$_2$ cells, no actual storage materials are present in the initial charge state and active material mass and volume definition become fuzzier. Li$_2$O$_2$ chemistry is not only based on electron conductor but also O$_2$ and Li$^+$ transport in the electrodes pore by the electrolyte, rather than seldom alkaline ions intercalation.

A more comparable descriptor of Li-O$_2$ electrode to intercalation materials is the concept of "super–host structure" representing the electrolyte filled porous electrode. Discharge products formation drives out the electrolyte from the pores but will still be present in the system and part of an extended host electrode definition. In Li-O$_2$ cells, the initial host mate-

rial is not confined to the electrode but includes the electrolyte filling the pores. The concept of super–host electrode is elaborate in fig. 1.19. Electrodes porosity holds primary importance for the capacity. Besides being needed to accommodate a high amount of active storage materials, high porosity implies a larger electrolyte/electrode proportion. This additional electrolyte, in turn, diminishes the true specific capacity compared to lower porosity. A capacity given per mass of electrodes alone can hence result in highly different "true" capacity depending on initial porosity; Only the "true" capacity based on the total super–host weight can be use to show a significant capacity improvement compare to intercalation materials, especially with limited capacity cycles.

(a)   (b)
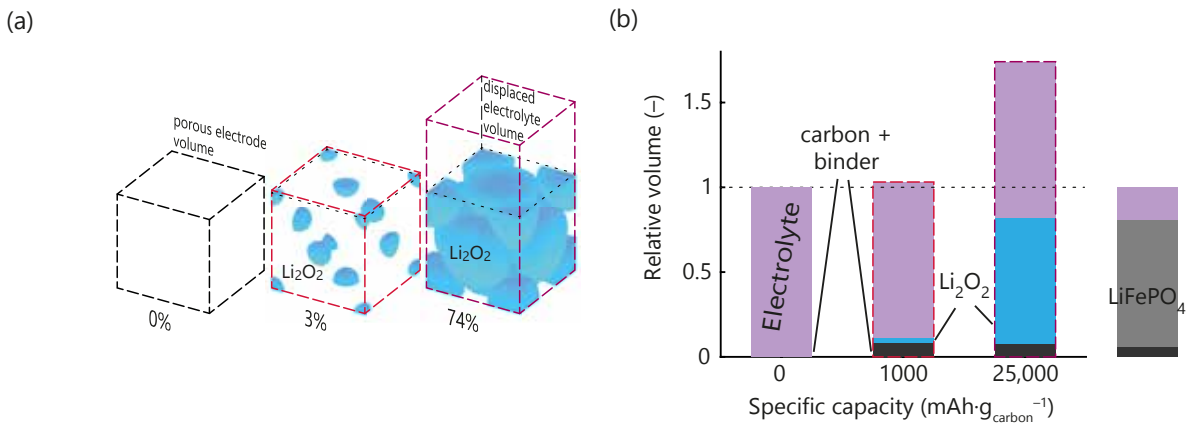
Figure 1.19: **Super–host structure, adapted from**[5]. (a) Scheme of the super–host structure expansion at different Li_2O_2 filling degrees. (b) Relative volumes of each super–host component at different state of discharge. The insertion material $LiFePO_4$ at 74% volume occupation is given for comparison.

To add more details, I need to know how the calculations were exactly done, could you give me your calculation sheet?
Only several easily obtained parameters are required to calculate true capacities. They are the electrode thickness, the mass fractions of all components (electrode, binder, and electrolyte), and their areal loading. Knowing the respective densities, the volume fractions can be obtained. With these measures, it is straightforward to convert the capacity with respect to substrate into true capacity per mass and volume of the total electrode including electrolyte. From crystallography, the maximum theoretical packing for Li_2O_2 is a face centred cubic structure corresponding to 74 % volume occupation. Using an electrode with 4% binder volume, a starting porosity of 92 % and a electrolyte with a **1.1 find why this value in the calculation sheet** density yield a "true" capacity of ≈ 700 mAh·g_{total}^{-1} and a volume occupation of 80 %, the results obtained is described in fig. 1.20.

Electrolyte/electrode ratio become even more predominant in the case of electrode material as porous Au or TiC, discussed in part 1.2.2.1. The specific capacity is naturally reduced considering their higher density. An increased porosity reduces the high–density material proportion hence nearing its theoretical capacity to a lighter one, like carbon. The use of alternatives cathode materials is therefore greatly dependent on their porosity as illustrated in fig. 1.20.

(a)

1000 mAh·g$_{carbon}^{-1}$

75% 85% 92%

LiFePO$_4$

True specific capacity (mAh·g$_{total}^{-1}$)

Specific capacity (× 10³ mAh·g$_{carbon}^{-1}$)

(b)

Specific capacity (mAh·g$_{total}^{-1}$)

C
TiC
Au
80% 100% pore filling

Initial porosity (%)
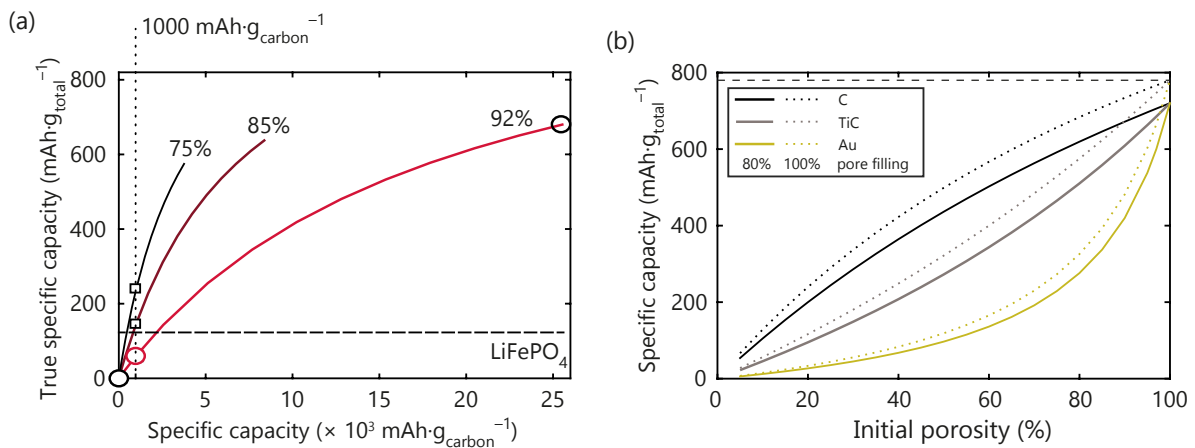
Figure 1.20: **Super-host true capacity.** The calculation protocol is described in the main text. (a) Recalculated capacity at different matrix porosity (75%, 85% and 92 %). The insertion material LiFePO$_4$ at 74% volume occupation is given for comparison, adapted from[5]. (b) Recalculated "true" capacity in function of the electrode porosity and density given for either 80% (full line) or 100% (dotted line) Li$_2$O$_2$ volume occupation, adapted form[140]. **The description is unclear, it is written in the book that you need an initial porosity of 92% to achieve 80% filling**

Even though accounting for "super–host structure" results in lower achievable capacity, Li–O$_2$ cathode still present a significant amelioration compared to lithium–ions cells. The only requirements are high Li$_2$O$_2$ packing density and a small inactive/active material ratio. Li–O$_2$ cathode is however not the only one to be subject to volume change during cycling. Lithium metal electrode itself will change volume/mass upon lithium plating/stripping or the surface electrolyte interphase formation[98,141]. This is often overlooked since the lithium metal is a very efficient reservoir of lithium ions and imposes overdesigning lithium anode.

True cathode specific capacity is sufficient for Li–O$_2$ technology to hold promises at research scales; Practical application needs to take into account specific cell design[4]. Stack capacity depends notably on binders that should be kept at a minimum, current collectors, the cell housing and stack[142]. The stack and cell housing are particularly important for Li–O$_2$ batteries where airflow to the cathode has to be insured. Development of such technologies is still in its infancy. If current predictions are pessimistic, it is too early to judge on the final achievable capacity of a Li–O$_2$ stack[6].

1.3   Main Reason and suspected origin of metal–air technologies set-backs

1.3.1   The side reactivity importance and metrics

The biggest challenge faced by non–aqueous metal-air batteries is high side reactions, preventing long term cycling amd maturing of the technology. Typical side products are lithium carbonates as Li_2CO_3, Li formate and Li acetate [75,114,143]. The parasitic products subsequently lead to quick cells death due to pore and surface clogging as well as higher charge potential [10,58]. The higher potential results itself in an acceleration of side reactions [58]. Only a deep understanding of the reaction mechanisms and the development of accurate measurement methods will allow truly technology advancement and prevent cell degradation.

The first and foremost characteristic of reversible cells is an efficient redox chemistry of O_2. For Li–O_2 chemistry, the amount of oxygen and peroxide consume/released compared to the capacity must comply with the Faraday law, given in eq. 1.9, and a deviation characterizes side reactions presence; Stoichiometry implies strict e^-/O_2, e^-/Li_2O_2 and O_2/Li_2O_2 ratio described in eq. 1.10 and eq. 1.11. O_2 and L are the only products in a perfectly reversible cell. No side reactivity results in a perfect coulombic yield, hence, all Li_2O_2 produce during discharge should readily be oxidized to O_2 during charge.

$$n = \frac{I \cdot t}{F \cdot z} \tag{1.9}$$

with n, the number of mole consumed/produced; I, the current (A); t, the time (s); F, the Faraday constant (96485.33289 $C \cdot mol^{-1}$); z, the valency number

$$O_2 + 2\,e^- + 2\,Li^+ \longleftrightarrow Li_2O_2 \tag{1.10}$$

$$e^-/O_2 = 2; \; e^-/Li_2O_2 = 2; \; O_2/Li_2O_2 = 1 \tag{1.11}$$

$$P \cdot V = n \cdot R \cdot T \tag{1.12}$$

with P, the pressure (Pa); V, the volume (m^3); n, the number of mole consumed/produced; R, the ideal gas constant (8.314 $m^3 \cdot Pa \cdot K^{-1} \cdot mol^{-1}$); T, the temperature (K)

These conditions are not mutually inclusive and all of them should be met to achieved complete reversibility. During discharge, oxygen consumption is often close to the theoretical ratio of 2 e^-/O_2. Such oxygen consumption does not necessary result in a 2 e^-/Li_2O_2 formation as side reactions might consume O_2. The observed side reactions are more severe during charges, represented by the orange gap between the O_2 production and Li_2O_2 consumption in fig. 1.21. The clear lack of oxygen results in a deviation from the ideal trend of 2 e^-/O_2. This representation defines the major issue of metal-air batteries, a far from ideal reactions due to parasitic reaction especially severe during charge.

(a)

(b)
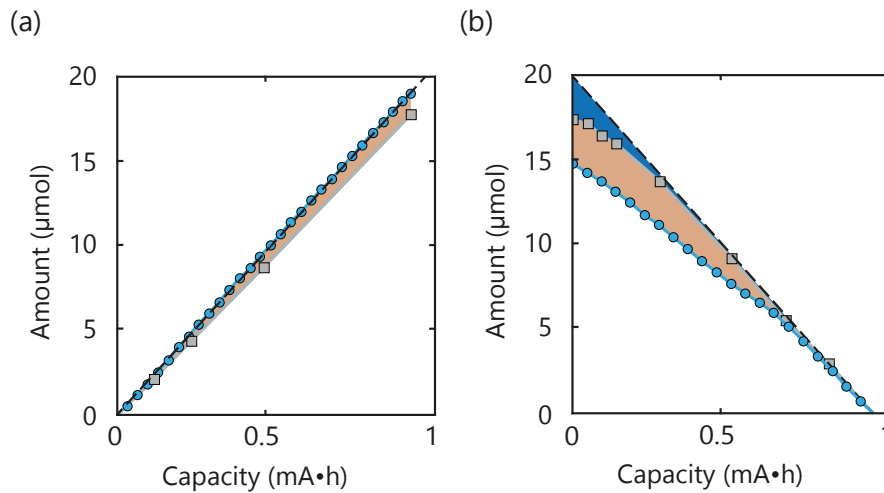
Figure 1.21: **Side reactivity characterized by Li$_2$O$_2$ and O$_2$ evolution, adapted from**[144]. O$_2$ evolution represented in light blue, Li$_2$O$_2$ in grey, side reaction in orange related to Li$_2$O$_2$ formation/dissolution and side reaction due to parasitic oxidation of other species in orange. (a) Discharge (b) Charge side reactivity characterized by Li$_2$O$_2$ and O$_2$ evolution

Analysis of the O$_2$ and Li$_2$O$_2$ production in evermore crucial when limited discharge/charge capacity is used. Apart from biasing the faradic yield by reducing the number of possible side reactions, the charge curves can falsely appear as reversible. The figure 1.22 illustrates this point. Full discharge/charge curves are characterized by a plateau at a characteristic voltage corresponding to the reagent consumption with a rate imposed by the current. This plateau followed by a sharp change at the end of the reaction due to insufficient reagent concentration at the electrode surface. It signifies the transition towards a new electro-chemical reaction as the electrolyte decomposition. In a limited capacity discharge case, a recharge at the same capacity should reach full consumption of the storage material and present the potential shift, except in the case of a complete absence of side reaction. The absence of potential shift indicates then the presence of side reactions. In a similar fashion, a side reaction at a potential close to the main reaction could appears as the main reaction overpotential as for LiCO$_3$ oxidation during Li–O$_2$ batterie charge[10,58]. In the extreme case of the black curve in fig. 1.22, the capacity is at least partly due to side reactivity, as indicated by the absence of peaks in the derivative scale. The faradic yield alone is not a good marker of reversibility.
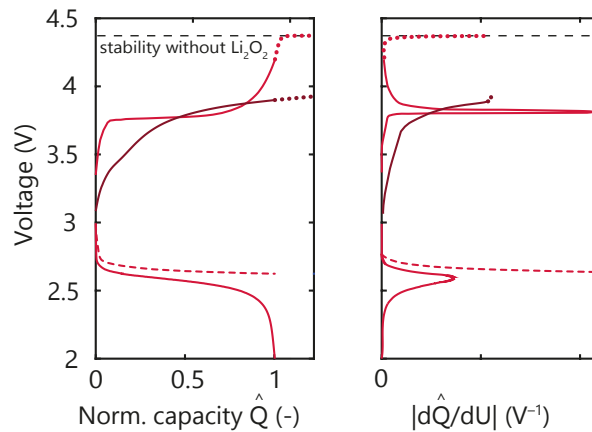
Figure 1.22: **Typical cycling curve of Li-O$_2$ cells, adapted from book chapter.** The dark curves represent charge with high amount of side reactions. The full curves shows cycling with voltage cut-off where the dashed curves shows capacitiy limited discharge.

The needs for more qualitative measurement gave rise to analytic protocols for the consumption/release of O$_2$ and the discharge/side products characterization that will be reviewed more in detailled in part 2.2.4.

It is important to consider metal-air batteries to be in its infancy. Most studies concerns indeed metal-O$_2$ chemistry and not metal-air. With the use of air, species as CO$_2$ or H$_2$O, highly reactive with both the anode and the cathode would increase the number of side reactions[36,145] and part. **??**. Due to the lack of technological insight on the metal-air, the rest of the thesis will only focus on metal-O$_2$ side reactivity as the first step to practical applications.

1.3.2   Reduced oxygen species as the side reactivity source

Finding culprits for the crippling parasitic reactions of metal-O2 cells have always been of major importance to unleash its potential. Reduced oxygen species, formed during the reaction, are easily desirable due to their nucleophilicity, basicity and radical nature; Such species as O$_2^-$, O$_2^{2-}$, HOO·, HOO$^-$, and HO· are prone to react with numerous organic molecules and are a possible source of parasitic chemistry[146,147]. Known reaction routes are for examples nucleophilic substitutions, H+, H-atom abstraction or oxidation. High polarity solvents are desirable to increase salt solubility; In view of their aprotic nature, solvents usually comprise electronegative moieties increasing susceptibility to nucleophilic substitution[147]. Common aprotic batteries electrolyte as carbonates are not stable with reduced oxygen species[119,148]. Alternatives solvents, as glyme, show increased stability[114,143].

Table 1.1: **Generic electrolyte side reactions with reduced oxygen species and molecular oxygen, adapted from[140].** The activation energy for the reaction are calculated by DFT. For O_2^- H^+ abastraction, example of pKa < 30: Fluorinated esters, $-(CH_2-CF_2)_n-$, aliphatic dinitriles, alkyl imides. Example of pKa > 30: acetonitrile, DMSO, N-alkyl amides and lactams, aliphatic ethers.

Reactant	Type of reaction	Reaction	E^{act} (kJ·mol^{-1})
O_2^-	nucleophilic substitution	$ROR' + O_2^- \longrightarrow RO^- + R'OO\cdot$	132[117] – 152[149] (DME) 121-193 with LiO_2[150] (DME derivative) 65[117] – 68[150] (PC) 96 with LiO_2 (PC) 105[117] (MeCN)
	H-atom abstraction	$RH + O_2^- \longrightarrow RO\cdot + HOO^-$	129[151] – 147[152] – 152[149] – 180[153] (DME)
	H^+ abstraction	$RH + O_2^- \longrightarrow R^- + HOO\cdot$	As first approx. pKa>30 is stable[154][155] see legend for examples
Li_2O_2	nucleophilic substitution	$ROR' + Li_2O_2 \longrightarrow [RO^-Li^+] + [ROO^-Li^+]$	67[150] (PC) 135 – 192[156] (DME) 112[150] (DME derivative)
	H-atom abstraction	$RH + Li_2O_2 \longrightarrow R\cdot + [Li_2O_2-H\cdot]$	132[156] (DME)
	H^+ abstraction	$RH + Li_2O_2^- \longrightarrow [R^-Li^+] + [HOO^-Li^+]$	116[156]
O_2	H-atom abstraction	$RH + O_2 \longrightarrow R\cdot + HOO\cdot$	163[151]

recheck table for safety

An activation energy higher than 100 kJ·mol^{-1} appears too endothermic to greatly contribute to the parasitic reaction[117]. On the contrary the carbonates, ~~the~~ aliphatic ether ~~solvent~~ as ~~the~~ common metal-air ~~solvent~~ glyme, present reactivity with the superoxide at energy activation above the 100 k·mol^{-1} threshold; This suggests a low occurrence of superoxide-solvents reactions. Li^+ ion addition furthermore stabilises against H-abstraction by O_2^- and O_2 ~~by dint~~ of solvent coordination[117,151,152].

Setting aside superoxide, HOO·, HOO$^-$, and HO· are still good candidate as the source of unwanted reactivity[80,151]. These species arise from proton source such as water or weak acids, with which O_2^- readily react according to eq. 1.13.

$$
\begin{aligned}
O_2^- + HA &\longrightarrow HOO\cdot + A^- \\
HOO\cdot + O_2^- &\longrightarrow HOO^- + O_2 \\
2\,HOO\cdot &\longrightarrow H_2O_2 + O_2 \\
HOO^- + H_2O_2 &\longrightarrow O_2^- + HO\cdot + H_2O \\
A^- + O_2 &\longrightarrow O_2^- + A\cdot \\
A\cdot + O_2 &\longrightarrow AOO\cdot \\
AOO\cdot + O_2^- &\longrightarrow AOO^- + O_2
\end{aligned}
\tag{1.13}
$$
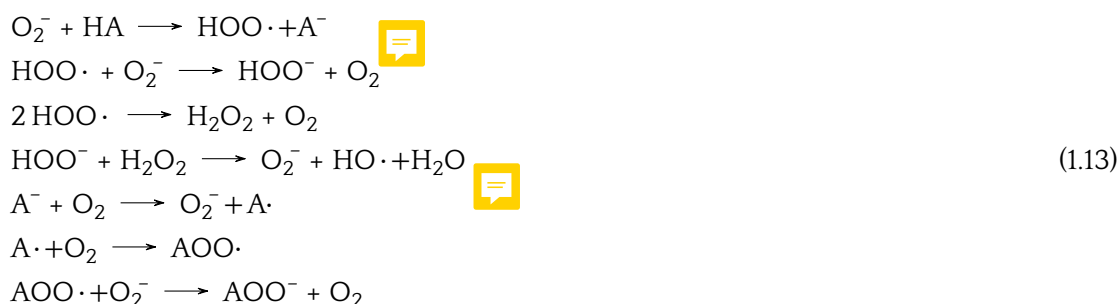
A proton source appears to be intertwined with nucleophilic attacks of the solvent; The parasitic chemistry in Li-O_2 actually increase with the addition of water[36]. The oxygen-pronated reduced species are stronger reactant as the HOO$^-$ base[80]. The stronger base facilitates H-abstraction and the initiator leads to a radical chain reaction and solvent autoxidation. K-O_2 cells can be cycled in DMSO reversibly for over thousands of cycles[22], as illustrated in fig. 1.23. To do so, the anode must be separated from the cathode with ceramic membrane to remove any proton contamination. KO_2 being a source of superoxide, the

electrolyte shows relative stability towards O_2^-; gas chromatography and cyclic voltametry corroborate adapted solvent stabilities after contact with dissolve KO_2 by 18-crown-6 ether during one week[117]. Water contamination can nevertheless not be assigned as solely responsible for side reactions. Side reactions are more proficient during charge than discharge, conflicting with the reduced presence of superoxide, as explained in part. 1.3.1. The major difference between K-O_2 and Na/Li-O_2 chemistry is the stability of alkaline superoxide as it will be discussed in part. **singlet disp**. The LiO_2 or NaO_2 disproportionation influence is of prime importance ~~when considering~~ the presence of singlet oxygen, an excited molecular oxygen species.
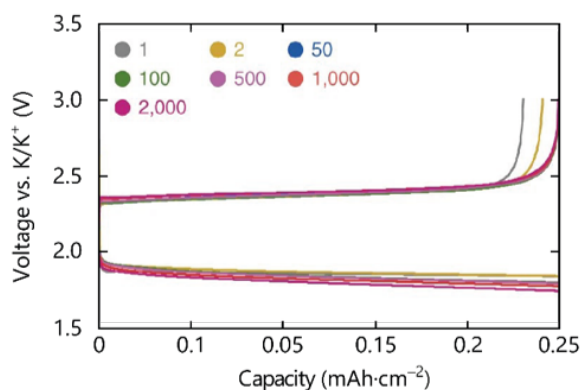
Figure 1.23: **Discharge/charge curves of a KO_2 cell for 2000 cycle at a current density of 2.0 mA·cm^{-2} and limited to 0.25 ma·h·cm^{-2}, adapted from[22]**.

Conclusion

Li–air technology is still in its infancy despite the promises of improve capacity. The new "beyond intercalation chemistries" paradigm ~~impose~~ new mechanistic descriptor to ensure maturation of Li–air cells. The ~~current~~ understanding of Li-air chemistry was ~~exposed through~~ this chapter and while still lacking deep understanding of the process in place, recent insight provided a better awareness of the Li_2O_2 formation/disappearance and associated parasitic chemistry.

~~The major Li–air mechanistic unraveling is the presence of superoxide disproportionation both on discharge and charge~~. This process leads to higher importance of the electrolyte composition which influences directly the discharge products geometry as well as the capacity achieved. Through superoxide solvation, the solution mechanism allows for higher discharge capacities. Li_2O_2 itself is a insulator which conductivity is now known to depend on its formation mechanism and potential applied. The high overpotential encounter during charge is mostly arising from the accumulation of side products from electrodes and electrolyte decomposition. The widely used carbon cathodes are increasingly degraded with the potential applied and results in carbonates formation. New materials are being developed to increase the cathode stability at the cost of weight increase. The anode is similarly problematic with instability towards organic and oxygenated species despite improve compatibility by dint of specially designed SEI. Typical lithium–ion batteries electrolyte are unstable in metal–air chemistry which gave rise to new organic solvent use as glyme presenting higher robustness. Ionic liquids and solid-states electrolyte are concurrently developed but reveals themselves as currently unadapted to the metal–air chemistry.

Although there has been tremendous improvement of the Li–air cell cyclability, parasitic

reactions stay their main hurdle. The achieved capacities per mass of cathode are often compared favourably to intercalation materials. This neglect the "beyond intercalation" nature of the technology and the complete stack characteristic should be taken in consideration before any assessment. They might moreover be the results of limited capacity, potentially covering the parasitic chemistry contribution to the capacity. To determine the real reaction yield and reversibility, specific analytical methods have been developed as pressure monitoring. Without such measurements, it is difficult to statute on improved performance claim due to the very nature of Li–air cells. The side reactions were mainly attributed by the presence of reduced oxygen species present during cell cycling. Superoxide species, yet, can not explain the increase side reaction production formation during charge. By DFT, it was moreover shown that the reduced oxygen species reactivity with adapted electrolyte is unlikely, comforted by the high stability achieved for K–O$_2$ cells. Recently, the very aggressive singlet oxygen was ascribed as a main source of side reactivity in Li–air chemistry.

Bibliography

[1] D. Larcher and J.-M. Tarascon, "Towards greener and more sustainable batteries for electrical energy storage," *Nature chemistry*, vol. 7, no. 1, p. 19, 2015.

[2] M. S. Whittingham, "Ultimate limits to intercalation reactions for lithium batteries," *Chemical reviews*, vol. 114, no. 23, pp. 11 414–11 443, 2014.

[3] A. C. Luntz and B. D. McCloskey, "Nonaqueous li–air batteries: a status report," *Chemical reviews*, vol. 114, no. 23, pp. 11 721–11 750, 2014.

[4] J. W. Choi and D. Aurbach, "Promise and reality of post-lithium-ion batteries with high energy densities," *Nature Reviews Materials*, vol. 1, no. 4, p. 16013, 2016.

[5] S. A. Freunberger, "True performance metrics in beyond-intercalation batteries," *Nature Energy*, vol. 2, p. 17091, 2017.

[6] K. G. Gallagher, S. Goebel, T. Greszler, M. Mathias, W. Oelerich, D. Eroglu, and V. Srinivasan, "Quantifying the promise of lithium–air batteries for electric vehicles," *Energy & Environmental Science*, vol. 7, no. 5, pp. 1555–1563, 2014.

[7] Z. Peng, S. A. Freunberger, L. J. Hardwick, Y. Chen, V. Giordani, F. Bardé, P. Novák, D. Graham, J.-M. Tarascon, and P. G. Bruce, "Oxygen reactions in a non-aqueous Li$^+$ electrolyte," *Angewandte Chemie International Edition*, vol. 50, no. 28, pp. 6351–6355, 2011.

[8] C. O. Laoire, S. Mukerjee, K. Abraham, E. J. Plichta, and M. A. Hendrickson, "Influence of nonaqueous solvents on the electrochemistry of oxygen in the rechargeable lithium-air battery," *The Journal of Physical Chemistry C*, vol. 114, no. 19, pp. 9178–9186, 2010.

[9] ——, "Elucidating the mechanism of oxygen reduction for lithium-air battery applications," *The Journal of Physical Chemistry C*, vol. 113, no. 46, pp. 20 127–20 134, 2009.

[10] B. D. McCloskey, R. Scheffler, A. Speidel, G. Girishkumar, and A. C. Luntz, "On the mechanism of nonaqueous Li–O$_2$ electrochemistry on C and its kinetic overpotentials: some implications for Li–air batteries," *The Journal of Physical Chemistry C*, vol. 116, no. 45, pp. 23 897–23 905, 2012.

[11] Y. Wang, N.-C. Lai, Y.-R. Lu, Y. Zhou, C.-L. Dong, and Y.-C. Lu, "A solvent-controlled oxidation mechanism of Li$_2$O$_2$ in lithium-oxygen batteries," *Joule*, vol. 2, no. 11, pp. 2364–2380, 2018.

[12] L. Johnson, C. Li, Z. Liu, Y. Chen, S. A. Freunberger, P. C. Ashok, B. B. Praveen, K. Dholakia, J.-M. Tarascon, and P. G. Bruce, "The role of LiO$_2$ solubility in O$_2$ reduction in aprotic solvents and its consequences for Li–O$_2$ batteries," *Nature chemistry*, vol. 6, no. 12, p. 1091, 2014.

[13] C. M. Burke, V. Pande, A. Khetan, V. Viswanathan, and B. D. McCloskey, "Enhancing electrochemical intermediate solvation through electrolyte anion selection to increase nonaqueous Li–O$_2$ battery capacity," *Proceedings of the National Academy of Sciences*, vol. 112, no. 30, pp. 9293–9298, 2015.

[14] Y. Zhang, X. Zhang, J. Wang, W. C. McKee, Y. Xu, and Z. Peng, "Potential-dependent generation of O$_2$–and LiO$_2$ and their critical roles in O$_2$ reduction to Li$_2$O$_2$ in aprotic Li–O$_2$ batteries," *The Journal of Physical Chemistry C*, vol. 120, no. 7, pp. 3690–3698, 2016.

[15] Z. Zhao, J. Huang, and Z. Peng, "Achilles' heel of lithium–air batteries: Lithium carbonate," *Angewandte Chemie International Edition*, vol. 57, no. 15, pp. 3874–3886, 2018.

[16] P. G. Bruce, S. A. Freunberger, L. J. Hardwick, and J.-M. Tarascon, "Li–O_2 and Li–S batteries with high energy storage," *Nature materials*, vol. 11, no. 1, p. 19, 2012.

[17] B. Dunn, H. Kamath, and J.-M. Tarascon, "Electrical energy storage for the grid: a battery of choices," *Science*, vol. 334, no. 6058, pp. 928–935, 2011.

[18] M. Obrovac and V. Chevrier, "Alloy negative electrodes for li-ion batteries," *Chemical reviews*, vol. 114, no. 23, pp. 11 444–11 502, 2014.

[19] V. Chevrier and G. Ceder, "Challenges for Na-ion negative electrodes," *Journal of The Electrochemical Society*, vol. 158, no. 9, pp. A1011–A1014, 2011.

[20] Z. Peng, S. A. Freunberger, Y. Chen, and P. G. Bruce, "A reversible and higher-rate Li–O_2 battery," *Science*, vol. 337, no. 6094, pp. 563–566, 2012.

[21] P. Hartmann, C. L. Bender, M. Vraar, A. K. Dürr, A. Garsuch, J. Janek, and P. Adelhelm, "A rechargeable room-temperature sodium superoxide (NaO_2) battery," *Nature materials*, vol. 12, no. 3, p. 228, 2013.

[22] G. Cong, W. Wang, N.-C. Lai, Z. Liang, and Y.-C. Lu, "A high-rate and long-life organic–oxygen battery," *Nature materials*, vol. 18, no. 4, p. 390, 2019.

[23] S. Evers and L. F. Nazar, "New approaches for high energy density lithium–sulfur battery cathodes," *Accounts of chemical research*, vol. 46, no. 5, pp. 1135–1143, 2012.

[24] D. Bresser, S. Passerini, and B. Scrosati, "Recent progress and remaining challenges in sulfur-based lithium secondary batteries – a review," *Chemical communications*, vol. 49, no. 90, pp. 10 545–10 562, 2013.

[25] B. D. McCloskey, J. M. Garcia, and A. C. Luntz, "Chemical and electrochemical differences in nonaqueous Li–O_2 and Na–O_2 batteries," *The journal of physical chemistry letters*, vol. 5, no. 7, pp. 1230–1235, 2014.

[26] Y. K. Petit and S. A. Freunberger, "Thousands of cycles," *Nature materials*, vol. 18, no. 4, p. 301, 2019.

[27] C. L. Bender, P. Hartmann, M. Vraar, P. Adelhelm, and J. Janek, "On the thermodynamics, the role of the carbon cathode, and the cycle life of the sodium superoxide (NaO_2) battery," *Advanced Energy Materials*, vol. 4, no. 12, p. 1301863, 2014.

[28] C. L. Bender, D. Schröder, R. Pinedo, P. Adelhelm, and J. Janek, "One-or two-electron transfer? The ambiguous nature of the discharge products in sodium–oxygen batteries," *Angewandte Chemie International Edition*, vol. 55, no. 15, pp. 4640–4649, 2016.

[29] X. Ren and Y. Wu, "A low-overpotential potassium–oxygen battery based on potassium superoxide," *Journal of the American Chemical Society*, vol. 135, no. 8, pp. 2923–2926, 2013.

[30] E. Mourad, Y. K. Petit, R. Spezia, A. Samojlov, F. F. Summa, C. Prehal, C. Leypold, N. Mahne, C. Slugovc, O. Fontaine *et al.*, "Singlet oxygen from cation driven superoxide disproportionation and consequences for aprotic metal–o 2 batteries," *Energy & Environmental Science*, vol. 12, no. 8, pp. 2559–2568, 2019.

[31] R. Cao, E. D. Walter, W. Xu, E. N. Nasybulin, P. Bhattacharya, M. E. Bowden, M. H. Engelhard, and J.-G. Zhang, "The mechanisms of oxygen reduction and evolution reactions in nonaqueous lithium–oxygen batteries," *ChemSusChem*, vol. 7, no. 9, pp. 2436–2440, 2014.

[32] D. Aurbach, M. Daroux, P. Faguy, and E. Yeager, "The electrochemistry of noble metal electrodes in aprotic organic solvents containing lithium salts," *Journal of electroanalytical chemistry and interfacial electrochemistry*, vol. 297, no. 1, pp. 225–244, 1991.

[33] D. G. Kwabi, V. S. Bryantsev, T. P. Batcho, D. M. Itkis, C. V. Thompson, and Y. Shao-Horn, "Experimental and computational analysis of the solvent-dependent O_2/Li^+-O_2^- redox couple: standard potentials, coupling ctrength, and implications for lithium–oxygen batteries," *Angewandte Chemie International Edition*, vol. 55, no. 9, pp. 3129–3134, 2016.

[34] V. Gutmann, "Solvent effects on the reactivities of organometallic compounds," *Coordination Chemistry Reviews*, vol. 18, no. 2, pp. 225–255, 1976.

[35] C. Bondue, P. Bawol, A. Abd-El-Latif, P. Reinsberg, and H. Baltruschat, "Gaining control over the mechanism of oxygen reduction in organic electrolytes: the effect of solvent properties," *The Journal of Physical Chemistry C*, vol. 121, no. 16, pp. 8864–8872, 2017.

[36] N. B. Aetukuri, B. D. McCloskey, J. M. García, L. E. Krupp, V. Viswanathan, and A. C. Luntz, "Solvating additives drive solution-mediated electrochemistry and enhance toroid growth in non-aqueous Li–O_2 batteries," *Nature chemistry*, vol. 7, no. 1, p. 50, 2015.

[37] D. Sharon, D. Hirsberg, M. Salama, M. Afri, A. A. Frimer, M. Noked, W. Kwak, Y.-K. Sun, and D. Aurbach, "Mechanistic role of Li^+ dissociation level in aprotic Li–O_2 battery," *ACS applied materials & interfaces*, vol. 8, no. 8, pp. 5300–5307, 2016.

[38] I. Gunasekara, S. Mukerjee, E. J. Plichta, M. A. Hendrickson, and K. Abraham, "A study of the influence of lithium salt anions on oxygen reduction reactions in Li-air batteries," *Journal of The Electrochemical Society*, vol. 162, no. 6, pp. A1055–A1066, 2015.

[39] D. Sharon, D. Hirsberg, M. Afri, F. Chesneau, R. Lavi, A. A. Frimer, Y.-K. Sun, and D. Aurbach, "Catalytic behavior of lithium nitrate in Li–O_2 cells," *ACS applied materials & interfaces*, vol. 7, no. 30, pp. 16 590–16 600, 2015.

[40] K. U. Schwenke, M. Metzger, T. Restle, M. Piana, and H. A. Gasteiger, "The influence of water and protons on Li_2O_2 crystal growth in aprotic Li-O_2 cells," *Journal of The Electrochemical Society*, vol. 162, no. 4, pp. A573–A584, 2015.

[41] D. G. Kwabi, T. P. Batcho, S. Feng, L. Giordano, C. V. Thompson, and Y. Shao-Horn, "The effect of water on discharge product growth and chemistry in Li–O_2 batteries," *Physical Chemistry Chemical Physics*, vol. 18, no. 36, pp. 24 944–24 953, 2016.

[42] C. Li, O. Fontaine, S. A. Freunberger, L. Johnson, S. Grugeon, S. Laruelle, P. G. Bruce, and M. Armand, "Aprotic Li–O_2 battery: influence of complexing agents on oxygen reduction in an aprotic solvent," *The Journal of Physical Chemistry C*, vol. 118, no. 7, pp. 3393–3401, 2014.

[43] X. Gao, Z. P. Jovanov, Y. Chen, L. R. Johnson, and P. G. Bruce, "Phenol-catalyzed discharge in the aprotic lithium-oxygen battery," *Angewandte Chemie*, vol. 129, no. 23, pp. 6639–6643, 2017.

[44] A. Khetan, A. Luntz, and V. Viswanathan, "Trade-offs in capacity and rechargeability in nonaqueous Li–O_2 batteries: solution-driven growth versus nucleophilic stability," *The journal of physical chemistry letters*, vol. 6, no. 7, pp. 1254–1259, 2015.

[45] S. Kang, Y. Mo, S. P. Ong, and G. Ceder, "A facile mechanism for recharging Li2O2 in Li–O$_2$ batteries," *Chemistry of Materials*, vol. 25, no. 16, pp. 3328–3336, 2013.

[46] B. D. Adams, C. Radtke, R. Black, M. L. Trudeau, K. Zaghib, and L. F. Nazar, "Current density dependence of peroxide formation in the Li–O$_2$ battery and its effect on charge," *Energy & Environmental Science*, vol. 6, no. 6, pp. 1772–1778, 2013.

[47] D. G. Kwabi, M. Tuodziecki, N. Pour, D. M. Itkis, C. V. Thompson, and Y. Shao-Horn, "Controlling solution-mediated reaction mechanisms of oxygen reduction using potential and solvent for aprotic lithium–oxygen batteries," *The journal of physical chemistry letters*, vol. 7, no. 7, pp. 1204–1212, 2016.

[48] J. Huang and B. Tong, "Probing the reaction interface in Li–O$_2$ batteries using electrochemical impedance spectroscopy: dual roles of Li$_2$O$_2$," *Chemical Communications*, vol. 53, no. 83, pp. 11 418–11 421, 2017.

[49] J. Huang, B. Tong, Z. Li, T. Zhou, J. Zhang, and Z. Peng, "Probing the reaction interface in li–oxygen batteries using dynamic electrochemical impedance spectroscopy: Discharge–charge asymmetry in reaction sites and electronic conductivity," *The journal of physical chemistry letters*, vol. 9, no. 12, pp. 3403–3408, 2018.

[50] A. Kushima, T. Koido, Y. Fujiwara, N. Kuriyama, N. Kusumi, and J. Li, "Charging/discharging nanomorphology asymmetry and rate-dependent capacity degradation in Li–oxygen battery," *Nano letters*, vol. 15, no. 12, pp. 8260–8265, 2015.

[51] V. Viswanathan, K. S. Thygesen, J. Hummelshøj, J. K. Nørskov, G. Girishkumar, B. McCloskey, and A. Luntz, "Electrical conductivity in Li$_2$O$_2$ and its role in determining capacity limitations in non-aqueous Li-O$_2$ batteries," *The Journal of chemical physics*, vol. 135, no. 21, p. 214704, 2011.

[52] K. B. Knudsen, T. Vegge, B. D. McCloskey, and J. Hjelm, "An electrochemical impedance spectroscopy study on the effects of the surface-and solution-based mechanisms in Li–O$_2$ cells," *Journal of The Electrochemical Society*, vol. 163, no. 9, pp. A2065–A2071, 2016.

[53] J. Yang, D. Zhai, H.-H. Wang, K. C. Lau, J. A. Schlueter, P. Du, D. J. Myers, Y.-K. Sun, L. A. Curtiss, and K. Amine, "Evidence for lithium superoxide-like species in the discharge product of a Li–O$_2$ battery," *Physical Chemistry Chemical Physics*, vol. 15, no. 11, pp. 3764–3771, 2013.

[54] Z. Li, S. Ganapathy, Y. Xu, J. R. Heringa, Q. Zhu, W. Chen, and M. Wagemaker, "Understanding the electrochemical formation and decomposition of Li$_2$O$_2$ and LiOH with operando X-ray diffraction," *Chemistry of Materials*, vol. 29, no. 4, pp. 1577–1586, 2017.

[55] V. Viswanathan, J. Nørskov, A. Speidel, R. Scheffler, S. Gowda, and A. Luntz, "Li–O$_2$ kinetic overpotentials: Tafel plots from experiment and first-principles theory," *The journal of physical chemistry letters*, vol. 4, no. 4, pp. 556–560, 2013.

[56] Y. Chen, S. A. Freunberger, Z. Peng, F. Bardé, and P. G. Bruce, "Li–O$_2$ battery with a dimethylformamide electrolyte," *Journal of the American Chemical Society*, vol. 134, no. 18, pp. 7952–7957, 2012.

[57] R. Black, J.-H. Lee, B. Adams, C. A. Mims, and L. F. Nazar, "The role of catalysts and peroxide oxidation in lithium–oxygen batteries," *Angewandte Chemie International Edition*, vol. 52, no. 1, pp. 392–396, 2013.

[58] M. M. Ottakam Thotiyl, S. A. Freunberger, Z. Peng, and P. G. Bruce, "The carbon electrode in nonaqueous Li–O$_2$ cells," *Journal of the American Chemical Society*, vol. 135, no. 1, pp. 494–500, 2012.

[59] M. D. Radin and D. J. Siegel, "Charge transport in lithium peroxide: relevance for rechargeable metal–air batteries," *Energy & Environmental Science*, vol. 6, no. 8, pp. 2370–2379, 2013.

[60] S. Ganapathy, B. D. Adams, G. Stenou, M. S. Anastasaki, K. Goubitz, X.-F. Miao, L. F. Nazar, and M. Wagemaker, "Nature of Li$_2$O$_2$ oxidation in a Li–O$_2$ battery revealed by operando X-ray diffraction," *Journal of the American Chemical Society*, vol. 136, no. 46, pp. 16 335–16 344, 2014.

[61] Y.-C. Lu and Y. Shao-Horn, "Probing the reaction kinetics of the charge reactions of nonaqueous Li–O$_2$ batteries," *The journal of physical chemistry letters*, vol. 4, no. 1, pp. 93–99, 2012.

[62] L. Luo, B. Liu, S. Song, W. Xu, J.-G. Zhang, and C. Wang, "Revealing the reaction mechanisms of Li–O$_2$ batteries using environmental transmission electron microscopy," *Nature nanotechnology*, vol. 12, no. 6, p. 535, 2017.

[63] Y. Mo, S. P. Ong, and G. Ceder, "First-principles study of the oxygen evolution reaction of lithium peroxide in the lithium-air battery," *Physical Review B*, vol. 84, no. 20, p. 205446, 2011.

[64] J. Hummelshøj, A. Luntz, and J. Nørskov, "Theoretical evidence for low kinetic overpotentials in Li-O$_2$ electrochemistry," *The Journal of chemical physics*, vol. 138, no. 3, p. 034703, 2013.

[65] D. Zhai, H.-H. Wang, J. Yang, K. C. Lau, K. Li, K. Amine, and L. A. Curtiss, "Disproportionation in Li–O$_2$ batteries based on a large surface area carbon cathode," *Journal of the American Chemical Society*, vol. 135, no. 41, pp. 15 364–15 372, 2013.

[66] Y. Zhang, Q. Cui, X. Zhang, W. C. McKee, Y. Xu, S. Ling, H. Li, G. Zhong, Y. Yang, and Z. Peng, "Amorphous Li$_2$O$_2$: chemical synthesis and electrochemical properties," *Angewandte Chemie International Edition*, vol. 55, no. 36, pp. 10 717–10 721, 2016.

[67] F. Tian, M. D. Radin, and D. J. Siegel, "Enhanced charge transport in amorphous Li$_2$O$_2$," *Chemistry of Materials*, vol. 26, no. 9, pp. 2952–2959, 2014.

[68] A. Dunst, V. Epp, I. Hanzu, S. Freunberger, and M. Wilkening, "Short-range Li diffusion vs. long-range ionic conduction in nanocrystalline lithium peroxide Li$_2$O$_2$ — the discharge product in lithium-air batteries," *Energy & environmental science*, vol. 7, no. 8, pp. 2739–2752, 2014.

[69] O. Gerbig, R. Merkle, and J. Maier, "Electron and ion transport in Li$_2$O$_2$," *Advanced materials*, vol. 25, no. 22, pp. 3129–3133, 2013.

[70] Y. Wang and Y.-C. Lu, "Isotopic labeling reveals active reaction interfaces for electrochemical oxidation of lithium peroxide," *Angewandte Chemie*, vol. 131, no. 21, pp. 7036–7040, 2019.

[71] J. Wang, Y. Zhang, L. Guo, E. Wang, and Z. Peng, "Identifying reactive sites and transport limitations of oxygen reactions in aprotic lithium-O$_2$ batteries at the stage of sudden death," *Angewandte Chemie International Edition*, vol. 55, no. 17, pp. 5201–5205, 2016.

[72] H. Zheng, D. Xiao, X. Li, Y. Liu, Y. Wu, J. Wang, K. Jiang, C. Chen, L. Gu, X. Wei *et al.*, "New insight in understanding oxygen reduction and evolution in solid–state lithium–oxygen batteries using an in situ environmental scanning electron microscope," *Nano letters*, vol. 14, no. 8, pp. 4245–4249, 2014.

[73] Y. Wang, Z. Liang, Q. Zou, G. Cong, and Y.-C. Lu, "Mechanistic insights into catalyst-assisted nonaqueous oxygen evolution reaction in lithium–oxygen batteries," *The Journal of Physical Chemistry C*, vol. 120, no. 12, pp. 6459–6466, 2016.

[74] Q. Peng, J. Chen, H. Ji, A. Morita, and S. Ye, "Origin of the overpotential for the oxygen evolution reaction on a well-defined graphene electrode probed by in situ sum frequency generation vibrational spectroscopy," *Journal of the American Chemical Society*, vol. 140, no. 46, pp. 15 568–15 571, 2018.

[75] B. McCloskey, A. Speidel, R. Scheffler, D. Miller, V. Viswanathan, J. Hummelshøj, J. Nørskov, and A. Luntz, "Twin problems of interfacial carbonate formation in non-aqueous li–o2 batteries," *The journal of physical chemistry letters*, vol. 3, no. 8, pp. 997–1001, 2012.

[76] J. Højberg, B. D. McCloskey, J. Hjelm, T. Vegge, K. Johansen, P. Norby, and A. C. Luntz, "An electrochemical impedance spectroscopy investigation of the overpotentials in li–o2 batteries," *ACS applied materials & interfaces*, vol. 7, no. 7, pp. 4039–4047, 2015.

[77] B. D. McCloskey, A. Valery, A. C. Luntz, S. R. Gowda, G. M. Wallraff, J. M. Garcia, T. Mori, and L. E. Krupp, "Combining accurate O_2 and Li_2O_2 assays to separate discharge and charge stability limitations in nonaqueous $Li–O_2$ batteries," *The journal of physical chemistry letters*, vol. 4, no. 17, pp. 2989–2993, 2013.

[78] D. M. Itkis, D. A. Semenenko, E. Y. Kataev, A. I. Belova, V. S. Neudachina, A. P. Sirotina, M. Hävecker, D. Teschner, A. Knop-Gericke, P. Dudin *et al.*, "Reactivity of carbon in lithium–oxygen battery positive electrodes," *Nano letters*, vol. 13, no. 10, pp. 4697–4701, 2013.

[79] J. K. Papp, J. D. Forster, C. M. Burke, H. W. Kim, A. C. Luntz, R. M. Shelby, J. J. Urban, and B. D. McCloskey, "Poly(vinylidene fluoride)(PVDF) binder degradation in $Li–O_2$ batteries: a consideration for the characterization of lithium superoxide," *The journal of physical chemistry letters*, vol. 8, no. 6, pp. 1169–1174, 2017.

[80] V. S. Bryantsev, "Predicting the stability of aprotic solvents in Li-air batteries: pKa calculations of aliphatic C–H acids in dimethyl sulfoxide," *Chemical Physics Letters*, vol. 558, pp. 42–47, 2013.

[81] C. V. Amanchukwu, J. R. Harding, Y. Shao-Horn, and P. T. Hammond, "Understanding the chemical stability of polymers for lithium–air batteries," *Chemistry of Materials*, vol. 27, no. 2, pp. 550–561, 2015.

[82] E. Nasybulin, W. Xu, M. H. Engelhard, Z. Nie, X. S. Li, and J.-G. Zhang, "Stability of polymer binders in $Li–O_2$ batteries," *Journal of Power Sources*, vol. 243, pp. 899–907, 2013.

[83] D. Kundu, R. Black, E. J. Berg, and L. F. Nazar, "A highly active nanostructured metallic oxide cathode for aprotic $Li–O_2$ batteries," *Energy & Environmental Science*, vol. 8, no. 4, pp. 1292–1298, 2015.

[84] M. M. Ottakam Thotiyl, S. A. Freunberger, Z. Peng, Y. Chen, Z. Liu, and P. G. Bruce, "A stable cathode for the aprotic $Li–O_2$ battery," *Nature materials*, vol. 12, no. 11, p. 1050, 2013.

[85] A. Y. Kozmenkova, E. Y. Kataev, A. I. Belova, M. Amati, L. Gregoratti, J. Velasco-Vélez, A. Knop-Gericke, B. Senkovsky, D. V. Vyalikh, D. M. Itkis *et al.*, "Tuning surface chemistry of TiC electrodes for lithium–air batteries," *Chemistry of Materials*, vol. 28, no. 22, pp. 8248–8255, 2016.

[86] Y. Bae, D.-H. Ko, S. Lee, H.-D. Lim, Y.-J. Kim, H.-S. Shim, H. Park, Y. Ko, S. K. Park, H. J. Kwon *et al.*, "Enhanced stability of coated carbon electrode for Li-O_2 batteries and its limitations," *Advanced Energy Materials*, vol. 8, no. 16, p. 1702661, 2018.

[87] M. Marinaro, U. Riek, S. E. Moorthy, J. Bernhard, U. Kaiser, M. Wohlfahrt-Mehrens, and L. Jörissen, "Au-coated carbon cathodes for improved oxygen reduction and evolution kinetics in aprotic Li–O_2 batteries," *Electrochemistry Communications*, vol. 37, pp. 53–56, 2013.

[88] N. Ding, S. W. Chien, T. A. Hor, R. Lum, Y. Zong, and Z. Liu, "Influence of carbon pore size on the discharge capacity of Li–O_2 batteries," *Journal of Materials Chemistry A*, vol. 2, no. 31, pp. 12 433–12 441, 2014.

[89] J. Zeng, J. Amici, A. H. M. Videla, C. Francia, and S. Bodoardo, "Synthesis of mesoporous carbons and reduced graphene oxide and their influence on the cycling performance of rechargeable Li-O_2 batteries," *Journal of Solid State Electrochemistry*, vol. 21, no. 2, pp. 503–514, 2017.

[90] S. B. Ma, D. J. Lee, V. Roev, D. Im, and S.-G. Doo, "Effect of porosity on electrochemical properties of carbon materials as cathode for lithium-oxygen battery," *Journal of Power Sources*, vol. 244, pp. 494–498, 2013.

[91] B. Sun, X. Huang, S. Chen, P. Munroe, and G. Wang, "Porous graphene nanoarchitectures: an efficient catalyst for low charge-overpotential, long life, and high capacity lithium–oxygen batteries," *Nano letters*, vol. 14, no. 6, pp. 3145–3152, 2014.

[92] A. Kraytsberg and Y. Ein-Eli, "The impact of nano-scaled materials on advanced metal–air battery systems," *Nano Energy*, vol. 2, no. 4, pp. 468–480, 2013.

[93] A. Torayev, P. C. M. M. Magusin, C. P. Grey, C. Merlet, and A. A. Franco, "Importance of incorporating explicit 3D-resolved electrode mesostructures in Li–O_2 battery models," *ACS Applied Energy Materials*, vol. 1, no. 11, pp. 6433–6441, 2018.

[94] H.-D. Lim, H. Song, J. Kim, H. Gwon, Y. Bae, K.-Y. Park, J. Hong, H. Kim, T. Kim, Y. H. Kim *et al.*, "Superior rechargeability and efficiency of lithium–oxygen batteries: hierarchical air electrode architecture combined with a soluble catalyst," *Angewandte Chemie International Edition*, vol. 53, no. 15, pp. 3926–3931, 2014.

[95] J. Liu, Z. Bao, Y. Cui, E. J. Dufek, J. B. Goodenough, P. Khalifah, Q. Li, B. Y. Liaw, P. Liu, A. Manthiram *et al.*, "Pathways for practical high-energy long-cycling lithium metal batteries," *Nature Energy*, p. 1, 2019.

[96] M. D. Tikekar, S. Choudhury, Z. Tu, and L. A. Archer, "Design principles for electrolytes and interfaces for stable lithium-metal batteries," *Nature Energy*, vol. 1, no. 9, p. 16114, 2016.

[97] D. Aurbach, M. Daroux, P. Faguy, and E. Yeager, "Identification of surface films formed on lithium in propylene carbonate solutions," *Journal of The Electrochemical Society*, vol. 134, no. 7, pp. 1611–1620, 1987.

[98] D. Aurbach, "Review of selected electrode–solution interactions which determine the performance of Li and Li ion batteries," *Journal of Power Sources*, vol. 89, no. 2, pp. 206–218, 2000.

[99] J. Qian, W. Xu, P. Bhattacharya, M. Engelhard, W. A. Henderson, Y. Zhang, and J.-G. Zhang, "Dendrite-free Li deposition using trace-amounts of water as an electrolyte additive," *Nano Energy*, vol. 15, pp. 135–144, 2015.

[100] G. Bieker, M. Winter, and P. Bieker, "Electrochemical in situ investigations of SEI and dendrite formation on the lithium metal anode," *Physical Chemistry Chemical Physics*, vol. 17, no. 14, pp. 8670–8679, 2015.

[101] A. Aryanfar, D. Brooks, B. V. Merinov, W. A. Goddard III, A. J. Colussi, and M. R. Hoffmann, "Dynamics of lithium dendrite growth and inhibition: Pulse charging experiments and Monte Carlo calculations," *The journal of physical chemistry letters*, vol. 5, no. 10, pp. 1721–1726, 2014.

[102] J.-i. Yamaki, S.-i. Tobishima, K. Hayashi, K. Saito, Y. Nemoto, and M. Arakawa, "A consideration of the morphology of electrochemically deposited lithium in an organic electrolyte," *Journal of Power Sources*, vol. 74, no. 2, pp. 219–227, 1998.

[103] F. Orsini, A. Du Pasquier, B. Beaudoin, J. M. Tarascon, M. Trentin, N. Langenhuizen, E. De Beer, and P. Notten, "In situ scanning electron microscopy (SEM) observation of interfaces within plastic lithium batteries," *Journal of power sources*, vol. 76, no. 1, pp. 19–29, 1998.

[104] B. G. Kim, J.-S. Kim, J. Min, Y.-H. Lee, J. H. Choi, M. C. Jang, S. A. Freunberger, and J. W. Choi, "A moisture- and oxygen- impermeable separator for aprotic Li-O_2 batteries," *Advanced functional materials*, vol. 26, no. 11, pp. 1747–1756, 2016.

[105] X.-B. Cheng, R. Zhang, C.-Z. Zhao, F. Wei, J.-G. Zhang, and Q. Zhang, "A review of solid electrolyte interphases on lithium metal anode," *Advanced Science*, vol. 3, no. 3, p. 1500213, 2016.

[106] V. Giordani, W. Walker, V. S. Bryantsev, J. Uddin, G. V. Chase, and D. Addison, "Synergistic effect of oxygen and $LiNO_3$ on the interfacial stability of lithium metal in a Li/O_2 battery," *Journal of The Electrochemical Society*, vol. 160, no. 9, pp. A1544–A1550, 2013.

[107] G. G. Eshetu, X. Judez, C. Li, O. Bondarchuk, L. M. Rodriguez-Martinez, H. Zhang, and M. Armand, "Lithium azide as an electrolyte additive for all-solid-state lithium–sulfur batteries," *Angewandte Chemie International Edition*, vol. 56, no. 48, pp. 15 368–15 372, 2017.

[108] W. Walker, V. Giordani, J. Uddin, V. S. Bryantsev, G. V. Chase, and D. Addison, "A rechargeable Li–O_2 battery using a lithium nitrate/N, N-dimethylacetamide electrolyte," *Journal of the American Chemical Society*, vol. 135, no. 6, pp. 2076–2079, 2013.

[109] J. Uddin, V. S. Bryantsev, V. Giordani, W. Walker, G. V. Chase, and D. Addison, "Lithium nitrate as regenerable SEI stabilizing agent for rechargeable Li/O_2 batteries," *The Journal of Physical Chemistry Letters*, vol. 4, no. 21, pp. 3760–3765, 2013.

[110] C. Schweitzer and R. Schmidt, "Physical mechanisms of generation and deactivation of singlet oxygen," *Chemical reviews*, vol. 103, no. 5, pp. 1685–1758, 2003.

[111] F. Ding, W. Xu, X. Chen, J. Zhang, Y. Shao, M. H. Engelhard, Y. Zhang, T. A. Blake, G. L. Graff, X. Liu *et al.*, "Effects of cesium cations in lithium deposition via self-healing

electrostatic shield mechanism," *The Journal of Physical Chemistry C*, vol. 118, no. 8, pp. 4043–4049, 2014.

[112] N. D. Trinh, D. Lepage, D. Aymé-Perrot, A. Badia, M. Dollé, and D. Rochefort, "An artificial lithium protective layer that enables the use of acetonitrile-based electrolytes in lithium metal batteries," *Angewandte Chemie International Edition*, vol. 57, no. 18, pp. 5072–5075, 2018.

[113] J.-l. Ma, F.-l. Meng, Y. Yu, D.-p. Liu, J.-m. Yan, Y. Zhang, X.-b. Zhang, and Q. Jiang, "Prevention of dendrite growth and volume expansion to give high-performance aprotic bimetallic Li-Na alloy–O_2 batteries," *Nature chemistry*, vol. 11, no. 1, p. 64, 2019.

[114] S. A. Freunberger, Y. Chen, N. E. Drewett, L. J. Hardwick, F. Bardé, and P. G. Bruce, "The lithium–oxygen battery with ether-based electrolytes," *Angewandte Chemie International Edition*, vol. 50, no. 37, pp. 8609–8613, 2011.

[115] K. R. Ryan, L. Trahey, B. J. Ingram, and A. K. Burrell, "Limited stability of ether-based solvents in lithium–oxygen batteries," *The Journal of Physical Chemistry C*, vol. 116, no. 37, pp. 19 724–19 728, 2012.

[116] F. Barde, Y. Chen, L. Johnson, S. Schaltin, J. Fransaer, and P. G. Bruce, "Sulfone-Based Electrolytes for Nonaqueous Li–O_2 Batteries," *The Journal of Physical Chemistry C*, vol. 118, no. 33, pp. 18 892–18 898, 2014.

[117] V. S. Bryantsev, V. Giordani, W. Walker, M. Blanco, S. Zecevic, K. Sasaki, J. Uddin, D. Addison, and G. V. Chase, "Predicting solvent stability in aprotic electrolyte Li–air batteries: nucleophilic substitution by the superoxide anion radical (O_2^-)," *The Journal of Physical Chemistry A*, vol. 115, no. 44, pp. 12 399–12 409, 2011.

[118] V. S. Bryantsev, J. Uddin, V. Giordani, W. Walker, D. Addison, and G. V. Chase, "The identification of stable solvents for nonaqueous rechargeable li-air batteries," *Journal of The Electrochemical Society*, vol. 160, no. 1, pp. A160–A171, 2013.

[119] S. A. Freunberger, Y. Chen, Z. Peng, J. M. Griffin, L. J. Hardwick, F. Bardé, P. Novák, and P. G. Bruce, "Reactions in the rechargeable lithium–O_2 battery with alkyl carbonate electrolytes," *Journal of the American Chemical Society*, vol. 133, no. 20, pp. 8040–8047, 2011.

[120] B. D. McCloskey, D. Bethune, R. Shelby, T. Mori, R. Scheffler, A. Speidel, M. Sherwood, and A. Luntz, "Limitations in rechargeability of Li-O_2 batteries and possible origins," *The journal of physical chemistry letters*, vol. 3, no. 20, pp. 3043–3047, 2012.

[121] B. D. Adams, R. Black, Z. Williams, R. Fernandes, M. Cuisinier, E. J. Berg, P. Novak, G. K. Murphy, and L. F. Nazar, "Towards a stable organic electrolyte for the lithium oxygen battery," *Advanced Energy Materials*, vol. 5, no. 1, p. 1400867, 2015.

[122] B. Zhou, L. Guo, Y. Zhang, J. Wang, L. Ma, W.-H. Zhang, Z. Fu, and Z. Peng, "A High-Performance Li–O_2 Battery with a Strongly Solvating Hexamethylphosphoramide Electrolyte and a LiPON-Protected Lithium Anode," *Advanced Materials*, vol. 29, no. 30, p. 1701568, 2017.

[123] D. Sharon, P. Sharon, D. Hirshberg, M. Salama, M. Afri, L. J. Shimon, W.-J. Kwak, Y.-K. Sun, A. A. Frimer, and D. Aurbach, "2, 4-Dimethoxy-2, 4-dimethylpentan-3-one: An aprotic solvent designed for stability in Li–O_2 cells," *Journal of the American Chemical Society*, vol. 139, no. 34, pp. 11 690–11 693, 2017.

[124] C. J. Allen, S. Mukerjee, E. J. Plichta, M. A. Hendrickson, and K. Abraham, "Oxygen electrode rechargeability in an ionic liquid for the Li–air battery," *The Journal of Physical Chemistry Letters*, vol. 2, no. 19, pp. 2420–2424, 2011.

[125] C. J. Allen, J. Hwang, R. Kautz, S. Mukerjee, E. J. Plichta, M. A. Hendrickson, and K. Abraham, "Oxygen reduction reactions in ionic liquids and the formulation of a general ORR mechanism for Li–air batteries," *The Journal of Physical Chemistry C*, vol. 116, no. 39, pp. 20755–20764, 2012.

[126] M. C. Buzzeo, O. V. Klymenko, J. D. Wadhawan, C. Hardacre, K. R. Seddon, and R. G. Compton, "Voltammetry of oxygen in the room-temperature ionic liquids 1-ethyl-3-methylimidazolium bis ((trifluoromethyl) sulfonyl) imide and hexyltriethylammonium bis ((trifluoromethyl) sulfonyl) imide: one-electron reduction to form superoxide. steady-state and transient behavior in the same cyclic voltammogram resulting from widely different diffusion coefficients of oxygen and superoxide," *The Journal of Physical Chemistry A*, vol. 107, no. 42, pp. 8872–8878, 2003.

[127] M. Hayyan, F. S. Mjalli, M. A. Hashim, and I. M. AlNashef, "An investigation of the reaction between 1-butyl-3-methylimidazolium trifluoromethanesulfonate and superoxide ion," *Journal of Molecular Liquids*, vol. 181, pp. 44–50, 2013.

[128] S. Das, J. Højberg, K. B. Knudsen, R. Younesi, P. Johansson, P. Norby, and T. Vegge, "Instability of ionic liquid-based electrolytes in Li–O$_2$ batteries," *The Journal of Physical Chemistry C*, vol. 119, no. 32, pp. 18084–18090, 2015.

[129] L. Grande, E. Paillard, G.-T. Kim, S. Monaco, and S. Passerini, "Ionic liquid electrolytes for li–air batteries: lithium metal cycling," *International journal of molecular sciences*, vol. 15, no. 5, pp. 8122–8137, 2014.

[130] G. Elia, J. Hassoun, W.-J. Kwak, Y.-K. Sun, B. Scrosati, F. Mueller, D. Bresser, S. Passerini, P. Oberhumer, N. Tsiouvaras *et al.*, "An advanced lithium–air battery exploiting an ionic liquid-based electrolyte," *Nano letters*, vol. 14, no. 11, pp. 6572–6577, 2014.

[131] Z. P. Rosol, N. J. German, and S. M. Gross, "Solubility, ionic conductivity and viscosity of lithium salts in room temperature ionic liquids," *Green Chemistry*, vol. 11, no. 9, pp. 1453–1457, 2009.

[132] M. Balaish, E. Peled, D. Golodnitsky, and Y. Ein-Eli, "Liquid-free lithium–oxygen batteries," *Angewandte Chemie International Edition*, vol. 54, no. 2, pp. 436–440, 2015.

[133] J. Janek and W. G. Zeier, "A solid future for battery development," *Energy*, vol. 500, no. 400, p. 300, 2016.

[134] N. Bonnet-Mercier, R. A. Wong, M. L. Thomas, A. Dutta, K. Yamanaka, C. Yogi, T. Ohta, and H. R. Byon, "A structured three-dimensional polymer electrolyte with enlarged active reaction zone for Li–O$_2$ batteries," *Scientific reports*, vol. 4, p. 7127, 2014.

[135] S. H. Lee, J.-B. Park, H.-S. Lim, and Y.-K. Sun, "An advanced separator for Li–O$_2$ batteries: maximizing the effect of redox mediators," *Advanced Energy Materials*, vol. 7, no. 18, p. 1602417, 2017.

[136] B. J. Bergner, M. R. Busche, R. Pinedo, B. B. Berkes, D. Schröder, and J. Janek, "How to improve capacity and cycling stability for next generation Li–O$_2$ batteries: approach with a solid electrolyte and elevated redox mediator concentrations," *ACS applied materials & interfaces*, vol. 8, no. 12, pp. 7756–7765, 2016.

[137] T. Liu, Q.-C. Liu, J.-J. Xu, and X.-B. Zhang, "Cable-type water-survivable flexible Li-O_2 battery," *Small*, vol. 12, no. 23, pp. 3101–3105, 2016.

[138] K. Zhang, S. Mu, W. Liu, D. Zhu, Z. Ding, and Y. Chen, "A flexible NASICON-type composite electrolyte for lithium-oxygen/air battery," *Ionics*, vol. 25, no. 1, pp. 25–33, 2019.

[139] N. Nitta, F. Wu, J. T. Lee, and G. Yushin, "Li-ion battery materials: present and future," *Materials today*, vol. 18, no. 5, pp. 252–264, 2015.

[140] N. Mahne, O. Fontaine, M. O. Thotiyl, M. Wilkening, and S. A. Freunberger, "Mechanism and performance of lithium–oxygen batteries–a perspective," *Chemical science*, vol. 8, no. 10, pp. 6716–6729, 2017.

[141] R. Koerver, W. Zhang, L. de Biasi, S. Schweidler, A. O. Kondrakov, S. Kolling, T. Brezesinski, P. Hartmann, W. G. Zeier, and J. Janek, "Chemo-mechanical expansion of lithium electrode materials–on the route to mechanically optimized all-solid-state batteries," *Energy & Environmental Science*, vol. 11, no. 8, pp. 2142–2158, 2018.

[142] J. Betz, G. Bieker, P. Meister, T. Placke, M. Winter, and R. Schmuch, "Theoretical versus practical energy: A plea for more transparency in the energy calculation of different rechargeable battery systems," *Advanced Energy Materials*, vol. 9, no. 6, p. 1803170, 2019.

[143] B. D. McCloskey, D. S. Bethune, R. M. Shelby, G. Girishkumar, and A. C. Luntz, "Solvents' critical role in nonaqueous lithium–oxygen battery electrochemistry," *The Journal of Physical Chemistry Letters*, vol. 2, no. 10, pp. 1161–1166, 2011.

[144] A. C. Luntz and B. D. McCloskey, "Li–air batteries: Importance of singlet oxygen," *Nature Energy*, vol. 2, no. 5, p. 17056, 2017.

[145] S. R. Gowda, A. Brunet, G. Wallraff, and B. D. McCloskey, "Implications of CO_2 contamination in rechargeable nonaqueous Li–O_2 batteries," *The journal of physical chemistry letters*, vol. 4, no. 2, pp. 276–279, 2012.

[146] D. T. Sawyer and J. S. Valentine, "How super is superoxide?" *Accounts of Chemical Research*, vol. 14, no. 12, pp. 393–400, 1981.

[147] D. Aurbach, B. D. McCloskey, L. F. Nazar, and P. G. Bruce, "Advances in understanding mechanisms underpinning lithium–air batteries," *Nature Energy*, vol. 1, no. 9, p. 16128, 2016.

[148] V. S. Bryantsev and M. Blanco, "Computational study of the mechanisms of superoxide-induced decomposition of organic carbonate-based electrolytes," *The Journal of Physical Chemistry Letters*, vol. 2, no. 5, pp. 379–383, 2011.

[149] B. Genorio, J. Staszak-Jirkovský, R. S. Assary, J. G. Connell, D. Strmcnik, C. E. Diesendruck, P. P. Lopes, V. R. Stamenkovic, J. S. Moore, L. A. Curtiss *et al.*, "Superoxide (electro) chemistry on well-defined surfaces in organic environments," *The Journal of Physical Chemistry C*, vol. 120, no. 29, pp. 15 909–15 914, 2016.

[150] Z. Zhang, J. Lu, R. S. Assary, P. Du, H.-H. Wang, Y.-K. Sun, Y. Qin, K. C. Lau, J. Greeley, P. C. Redfern *et al.*, "Increased stability toward oxygen reduction products for lithium-air batteries with oligoether-functionalized silane electrolytes," *The Journal of Physical Chemistry C*, vol. 115, no. 51, pp. 25 535–25 542, 2011.

[151] V. S. Bryantsev and F. Faglioni, "Predicting autoxidation stability of ether-and amide-based electrolyte solvents for Li–air batteries," *The Journal of Physical Chemistry A*, vol. 116, no. 26, pp. 7128–7138, 2012.

[152] B. Liu, W. Xu, P. Yan, X. Sun, M. E. Bowden, J. Read, J. Qian, D. Mei, C.-M. Wang, and J.-G. Zhang, "Enhanced cycling stability of rechargeable Li-O$_2$ batteries using high-concentration electrolytes," *Advanced Functional Materials*, vol. 26, no. 4, pp. 605–613, 2016.

[153] M. Carboni, A. G. Marrani, R. Spezia, and S. Brutti, "1,2-Dimethoxyethane degradation thermodynamics in Li-O$_2$ Redox Environments," *Chemistry–A European Journal*, vol. 22, no. 48, pp. 17 188–17 203, 2016.

[154] A. Khetan, H. Pitsch, and V. Viswanathan, "Solvent degradation in nonaqueous Li-O$_2$ batteries: oxidative stability versus H-abstraction," *The journal of physical chemistry letters*, vol. 5, no. 14, pp. 2419–2424, 2014.

[155] V. S. Bryantsev, "Predicting the stability of aprotic solvents in Li-air batteries: pKa calculations of aliphatic C–H acids in dimethyl sulfoxide," *Chemical Physics Letters*, vol. 558, pp. 42–47, 2013.

[156] R. S. Assary, K. C. Lau, K. Amine, Y.-K. Sun, and L. A. Curtiss, "Interactions of dimethoxy ethane with Li$_2$O$_2$ clusters and likely decomposition mechanisms for Li–O$_2$ batteries," *The Journal of Physical Chemistry C*, vol. 117, no. 16, pp. 8041–8049, 2013.

Singlet oxygen in aqueous batteries, an affliction

Oxigen (sic), as you well know, is my hero as well as my foe.
Christian Friedrich Schonbein

Contents

Figures

Introduction

Metal-air batteries suffer from severe parasitic reactions preventing their long term cycling. Among other consequences, side reactions provoke electrolyte and electrode decomposition resulting in low efficiency, high overpotential and poor rechargeability due to side products accumulation. As described in the previous chapter, superoxide presence does not suffice to explain such degradation in regards to the improved K-O_2 cyclabi... compared to Li-O_2 and Na-O_2 chemistries. Other culprits must emerge to underpin an improved metal-air cells cyclability. Considering the metal-air mechanistic, the most indicate species are excited oxygen. Due to their detection difficulties, their presence in metal-air devices was often overlooked despite their high reactivity. From peroxide chemical oxidation, singlet oxygen, the first oxygen excited state, can be produced[4–6]. Our group main reasoning, presented this chapter, is the production of this aggressive species in metal-air devices and deciphering its possible productions pathways.

Singlet oxygen, as an excited species, possesses a peculiar chemistry compared to its ground state counterpart. Singlet oxygen reactivity lies in its electronic structures. On the contrary of the triplet state, singlet oxygen has two uncoupled electrons in its valence shell giving it a dienophile character. This particularity is made use of in organic chemistry. In metal-air batteries context, singlet oxygen was shown to react with and degrade cells component as the electrolyte or carbonaceous electrode. Parasitic reactions could be thus partly attributed to $^1O_2$ if present in the cells.

To characterize and quantify the suspected $^1O_2$ presence in metal-air batteries, our group developed a number of adapted analytical methods. These analyses allow quantification in-situ or ex-situ of singlet oxygen and side reaction presences by a combination of techniques, i.e., high precision liquid chromatography (HPLC), UV-vis spectrometry, mass spectroscopy (MS) or pressure monitoring. The development of these methods repose on the production of photochemically produced $^1O_2$ at on controlled rate by dint of a photo-sensitizer.
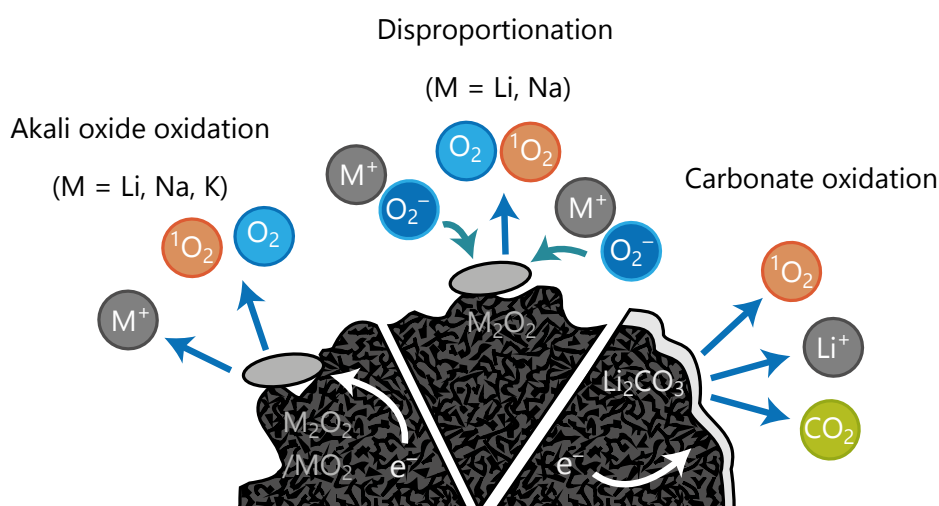
Figure 2.1: **Illustration of the proposed singlet oxygen production pathways in metal–air batteries.**

The singlet oxygen presence will be demonstrated in metal–air as well as Li–based non-organic batteries and its production mechanism described, either via a direct electrochemical or chemical process. The formation of singlet oxygen is directly intertwined with the energy

storage reactions in metal-air batteries. Its formation at high overpotential can ~~process~~ by oxidation of either alkali oxide, at potential sufficient to overcome the $^1O_2$ formation energy barrier, or lithium carbonate, a common by-products of organic based lithium batteries. We show ~~as well the~~ $^1O_2$ formation via alkali superoxide disproportionation thermodynamically favoured for LiO_2 and NaO_2, process partially responsible for NaO_2 decomposition at rest. The singlet oxygen ~~importance~~ to understand the side reactions ~~process~~ in metal-air batteries will be presented in this chapter and the rest of this thesis will try to unfold these mechanisms more in-depth.

2.1 Excited molecular oxygen as a source of side reactivity

2.1.1 Theoretical considerations

Oxygen redox chemistry is so crucial that the word oxidation was forged from this molecule. Oxygen is ever so ominous due to cellular respiration. This reaction, which shaped current animal evolution[7], rely on oxygen reduction in a similar fashion to metal-O_2 cells[8]. These reactions are based on the oxygen chemistry in its ground state. The ground state of molecular dioxygen is a triplet state due to its open electron shell, on the contrary of most molecules who have a closed shell (cf. the octet and eighteen-electron rules)[9], reducing electronic screening of the nucleus according to Hund's rule of maximum multiplicity[10,11]. The ground triplet state is noted as $^3\Sigma_g^-$ in molecular term symbol (3 is the total spin quantum number, Σ the projection of the orbital angular momentum along the internuclear axis and $^-$ the reflection symmetry along an arbitrary plane containing the internuclear axis). The $^3\Sigma_g^-$ state is characterized by two uncoupled electron on the valence shell; These are situated on the 2-π antibonding orbitals in the case of dioxygen ($\pi_{2p_x}^*$ and $\pi_{2p_y}^*$)[10][12], as illustrated in fig. 2.2. The ground state dioxygen is not the only molecular oxygen involve in biological process[13,14]. Dioxygen can exist in excited states; The lowest energy one are singlet states with the change of one electron spin at 94 and 157 kJ·mol^{-1} for $^1\Delta_g$ and $^1\Sigma_g^+$, respectively from the ground state[12,15-17]. As single state, $^1\Delta_g$ and $^1\Sigma_g^+$ present two coupled electron on the valence shell, as indicated in fig. 2.2. The $^1\Delta_g$ has both electrons situated on the same π_{2p}^* orbital where the $^1\Sigma_g^+$ has electrons on the two different π_{2p}^* orbitals[5].
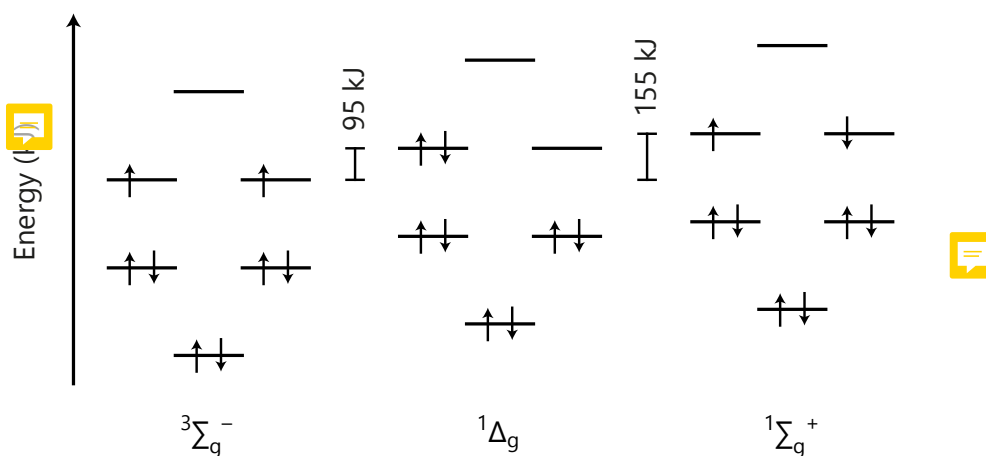
Figure 2.2: **Electronics structures of dioxygen at ground state and its two lower excited state ($^3\Sigma_g^-$, $^1\Delta_g$ and $^1\Sigma_g^+$).**

$^1\Delta_g$ and $^1\Sigma_g^+$ states decay towards the ground state at largely different kinetics[14]. $^1\Sigma_g^+$ quickly decay to the $^1\Delta_g(/^3\Sigma_g^-)$ state(s)[14], with a lifetime of 7 sec in absence of external perturbation, 2.4 μs in dry air and inferior to 1 ns in common solvent[14,16]. The $^1\Delta_g$ transition to the ground state is however spin forbidden[15]. The $^1\Delta_g$ state can be called a metastable species, with a lifetime of 45-72 min in absence of external perturbation, 86 ms in dry air and between approximatelly 10^{-6} up to 10^{-2} seconds in solution depanding on the solvent[14,16,18]. The lifetime of the $^1\Delta_g$ depend strongly on the nature of the solvent and notably the water content and proton moeties[14].

2.1.2 Singlet oxygen reactivity

Due to the lifetime difference of $^1\Delta_g$ and $^1\Sigma_g$, only the $^1\Delta_g$ state will be considered ~~as stable enough to be reactive~~ and simplified as singlet oxygen or $^1O_2$ through the rest of this thesis. Singlet oxygen is highly reactive and its singlet nature allows direct two–electron reaction with singlet organic molecules that would be spin-forbidden for the ground state[19]. The chemistry of singlet oxygen is widely different, being dienophile, than its ground state who behave more as a diradical[4]. Several singlet oxygen reactions are well known and use in organic synthesis as for "ene" reaction, Diels–Alder reaction or addition to activated double bonds[12,20–22]. $^1O_2$ reactions usually involve direct reaction with double bonds. Singlet oxygen is also known to oxidize heteratoms as organosulfur for example[23]. More recently, singlet oxygen was shown to selectively perform hydroperoxidation of ethereal hydrocarbons[24].

~~Glymes, common metal–air battery electrolytes, are not stable in presence of singlet oxygen~~[25]. A typical lithium–air electrolyte, 0.1 M LiClO$_4$ in DME, in presence of singlet oxygen for 30 min did not release any CO_2 ~~from mass spectroscopy measurement.~~ The addition of H_3PO_4 to decompose possibly formed LiCO$_3$, according to Annexe **Annexes of this chapter for Bettina Method**, ~~yielded~~ however a significant CO_2 release as shown in fig. 2.3a. Singlet oxygen is thus able to decompose the electrolyte and produce lithium carbonates. In addition, ^1H-NMR of the electrolyte dissolved in D_2O after $^1O_2$ exposition, presented in fig. 2.3b, ~~exhibit~~ the production of ~~organic~~ lithium ~~carbonates~~ as ~~lithium~~ formate and acetate. Metal–air electrolyte ~~reaction~~ with singlet oxygen produce the ~~most~~ common side products found in theses chemistry, as discussed in part. **??**. Singlet oxygen reactions involve commonly formation of peroxide as discussed in the previous paragraph; It was hypothesised that singlet oxygen generates ROOH, ROO· and R· species that initiate degradation at higher ~~scale~~ as suggested in previous studies[26,27]. ~~On the contrary of~~ triplet oxygen, singlet oxygen is capable to react by Diels–Alder [4+2] cycloaddition with the electrode carbon surface ~~and~~ leads to the formation of quinone moeties at the surface[28]. The ~~addition~~ of quinone at the surface could ~~catalysed~~ to further side reaction[28] and change the hydrophilicity of the carbon surface, reducing further the electrode stability as discussed in **??**. Singlet oxygen can also react with common organic additives in metal–air batteries containing double bonds as redox mediators[29].

(a)   (b)
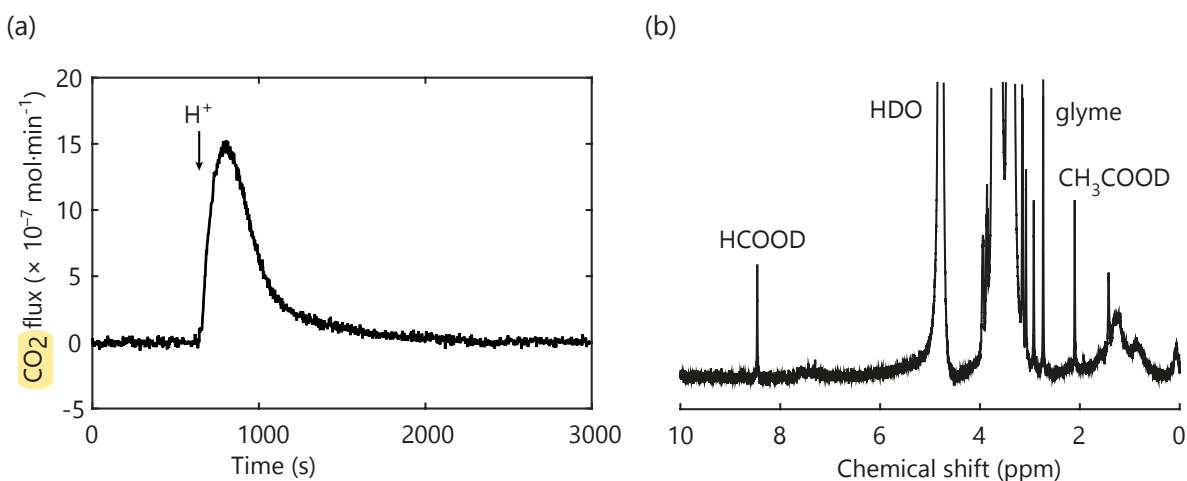
Figure 2.3: **Electrolyte reactivity towards $^1O_2$, adapted from[25].** (a) CO_2 evolution form LiCO$_3$ decomposition formed by O2 saturated 0.1 M LiClO4 in DME electrolyte exposure to $^1O_2$ for 30 minutes. (b) ^1H-NMR of the electrolyte dissolved in D_2O after $^1O_2$ exposition.

2.2 Detecting singlet oxygen

2.2.1 Production of singlet oxygen

As singlet oxygen appears to be a possible source of metal–air side reactivity, it is necessary to detect and quantify it. To conceive and calibrate singlet oxygen analytical methods, controlled production must be achieved. Singlet oxygen can not be produced chemically from its ground state, due to spin forbidden transition. Singlet oxygen can, yet, be chemically produced from superoxide and peroxide [4–6]; Such methods involves reactive species that could forged reactivity of $^1O_2$ alone. A more "soft" $^1O_2$ production is possible through photo-sensitizers. This production method is based on a sensitizer excitation by photon at a specific wavelength [14,15]. The sensitizer transfers the energy to the ground state oxygen forming its singlet state. Photosensitization of oxygen is especially efficient since oxygen transition form triplet to singlet state is lower in energy than most organic molecules that could quench the excited sensitizer and oxygen diffuse quickly in most media, increasing energy transfer chance [14]. The photosensitization main mechanism is O_2 quenching of the sensitizer excited triplet state [14,15]. To do so, the sensitizer is excited by photon emission to its singlet excited states, through a one photon transition. According to Kasha's rule, molecules in states above the lower excited state will deactivate through vibration until reaching the first excited singlet state (S_1) [15,30]. Intersystem crossing allows the production of the first triplet state (T_1) of the sensitizer despite its spin forbidden nature [14,15,30]. Once formed, T_1 state lifetime is long enough to collide with a ground state oxygen molecule, due to kinetically unfavoured deexcitation by spin forbidden transition [15]. Upon collision, the sensitizer can transfer its energy to the oxygen as they are both in triplet state, generating a singlet oxygen molecule. The photosensitisation process is systematized in fig. 2.4.
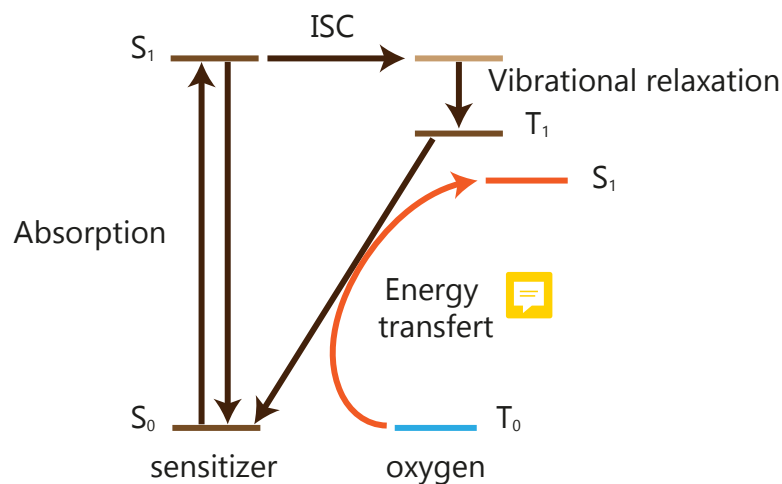
Figure 2.4: **Schematized electronic states transition for photo-sensitized singlet oxygen production, adapted form** [31].

To allow an efficient photosensitization, a sensitizer must have high absorption at a specific wavelength to have a good excitation yield, a T_1 state higher in energy than the transition of $^3\Delta_g$ to $^1\Delta_g$, a good quantum yield of the triplet state with a long lifetime and a good stability [15]. Several chemical groups are identified as good oxygen photosensitizers, i.e. organic dyes, porphyrins, phthalocyanines, tetrapyrroles or transition metal complexes [15]. Palladium (II) meso-tetra(4-fluorophenyl-9-tetrabenzoporphyrin) (or PdF 4) has been used in metal–air battery environments to produce singlet oxygen and is relatively stable towards photobleaching and singlet oxygen [25] [32].

2.2.2 Phosphorescence

Deexcitation of the singlet state to the triplet state through photoemission is called phosphorescence. Singlet oxygen phosphorescence emits photon at the specific wavelength of 1275 nm in the near-infrared that does not vary importantly with the solvent used[13,14,33]. Detection of the photon at this specific wavelength allows to characterize the singlet oxygen presence as other species usually release photon at shorter wavelengths[13]. The characteristic phosphorescence signal is nevertheless weak due to its low quantum yield and spin-forbidden nature[13,14,33]; Its detection is also sensitivite to the solvent as singlet oxygen might deactivate through other pathways. $^1O_2$ spontaneously emitted light, which characterize the singlet to the triplet state transition, can be detected in operando using a specially design cell based on modified sealed quartz cuvette[25].

2.2.3 Use of a chemical trap

Singlet oxygen quantification can be improved by fluorescent probes. These probes are usually composed of a highly fluorescent chromophore, as fluorescein, and a singlet oxygen trap, as 9,10-diphenylanthracene (DPA)[13,34,35]. The chemical trap are based on anthracene that will react selectively with $^1O_2$ to forms its endoperoxide at high rate (2·10⁷ – 9·10⁸ mol·L⁻¹·s⁻¹ for 9,10-Dimethylanthracene (DMA)[35]). The endoperoxide formation via [4+2]-cycloaddition result in a change in fluorescence. Such fluorescent species are yet not electrochemically stable in the metal-air potential range[25]. The actual singlet production can moreover be higher than the trap consumption as other decay roads are still present.

Anthracenes themselves present fluorescence albeit with a lower sensitivity. The detection is then based on decreasing absorbance, the endoperoxide being non-fluorescent as presented in fig. 2.5(b)[25,34,35]. DMA and DPA kinetic comparison in Li-air electrolyte by in-situ photo-generated $^1O_2$ showed improved reactivity for DMA most likely from steric hindrance[25]. DMcA and its endoperoxide are stable chemically in contact with triplet oxygen, superoxide, peroxide as well as lithium carbonate and electrochemically up to ∼ 4 V_{Li/Li^+} on glassy carbon[25,36]. The DMA endoperoxide (DMA-O₂) production is specific to singlet oxygen in the metal-air chemistry. DMA used as in operando measurement requires yet low concentration for high sensitivity as the absorbtion decline is stronger for a low probe starting amount, which increases the measurement noise and degrades the detection limits[25].

(a)   (b)
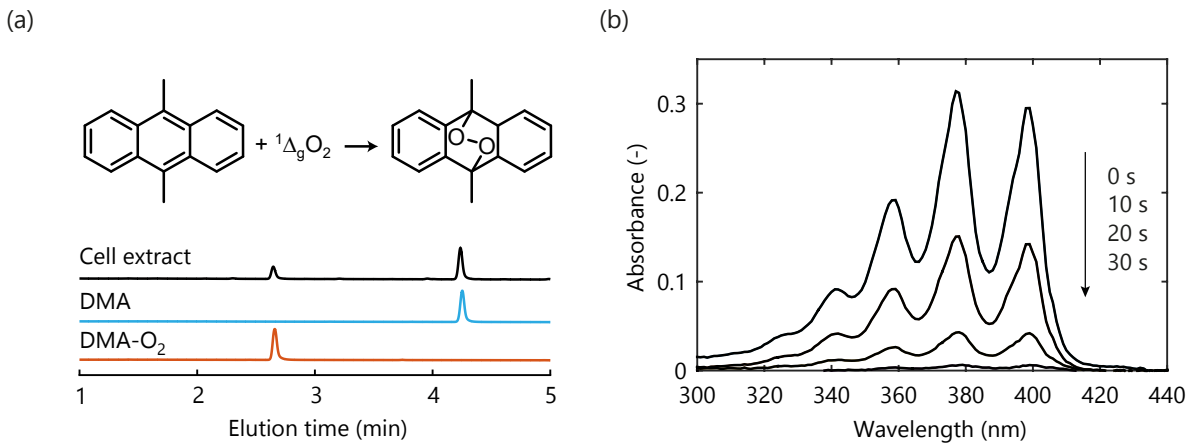
Figure 2.5: **Use of a chemical trap for singlet oxygen detection.** (a) DMA reaction to form~~s~~ its endoperoxide in presence of ~~oxygen~~ and the~~ir respective~~ elution times compared to a cell extract after cycling. (b) ~~DMA~~ UV vis absorption spectra ~~and its disappearance after~~ exposure to $^1O_2$ for different times, adapted from [25].

To bypass this limitation, ex-situ DMA detection by high-performance liquid chromatography (HPLC) permits a near saturated concentration [25]. Using a specific procedure described more precisely in ~~Annexe~~ **Annexe method HPLC**, DMA and its endoperoxide ~~present~~ different elution times. Their respective amount are quantified by the peak surface area compared to a control sample ~~at~~ known concentration, as illustrated in fig. 2.5(a). This involves ~~DMA and DMA-O₂ extraction from the~~ electrolyte after electrochemical cycling by a ~~lower vapour pressure~~ solvent, ~~by dint of a Swagelock cell design presented in~~ **Annexes scheme swagelock**, ~~and a subsequent dilution to the detection limit of the HPLC apparatus.~~

2.2.4 Side reaction characterization

Side reactivity can be ~~partly~~ attributed to singlet oxygen ~~if it~~ forms in metal–air batteries. As discussed in ~~part,~~ 1.3.1, quantitative measurements are necessary ~~characterizations~~ to ~~decide on~~ the reversibility of a cell. Taking into consideration the gaseous nature of O_2, two specific methods have been developed to measure its consumption/release over time. The first one is operando electrochemical mass spectrometry (OEMS) [37–40]. In this case, the cell ~~possesses a~~ headspace flushed to a mass spectrometer which allows for gas analysis. Quantification of the O_2 consumption ~~demands~~ the use of a known ~~O₂/Ar mix~~ as ~~a baseline for gas flushing. The spectrometer can then quantify the amount of gas produced and consumed. Unfortunately, this method does not follow the rate of O₂ evolution in time but only over the full capacity passed.~~ To quantify ~~gas evolution rate over time~~, the pressure in a cell closed headspace can be measured during charge/discharge; ~~P~~ressure change can ~~rely~~ the gas formation to the electron flux using the Faraday law (eq. 1.9) and the ideal gas law (eq. 1.12) [41,42], as shown in fig. 2.6(b) and described more precisely in ~~Annexes~~ **Annexes method pressure cell**. The nature of the gas is, however, unknown.

The discharge~~d~~ product being a solid attached to a conductive matrix, only destructive ex-situ method can be used. Iodometric titration (eq: 2.1) or $[Ti(O_2^{2-})]^{2+}$ complex spectrophotometry (eq. 2.2) are, for example, destructive but quantitative measurements of (su)peroxide quantity [43–45]. The amount of side reaction can be ~~approximate~~ by ~~carbonates content, a common side product for both Li–air and Na–air cells discussed in part.~~ **side products, electrode and discharge products** [37,43,46–48], acting as a proxy for the total side reaction amounts. Both organic and inorganic carbonaceous species are quantifiable through an

ex-situ destructive method[43]. The addition of acid ~~on~~ a washed electrode provoke a CO_2 release from inorganic carbonate as Li_2CO_3 (eq. 2.3) and the addition of ~~a~~ Fenton reactant evolve CO_2 from organic ~~carbonates~~ (eq. 2.4), stable to the sulphuric acid used at the right concentration. Mass spectrometry quantifies the CO_2 evolution for both ~~subsequent~~ steps. We present a refinement which combines both Li_2O_2 and carbonates quantification and is described in Annexe **Annexe method Bettina**; Only one measurement ~~can characterize~~ both Li_2O_2 amounts and the side reactions ~~tendency~~[1], as illustrated in fig. 2.6(a). The Fenton reagent use ~~necessitates~~ precautionary electrode ~~washing~~ to prevent reaction with the organic electrolyte. Unwashed electrodes ~~are preferable for~~ poorly attached Li_2O_2 ~~that might be washed away~~. Two electrodes are then required for full characterization. If more precise speciation of the carbonate products is necessary, their separate quantification can be obtained by ^{1}H-NMR of a D_2O solution after ~~the~~ electrode immersion[44,49]. Altogether, these methods can capture the reversibility ~~nature~~ of a cell in its entirety. ~~If~~ the methods explained here ~~are~~ more thourougly ~~described~~ for $Li-O_2$ chemistries, they can be applied ~~for~~ other non-aqueous metal-air batteries with simple adjustments[1,50].
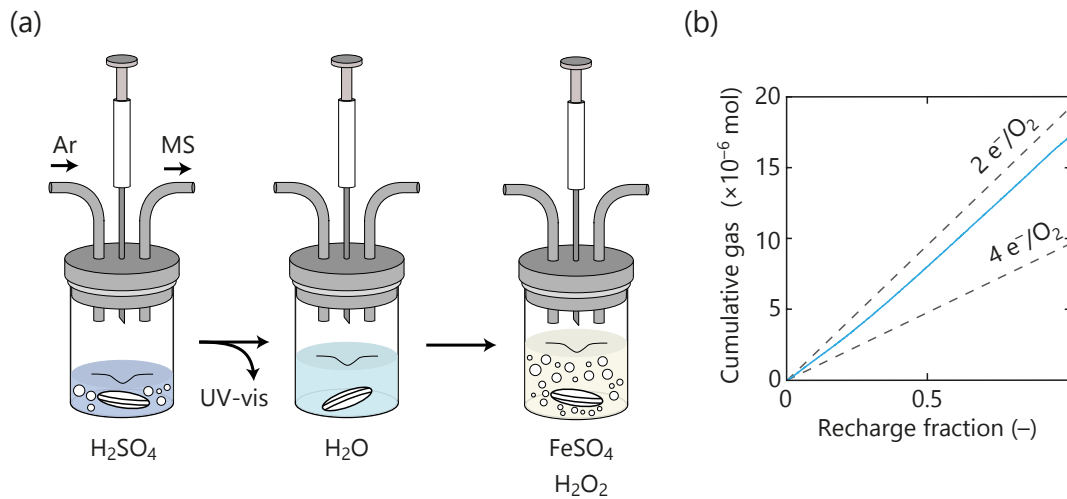
Figure 2.6: ~~Example of~~ **quantitative characterizations.** (a) Scheme of the Li_2O_2 and inorganic/organic carbonates quantification by mass spectroscopy and ultraviolet-visible spectroscopy, adapted from[1]. (b) Gas evolution during a $Li-O_2$ cell charge obtained by pressure monitoring in tetraglyme with 1M LiTFSI compared to theoretical yields of O_2, adapted from[3].

$$Li_2O_2 + 2\,H_2O \longrightarrow 2\,LiOH + H_2O_2$$
$$H_2O_2 + 2\,KI + H_2SO_4 \longrightarrow I_2 + K_2SO_4 + 2\,H_2O \tag{2.1}$$
$$I_2 + 2\,Na_2S_2O_3 \longrightarrow Na_2S_4O_6 + 2\,NaI$$

$$Li_2O_2 + 2\,H_2O \longrightarrow 2\,LiOH + H_2O_2$$
$$TiOSO_4 + H_2O_2 \longrightarrow TiO_2^{2+} + SO_4^{2-} + H_2O \tag{2.2}$$

$$CO_3^{2-} \rightleftharpoons HCO_3^- \rightleftharpoons CO_2 \tag{2.3}$$
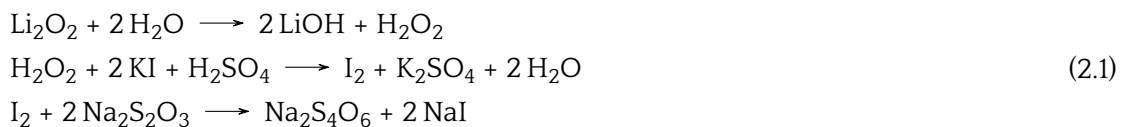
~~This~~ equilibrium highly favour CO_2 formation at ~~high~~ pH.

$$Fe^{2+} + H_2O \longrightarrow Fe^{3+} + OH\cdot + OH^- \tag{2.4}$$

~~Carbonate radical decompositions give rise to CO_2 evolution~~.

Qualitative measurement, despite the ~~information~~ loss ~~on quantities,~~ have the advantages to permit ~~direct visualization~~ of the charge/discharge process or characterize specific products. Recent effort addresses in situ characterization to understand the reactions ~~in presence:~~ TEM [51,52], X-ray and neutron tomography [53], XRD [54–56], XPS [57], Raman [58], IR [59] or AFM [60] are a few example of available techniques.

2.3 Formation mechanism of singlet oxygen

2.3.1 Presence of singlet oxygen in metal–air batteries

~~The~~ previously analytical methods to detect singlet oxygen ~~and side reactions are~~ adapted to metal–air batteries, where singlet oxygen formation was suggested in an early stage of research[61]. In-situ measurements of singlet oxygen phosphorescence ~~settled~~ $^1O_2$ formation in Li-air chemistry at all stage of charge[25], as shown in fig. 2.7. The absence of ~~singlet oxygen~~ detection during discharge ~~can~~ not ~~be related to its non-appearance but ascribed to a lower rate considering the high reactivity of $^1O_2$~~. Similarly, EPR measurement showed production of singlet oxygen above 3.55 V_{Li/Li^+}[62].
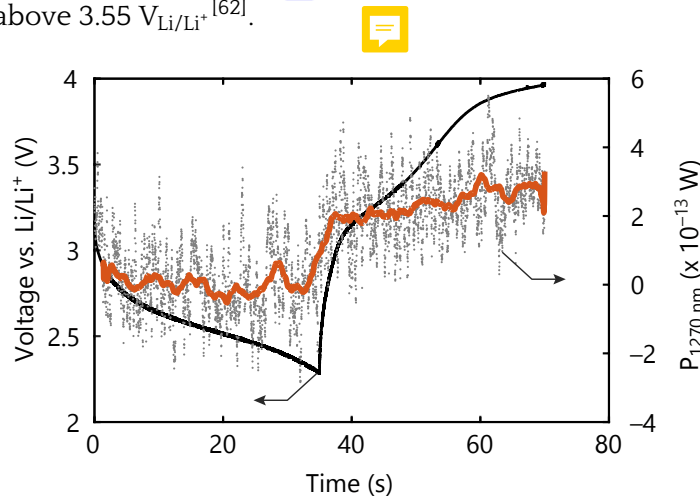
Figure 2.7: ~~Detection in situ~~ **of singlet oxygen during ~~charge~~ by phosphorescence, adapted from[25].** In black, the voltage profile during a Au grid electrode galvanostatic cycling in O_2 saturated 0.1 M $LiClO_4$ deuterated acetonitrile electrolyte with 1000 ppm D_2O. In light grey, the power of the optical emission at 1270 nm, related to $^1O_2$ phosphorescence. In orange, the moving average of the phosphorescence output.

DMA in-situ fluorescence monitoring during Li-air cell cycling shows ~~as well~~ clear consumption of the trap by singlet oxygen from the charge onset with improved sensitivity in a classical electrolyte (0.1 mol.L^{-1} $LiClO_4$ in TEGDME). The $^1O_2$ production rate increase with the overpotential during the charge, yet, no clear singlet oxygen production appears during discharge[25]. The addition of 1000 ppm of water as additive~~s~~, known to increase solution pathway and ~~so~~ solvated superoxide[63], changes drastically the results as presented in fig. 2.8(a). A slight DMA consumption can be seen also through the discharge in this case, indicating singlet oxygen formation at all stage of cycling[25]. ~~Solution pathway seems~~ to enhance $^1O_2$ production, especially during discharge. Using a similar method in Na–O_2 cells showed production of singlet oxygen during ~~charge~~ in a similar fashion as well[50], as depicted in fig. 2.8(b). The production of singlet oxygen ~~is then not confined to~~ Li-air chemistry but encompass~~es~~ the metal–air ~~problematic~~.

(a)   (b)
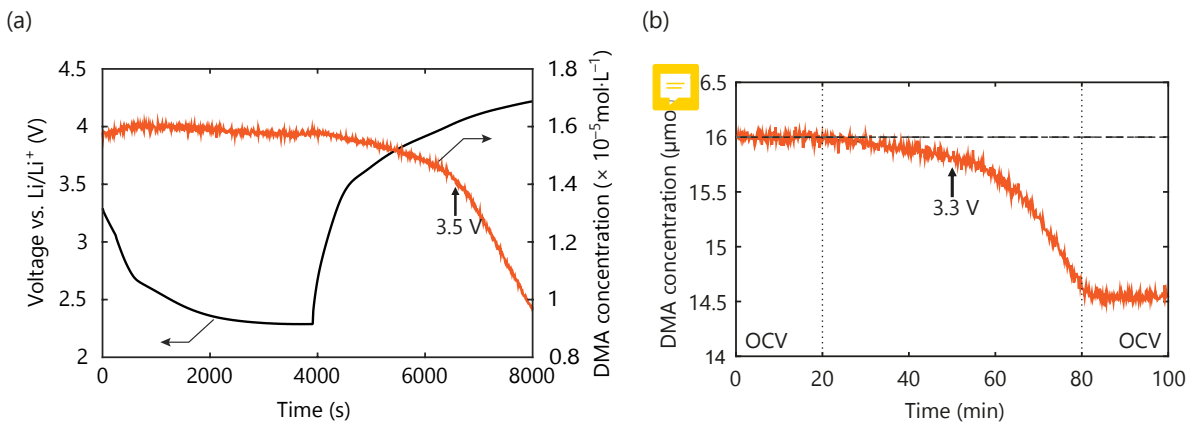
Figure 2.8: **Detection in situ of singlet oxygen by DMA fluoresence.** (a) $^1O_2$ detection by fluoresence spectroscopy in Li-air cells, adapted from[25]. In black, the voltage profile of Li-O_2 cell during galvonostatic cycling in O_2 saturated 16 μM DMA, a 0.1 M LiClO$_4$ and 1000 ppm H$_2$O TEGDME electrolyte at 25 mA·cm–2. In orange, the DMA concentration evolution. (b) $^1O_2$ detection by fluoresence spectroscopy in Na-air cells, adapted from[50]. In orange, the DMA concentration evolution during potentiostatic charge. Prior to charge, the cathode was first discharged at 75 mA·h·cm^{-2} in a O_2 saturated 0.5 M NaOTf and 40 ppm H$_2$O diglyme electrolyte and used in a the operando setup containing the same electrolyte and 16 μM DMA as additive.

To clarify the singlet oxygen production during discharge even without additives in Li-air cells, HPLC characterization of the DMA-to-DMA-O_2 conversion has been performed at different stages of discharge and recharge in Li-O_2 cells[25]. The results, shown in fig. 2.9(a)-(b), present a $^1O_2$ production during discharge albeit in lower amount than charge, in concordance with the in-situ measurements. Similarly, DMA-O_2 is produced during charge as well as discharge at smaller rate in Na-O_2 cells[50], as represented in fig 2.9(c)-(d).
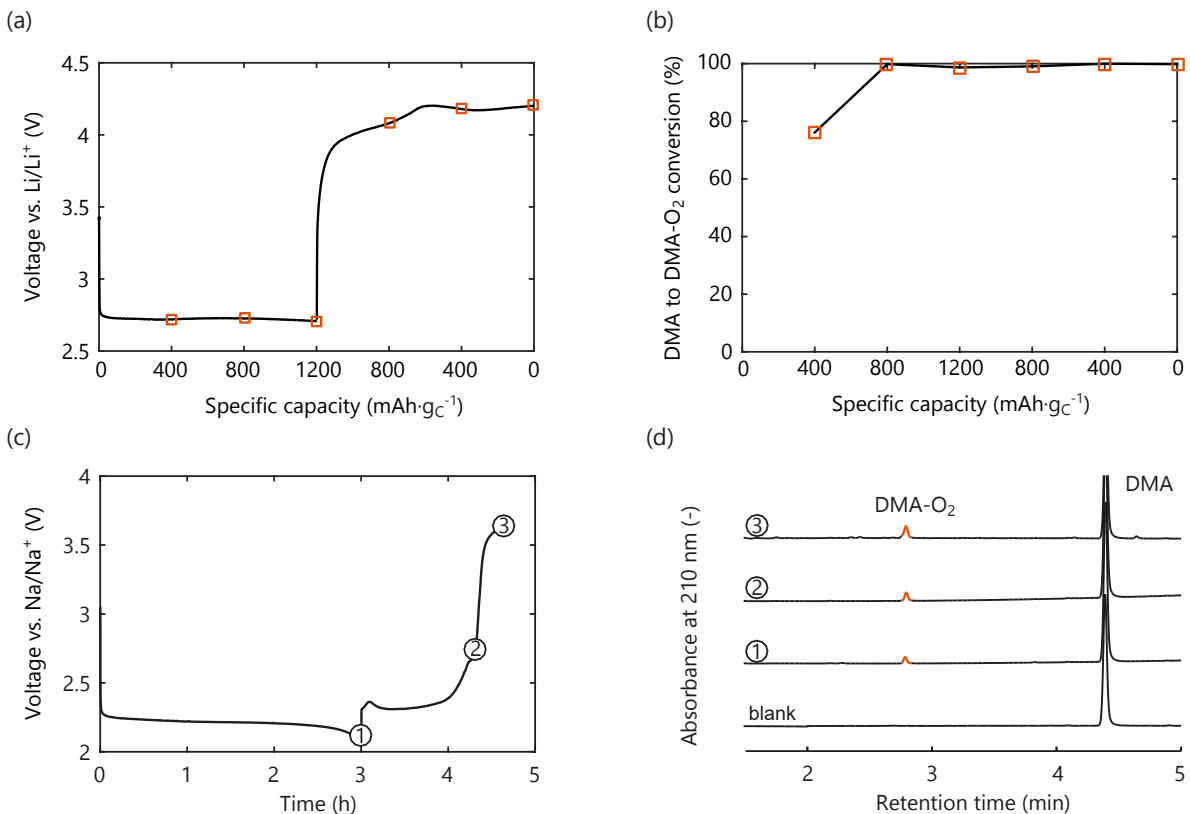
Figure 2.9: **~~Detection~~ ex situ of singlet oxygen by HPLC.** (a-b) $^1O_2$ detection by DMA–O_2 formation in Li–air cells, adapted from [25]. (a) The voltage profile of a porous carbon black electrode during cycling in a O_2 saturated 30 mM DMA, 0.1 M $LiClO_4$ TEGDME electrolyte at 70 mA·g_c^{-1}. The orange square ~~represent~~ a HPLC quantification. (b) ~~Reaction yield of DMA to its peroxide by via reaction with~~ $^1O_2$. (c–d) $^1O_2$ detection by DMA–O_2 formation in Na–air cells, adapted from [50]. (a) The voltage profile of a carbon paper electrode during cycling in a O_2 saturated 30 mM DMA, 0.5 M NaOTf and 40 ppm H_2O diglyme electrolyte at 90 mA·cm^{-2}. The numbered circles represent a HPLC quantification. (b) HPLC runs corresponding to the numbered circles in (c) indicating in orange DMA to DMA–O_2 conversion.

The $^1O_2$ formation rate displays striking similarity with the side reactions rate illustrated in Fig. 1.21, namely a small rate during discharge and an increased rate as the charge progress. DMA ~~incorporation~~ to the electrolyte ~~as additives~~ reduces the carbonate production through most of the cycling [25]. The reduced carbonate production ~~difference~~ between the cells with or without DMA is due to the DMA ~~amount diminution~~; DMA effectiveness will be reduced through the cycling as it is consumed over time. ~~Singlet oxygen can then be ascribed as one of the side reactivity pathways in metal–air batteries.~~ To confirm singlet oxygen influence on parasitic chemistry, OEMS measurement monitored the O_2 and CO_2 release during recharge in electrolytes with or without DMA as additives in Li–air cells, respectively from Li_2O_2 and $LiCO_3$ oxidation [25]. The DMA addition resulted in lower overpotential through ~~the~~ charge attributed to lower production of carbonates during discharge; Carbonate accumulation and oxidation provokes in part the overpotential rise as described in part. **discharge products part**. ~~The gas~~ evolution follows ~~a yield~~ closer to the theoretical yield ~~for the oxygen~~ accompanied by a ~~lower~~ CO_2 release with ~~the~~ DMA containing electrolyte, indicating reduced parasitic reactivity both in discharge and charge.

2.3.2   Alkali oxide oxidation

As singlet oxygen is partially responsible for metal–air parasitic chemistry, the biggest hindrance to their cyclability, underpinning and understanding its formation mechanism is of prime importance. Alkaline peroxide chemical oxidation is a known production pathway for $^1O_2$[6]. The most direct formation mechanism in metal–air chemistries is alkaline oxide oxidation. Despite being unfavoured thermodynamically, singlet oxygen can be produced if the applied overpotential is high enough to overcome the energy barrier. The required energy to pass oxygen from ground state to singlet state is 94 kJ.moL^{-1} or 0.97 eV[17]. Assuming this energy as a first estimate of the Gibbs free energy difference between the singlet and triplet state [25,62], a singlet oxygen potential threshold estimation is possible from the triplet state release according to the eq. 2.5. The $^1O_2$ formation overpotential is then approximate as 0.97 V for the alkali peroxide (considering a 2 e$^-$ process) and 0.49 V for the alkali superoxide (1 e$^-$ process). A direct two electron reaction appears unlikely form the mechanism described in part. 1.2.1.2, this case is still useful to be discussed as an extreme case. The different potential threshold for $^1O_2$ formation obtained from the thermodynamical potentials of the different alkali oxide are compiled in **put in annexes tab. 2.1** and illustrated in fig. 2.10. Potassium peroxide being not stable as discussed in part. **introduction**, its value is give only for completeness. The exact LiO_2 potential ranged around 3.55 V_{Li/Li^+} but is still under debate as several values has been reported in the literature since lithium superoxide is unstable in a solid form[64].

$$\Delta_r G = nFE \qquad \text{in charge}$$
$$E_{^1O_2} = E_{^3O_2} + \frac{\Delta_r G(^3O2 \longrightarrow {^1O2})}{nF} \tag{2.5}$$

with $\Delta_r G$, the Gibbs energy per mole of reaction (J.mol^{-1}); n, the number of e$^-$ transferred (mol); F, the Faraday constant (96485.33289 C · mol^{-1}) and E, the reaction potential (V).

put in annexes

Table 2.1: **Potential of alkali oxide oxidation and $^1O_2$ production ($^3O_2$/$^1O_2$)**

Oxide	Li–O$_2$ (V_{Li/Li^+})	Na–O$_2$ (V_{Na/Na^+})	K–O$_2$ (V_{K/K^+})
superoxide	2.46/3.43[65], 2.61/3.58[66], 2.68/3.65[67]	2.28/3.25[64]	2.48/3.45[68]
peroxide	2.96/3.45[69]	2.33/2.82[64]	2.20/2.69[68]
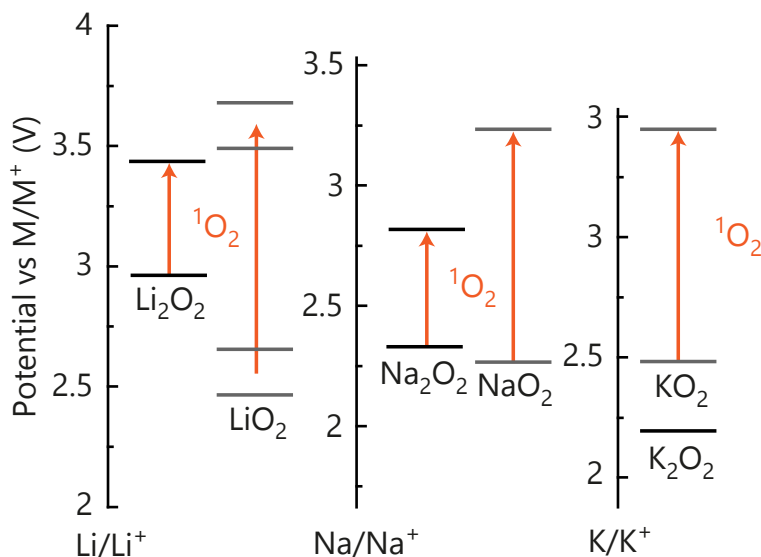
Figure 2.10: **Potential of $^1O_2$ production by alkali oxide oxidation.** The orange arrow represent the 0.97/0.49 eV needed for $^1O_2$ formation. The potential are given in tab. 2.1.

These potential thresholds correspond to the increase $^1O_2$ formation rate during charge both for Na-O_2 and Li-O_2 seen by in-situ fluorescence, presented in fig 2.8, as well as the detection start for in operando EPR[25,50,62]. Alkaline oxide electrochemical oxidation appears to be responsible for the $^1O_2$ formation at high overpotantial; This process is moreover not limited to lithium peroxide and continue with the oxidation of superoxide like species formed during Li-O_2 cell charge, as discussed in part. **charge**.

2.3.3 Disproportionation as source of singlet oxygen

Singlet oxygen was shown to form at all stage of cycling in Li-air and Na-air batteries, phenomenon that can not be explain by alkali oxide direct oxidations alone[25,50]. Another reaction releasing oxygen while cycling Li-O_2 and Na-O_2 cells is the superoxide disproportionation towards peroxide, thermodynamically favoured as shown in fig. 2.10. In agreement with Pearson acid-base concept, harder lewis acid cations as Li$^+$ or Na$^+$ rather form peroxide, albeit with a lower driving force for the latter[47,70,71]. On the other hand, softer Lewis acid cations as K$^+$ or TBA$^+$ and imidazolium are known to favour superoxide formation[68,72–77]. The relative Lewis acidity of these cations has been determined in litterature by ^{13}C NMR[78].

NaO$_2$ might appear kinetically stable due to the low disproportionation driving force (-12.2 kJ.mol^{-1} [65]), especially considering its enhanced stability during nucleation due to a lower surface energy[79]; Discharge product in Na-O_2 chemistry is then often characterized as superoxide[45,80,81]. Resting of Na-O_2 cells after discharge, yet, showed severe superoxide degradation accompanied by formation of peroxide and decomposition products as cabonates, illustrated in fig. 2.11(a)-(b)[47,48,70,71,82,83]. After discharge in a classical electrolyte (0.5 M NaOTf in diglyme containing 40 ppm H$_2$O), resting of a Na-O_2 cathode in the same electrolyte containing in addition 30 mM of DMA exhibited DMA-O_2 conversion over time, accompanied by Na$_2$CO$_3$ formation. $^1O_2$ oxygen appears to be released during cell resting coinciding with degradation products formation as shown in fig. 2.11(c)[50].
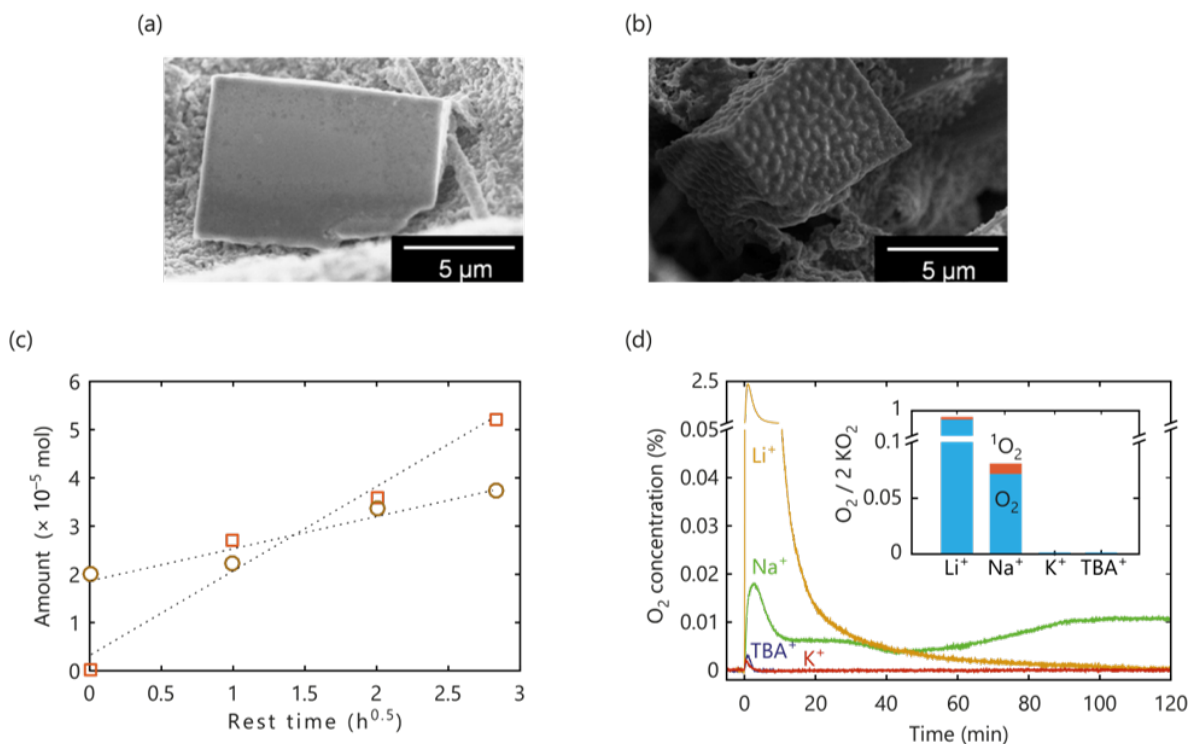
Figure 2.11: **Disproportionation as a source of singlet oxygen.** (a) SEM image of Na-O_2 discharge products analysed directly after discharge. (b) SEM images of Na-O_2 discharge products analysed after 30 hours resting showing clear surface degradation. (c) DMA-O_2 (orange squares) and NaCO_3 (brown circles) production overtime during resting in a Na-O_2 cell. The cells were first discharged in a 0.5 M NaOTf and 40 ppm H_2O diglyme electrolyte. the washed cathodes were immersed in the same electrolyte containing additionally 30 mM DMA for a given amount of time before analysis. (d) O_2 evolution induced by disproportionation overtime upon mixing KO_2 with TEGDME electrolytes containing 0.1 M of the indicated cations and 30 mM DMA. The inset shows the evolved $^3O_2$ (as measured by MS) and $^1O_2$ (as measured by HPLC) after 2 hours reaction time.

KO_2 put in contact with water was shown to results in singlet oxygen production[84]. If KO_2 by itself is stable, the addition of protic species to superoxide could induces water assisted disproportionation with H_2O_2 as intermediate product despite contradictory results[25,50,85]. Poor NaO_2 chemical stability and parasitic chemistry might arise partly from the superoxide disproportionation; This one can disporportionate via from solvated superoxide despite lower solubility than LiO_2[70,71]. A parallel can be drawn between Li-air and Na-air chemistries with the formation of lithium superoxide or superoxide-like through all stage of cycling.

Using KO_2 as stable superoxide, we modeled the disproportionation reaction in presence of different cations, as presented in fig 2.11(d)[2] and further described in Annexe **Annexe HPLC EES**. The reaction was followed by mass spectrometry in a closed reactor with a headspace continuously purged. Disproportionation was initiated by injecting an electrolyte containing different cations, chosen for their different Lewis acidity (0.03 M DMA and 0.1 M Li$^+$, Na$^+$, K$^+$, or TBA$^+$ in TEGMDE) on a KO_2 powder. The electrolyte was further analysed by HPLC after reaction to quantify the $^1O_2$ production, as shown in the insert of fig 2.11(d) and detailed in **Annexes HPLC disp**. As expected, disproportionation induced by Li$^+$ cations, the harder Lewis acid, quickly releases oxygen and reach completion within 2 hours. Na$^+$ electrolyte addition to KO_2 powder also produces oxygen albeit at a slower rate and is still in

progress after 2 hours. Slower rate is expected considering the lower driving force compare to Li^+. As for K^+ and TBA^+ cations, only negligible oxygen amount evolves as peroxide formation is unfavoured. Li^+ induced disproportionation resulted in 93% $^3O_2$ and 2% $^1O_2$ of the theoretical amount obtain from eq. 2.6 , i.e., 1 mol O_2 per 2 mol KO_2. The Na^+ disproportionation reaches value farther from the expected amount, as the reaction did not finish; Only 8% of the KO_2 have reacted of which 12% resulted in $^1O_2$, a higher amount than for Li^+. Disproportionation in presence of alkali cations yields significant fractions of $^1O_2$ with its fraction increasing as the Lewis acidity of the cations decreases. $K-O_2$ cells show improved stability compare to $Na-O_2$ and $Li-O_2$ as well lithium and sodium peroxide based chemistry compared to superoxide over time, as discussed in part. **side product**; Increased side reactivity correlate with the presence of disproportionation and originate at least partly from $^1O_2$ reactivity.

$$2\,O_2^- \longrightarrow O_2^{2-} + x\,^3O_2 + (1-x)^1O_2 \tag{2.6}$$

2.3.4   Importance of singlet oxygen for non aqueous batteries

Li_2CO_3 is a common by-products in Li-air batteries but also in every non organic lithium based batteries [37,43,44,86,87], as discussed in **side products, electrode**. Carbonate oxidation can proceed at potential observed in Li-air batteries (E^0 = 3.82 V_{Li/Li^+} for Li_2CO_3 [88,89]) and are held responsible for the increased overpotantial during charge, as discussed in part. **discharge products** [43,44,46,49,88,90,91]. If Li_2CO_3 oxidation could proceed via reaction eq. 2.7, only CO_2 release can be detect during Li_2CO_3 decompostion [88–90,92–94]; Oxygen release is lacking and have been attributed to superoxide formation [89,92].

$$2\,Li_2CO_3 \longrightarrow 4\,Li^+ + 4\,e^- + 2\,CO_2 + O_2 \tag{2.7}$$
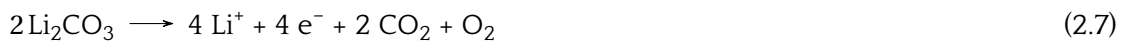
To explain the lack of oxygen release, $^1O_2$ formation instead of the ground state oxygen have been proposed [36]. The lack of oxygen release could be explained by the singlet oxygen reactivity with cell components. Charge of a prefilled electrode with chemical Li_2CO_3 in a electrolyte containing DMA (0.03 M DMA and 0.1 M LiTFSI DME) give rise to $DMA-O_2$ formation, indicating formation $^1O_2$ presence, above 3.8 V_{Li/li^+} as shown in fig. 2.12 [36]. The singlet oxygen release correspond to more than 50% of the theoritical production, from eq. 2.7, at all stage of charge above 3.8 V_{Li/li^+}; This value represents the low extrema since part of the $^1O_2$ might react by other decay roads. As $DMA-O_2$ is only stable up to approximately 4 V_{Li/li^+}, the reduced $^1O_2$ production above 4.05 V_{Li/li^+} can be ascribed to $DMA-O_2$ oxidation [36].
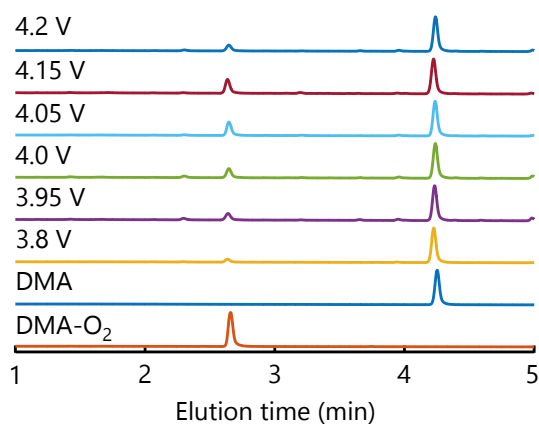
Figure 2.12: **Lithium carbonate oxidation as a source of singlet oxygen.** The cells composed of a prefilled LicO$_3$ carbon electrode were charged at a fixed potential to reach 0.64 mA·h in a DME electrolyte containing 0.03 M DMA and 0.1 M LiTFSI. HPLC runs of the electrolyte at different charge potential shows the production of singlet oxygen upon LiCO$_3$ oxidation.

Concurrently to alkali oxide oxidation, $^1O_2$ production at high overpotential can proceed via carbonate oxidation; More precisely, LiCO$_3$ releases singlet oxygen during its oxidation[36]. As Li$_2$CO$_3$ is a common passivation agent, notably formed during synthesis of transition metal oxide[94], singlet oxygen parasitic chemistry is not confined to metal–air batteries[95,96].

Conclusion

Singlet oxygen, owing to its very chemical natures, is a very reactive species able to react with ~~the~~ batteries component. $^1O_2$ formation is unquestionable in metal-air batteries and has serious mechanistic consequences. By dint of adapted analytical methods, our group showed $^1O_2$ presence through all stage of cycling and corroborate the influence of $^1O_2$ on the metal-air cells degradation mechanism. $^1O_2$ chemical traps stable in metal–air conditions, as DMA, were shown to quantify the presence of singlet oxygen both in or ex situ. The reactions yield can be further determined by pressure monitoring, as the principal reagent/product is a gas (O_2). Finally we show that the reactions products can be quantified with one electrode ~~only~~ using a combination of ultra violet spectrometry and mass spectrometry. As the presence of $^1O_2$ can be related to the formation of side products, there characterization is a relevant indicator to its formation.

Using the afore mentioned methods, singlet oxygen formation appears ~~as an inevitable consequence of~~ the discharge and charge process in metal-air batteries. It can forms either directly by oxidation above a given threshold potential or by superoxide disproportionation. The importance of singlet oxygen goes further than metal-air batteries. Formation of $^1O_2$ by carbonate oxidation widen the ~~application spectra~~ of singlet oxygen mitigations means to all Li-based cells reaching high potential. The $^1O_2$ formation mechanism needs to be better understood to reduce and control its production and permits the realistic cyclability of metal–air redox chemistries.

Reckoning the presence of $^1O_2$ in non-aqueous batteries, the rest of this manuscript will ~~try to provide more~~ in-depth mechanistic descriptor and $^1O_2$ consequence alleviation in electrochemical energy storage devices. $^1O_2$ formation by alkali oxide or carbonate oxidation in metal–air batteries could be avoided for example through the use of adapted catalyst or redox mediators, reducing the applied overpotential. The disproportionation reaction, yet, is spontaneous in Li$^+$ and Na$^+$ electrolytes and ~~its mechanistic should be unravelled to understand~~ $^1O_2$ production in metal air batteries.

Bibliography

[1] B. Schafzahl, E. Mourad, L. Schafzahl, Y. K. Petit, A. R. Raju, M. O. Thotiyl, M. Wilkening, C. Slugovc, and S. A. Freunberger, "Quantifying Total Superoxide, Peroxide, and Carbonaceous Compounds in Metal–O_2 Batteries and the Solid Electrolyte Interphase," *ACS Energy Letters*, vol. 3, no. 1, pp. 170–176, 2017.

[2] E. Mourad, Y. K. Petit, R. Spezia, A. Samojlov, F. F. Summa, C. Prehal, C. Leypold, N. Mahne, C. Slugovc, O. Fontaine *et al.*, "Singlet oxygen from cation driven superoxide disproportionation and consequences for aprotic metal–O_2 batteries," *Energy & Environmental Science*, vol. 12, no. 8, pp. 2559–2568, 2019.

[3] Y. K. Petit, C. Leypold, N. Mahne, E. Mourad, L. Schafzahl, C. Slugovc, S. M. Borisov, and S. A. Freunberger, "DABCOnium: an efficient and high-voltage stable singlet oxygen quencher for metal–O_2 cells," *Angewandte Chemie International Edition*, vol. 58, no. 20, pp. 6535–6539, 2019.

[4] E. McKeown and W. A. Waters, "The oxidation of organic compounds by "singlet" oxygen," *Journal of the Chemical Society B: Physical Organic*, pp. 1040–1046, 1966.

[5] M. Kasha and A. U. Khan, "The physics, chemistry, and biology, of singlet molecular oxygen," *Annals of the New York Academy of Sciences*, vol. 171, no. 1, pp. 5–23, 1970.

[6] Q. Li, F. Chen, W. Zhao, M. Xu, B. Fang, Y. Zhang, L. Duo, Y. Jin, and F. Sang, "A spectroscopic study on singlet oxygen production from different reaction paths using solid inorganic peroxides as starting materials," *Bulletin of the Korean Chemical Society*, vol. 28, no. 10, pp. 1656–1660, 2007.

[7] P. G. Falkowski, M. E. Katz, A. J. Milligan, K. Fennel, B. S. Cramer, M. P. Aubry, R. A. Berner, M. J. Novacek, and W. M. Zapol, "The rise of oxygen over the past 205 million years and the evolution of large placental mammals," *Science*, vol. 309, no. 5744, pp. 2202–2204, 2005.

[8] J. J. Zimmerman, A. von Saint André-von Arnim, and J. McLaughlin, "Cellular respiration," in *Pediatric Critical Care*. Elsevier, 2011, pp. 1058–1072.

[9] G. Parkin, "Valence, oxidation number, and formal charge: three related but fundamentally different concepts," *Journal of chemical education*, vol. 83, no. 5, p. 791, 2006.

[10] C. A. Coulson, "Representation of simple molecules by molecular orbitals," *Quarterly Reviews, Chemical Society*, vol. 1, no. 2, pp. 144–178, 1947.

[11] I. Levine, *Quantum Chemistry*. Pearson, 2014.

[12] D. Min and J. Boff, "Chemistry and reaction of singlet oxygen in foods," *Comprehensive reviews in food science and food safety*, vol. 1, no. 2, pp. 58–72, 2002.

[13] P. R. Ogilby, "Singlet oxygen: there is indeed something new under the sun," *Chemical Society Reviews*, vol. 39, no. 8, pp. 3181–3209, 2010.

[14] C. Schweitzer and R. Schmidt, "Physical mechanisms of generation and deactivation of singlet oxygen," *Chemical reviews*, vol. 103, no. 5, pp. 1685–1758, 2003.

[15] M. C. DeRosa and R. J. Crutchley, "Photosensitized singlet oxygen and its applications," *Coordination Chemistry Reviews*, vol. 233, pp. 351–371, 2002.

[16] S. Arnold, M. Kubo, and E. Ogryzlo, "Relaxation and reactivity of singlet oxygen," *Adv. Chem. Ser*, vol. 77, pp. 133–142, 1968.

[17] F. Wilkinson, W. P. Helman, and A. B. Ross, "Rate constants for the decay and reactions of the lowest electronically excited singlet state of molecular oxygen in solution. An expanded and revised compilation," *Journal of Physical and Chemical Reference Data*, vol. 24, no. 2, pp. 663–677, 1995.

[18] P. B. Merkel and D. R. Kearns, "Remarkable solvent effects on the lifetime of $^1\delta_g$ oxygen," *Journal of the American Chemical Society*, vol. 94, no. 3, pp. 1029–1030, 1972.

[19] R. Y. Ho, J. F. Liebman, and J. S. Valentine, "Overview of the energetics and reactivity of oxygen," in *Active Oxygen in Chemistry*. Springer, 1995, pp. 1–23.

[20] H. H. Wasserman and J. L. Ives, "Singlet oxygen in organic synthesis," *Tetrahedron*, vol. 37, no. 10, pp. 1825–1852, 1981.

[21] P. D. Bartlett, G. D. Mendenhall, and A. P. Schaap, "Competitive modes of reaction of singlet oxygen," *Annals of the New York Academy of Sciences*, vol. 171, no. 1, pp. 79–88, 1970.

[22] A. A. Frimer, "The reaction of singlet oxygen with olefins: the question of mechanism," *Chemical Reviews*, vol. 79, no. 5, pp. 359–387, 1979.

[23] E. Clennan and A. Pace, "Advances in singlet oxygen chemistry," *TETRAHEDRON*, vol. 61, pp. 6665–6691, 10 2005.

[24] A. Sagadevan, K. C. Hwang, and M.-D. Su, "Singlet oxygen-mediated selective C–H bond hydroperoxidation of ethereal hydrocarbons," *Nature communications*, vol. 8, no. 1, p. 1812, 2017.

[25] N. Mahne, B. Schafzahl, C. Leypold, M. Leypold, S. Grumm, A. Leitgeb, G. A. Strohmeier, M. Wilkening, O. Fontaine, D. Kramer *et al.*, "Singlet oxygen generation as a major cause for parasitic reactions during cycling of aprotic lithium–oxygen batteries," *Nature Energy*, vol. 2, no. 5, p. 17036, 2017.

[26] V. S. Bryantsev, V. Giordani, W. Walker, M. Blanco, S. Zecevic, K. Sasaki, J. Uddin, D. Addison, and G. V. Chase, "Predicting solvent stability in aprotic electrolyte Li–air batteries: nucleophilic substitution by the superoxide anion radical ($O_2{\cdot}^-$)," *The Journal of Physical Chemistry A*, vol. 115, no. 44, pp. 12 399–12 409, 2011.

[27] V. S. Bryantsev and F. Faglioni, "Predicting autoxidation stability of ether-and amide-based electrolyte solvents for Li–air batteries," *The Journal of Physical Chemistry A*, vol. 116, no. 26, pp. 7128–7138, 2012.

[28] K. Chaisiwamongkhol, C. Batchelor-McAuley, R. G. Palgrave, and R. G. Compton, "Singlet oxygen and the origin of oxygen functionalities on the surface of carbon electrodes," *Angewandte Chemie*, vol. 130, no. 21, pp. 6378–6381, 2018.

[29] W.-J. Kwak, H. Kim, Y. K. Petit, C. Leypold, T. T. Nguyen, N. Mahne, P. Redfern, L. A. Curtiss, H.-G. Jung, S. M. Borisov *et al.*, "Deactivation of redox mediators in lithium–oxygen batteries by singlet oxygen," *Nature communications*, vol. 10, no. 1, p. 1380, 2019.

[30] C. M. Marian, "Spin–orbit coupling and intersystem crossing in molecules," *Wiley Interdisciplinary Reviews: Computational Molecular Science*, vol. 2, no. 2, pp. 187–203, 2012.

[31] R. Bonnett, "Photosensitizers of the porphyrin and phthalocyanine series for photody-namic therapy," *Chemical Society Reviews*, vol. 24, no. 1, pp. 19–33, 1995.

[32] S. Borisov, G. Nuss, W. Haas, R. Saf, M. Schmuck, and I. Klimant, "New NIR-emitting complexes of platinum (II) and palladium (II) with fluorinated benzoporphyrins," *Journal of Photochemistry and Photobiology A: Chemistry*, vol. 201, no. 2-3, pp. 128–135, 2009.

[33] S. Nonell and C. Flors, "Steady-state and time-resolved singlet oxygen phosphorescence detection in the near-IR," *Compr Ser. Photoch*, vol. 2, pp. 7–26, 2016.

[34] N. Umezawa, K. Tanaka, Y. Urano, K. Kikuchi, T. Higuchi, and T. Nagano, "Novel fluorescent probes for singlet oxygen," *Angewandte Chemie International Edition*, vol. 38, no. 19, pp. 2899–2901, 1999.

[35] A. Gomes, E. Fernandes, and J. L. Lima, "Fluorescence probes used for detection of reactive oxygen species," *Journal of biochemical and biophysical methods*, vol. 65, no. 2-3, pp. 45–80, 2005.

[36] N. Mahne, S. E. Renfrew, B. D. McCloskey, and S. A. Freunberger, "Electrochemical oxida-tion of lithium carbonate generates singlet oxygen," *Angewandte Chemie International Edition*, vol. 57, no. 19, pp. 5529–5533, 2018.

[37] B. D. McCloskey, D. S. Bethune, R. M. Shelby, G. Girishkumar, and A. C. Luntz, "Solvents' critical role in nonaqueous lithium–oxygen battery electrochemistry," *The Journal of Physical Chemistry Letters*, vol. 2, no. 10, pp. 1161–1166, 2011.

[38] Z. Peng, S. A. Freunberger, Y. Chen, and P. G. Bruce, "A reversible and higher-rate Li-O_2 battery," *Science*, vol. 337, no. 6094, pp. 563–566, 2012.

[39] Y. Chen, S. A. Freunberger, Z. Peng, F. Bardé, and P. G. Bruce, "Li–O_2 battery with a dimethylformamide electrolyte," *Journal of the American Chemical Society*, vol. 134, no. 18, pp. 7952–7957, 2012.

[40] M. M. Ottakam Thotiyl, S. A. Freunberger, Z. Peng, Y. Chen, Z. Liu, and P. G. Bruce, "A stable cathode for the aprotic Li–O_2 battery," *Nature materials*, vol. 12, no. 11, p. 1050, 2013.

[41] B. D. McCloskey, D. Bethune, R. Shelby, T. Mori, R. Scheffler, A. Speidel, M. Sherwood, and A. Luntz, "Limitations in rechargeability of Li-O_2 batteries and possible origins," *The journal of physical chemistry letters*, vol. 3, no. 20, pp. 3043–3047, 2012.

[42] S. Das, J. Højberg, K. B. Knudsen, R. Younesi, P. Johansson, P. Norby, and T. Vegge, "In-stability of ionic liquid-based electrolytes in Li–O_2 batteries," *The Journal of Physical Chemistry C*, vol. 119, no. 32, pp. 18 084–18 090, 2015.

[43] M. M. Ottakam Thotiyl, S. A. Freunberger, Z. Peng, and P. G. Bruce, "The carbon electrode in nonaqueous Li–O_2 cells," *Journal of the American Chemical Society*, vol. 135, no. 1, pp. 494–500, 2012.

[44] B. D. McCloskey, A. Valery, A. C. Luntz, S. R. Gowda, G. M. Wallraff, J. M. Garcia, T. Mori, and L. E. Krupp, "Combining accurate O_2 and Li_2O_2 assays to separate discharge and charge stability limitations in nonaqueous Li–O_2 batteries," *The journal of physical chemistry letters*, vol. 4, no. 17, pp. 2989–2993, 2013.

[45] P. Hartmann, C. L. Bender, J. Sann, A. K. Dürr, M. Jansen, J. Janek, and P. Adelhelm, "A comprehensive study on the cell chemistry of the sodium superoxide (NaO_2) battery," *Physical Chemistry Chemical Physics*, vol. 15, no. 28, pp. 11 661–11 672, 2013.

[46] B. McCloskey, A. Speidel, R. Scheffler, D. Miller, V. Viswanathan, J. Hummelshøj, J. Nørskov, and A. Luntz, "Twin problems of interfacial carbonate formation in nonaqueous Li–O_2 batteries," *The journal of physical chemistry letters*, vol. 3, no. 8, pp. 997–1001, 2012.

[47] I. Landa-Medrano, R. Pinedo, X. Bi, I. Ruiz de Larramendi, L. Lezama, J. Janek, K. Amine, J. Lu, and T. Rojo, "New insights into the instability of discharge products in Na–O_2 batteries," *ACS applied materials & interfaces*, vol. 8, no. 31, pp. 20 120–20 127, 2016.

[48] R. Black, A. Shyamsunder, P. Adeli, D. Kundu, G. K. Murphy, and L. F. Nazar, "The nature and impact of side reactions in glyme-based sodium–oxygen batteries," *ChemSusChem*, vol. 9, no. 14, pp. 1795–1803, 2016.

[49] S. A. Freunberger, Y. Chen, Z. Peng, J. M. Griffin, L. J. Hardwick, F. Bardé, P. Novák, and P. G. Bruce, "Reactions in the rechargeable lithium–O_2 battery with alkyl carbonate electrolytes," *Journal of the American Chemical Society*, vol. 133, no. 20, pp. 8040–8047, 2011.

[50] L. Schafzahl, N. Mahne, B. Schafzahl, M. Wilkening, C. Slugovc, S. M. Borisov, and S. A. Freunberger, "Singlet oxygen during cycling of the aprotic sodium–O_2 battery," *Angewandte Chemie International Edition*, vol. 56, no. 49, pp. 15 728–15 732, 2017.

[51] A. Kushima, T. Koido, Y. Fujiwara, N. Kuriyama, N. Kusumi, and J. Li, "Charging/discharging nanomorphology asymmetry and rate-dependent capacity degradation in Li–oxygen battery," *Nano letters*, vol. 15, no. 12, pp. 8260–8265, 2015.

[52] C. Yang, J. Han, P. Liu, C. Hou, G. Huang, T. Fujita, A. Hirata, and M. Chen, "Direct observations of the formation and redox-mediator-assisted decomposition of Li_2O_2 in a liquid-cell Li–O_2 microbattery by Scanning Transmission Electron Microscopy," *Advanced Materials*, vol. 29, no. 41, p. 1702752, 2017.

[53] F. Sun, R. Gao, D. Zhou, M. Osenberg, K. Dong, N. Kardjilov, A. Hilger, H. Markötter, P. M. Bieker, X. Liu *et al.*, "Revealing hidden facts of Li anode in cycled Lithium–Oxygen Batteries through X-ray and neutron tomography," *ACS Energy Letters*, vol. 4, no. 1, pp. 306–316, 2018.

[54] Z. Li, S. Ganapathy, Y. Xu, J. R. Heringa, Q. Zhu, W. Chen, and M. Wagemaker, "Understanding the electrochemical formation and decomposition of Li_2O_2 and LiOH with operando X-ray diffraction," *Chemistry of Materials*, vol. 29, no. 4, pp. 1577–1586, 2017.

[55] S. Ganapathy, B. D. Adams, G. Stenou, M. S. Anastasaki, K. Goubitz, X.-F. Miao, L. F. Nazar, and M. Wagemaker, "Nature of Li_2O_2 oxidation in a Li–O_2 battery revealed by operando X-ray diffraction," *Journal of the American Chemical Society*, vol. 136, no. 46, pp. 16 335–16 344, 2014.

[56] J.-L. Shui, J. S. Okasinski, C. Chen, J. D. Almer, and D.-J. Liu, "In Operando spatiotemporal study of Li_2O_2 grain growth and its distribution inside operating Li–O_2 batteries," *ChemSusChem*, vol. 7, no. 2, pp. 543–548, 2014.

[57] Y.-C. Lu, E. J. Crumlin, T. J. Carney, L. Baggetto, G. M. Veith, N. J. Dudney, Z. Liu, and Y. Shao-Horn, "Influence of hydrocarbon and CO_2 on the reversibility of Li–O_2 chemistry using in situ ambient pressure X-ray photoelectron spectroscopy," *The Journal of Physical Chemistry C*, vol. 117, no. 49, pp. 25 948–25 954, 2013.

[58] F. S. Gittleson, W.-H. Ryu, and A. D. Taylor, "Operando observation of the gold–electrolyte interface in Li–O_2 batteries," *ACS applied materials & interfaces*, vol. 6, no. 21, pp. 19 017–19 025, 2014.

[59] J. P. Vivek, N. G. Berry, J. Zou, R. J. Nichols, and L. J. Hardwick, "In situ surface-enhanced infrared spectroscopy to identify oxygen reduction products in nonaqueous metal–oxygen batteries," *The Journal of Physical Chemistry C*, vol. 121, no. 36, pp. 19 657–19 667, 2017.

[60] R. Wen, M. Hong, and H. R. Byon, "In situ AFM imaging of Li–O_2 electrochemical reaction on highly oriented pyrolytic graphite with ether-based electrolyte," *Journal of the American Chemical Society*, vol. 135, no. 29, pp. 10 870–10 876, 2013.

[61] J. Hassoun, F. Croce, M. Armand, and B. Scrosati, "Investigation of the O_2 electrochemistry in a polymer electrolyte solid-state cell," *Angewandte Chemie International Edition*, vol. 50, no. 13, pp. 2999–3002, 2011.

[62] J. Wandt, P. Jakes, J. Granwehr, H. A. Gasteiger, and R.-A. Eichel, "Singlet oxygen formation during the charging process of an aprotic lithium–oxygen battery," *Angewandte Chemie International Edition*, vol. 55, no. 24, pp. 6892–6895, 2016.

[63] N. B. Aetukuri, B. D. McCloskey, J. M. García, L. E. Krupp, V. Viswanathan, and A. C. Luntz, "Solvating additives drive solution-mediated electrochemistry and enhance toroid growth in non-aqueous Li–O_2 batteries," *Nature chemistry*, vol. 7, no. 1, p. 50, 2015.

[64] C. L. Bender, D. Schröder, R. Pinedo, P. Adelhelm, and J. Janek, "One-or two-electron transfer? The ambiguous nature of the discharge products in sodium–oxygen batteries," *Angewandte Chemie International Edition*, vol. 55, no. 15, pp. 4640–4649, 2016.

[65] C. L. Bender, P. Hartmann, M. Vraar, P. Adelhelm, and J. Janek, "On the thermodynamics, the role of the carbon cathode, and the cycle life of the sodium superoxide (NaO_2) battery," *Advanced Energy Materials*, vol. 4, no. 12, p. 1301863, 2014.

[66] S. Kang, Y. Mo, S. P. Ong, and G. Ceder, "A facile mechanism for recharging Li_2O_2 in Li–O_2 batteries," *Chemistry of Materials*, vol. 25, no. 16, pp. 3328–3336, 2013.

[67] Y. Zhang, X. Zhang, J. Wang, W. C. McKee, Y. Xu, and Z. Peng, "Potential-dependent generation of O_2–and LiO_2 and their critical roles in O_2 reduction to Li_2O_2 in aprotic Li–O_2 batteries," *The Journal of Physical Chemistry C*, vol. 120, no. 7, pp. 3690–3698, 2016.

[68] X. Ren and Y. Wu, "A low-overpotential potassium–oxygen battery based on potassium superoxide," *Journal of the American Chemical Society*, vol. 135, no. 8, pp. 2923–2926, 2013.

[69] B. D. McCloskey, R. Scheffler, A. Speidel, G. Girishkumar, and A. C. Luntz, "On the mechanism of nonaqueous Li–O_2 electrochemistry on C and its kinetic overpotentials: some implications for Li–air batteries," *The Journal of Physical Chemistry C*, vol. 116, no. 45, pp. 23 897–23 905, 2012.

[70] C. Sheng, F. Yu, Y. Wu, Z. Peng, and Y. Chen, "Disproportionation of sodium superoxide in metal–air batteries," *Angewandte Chemie*, vol. 130, no. 31, pp. 10 054–10 058, 2018.

[71] J. Kim, H. Park, B. Lee, W. M. Seong, H.-D. Lim, Y. Bae, H. Kim, W. K. Kim, K. H. Ryu, and K. Kang, "Dissolution and ionization of sodium superoxide in sodium–oxygen batteries," *Nature communications*, vol. 7, p. 10670, 2016.

[72] W. Wang, N.-C. Lai, Z. Liang, Y. Wang, and Y.-C. Lu, "Superoxide stabilization and a universal KO_2 growth mechanism in potassium–oxygen batteries," *Angewandte Chemie International Edition*, vol. 57, no. 18, pp. 5042–5046, 2018.

[73] Y. Chen, Z. P. Jovanov, X. Gao, J. Liu, C. Holc, L. R. Johnson, and P. G. Bruce, "High capacity surface route discharge at the potassium-O_2 electrode," *Journal of Electroanalytical Chemistry*, vol. 819, pp. 542–546, 2018.

[74] L. Johnson, C. Li, Z. Liu, Y. Chen, S. A. Freunberger, P. C. Ashok, B. B. Praveen, K. Dholakia, J.-M. Tarascon, and P. G. Bruce, "The role of LiO_2 solubility in O_2 reduction in aprotic solvents and its consequences for Li–O_2 batteries," *Nature chemistry*, vol. 6, no. 12, p. 1091, 2014.

[75] C. O. Laoire, S. Mukerjee, K. Abraham, E. J. Plichta, and M. A. Hendrickson, "Elucidating the mechanism of oxygen reduction for lithium-air battery applications," *The Journal of Physical Chemistry C*, vol. 113, no. 46, pp. 20 127–20 134, 2009.

[76] C. J. Allen, J. Hwang, R. Kautz, S. Mukerjee, E. J. Plichta, M. A. Hendrickson, and K. Abraham, "Oxygen reduction reactions in ionic liquids and the formulation of a general ORR mechanism for Li–air batteries," *The Journal of Physical Chemistry C*, vol. 116, no. 39, pp. 20 755–20 764, 2012.

[77] C. V. Amanchukwu, H.-H. Chang, M. Gauthier, S. Feng, T. P. Batcho, and P. T. Hammond, "One-electron mechanism in a gel–polymer electrolyte Li–O_2 battery," *Chemistry of Materials*, vol. 28, no. 19, pp. 7167–7177, 2016.

[78] K. Abraham, "Electrolyte-directed reactions of the oxygen electrode in lithium-air batteries," *Journal of The Electrochemical Society*, vol. 162, no. 2, pp. A3021–A3031, 2015.

[79] S. Kang, Y. Mo, S. P. Ong, and G. Ceder, "Nanoscale stabilization of sodium oxides: implications for Na–O2 batteries," *Nano letters*, vol. 14, no. 2, pp. 1016–1020, 2014.

[80] P. Hartmann, C. L. Bender, M. Vraar, A. K. Dürr, A. Garsuch, J. Janek, and P. Adelhelm, "A rechargeable room-temperature sodium superoxide (NaO_2) battery," *Nature materials*, vol. 12, no. 3, p. 228, 2013.

[81] N. Ortiz-Vitoriano, T. P. Batcho, D. G. Kwabi, B. Han, N. Pour, K. P. C. Yao, C. V. Thompson, and Y. Shao-Horn, "Rate-dependent nucleation and growth of NaO_2 in Na–O_2 batteries," *The journal of physical chemistry letters*, vol. 6, no. 13, pp. 2636–2643, 2015.

[82] T. Liu, G. Kim, M. T. Casford, and C. P. Grey, "Mechanistic insights into the challenges of cycling a nonaqueous Na–O_2 battery," *The journal of physical chemistry letters*, vol. 7, no. 23, pp. 4841–4846, 2016.

[83] S. Y. Sayed, K. P. Yao, D. G. Kwabi, T. P. Batcho, C. V. Amanchukwu, S. Feng, C. V. Thompson, and Y. Shao-Horn, "Revealing instability and irreversibility in nonaqueous sodium–O_2 battery chemistry," *Chemical Communications*, vol. 52, no. 62, pp. 9691–9694, 2016.

[84] A. U. Khan, "Direct spectral evidence of the generation of singlet molecular oxygen ($^1\Delta_g$) in the reaction of potassium superoxide with water," *Journal of the American Chemical Society*, vol. 103, no. 21, pp. 6516–6517, 1981.

[85] J. Aubry, J. Rigaudy, C. Ferradini, and J. Pucheault, "Search for singlet oxygen in the disproportionation of superoxide anion," *Journal of the American Chemical Society*, vol. 103, no. 16, pp. 4965–4966, 1981.

[86] K. Xu, "Electrolytes and interphases in Li-ion batteries and beyond," *Chemical reviews*, vol. 114, no. 23, pp. 11 503–11 618, 2014.

[87] P. Verma, P. Maire, and P. Novák, "A review of the features and analyses of the solid electrolyte interphase in Li-ion batteries," *Electrochimica Acta*, vol. 55, no. 22, pp. 6332–6341, 2010.

[88] W. Yin, A. Grimaud, F. Lepoivre, C. Yang, and J. M. Tarascon, "Chemical vs electrochemical formation of Li_2CO_3 as a discharge product in Li–O_2/CO_2 batteries by controlling the superoxide intermediate," *The journal of physical chemistry letters*, vol. 8, no. 1, pp. 214–222, 2016.

[89] S. Yang, P. He, and H. Zhou, "Exploring the electrochemical reaction mechanism of carbonate oxidation in Li–air/CO_2 battery through tracing missing oxygen," *Energy & Environmental Science*, vol. 9, no. 5, pp. 1650–1654, 2016.

[90] S. R. Gowda, A. Brunet, G. Wallraff, and B. D. McCloskey, "Implications of CO_2 contamination in rechargeable nonaqueous Li–O_2 batteries," *The journal of physical chemistry letters*, vol. 4, no. 2, pp. 276–279, 2012.

[91] J. Højberg, B. D. McCloskey, J. Hjelm, T. Vegge, K. Johansen, P. Norby, and A. C. Luntz, "An electrochemical impedance spectroscopy investigation of the overpotentials in Li–O_2 batteries," *ACS applied materials & interfaces*, vol. 7, no. 7, pp. 4039–4047, 2015.

[92] Z. Zhao, J. Huang, and Z. Peng, "Achilles' heel of lithium–air batteries: Lithium carbonate," *Angewandte Chemie International Edition*, vol. 57, no. 15, pp. 3874–3886, 2018.

[93] S. Meini, N. Tsiouvaras, K. U. Schwenke, M. Piana, H. Beyer, L. Lange, and H. A. Gasteiger, "Rechargeability of Li–air cathodes pre-filled with discharge products using an ether-based electrolyte solution: implications for cycle-life of Li–air cells," *Physical Chemistry Chemical Physics*, vol. 15, no. 27, pp. 11 478–11 493, 2013.

[94] S. E. Renfrew and B. D. McCloskey, "Residual lithium carbonate predominantly accounts for first cycle CO_2 and CO outgassing of Li-stoichiometric and Li-rich layered transition-metal oxides," *Journal of the American Chemical Society*, vol. 139, no. 49, pp. 17 853–17 860, 2017.

[95] T. Hatsukade, A. Schiele, P. Hartmann, T. Brezesinski, and J. Janek, "Origin of carbon dioxide evolved during cycling of nickel-rich layered ncm cathodes," *ACS applied materials & interfaces*, vol. 10, no. 45, pp. 38 892–38 899, 2018.

[96] J. Wandt, A. T. Freiberg, A. Ogrodnik, and H. A. Gasteiger, "Singlet oxygen evolution from layered transition metal oxide cathode materials and its implications for lithium-ion batteries," *Materials Today*, vol. 21, no. 8, pp. 825–833, 2018.

Cations influence on disproportionation induced $^1O_2$

For many centuries chemists labored to change lead into precious gold, and eventually found that precious uranium turned to lead without any human effort at all.

Isaac Asimov

Contents

Figures

Introduction

Singlet oxygen presence in metal-air batteries has been established in the previous chapter. Considering its high reactivity, $^1O_2$ can be ascribed as a culprit for the severe parasitic reactions encountered in metal-air technologies. If singlet oxygen can be produced by alkali direct oxidation, it was also found during discharge in Li-O_2 cells and while resting after discharge in Na-O_2 ones. Superoxide disproportion, directly related to the formation of lithium and sodium peroxide as illustrated in 3.1, produce singlet oxygen and correspond well to the decrease yield observed. A sizeable part of the metal-air cells uncyclability could hence be imputed to disproportionation. This reaction is the only known mechanism capable of producing $^1O_2$ during discharge or at rest in Li/Na-O_2 chemistry.

Superoxide disproportionation relationship with side reactivity impose a strive to understand its underlying chemical mechanism. Disproportionation was already consider as a crucial process in lithium-air batteries through the so-called solution mechanism, already described in part. **Intro discharge**. As (su)peroxide are insulating solids, they can quickly passivate the electrode surface, reducing the achievable capacities. Disproportionation allows solid peroxide formation in solution resulting in higher capacities. A consequence is the search for favourized solution pathway by the choice of electrolyte or additives use. Yet, $^1O_2$ production by disproportionation imposes a certain plight to the technology and only unravelling more in–depth mechanistic descriptor for this reaction will enable full potential of metal-air batteries.

Disproportionation, as a chemical process, is greatly influenced by the media. In part. **Intro discharge**, it was shown that the solvent or additives choice influence superoxide disproportionation by stabiliwing its solvated state. Concerning $^1O_2$ production rate, we observed a higher singlet oxygen yield with Na$^+$ than with Li$^+$ in part. **Production of singlet oxygen disp**, despite sodium lower Lewis acidity. The cations appears thus to have a strong influence on $^1O_2$ production induced by disproportionation.
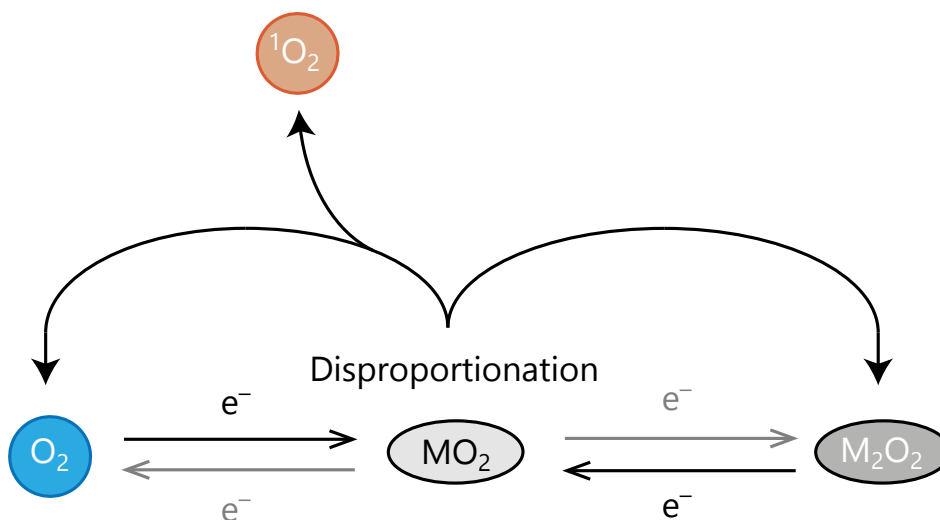
Figure 3.1: **Illustration of the disproportionation process in Li/Na-O_2 cells and the induced $^1O_2$ production.**

To decipher the cations influence on the disproportionation reaction, we put in place mechanistic descriptor confirmed both experimentally and by calculations. To do so, we first studied the disproportionation reaction of chemically produced solvated superoxide in

presence of different cations and their influence. As the cations Lewis acidity governs the disproportionation driving force (formation of solid peroxide), the cations studied covers a large range of Lewis acidity used in metal–air batteries as alkaline cations or typical ionic liquids cations. The results confirms that inversely to the driving force, the $^1O_2$ production increase with soft Lewis acid presence. As low Lewis acidity cations would not drive by themselves, this increase is only see for cations mixtures with Li^+ or Na^+.

Density functional theory (DFT) calculation were conducted in collaboration with Sapienza university to understand the reaction pathways in presence of the different cations. As disproportion evolves through LiO_2 clusters formation, here strictly modelled by dimers, these clusters can be formed in the singlet state with a certain energy cost. The presence of low Lewis acidity cations appears to reduce the activation energy to the singlet state, enhancing the proportion of $^1O_2$ compared to $^3O_2$.

Li-O_2 cells were analysed further during (dis)charge to show the presence of disproportionation process as well as cations influence during actual cells cycling. The consumption/production of O_2 clearly showed presence of disproportionation and its influence on side products formation. The presence of low Lewis acid increased the formation of carbonates on discharge where $^1O_2$ is produced by disproportionation in higher proportion. Presence of disporoportionation in metal–air cells has serious consequences, notably on electrolyte, additives and aimed discharge products that will be discussed more in-depth.

3.1 Disproportionation of chemically produced solvated superoxide

As disproportionation is a spontaneous chemical reaction, it can be studied outside a cell by dint of the stable potassium superoxide. To characterized disproportionation chemistry, solvated peroxide occurs as a better proxy than KO_2 powder to avoid possible surface chemistry effects. KO_2 can be solvated by crown ether (as 18-crown-6(1,4,7,10,13,16-hexaoxacyclooctadecane)) in TEGDME[2]. In a similar fashion than discussed in part **Singlet oxygen disporoprtionation**, disproportionation reaction could be characterized by the amount of $^3O_2/^1O_2$ release as well as Li_2O_2/Na_2O_2 yield and carbonate production. The disproportionation was driven by injecting different cations in TEGDME based electrolytes. The reaction yield and carbonate amount were determined by coupling mass spectroscopy and UV titration after complete reaction according to the oxygen release, as described in **Annexes method**[3].

     The O_2, $^1O_2$, peroxide and carbonates production via dissolved superoxide disproportionation are given in fig. 3.2. With Li^+ addition, the reaction yield similar amount of $^3O_2$ and $^1O_2$ than with solid KO_2 shown in part **Singlet oxygen disporoprtionation**, i.e. $\sim 93\% ^3O_2$, $\sim 2\%$ $^1O_2$ and a correspondant $\sim 93\%$ peroxide. Na^+ electrolyte addition gives in turn similar results than on solid KO_2, i.e., $\sim 83\% ^3O_2$, $\sim 13\%$ $^1O_2$ and a $\sim 85\%$ peroxide yield as the reaction reached completeness. Simulating proton source by adding 0.1 M trifluoroacetic acid (F_3CCOOH) as additive to the lithium electrolyte, singlet oxygen production presents a slight increase with $\sim 91\%$ $^3O_2$/peroxide yield and 3% $^1O_2$. Albeit shallow, this $^1O_2$ increase might indicates water assisted disporoportion and partly explain the increased $^1O_2$ production in Li–air cell with addition of water[4].

Change Na+ + H+ for Na+ + TBA+
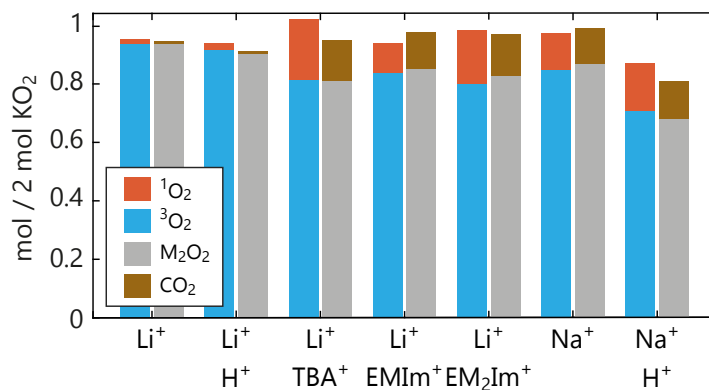
Figure 3.2: **O_2, $^1O_2$, peroxide and carbonates production via dissolved superoxide disproportionation.** Dissolved peroxide in TEGDME is obtained by mixing KO_2 powder in presence of an 18-crown-6 ether equimolar ratio in solution. To drive disproportionation and quantify singlet oxygen, a TEGDME electrolyte composed of 30 mM DMA, 0.5 M Li^+/Na^+ and either no additives, 0.1 M TBA^+, $EMIm^+$, EM_2Im^+ or F_3CCOOH is added to the dissolved O_2^-. THe scale represent the theoretical yield of 1 mol O_2 and peroxide per 2 mol of KO_2 according to eq. 2.6. The repeatability of the obtained value can be found in **Annexes Repetatbility S4**

     Rather than only testing pure Li^+ or Na^+ electrolytes, salt combinations to drive superoxide disproportionation in soft Lewis acid presence were also tested. The chosen organic cations covers a different range of Lewis acidity, namely in descending Lewis acidity TBA^+, $EMIm^+$, and EM_2Im^+[5]. As described in part. **singlet reactivity and side reactivity**, super-

oxide and singlet oxygen are prone to react with organic species and their stability was assessed beforehand. TBA is known to be stable coupled with superoxide[6,7]. Imidazolium salt stabilities towards superoxide were tested by ^{1}H-NMR before after 1 hour contact either with KO_2 powder or photochemically produced singlet oxygen according to **Annexes singlet photochemical**. On one hand, the cations showed good stability towards singlet oxygen, as illustrated in fig. 3.3(a). Singlet oxygen, being electrophile, appears mainly active towards electron-rich species[8]. On the other hand, imidazolium are unstable with KO_2 with the numerous apparition of decomposition products on the ^{1}H-NMR spectrum as shown in fig. 3.3(b). These results concords with previous instability report[9].
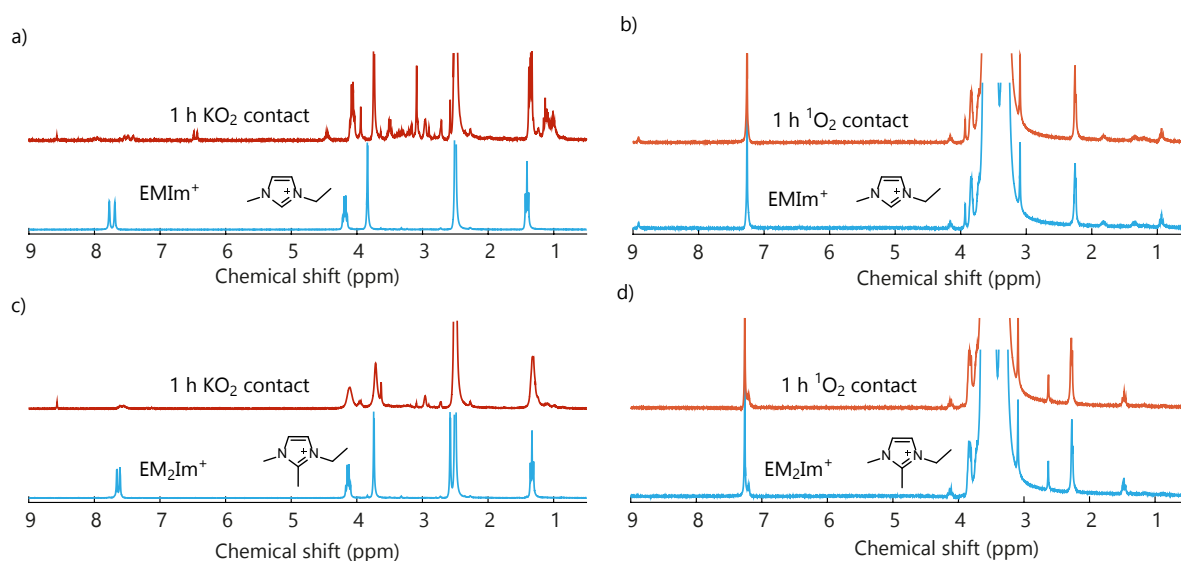
Figure 3.3: Imidazolium stability study in presence of KO_2 and $^1O_2$ by ^{1}H-NMR in CDCl$_3$. The first line characterize EMIm$^+$ and the second line EM$_2$Im$^+$. (a) and (c) show ^{1}H-NMR of imidazolium before and after 1 hour contact with KO_2 dissolved in TEGDME, respectively in blue and red. (b) and (d) show ^{1}H-NMR of imidazolium before and after 1 hour contact with $^1O_2$ in O_2 saturated TEGDME, respectively in blue and orange. $^1O_2$ was produced photochemically, according to a previously described method[4] and further described in **Annexes**, by dint of 1 μM *meso*-tetra(4-fluorophenyl9tetrabenzoporphyrin (Pd$_4$F) and illumination at 643 nm.

Tertiary amines are known $^1O_2$ quenchers that physically deactivate (quench) $^1O_2$ to $^3O_2$[10]. By their chemical natures, Imidazoliums could partially quench singlet oxygen and reduced the detected amount by DMA–O_2 conversion. At low imidazolium concentrations, the quenching effect is not expected to be significant as the amine quenching efficiency decrease with the species oxidation potential[10? ,11] **citer mediator paper**; At high concentration, imidazolium salt showed appreciable quenching effect. As a token of quenching, the consumption of DMA were measured by UV spectrometry in presence of photochemically produced $^1O_2$ with or without quencher addition. Competitive reactions between the quencher and DMA with $^1O_2$ leads to a slower reaction DMA reaction rate which indicates a good quenching efficiency compare to DMA reactivity. More detail on this method is given in **Annexe Quencher**. As shown in fig. 3.4, 0.1 M EMIm$^+$ in TEGDME results in a much slower DMA decay; The amount of $^1O_2$ quenched during the experiment cannot be neglected. Imidazolium experiments were still conducted, keeping in mind that the $^1O_2$ yield presented are underestimated and a part of the side reactions imputed to its superoxide instability.
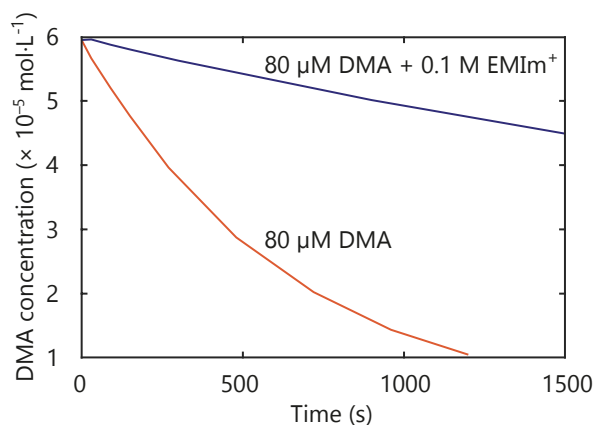
Figure 3.4: $^1O_2$ quenching effect of Imidazolium cation. In orange, DMA concentration decay over time in presence of photochemically produced $^1O_2$ according to **Annexes**. In purple, DMA concentration decay over time in presence of photochemically produced $^1O_2$ and 0.1 M EmIm$^+$. The decrease of the DMA reaction rate indicates other $^1O_2$ decays pathways as quenching by EMIm$^+$. The electrolytes used are based one 80 μM DMA and 1 μM Pd$_4$F in TEGDME illuminated at 643 nm.

Disproportionation in presence of weak Lewis acid organic cations enhanced noticeably the production of $^1O_2$ in 3.2. For Li$^+$ electrolyte, the value cut down to value close to the pure Na$^+$ electrolyte with $\sim$ 80–85% yields for $^3O_2$ and Li$_2O_2$ accompanied by a growth of $^1O_2$ and carbonates yields ($\sim$ 10–20%). Mixing Na$^+$ and TBA$^+$ results in a similar trends; $^3O_2$ and Na$_2O_2$ yields decrease to $\sim$ 70% while $^1O_2$ reached $\sim$ 16%. This similar trend with TBA$^+$ suggests that the presence of weaker Lewis acidic cations during disproportionation drives $^1O_2$. In any case, the increase of $^1O_2$ is always accompanied by an increase in carbonates, hence side-products formation, as well as a decrease in $^3O_2$ and peroxide yield; These yields are moreover similar. The missing peroxide and the side-productions formation appears well connected to the formation of $^1O_2$ as suggested before[4,12].
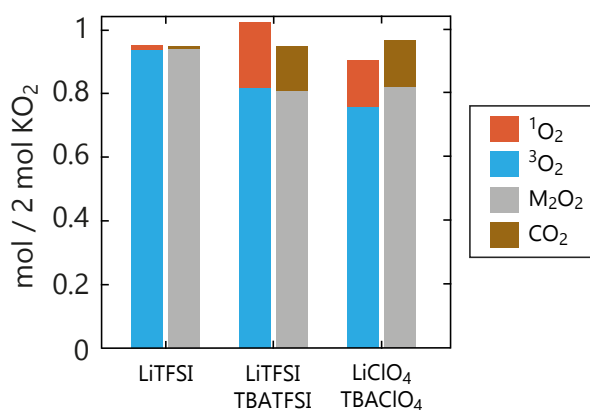
Figure 3.5: Influence of the anions used during this study on disproportionation. O$_2$, $^1O_2$, peroxide and carbonates production via dissolved superoxide disproportionation using electrolytes with different counter anions. Dissolved peroxide in TEGDME is obtained by mixing KO$_2$ powder in presence of an 18–crown–6 ether equimolar ratio in solution. The electrolyte injected to drive disproportionation is either 0.5 M LiTFSI, or 0.2 M Li$^+$/TBA$^+$ (5:1 ratio) with TFSI$^-$ or ClO$_4^-$ as counter ions. Albeit slight variation of amount detected, the same conclusion can be drawn upon cations influence.

Disproportionation characterizations in presence of the different counter anions used in

this study (TFSI$^-$ and ClO$_4^-$) shows a similar trend for the same cations, as depioted in fig 3.5. The influence of the anions is then disregarded in the rest of this chapter has they possess rather similar donor numbers and should not affect the result conclusions[13,14], as discussed in part. **Intro Discharge**.

3.2 Thermodynamic aspect of cations influence

~~Low~~ Lewis acid cations drive $^1O_2$ production; The reaction ~~mechanistic~~ must thus be influenced by the cations ~~in~~ presence. To understand the ~~different~~ disproportionation ~~relative~~ energies and their underlying reaction pathways, DFT calculation were performed. The different routes to $^3O_2$ and $^1O_2$ were scrutinized in presence of LiO_2 and NaO_2 as starting materials in presence of H^+, TBA^+, K^+ or Li^+/Na^+ respectively.

Energies were calculated for solvated species using the continuous C–PCM solvation model with a mean dielectric constant of $\epsilon = 7.28$ (resembling that of glyme as previously done[15]) and using the hybrid GGA DFT M06–2X functional. More details on the calculation method can be found in **Appendix calculation DFT**. As disproportionation ~~favours clusters~~ formations over superoxide monomers[7,16,17], different pathways might arise through the formation of different superoxide dimer $M(O_2)_2M'$ (M being Li^+ or Na^+, and M' being Li^+, Na^+ K^+ H^+ or TBA^+). The dimers consequently release O_2 molecules and a MO_2M' peroxide. After ion exchanges, M_2O_2 is obtained and precipitate as solid peroxide **Add Table S4 in appendix**. The overall driving force is, in this case, the formation of solid $M_2O_2(s)$ as previously shown in the case of Li chemistry both in gas and liquid phase[7,16] and illustrated in fig. 3.6. As a side note, the calculations presented here presuppose that only superoxide dimers will be formed as a first approximation. The formation and disproportionation of more complex superoxide clusters might be favoured at longer terms and change the energy difference but the energy tendencies were hypothesised to be similar[17].
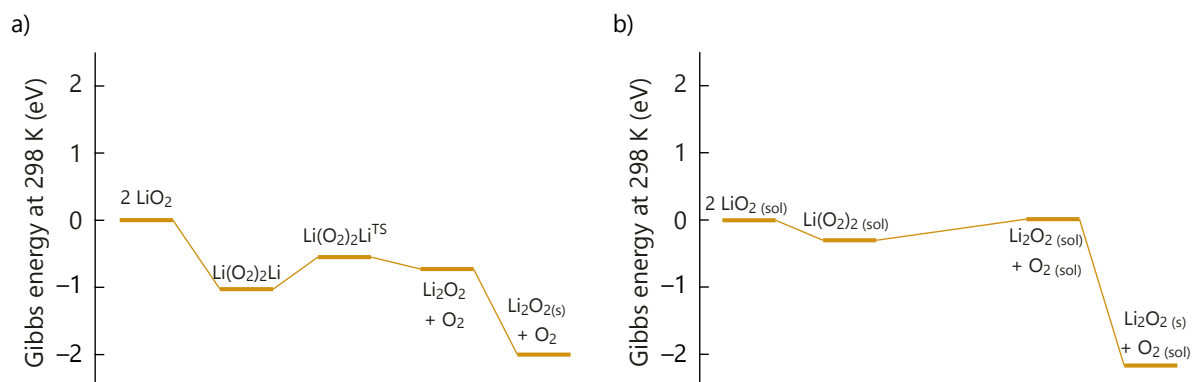
Figure 3.6: **Literature reported reaction free energy profiles for $^3O_2$ release from LiO_2 disproportionation as reported in the gas phase[16] or solution phase[7].** The reaction pathways are adapted from the two previously cited publications. If unspecified (either solvated or solid state), the species are in the gas phase. As indicated by the energy profiles, the ~~reaction~~ overall driving force is the largely favoured peroxide precipitation.

Superoxide dimers $M(O_2)_2M'$ (M,M') = H, Li, Na, K

Bi-pyramid (D_{2th})   Cage (C_{2v})

Chain (C_{2v})   Chair (C_i)

Superoxide dimer anions $[M(O_2)_2]^-$ (M,M') = H, Li, Na, K

Distorted Tetrahedron (D_4)   Distorted Tetrahedron (D_4)
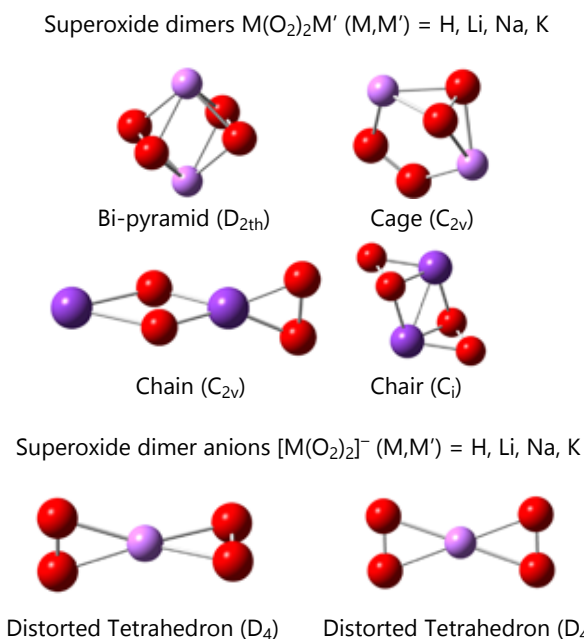
Figure 3.7: **Computed structures of neutral and negatively charge superoxide dimers ($M(O_2)_2M'$ and $M(O_2)_2^-$) with M and M' being H, Li, Na or K.**

As superoxide dimers can have different configurations[16], only the most stable ground state structures collected after calculation will be presented in the following chapter **Add Table S1 and the text with it in annexes**. The considered dimers configurations are given in fig. 3.7. The reaction energy for the precipitation to solid peroxides was calculated with thermochemical cycles starting from DFT calculations, the assessed thermodynamic properties of solid phases and for neutral atoms in the gas phase[18]. **put in appendix** The thermodynamics of the $TBA^+O_2^-$ ion couple was calculated at the same level of theory by relaxing the solid ionic couple in the simulated solvent to a ground state minimum[19]. **put in appendix** The energy are presented taking the more favoured pure solvated alkali superoxide as reference (2 LiO_2 or 2 NaO_2). The energetic influence of cation additions and the new reaction pathways are more easily comparable with such scales. As discussed in part. **Side reaction intro**, activation energies superior to 1 eV (100 kJ.mol^{-1}) are considered to be sufficiently high to ensure low reaction kinetic at room temperature.

The present model rests on superoxide dimer formations either in a triplet state or a singlet state, releasing respectively $^3O_2$ and $^1O_2$ during disproportionation. The most simple pathway is the one of a pure Li^+ or Na^+ electrolyte presented in fig. 3.8 and 3.9, respectively in yellow and green. The dimerization free energies are given in tab. 3.1 for the different cations **mettre en annexes**. The pathway resulting in triplet oxygen with LiO_2 is similar to the one already accepted from literature and showed in fig. 3.6(b)[7]. First, a $^3Li(O_2)_2Li$ dimer is form due to a slight stabilization compared to two LiO_2 monomers. The dimer then disproportionate in Li_2O_2 and $^3O_2$ in a second step despite being weakly endergonic by dint of a strong driving force to precipitate and form the stabilized solid Li_2O_2 as a final product, as given in tab. 3.2. Now considering the singlet oxygen pathway for pure Li^+ electrolyte, the consecutive steps are similar but the energy profile differently distributed. The most unfavourable step is the $^1Li(O_2)_2Li$ dimer formation with a ~ 1 eV thermodynamic barrier, the reaction being favourable for the rest of the reaction up to the formation Li_2O_2. The ~ 1 eV activation energy leads to small formation occurrence despite the strongly favoured overall disproportionation.
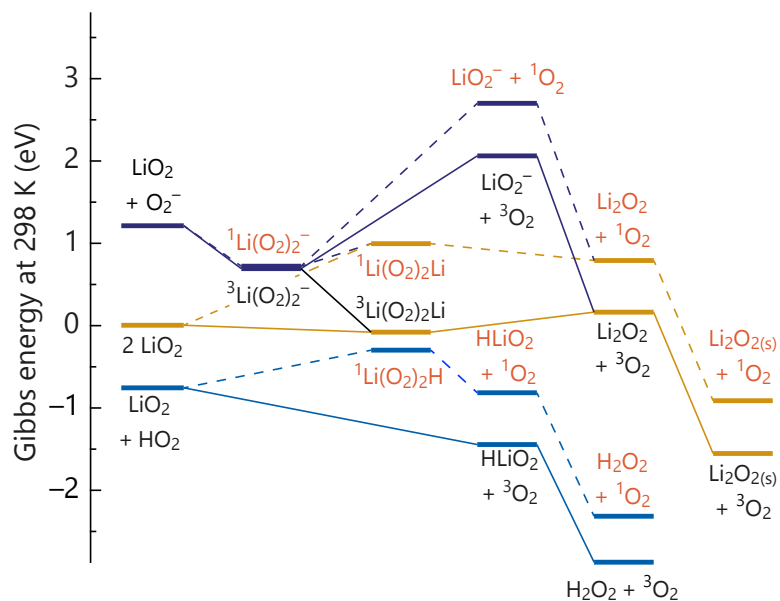
Figure 3.8: **Calculated free energy profiles for superoxide disproportionation in presence of Li+ and H+ traces.** The reaction forms peroxide and O_2, either in singlet (dashed line) or triplet state (full line). More details about the calculation can be found in **Annexes calculation**.
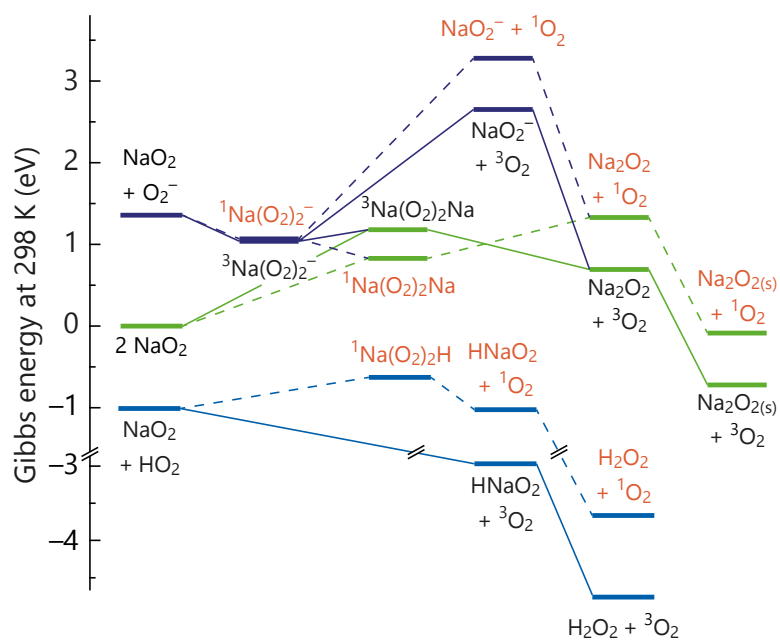
Figure 3.9: **Calculated free energy profiles for superoxide disproportionation in presence of Na+ and H+ traces.** The reaction forms peroxide and O_2, either in singlet (dashed line) or triplet state (full line). More details about the calculation can be found in **Annexes calculation**.

Table 3.1: **Calculated superoxide dimerization free energy at 298 K in presence of respectively Li$^+$ and H$^+$ traces or Na$^+$ and H$^+$ traces illustrated in fig. 3.8 and 3.9.** A blank cell represent a vibrationally unstable molecules. More details on the calculations are given in **Annexes Calculation**

Stoichiometry	$\Delta_r G^0_{298\,K}$ singlet (eV)	$\Delta_r G^0_{298\,K}$ triplet (eV)
2 LiO$_2$ $\longrightarrow$ Li(O$_2$)$_2$Li	0.99	−0.08
LiO$_2$ + O$_2^-$ $\longrightarrow$ Li(O$_2$)$_2^-$	−0.49	−0.52
LiO$_2$ + HO$_2$ $\longrightarrow$ H(O$_2$)$_2$Li	0.45	
2 NaO$_2$ $\longrightarrow$ Na(O$_2$)$_2$Na	0.83	1.18
NaO$_2$ + O$_2^-$ $\longrightarrow$ Na(O$_2$)$_2^-$	−0.29	−0.32
NaO$_2$ + HO$_2$ $\longrightarrow$ H(O$_2$)$_2$Na	0.38	

Table 3.2: **Precipitation free energy of solid alkaline peroxides form solution phase at 298 K.**

Peroxide	$\Delta_r G^0_{298\,K}$ (eV)
Li$_2$O$_{2\text{(solvated)}}$ $\longrightarrow$ Li$_2$O$_{2\text{(solid)}}$	−1.71
Na$_2$O$_{2\text{(solvated)}}$ $\longrightarrow$ Na$_2$O$_{2\text{(solid)}}$	−1.40
K$_2$O$_{2\text{(solvated)}}$ $\longrightarrow$ K$_2$O$_{2\text{(solid)}}$	−2.31

Considering NaO$_2$, the overall disproportionation process results also in products stabilization although less than for LiO$_2$. The dimers formation is yet energy costly for NaO$_2$ in both triplet and singlet states. Nevertheless, the singlet dimer is less endergonic than the triplet state with 0.83 eV compared to a 1.2 eV barrier. The $^1O_2$ disproportionation step is however unfavored by 0.5 eV while $^3O_2$ release is exergonic by −0.5 eV. The total energy needed for Na$^+$ disproportionation towards $^1O_2$ is then more exergonic by $\sim$ 0.1 eV compared to $^3O_2$. NaO$_2$ disproportionation is highly depend on the solvent use[20]. Solvated NaO$_2$ appears almost kinetically stable in high DN solvent while disproportionate relatively fast in low DN solvent. A low DN stabilize less the superoxide in solution as described in part **intro discharge** and might rise the solvated NaO$_2$ energy decreasing at the same time the energy difference with the dimer formation. Nevertheless the endergonicity of the dimers formation for NaO$_2$ could partly explain its relative stability in Na–O$_2$ cells[21].

The experimental differences observed between LiO$_2$ and NaO$_2$ concord well with the calculated single step barriers and overall driving forces. The low activation energy for LiO$_2$ results in fast disproportionation kinetic and low amount of $^1O_2$ due to the strong energy barrier difference between the singlet and triplet pathways. While NaO$_2$ singlet and triplet have more similar energy barriers, causing larger $^1O_2$ release, the comparably high exergonic character of sodium superoxide disproportionation impose a slower kinetic. The high driving force due to solid peroxide formation allows relatively high energy barrier to be pass and form singlet oxygen by disproportionation.

The addition of protons opens new highly favoured disproportionation pathways in Li$^+$ electrolyte, as shown in fig. 3.8. The HO$_2$ formation is by himself endothermic and leads to the HLiO$_2$ mixed peroxide formation accompanied by a release of $^3O_2$ without formation an intermediate dimer; The reaction results in the more stable H$_2$O$_2$. Even though one might consider 2 HO$_2$ as a preferable state than mixed superoxide, H$^+$ is considered here as a contaminant and in presence of a Li$^+$ large excess. The singlet reaction path still requires the

$^1Li(O_2)_2H$ dimer formation via a 0.46 eV barrier, which releases $HLiO_2$ and $^1O_2$ in a -0.52 eV exergonic step that continue downhill to reach H_2O_2. Analogous results were obtained for the NaO_2–HO_2 pairing as illustrated in fig. 3.9. As singlet path is exergonic, albeit less than for Li^+/Na^+ alone, and the triplet path only endothermic, only minor yield of $^1O_2$ can be expected by water induced disproportionation. This is in accord with experimental findings in fig. 3.2, which shows very light additional $^1O_2$ production with protons traces compared to pure Li^+ electrolyte. From the calculations and experiments, proton sources appear to cause only minor additional $^1O_2$ compared to disproportionation in Li^+ electrolyte.

Disproportionation induces more $^1O_2$ production in presence of the weak Lewis acid TBA^+ as shown in fig. 3.2 and fig. 3.5. The main developed hypothesis is based on the weaker O_2^-–TBA^+ interaction than O_2^-–M^+ [6,22,23]; The asymmetric pairing of superoxide would destabilize intermediates, reduce the energy barriers, and hence make $^1O_2$ production more favourable. Computing the asymmetric $Li(O_2)_2TBA$ would be extremely difficult because of the large number of electrons. Considering the weak association of the O_2^-–TBA^+ ion pair even in low dielectric constant solvents like DME ($\Delta_{diss}G^0 = 0.44$ eV), $TBAO_2$ may be at first approximated by the free solvated O_2^- anion. O_2/LiO_2 and $O_2/TBAO_2$ standard potentials in DME differs by 1.24 V[23], which agrees well with the estimated 1.21 eV for the dissociation energy of LiO_2 to free O_2^- anions, as given in **Annexes S4**. O_2^- does not have to form via dissociation of LiO_2 which would not result in appreciable O_2^- concentration; O_2^- may form as a transient species upon O_2^- generation before the initially formed O_2^- binds with Li^+ [6,24]. O_2^- exist in Li^+/TBA^+ mixtures even in low DN solvent as MeCN, where LiO_2 dissociates particularly poorly[6]. In more strongly solvating electrolytes such as DMSO, O_2^- life time is long enough in 0.1 M Li^+, TBA^+ free, electrolyte to allow for some reversiblility to the O_2/O_2^- couple. Glyme used in this study lies between MeCN and DMSO in terms of LiO_2 solvation strength, as explained in part. **Discharge intro**. The fig 3.2 shows well that TBA^+ strongly impact disproportionation in mixtures with Na^+ or Li^+ and must hence influence the O_2^- binding state.

The DFT calculations showed in fig. fig. 3.8 and 3.9 confirm the suggested destabilizing mechanism, respectively in presence of Li^+ and Na^+. The first step for Li^+ proceeds via formation of $^3Li(O_2)_2^-$ or $^1Li(O_2)_2^-$ dimers that are stabilized to a close value versus $LiO_2 + O_2^-$, -0.52 eV and -0.49 eV, respectively. Ongoing disproportionation pathways to the charged LiO_2^- peroxide species would face prohibitively high energy barriers in either states because of the large Li_2O_2 dissociation energy to $LiO_2^- + Li^+$. A more facile pathways is however possible, as a $Li(O_2)_2^-$ dimer can easily proceed to an ion exchange to form a $Li(O_2)_2Li$ dimer. The disproportionation can then continue through the pure lithium disproportionation mechanism described previously. If the reaction road is then similar to that of a pure Li^+ electrolyte, the presence of TBA^+ decreases the barrier towards $^1O_2$; In any case, the most endergonic step is $^1Li(O_2)_2Li$ formation which pass from ~ 1 eV to a mere 0.27 eV in presence of TBA^+. The proportion to each pathway is not given by the energy difference between $^1Li(O_2)_2Li$ and $^3Li(O_2)_2Li$, but the largest barrier in the respective free energy profiles; The smaller $^1Li(O_2)_2Li$ formation energy result in acceleration of the singlet path. Analogously, the asymmetric $NaO_2 + O_2^-$ pairing passes via $Na(O_2)_2^-$ and $Na(O_2)_2Na$ dimers and the barrier towards $^1O_2$ decreases from 1.2 eV to 0.4 eV. The weak Lewis acid TBA^+ opens paths that facilitate the most unfavourable reaction steps and hence strongly enhance $^1O_2$ evolution.

Several recent works have proposed mixed alkali cation electrolytes for metal-O_2 cells to influence solution equilibria and possibly improve cell characteristics[25–29]. For completeness, LiO_2 with KO_2 as well as NaO_2 with KO_2 or LiO_2 disproportionation pathways have been calculated and are respectively illustrated in fig. 3.10, 3.11 and 3.12. The asymmetric intermediates and peroxide products (LiO_2Na, NaO_2K, and LiO_2K) are not likely compared to

the symmetric pathways. Disproportionation of mixed dimers is less favourable since more exergonic; Li_2O_2 or Na_2O_2 production will hence more likely involves ion exchange towards the stronger lewis acid ~~in presence~~ and further proceed via the symmetric cases described earlier.
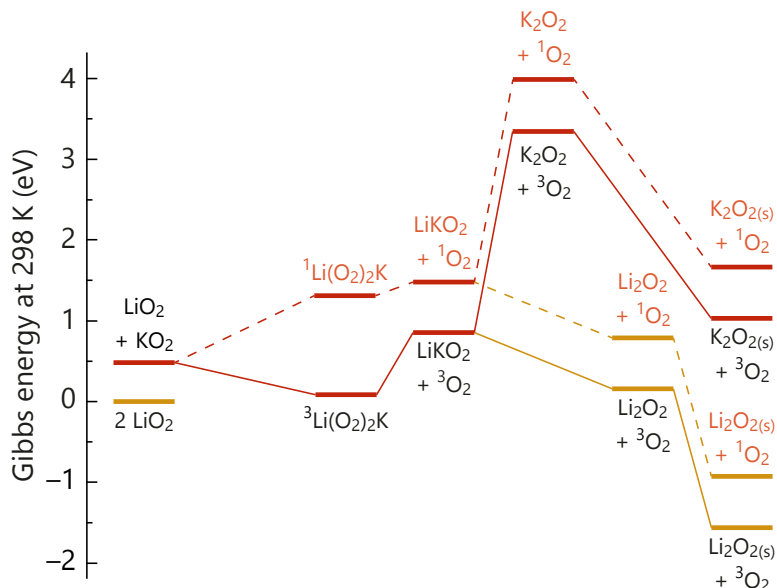
Figure 3.10: **Calculated free energy profiles for superoxide disproportionation in the presence of Li⁺ and K⁺.** The reaction forms peroxide and O_2, either in singlet (dashed line) or triplet state (full line). More details about the calculation can be found in *Annexes calculation*.
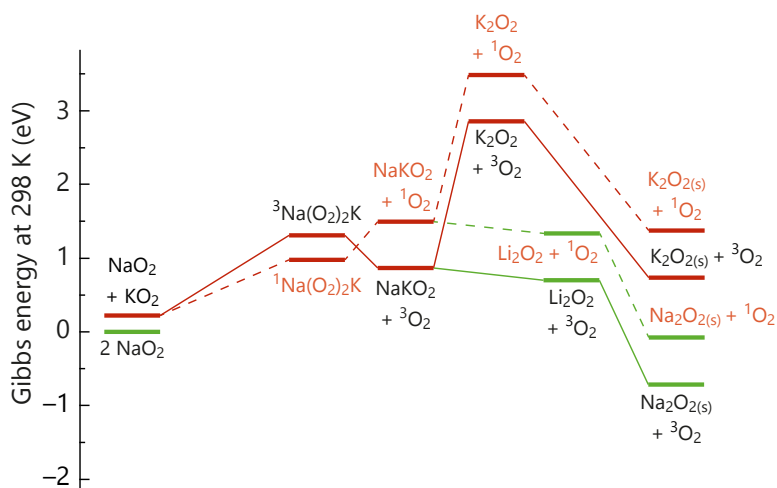
Figure 3.11: **Calculated free energy profiles for superoxide disproportionation in the presence of Na⁺ and K⁺.** The reaction forms peroxide and O_2, either in singlet (dashed line) or triplet state (full line). More details about the calculation can be found in *Annexes calculation*.
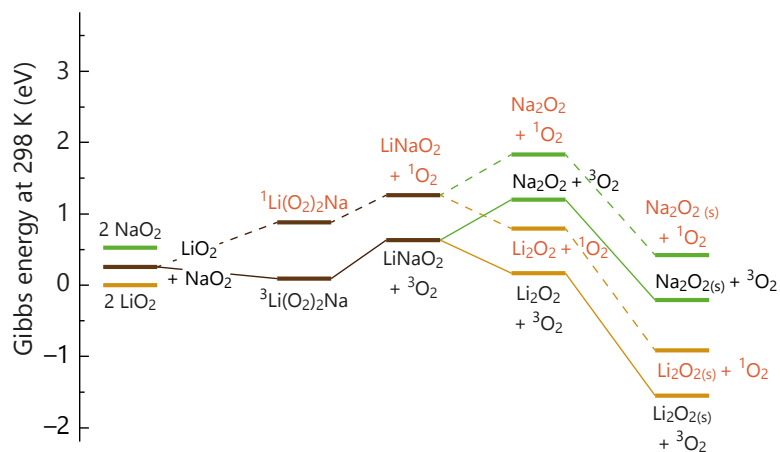
Figure 3.12: **Calculated free energy profiles for superoxide disproportionation in the presence of Li⁺ and Na⁺.** The reaction forms peroxide and O_2, either in singlet (dashed line) or triplet state (full line). More details about the calculation can be found in *Annexes calculation*.

3.3 Disproportionation during Li-O$_2$ cell cycling

Both chemical study and DFT calculation show $^1O_2$ production can be induced by superoxide disproportion. This phenomena remains to be proven during cells operation. The reaction yield and $^1O_2$ as well as carbonates production have been characterized during -O$_2$ cells cycling in either pure or mixed with weak Lewis acid cations Li$^+$ electrolyte. Li-O$_2$ chemistry was chosen since disproportionation is most significantly driven by thermodynamics, as shown in fig. 2.11(d). The cells are composed of carbon black cathodes and TEGDME electrolytes containing 30 mM DMA with either only 0.1 M Li$^+$ or a total of 1 M salt with a Li$^+$/TBA$^+$ ratio of 1:9 or 1:99. The emphasis is put on TBA$^+$ as weak Lewis acid since it avoids the further complications of imidazolium instability with O_2^-: The measurement details are given in **Annexes**.

3.3.1 Discharge

Considering first discharge, the cells were run at constant current and the gaz consumption followed using a pressure transducer and represented in fig. 3.13(a)-(b). The method is further described in **annexes + methods singlet**, assuming that the only gas consume is oxygen[30]. $^1O_2$, Li$_2$O$_2$, and carbonate were quantified after electrolyte and cathodes extraction by a HPLC, mass spectroscopie and UV-vis spectroscopy combination as defined in **annexes + methods singlet**. The values are expressed in mol per 2 mol e$^-$ passed in fig 3.13(c); An ideal reaction yields/consumes 1 mol Li$_2$O$_2$/O$_2$ per 2 mol e$^-$ according to eq. 2.6.

Discharge in pure Li$^+$ electrolyte resulted in a ratio of 1.98 e$^-$/O$_2$ in fig. 3.13(a), close to the ideal ratio of 2 e$^-$/O$_2$, and a Li$_2$O$_2$ yield of 94%, both in accord with previous reports for similar cells[31][30][32][33]. The $^1O_2$ yield is $\sim 3\%$ and hence similar to that found by chemical disproportionation with a similar electrolyte, illustrated in fig. 3.2. Using a mixed electrolyte with Li$^+$:TBA$^+$ ratio of 1:9 (1:99), the reaction yield remarkably decreases in fig. 3.13(a)-(b); The e$^-$/O2 ratio and Li$_2$O$_2$ yield dropped to 1.74 (1.70) and 85% (81%), respectively. As the Li$_2$O$_2$ yield decreases, the amount of $^1O_2$ and carbonate follows an inverse trends which correlate well the presence of $^1O_2$ and side reactions. Increasing $^1O_2$ yield together with decreasing Li$_2$O$_2$ yield as the electrolyte is changed from Li$^+$ to Li$^+$/TBA$^+$ mix mirrors the results obtain with dissolved superoxide in fig 3.2. The increase presence of TBA$^+$ result in a higher TBAO$_2$ occurrence and so $^1O_2$ production.
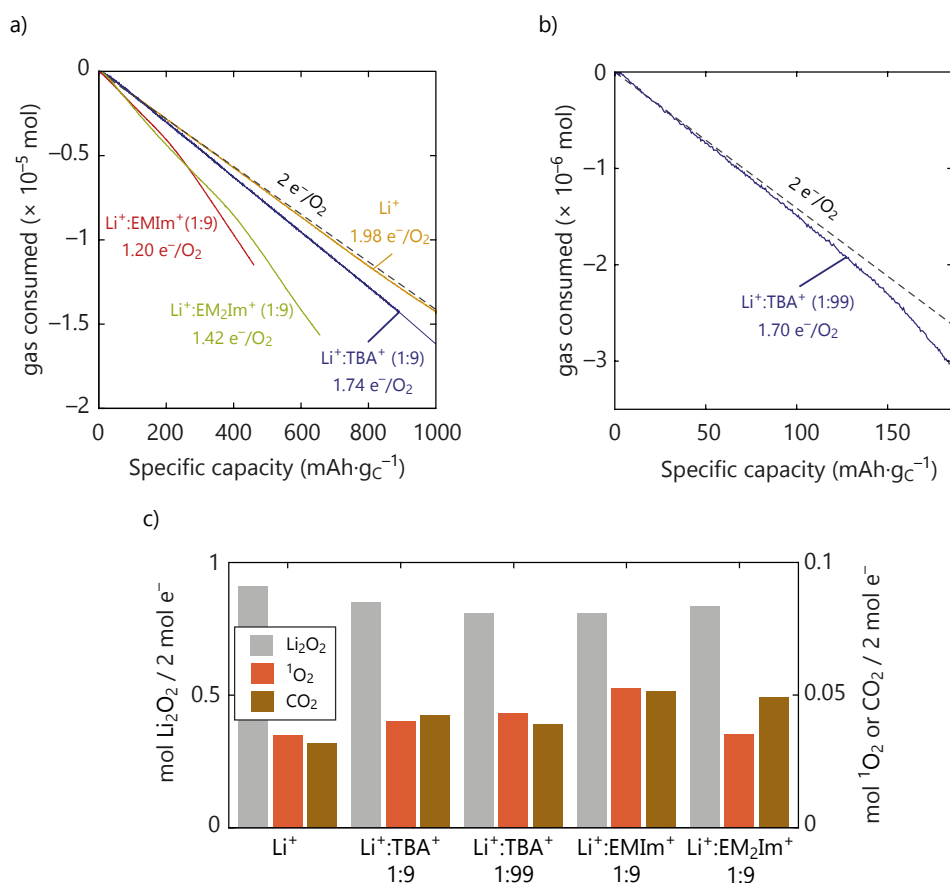
Figure 3.13: **Disproportionation and cations influence during Li–O$_2$ cells discharge.** (a)–(b) Gas evolution during a Li–O$_2$ cell discharge with a carbon black cathode and LFP counter electrode at 100 mA·g$_c$$^{-1}$. The O$_2$ saturated TEGDME elecrolytes used are composed of 30 mM DMA and either. The dashed line represent the theoritical 2 e$^-$/O$_2$. (a) 0.1 M+ or a combined 1 M salt of Li$^+$/TBA$^+$, Li$^+$/EMIm$^+$, Li$^+$/EM$_2$Im$^+$ (1:9 ratio) and (b) Li$^+$/TBA$^+$ (1:99 ratio). The method is further described in **Annexes discharge EES**. (c) O$_2$, ^{1}O$_2$, peroxide and carbonates production during discharge of the aforementioned cells. The discharge curves associated can be found in **Annexe S9**.

Deviation of the e$^-$/^{3}O$_2$ ratio from 2 does not necessarily arise from ^{1}O$_2$; Side reactions with the cations can also act as a O$_2^-$ sink, preventing alkaline peroxide formation. Discharge with imidazolium cations instead of TBA+ (1:9 ratio) further corroborates their instability with lower e$^-$/O$_2$ ratios, 1.42 and 1.2 for EM$_2$Im$^+$ and EMIm$^+$, respectively. A part of the stronger deviation compared to TBA$^+$ can be attributed to the O$_2^-$ reaction with the imidazolium cations, even though the ^{1}O$_2$ still increase compare to pure Li$^+$ electrolyte. Given the known stability of TBA$^+$ with O$_2^-$, as discussed earlier, a direct reaction can be excluded as the sink causing the decrease to 1.74 (1.70) e–/gaz. Instead, the lower ratio is in accord with TBA$^+$ enhancing the ^{1}O$_2$ fraction from O$_2^-$ disproportionation. The ^{1}O$_2$ reacting with the cell component can not be detected by the pressure transducer as it will react before.

The results on discharge are in good agreement with the chemical experiments shown in fig. 3.2, which have shown that O$_2^-$ disproportionation partly releases ^{1}O$_2$ and that the ^{1}O$_2$ fraction increases with the presence of weak Lewis acid cations as TBA$^+$. Overall, the results indicates O$_2^-$ disproportionation is the source of ^{1}O$_2$ on discharge in Li–O$_2$ cells and at rest in Na–O$_2$ cells.

3.3.2 Charge

Intermediate $Li_{2-x}O_2$ or soluble superoxide species are produced during charge in Li-O2 cells, as discussed in part. **Intro charge**[34–36]. They might undergo disproportionation to form Li_2O_2 and O_2. Through the same mechanism than during discharge, disproportionation induced $^1O_2$ could be formed and influenced by the cations in presence. To avoid influence of side products that would be formed at different rate during discharge depending on the electrolyte used, working electrode filled with chemically produced Li_2O_2 were produced according to **annexes Li_2O_2**. Similarly to discharge, the cells build with prefilled electrode were charged at constant current with TEGDME electrolytes that contained 0.03 M DMA and either only Li^+ (0.1 M) or a Li^+/TBA^+ mix (0.1 M/0.9 M); The $^3O_2$ and $^1O_2$ yield were measured by pressure monitoring and DMA conversion by HPLC after extraction as in **previous part**, assuming that the large majority of released gas is oxygen[30,32,37]. An ideal reaction yields 1 mol O_2 per 2 mol e^- according to eq. 2.6 and as for discharge the value are expressed consequently in fig. 3.14(e)–(f).

The charge voltage was first limited to 3.95 V_{Li/Li^+} since this voltage was reported to be the upper limit for quasi-equilibrium decomposition in TEGDME for similarly prefilled working electrode[35]. Charge in pure Li^+ electrolyte shows high side reactivity with a 2.40 e^-/O_2 yield in fig. 3.14(a) corresponding to ~83% of the expected O_2 evolved based on charge passed, in good agreement with previous study[31–33]. This $^3O_2$ loss is accompanied by $^1O_2$ detection which can partially be accounted for side reactions. Changing for a Li^+/TBA^+ electrolyte in fig. 3.14(b), Li_2O_2 oxidation drift even more from the theoritical yield with a 2.95 e^-/gas ratio and hence only ~68% of the expected O_2. Roughly doubled missing $^3O_2$ evolution goes along with the $^1O_2$ amount being more than doubled. Cells restricted to 3.45 V_{Li/Li^+} were also charged to exclude the possibility of $^1O_2$ evolution from a direct Li_2O_2 oxidation above ~3.5 V_{Li/Li^+}, as described in part **singlet mechanism**. Albeit reduced sensitivity due to the lower capacity passed, similar trends are observed for both $^3O_2$ and $^1O_2$, as shown in fig. 3.14(c)–(d).
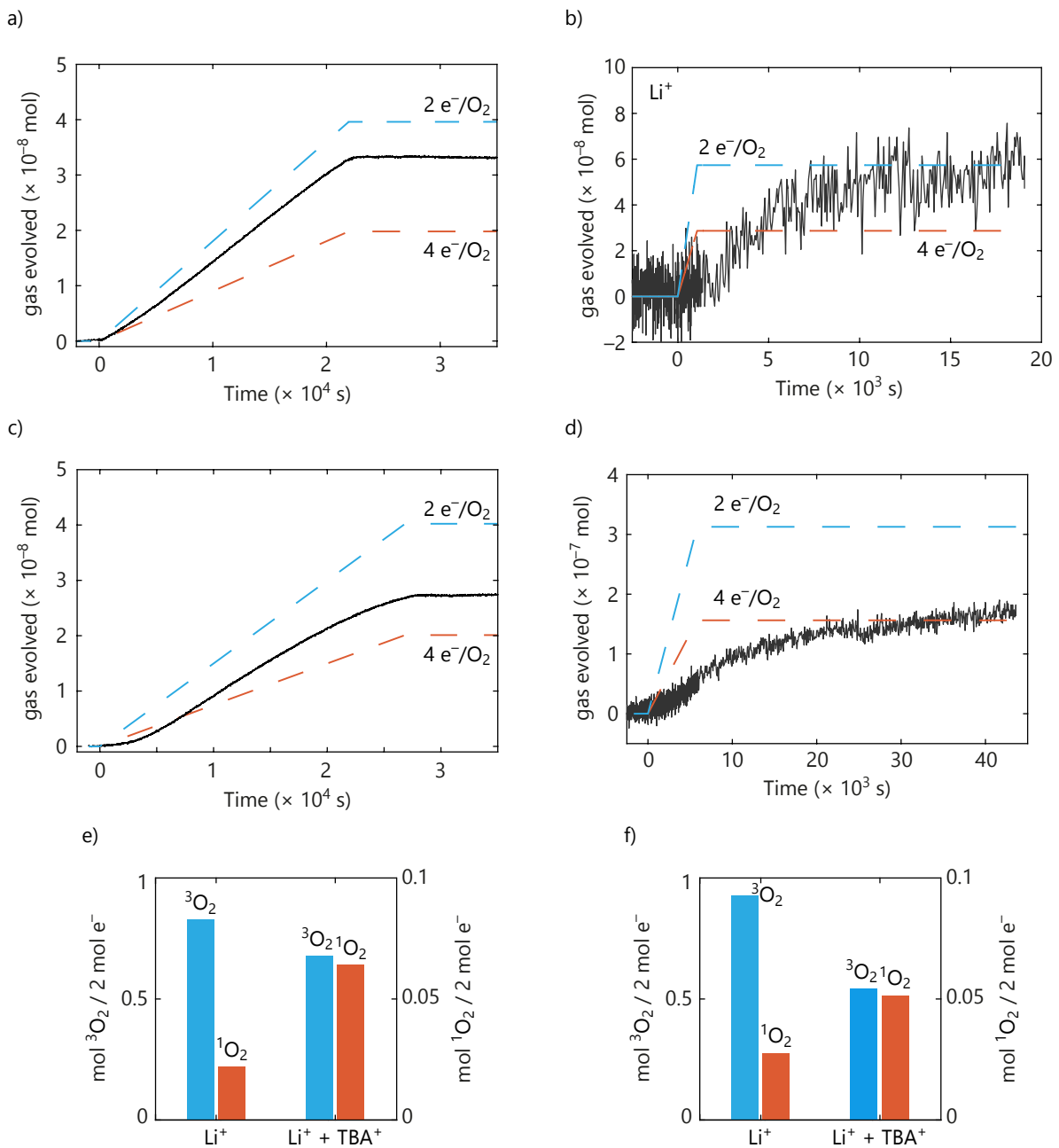
Figure 3.14: **Disproportionation and cations influence during Li-O$_2$ cells charge.** (a)-(d) Gas evolution during a Li-O$_2$ cell charge. The O$_2$ saturated TEGDME elecrolytes used are composed of 30 mM DMA and 0.1 M Li$^+$ on the first line ((a)-(b)) or a combined 1 M salt of Li$^+$/TBA$^+$ (1:9 ratio) on the second line ((c)-(d)). The prefilled carbon black cathode with chemically produced Li$_2$O$_2$ are charge at 10 mA·g$_c^{-1}$ until reaching a cut off voltage of either 3.95 V$_{Li/Li^+}$ ((a) and (c)) or 3.45 V$_{Li/Li^+}$ ((b) and (d)). After charge, the cells were kept at open circuit voltage until pressure stabilization. The blue dashed line represent the theoretical 2 e$^-$/O$_2$ and the orange one 4 e$^-$/O$_2$. More details on the cells and the method can be found in **Annexes charge EES**. (e)-(f) O$_2$, ^{1}O$_2$, peroxide and carbonates production during discharge of the aforementioned cells either up to 3.95 V$_{Li/Li^+}$ (e) or 3.45 V$_{Li/Li^+}$ (f). The discharge curves associated can be found in **Annexe S9**.

3.3.3 Mechanistic consequences of disproportionation

Altogether, the DFT calculation, as well as chemical and electrochemical experiments show that superoxide disproportionation, driven by the higher stability of the peroxide with strong Lewis acids, generates in part $^1O_2$. Additional presences of weakly Lewis acidic organic cations increases the $^1O_2$ yield. As $^1O_2$ can not be produced by direct oxidation below 3.5 V_{Li/Li^+} in Li-O_2; $^1O_2$ production below this potential threshold indicates disproportionation reaction, especially when influenced by the presence of weak Lewis acid as TBA$^+$. Taken as an indicator for disproportionation, the presence of $^1O_2$ at all stage of cycling have sizeable consequences on the reaction mechanism in metal–air batteries, especially on the second electron transfer pathway.

The correlation between missing $^3O_2$ evolution and the $^1O_2$ yield influenced by weak acid Lewis cations during discharge shows that a substantial part of the Li$_2$O$_2$ formation proceeds via disproportionation. As discussed in part. **Discharge Intro**, the disproportionation is favoured by solvent with high DN number and strongly coordinating Li$^+$ counter ions[38–40]. Disproportion is yet occurring even for weak coordinating TFSI$^+$ and medium DN solvent TEGDME as shown previously and is a crucial mechanism during discharge, especially at low overpotential[6,41]. On Au(111) in DMSO, calculated free energy of absorbed superoxide shows disproportionation to dominate direct reduction of superoxide to peroxide above 2 V_{Li/Li^+}[7].

As TBA$^+$ addition results in a continuous deviation from the 2e$^-$/O$_2$ ratio, it could indicate that solvated superoxide is present at the same concentration even at relatively high potential as ion exchange with TBA$^+$ is unlikely, see table **cite table S4 form previous subpart**. At high overpotential absorbed superoxide could be formed by supersaturation at the vicinity electrode, especially in relatively low DN number solvent. Solid superoxide facilitated formation by supersaturation was already proposed for the formation of the less soluble NaO$_2$ and hinted as influence at high overpotential in Li-O_2 chemistry[41–43]. Supersaturation effect could explain absence or low detection of solvated superoxide independently to the solvent used[6,41] and the TBAO$_2$ formation through all the discharge. A consequence of supersaturation would be an enhanced disproportionation rate at high overpotential reducing solvated superoxide concentration far away from the electrode and its detection in solution.

Concerning the charge, the presence of $^1O_2$ before 3.5 V_{Li/Li^+} demonstrates disproportionation during charge in TEGDME. Formation of soluble superoxide and subsequent disproportionate was shown during charge in high DN number[35]. Soluble superoxide was yet not detected in lower DN solvent as TEGDME. As Li$_2$O$_2$ oxidation proceed first via progressive delithiation as presented in part. **Intro charge**, the superoxide like species formed were hypothesised to disproportionate[44]. Since PITT showed a quasi-equilibrium potential around 3.5 – 3.96 V_{Li/Li^+} in glymes[44][35], oxygen evolution must proceed via disproportionation at least for early steps of charge. The influence of TBA$^+$ on the $^1O_2$ seems yet to indicate at least partially soluble superoxide in vicinity of the electrode during charge even in TEGDME despite the absence of superoxide detection afar from the electrode.

Superoxide disproportionation is then a $^1O_2$ and parasitic chemistry source during all step of cell cycling in Li-O_2 cells. NaO$_2$ is also susceptible to disproportionate albeit at slower rate due to its lower driving force and solubility[43]. NaO$_2$ is yet subject to severe degradation and peroxide formation at rest which is correlated with $^1O_2$ release as discussed in part. **Disp singlet chapter**. Singlet oxygen at rest can arise by NaO$_2$ disproportionation which also induces side reactions in Na-O_2 cells. Only KO$_2$ does not undergo disproportionation. The disproportionation reaction partially explains the higher stability of K-O_2 chemistry, especially in complete absence of protons[45], compared to lithium and sodium cells as discussed

in part. **side reactions**. Disproportionation is ~~then~~ an important process to understand side reactivity in metal–air batteries.

3.4 Direct consequences of disproportion induced singlet oxygen

Recognizing that $^1O_2$ formation is deeply rooted in the way current metal–O_2 cells operate has serious consequences on cell design, notably on the electrolyte. Weak Lewis acids are proposed as additives to enhance the solution mechanism, resulting in higher capacity as described in part. **Discharge Intro**[46,47]. Caution must be exercised with such additives as they could likewise drives $^1O_2$ production. The selected quaternary ammonium and imidazolium cations are prototypical motifs for the cations used so far in ionic liquid electrolytes for metal–O2 cells, as discussed in part. **Electrolyte Intro**[9]. Imidazoliums can be ruled out as metal-O_2 electrolytes since they readily decompose with superoxide. As ionic liquid cations suitable for electrolytes are most typically weak Lewis acids, the effect can likely be generalized considering that the organic cations would boost $^1O_2$ production[9]. Favoured $^1O_2$ formation explains why quantitative studies of metal–O2 chemistry with a broad variety of ionic liquids have shown worse parasitic chemistry on discharge and charge than molecular electrolytes, as described in part. **part electrolyte Intro**[32,48,49]. Protic additives drive $^1O_2$ formation insignificantly but may drive parasitic chemistry in other ways as by reacting with intermediate decomposition products. This is in accord with reports that found increased side reactions when water or other Brønsted acids were added[31,50,51].

Considering the discharge products itself, superoxide presence should be avoided as its favoured disproportionation in presence of Li^+ and Na^+ leads to cell degradations through $^1O_2$ release. As cells based on metastable LiO_2 or NaO_2 has been proposed to reduce the cells overpotential[21,52], its practical feasibility faces high disproportionation rate during either low rate cycling or at rest since superoxide gradually convert to peroxide and side products over time.[20,43,53–56]. Lithium and sodium peroxide, which are the thermodynamically stable products illustrated in fig. 2.10 and tab. 2.1, should be preferred. Peroxide based chemistry does not, however, prevent disproportionation during cycling; Reaction pathways by-passing the free superoxide formation steps needs to be developed. Solution to the disproportionation issue could be provided by catalyst on charge, stabilizing superoxide–like cluster[57].

Conclusion

To conclude, we ~~presented a mechanistic description for~~ $^1O_2$ ~~presence~~ at all stage of cycling and consequently a reason for parasitic chemistry in non-aqueous alkali metal–O_2 cells. We show that alkali superoxide disproportionation forms $^1O_2$ and detailed the underlying mechanism pathways and its repercussions on metal-O_2 chemistries. The different side reactivity propensity of K-, Na- and Li-O_2 ~~at least partly~~ originate from the disproportionation susceptibility of the superoxide. As disproportionation is driven by the peroxide formation for hard Lewis acid as Li$^+$, Na$^+$ or H$^+$, KO_2 remains stable in absence of additives or pollutants.

If hard Lewis acid drives disproportionation, soft Lewis acids on the contrary facilitate the formation of singlet oxygen. Superoxide disproportionation evolves oxygen via formation of a superoxide cluster either in triplet or singlet state. The presence of a weak Lewis acid, even if not driving disproportionation ~~by~~ itself, results in a lower energy barrier to a singlet state superoxide dimer and cause experimentally ~~a~~ higher $^1O_2$ formation. Since H$^+$ as additives results in ~~trivial~~ augmentation of the $^1O_2$ release, the previous $^1O_2$ production mechanism based on water induced disproportionation can be revised to alkali oxide disproportionation. Furthermore, the promising ionic liquid based electrolytes are not necessarily indicated in the case of metal-air batteries. Ionic liquids are based on soft Lewis acid organic cations that ~~would~~ enhance $^1O_2$ formation and suffers greatly from degradations. In the same vein, ~~low~~ Lewis acid additives should be used with caution~~s~~.

From our results, disproportionation is active and superoxide is at least partly present in solvated state during every reaction steps. This results in a significant degradation route in metal–O_2 cells, especially in Li$^+$/Na$^+$ containing electrolytes. The formation of metastable NaO_2 as discharge products is hence synonymous with ~~important~~ degradation during rest due to ~~low rate disproportionation~~. Advocating solution pathways for Li-O_2 for increased capacity is a double edge sword as it ~~imposes~~ $^1O_2$ ~~presence~~. Solution should be found to mediate superoxide reactivity and avoid superoxide disproportionation. As the current understanding of Na/Li-O_2 inevitably engenders $^1O_2$, its ~~reactivity should~~ be mitigated. Singlet oxygen quenchers appear well indicated to ~~deexcitate~~ $^1O_2$ before parasitic reaction with the cell components.

Bibliography

[1] E. Mourad, Y. K. Petit, R. Spezia, A. Samojlov, F. F. Summa, C. Prehal, C. Leypold, N. Mahne, C. Slugovc, O. Fontaine *et al.*, "Singlet oxygen from cation driven superoxide disproportionation and consequences for aprotic metal–O2 batteries," *Energy & Environmental Science*, vol. 12, no. 8, pp. 2559–2568, 2019.

[2] J. S. Valentine and A. B. Curtis, "Convenient preparation of solutions of superoxide anion and the reaction of superoxide anion with a copper (II) complex," *Journal of the American Chemical Society*, vol. 97, no. 1, pp. 224–226, 1975.

[3] B. Schafzahl, E. Mourad, L. Schafzahl, Y. K. Petit, A. R. Raju, M. O. Thotiyl, M. Wilkening, C. Slugovc, and S. A. Freunberger, "Quantifying Total Superoxide, Peroxide, and Carbonaceous Compounds in Metal–O_2 Batteries and the Solid Electrolyte Interphase," *ACS Energy Letters*, vol. 3, no. 1, pp. 170–176, 2017.

[4] N. Mahne, B. Schafzahl, C. Leypold, M. Leypold, S. Grumm, A. Leitgeb, G. A. Strohmeier, M. Wilkening, O. Fontaine, D. Kramer *et al.*, "Singlet oxygen generation as a major cause for parasitic reactions during cycling of aprotic lithium–oxygen batteries," *Nature Energy*, vol. 2, no. 5, p. 17036, 2017.

[5] K. Abraham, "Electrolyte-directed reactions of the oxygen electrode in lithium-air batteries," *Journal of The Electrochemical Society*, vol. 162, no. 2, pp. A3021–A3031, 2015.

[6] L. Johnson, C. Li, Z. Liu, Y. Chen, S. A. Freunberger, P. C. Ashok, B. B. Praveen, K. Dholakia, J.-M. Tarascon, and P. G. Bruce, "The role of LiO_2 solubility in O_2 reduction in aprotic solvents and its consequences for Li–O_2 batteries," *Nature chemistry*, vol. 6, no. 12, p. 1091, 2014.

[7] Y. Zhang, X. Zhang, J. Wang, W. C. McKee, Y. Xu, and Z. Peng, "Potential-dependent generation of O_2^- and LiO_2 and their critical roles in O_2 reduction to Li_2O_2 in aprotic Li–O_2 batteries," *The Journal of Physical Chemistry C*, vol. 120, no. 7, pp. 3690–3698, 2016.

[8] I. Saito, T. Matsuura, and K. Inoue, "Formation of superoxide ion via one-electron transfer from electron donors to singlet oxygen," *Journal of the American Chemical Society*, vol. 105, no. 10, pp. 3200–3206, 1983.

[9] M. Hayyan, M. A. Hashim, and I. M. AlNashef, "Superoxide ion: generation and chemical implications," *Chemical reviews*, vol. 116, no. 5, pp. 3029–3085, 2016.

[10] C. Schweitzer and R. Schmidt, "Physical mechanisms of generation and deactivation of singlet oxygen," *Chemical reviews*, vol. 103, no. 5, pp. 1685–1758, 2003.

[11] Y. K. Petit, C. Leypold, N. Mahne, E. Mourad, L. Schafzahl, C. Slugovc, S. M. Borisov, and S. A. Freunberger, "DABCOnium: an efficient and high-voltage stable singlet oxygen quencher for metal–O_2 cells," *Angewandte Chemie International Edition*, vol. 58, no. 20, pp. 6535–6539, 2019.

[12] L. Schafzahl, N. Mahne, B. Schafzahl, M. Wilkening, C. Slugovc, S. M. Borisov, and S. A. Freunberger, "Singlet oxygen during cycling of the aprotic sodium–O_2 battery," *Angewandte Chemie International Edition*, vol. 56, no. 49, pp. 15 728–15 732, 2017.

[13] W. Linert, A. Camard, M. Armand, and C. Michot, "Anions of low Lewis basicity for ionic solid state electrolytes," *Coordination Chemistry Reviews*, vol. 226, no. 1-2, pp. 137–141, 2002.

[14] M. Schmeisser, P. Illner, R. Puchta, A. Zahl, and R. van Eldik, "Gutmann donor and acceptor numbers for ionic liquids," *Chemistry–A European Journal*, vol. 18, no. 35, pp. 10 969–10 982, 2012.

[15] M. Carboni, A. G. Marrani, R. Spezia, and S. Brutti, "1, 2-dimethoxyethane segradation thermodynamics in Li-O$_2$ redox environments," *Chemistry–A European Journal*, vol. 22, no. 48, pp. 17 188–17 203, 2016.

[16] V. S. Bryantsev, M. Blanco, and F. Faglioni, "Stability of lithium superoxide LiO$_2$ in the gas phase: computational study of dimerization and disproportionation reactions," *The Journal of Physical Chemistry A*, vol. 114, no. 31, pp. 8165–8169, 2010.

[17] U. Das, K. C. Lau, P. C. Redfern, and L. A. Curtiss, "Structure and stability of lithium superoxide clusters and relevance to Li–O$_2$ batteries," *The journal of physical chemistry letters*, vol. 5, no. 5, pp. 813–819, 2014.

[18] M. Chase Jr, "NIST-JANAF thermochemical tables," *Washington, DC, American Chemical Society American Institute of Physics for the National Institute of Standards and Technology, Monograph*, vol. 9, p. 1963, 1998.

[19] P. D. Dietzel, R. K. Kremer, and M. Jansen, "Tetraorganylammonium superoxide compounds: Close to unperturbed superoxide ions in the solid state," *Journal of the American Chemical Society*, vol. 126, no. 14, pp. 4689–4696, 2004.

[20] C. Sheng, F. Yu, Y. Wu, Z. Peng, and Y. Chen, "Disproportionation of sodium superoxide in metal–air batteries," *Angewandte Chemie*, vol. 130, no. 31, pp. 10 054–10 058, 2018.

[21] P. Hartmann, C. L. Bender, M. Vraar, A. K. Dürr, A. Garsuch, J. Janek, and P. Adelhelm, "A rechargeable room-temperature sodium superoxide (nao 2) battery," *Nature materials*, vol. 12, no. 3, p. 228, 2013.

[22] C. J. Allen, J. Hwang, R. Kautz, S. Mukerjee, E. J. Plichta, M. A. Hendrickson, and K. Abraham, "Oxygen reduction reactions in ionic liquids and the formulation of a general ORR mechanism for Li–air batteries," *The Journal of Physical Chemistry C*, vol. 116, no. 39, pp. 20 755–20 764, 2012.

[23] D. G. Kwabi, V. S. Bryantsev, T. P. Batcho, D. M. Itkis, C. V. Thompson, and Y. Shao-Horn, "Experimental and computational analysis of the solvent-dependent O$_2$/Li$^+$-O$_2^-$ redox couple: standard potentials, coupling strength, and implications for lithium–oxygen batteries," *Angewandte Chemie International Edition*, vol. 55, no. 9, pp. 3129–3134, 2016.

[24] Z. Peng, S. A. Freunberger, L. J. Hardwick, Y. Chen, V. Giordani, F. Bardé, P. Novák, D. Graham, J.-M. Tarascon, and P. G. Bruce, "Oxygen reactions in a non-aqueous Li$^+$ electrolyte," *Angewandte Chemie International Edition*, vol. 50, no. 28, pp. 6351–6355, 2011.

[25] W. Yu, H. Wang, L. Qin, J. Hu, L. Liu, B. Li, D. Zhai, and F. Kang, "Controllable electrochemical fabrication of KO$_2$-decorated binder-free cathodes for rechargeable lithium–oxygen batteries," *ACS applied materials & interfaces*, vol. 10, no. 20, pp. 17 156–17 166, 2018.

[26] I. Landa-Medrano, I. R. de Larramendi, and T. Rojo, "Modifying the ORR route by the addition of lithium and potassium salts in Na-O$_2$ batteries," *Electrochimica Acta*, vol. 263, pp. 102–109, 2018.

[27] C. Li, Z. Qian, Y. Ma, P. Zuo, C. Du, H. Huo, and G. Yin, "Bifunctional electrolyte additive KI to improve the cycling performance of Li–O$_2$ batteries," *New Journal of Chemistry*, vol. 42, no. 21, pp. 17 311–17 316, 2018.

[28] I. Landa-Medrano, M. Olivares-Marín, B. Bergner, R. Pinedo, A. Sorrentino, E. Pereiro, I. Ruiz de Larramendi, J. Janek, T. Rojo, and D. Tonti, "Potassium salts as electrolyte additives in lithium–oxygen batteries," *The Journal of Physical Chemistry C*, vol. 121, no. 7, pp. 3822–3829, 2017.

[29] J.-l. Ma, F.-l. Meng, Y. Yu, D.-p. Liu, J.-m. Yan, Y. Zhang, X.-b. Zhang, and Q. Jiang, "Prevention of dendrite growth and volume expansion to give high-performance aprotic bimetallic Li-Na alloy–O_2 batteries," *Nature chemistry*, vol. 11, no. 1, p. 64, 2019.

[30] B. D. McCloskey, A. Valery, A. C. Luntz, S. R. Gowda, G. M. Wallraff, J. M. Garcia, T. Mori, and L. E. Krupp, "Combining accurate O_2 and Li_2O_2 assays to separate discharge and charge stability limitations in nonaqueous Li–O_2 batteries," *The journal of physical chemistry letters*, vol. 4, no. 17, pp. 2989–2993, 2013.

[31] N. B. Aetukuri, B. D. McCloskey, J. M. García, L. E. Krupp, V. Viswanathan, and A. C. Luntz, "Solvating additives drive solution-mediated electrochemistry and enhance toroid growth in non-aqueous Li–O_2 batteries," *Nature chemistry*, vol. 7, no. 1, p. 50, 2015.

[32] B. D. McCloskey, D. Bethune, R. Shelby, T. Mori, R. Scheffler, A. Speidel, M. Sherwood, and A. Luntz, "Limitations in rechargeability of Li-O_2 batteries and possible origins," *The journal of physical chemistry letters*, vol. 3, no. 20, pp. 3043–3047, 2012.

[33] B. D. McCloskey, J. M. Garcia, and A. C. Luntz, "Chemical and electrochemical differences in nonaqueous Li–O_2 and Na–O_2 batteries," *The journal of physical chemistry letters*, vol. 5, no. 7, pp. 1230–1235, 2014.

[34] S. Ganapathy, B. D. Adams, G. Stenou, M. S. Anastasaki, K. Goubitz, X.-F. Miao, L. F. Nazar, and M. Wagemaker, "Nature of Li_2O_2 oxidation in a Li–O_2 battery revealed by operando X-ray diffraction," *Journal of the American Chemical Society*, vol. 136, no. 46, pp. 16 335–16 344, 2014.

[35] Y. Wang, N.-C. Lai, Y.-R. Lu, Y. Zhou, C.-L. Dong, and Y.-C. Lu, "A solvent-controlled oxidation mechanism of Li_2O_2 in lithium-oxygen batteries," *Joule*, vol. 2, no. 11, pp. 2364–2380, 2018.

[36] S. Kang, Y. Mo, S. P. Ong, and G. Ceder, "A facile mechanism for recharging Li_2O_2 in Li–O_2 batteries," *Chemistry of Materials*, vol. 25, no. 16, pp. 3328–3336, 2013.

[37] B. D. McCloskey, D. S. Bethune, R. M. Shelby, G. Girishkumar, and A. C. Luntz, "Solvents' critical role in nonaqueous lithium–oxygen battery electrochemistry," *The Journal of Physical Chemistry Letters*, vol. 2, no. 10, pp. 1161–1166, 2011.

[38] D. Aurbach, B. D. McCloskey, L. F. Nazar, and P. G. Bruce, "Advances in understanding mechanisms underpinning lithium–air batteries," *Nature Energy*, vol. 1, no. 9, p. 16128, 2016.

[39] H.-D. Lim, B. Lee, Y. Bae, H. Park, Y. Ko, H. Kim, J. Kim, and K. Kang, "Reaction chemistry in rechargeable Li–O_2 batteries," *Chemical Society Reviews*, vol. 46, no. 10, pp. 2873–2888, 2017.

[40] D. Sharon, D. Hirsberg, M. Salama, M. Afri, A. A. Frimer, M. Noked, W. Kwak, Y.-K. Sun, and D. Aurbach, "Mechanistic role of Li^+ dissociation level in aprotic Li–O_2 battery," *ACS applied materials & interfaces*, vol. 8, no. 8, pp. 5300–5307, 2016.

[41] D. G. Kwabi, M. Tuodziecki, N. Pour, D. M. Itkis, C. V. Thompson, and Y. Shao-Horn, "Controlling solution-mediated reaction mechanisms of oxygen reduction using potential

and solvent for aprotic lithium–oxygen batteries," *The journal of physical chemistry letters*, vol. 7, no. 7, pp. 1204–1212, 2016.

[42] N. Ortiz-Vitoriano, T. P. Batcho, D. G. Kwabi, B. Han, N. Pour, K. P. C. Yao, C. V. Thompson, and Y. Shao-Horn, "Rate-dependent nucleation and growth of NaO_2 in Na–O_2 batteries," *The journal of physical chemistry letters*, vol. 6, no. 13, pp. 2636–2643, 2015.

[43] J. Kim, H. Park, B. Lee, W. M. Seong, H.-D. Lim, Y. Bae, H. Kim, W. K. Kim, K. H. Ryu, and K. Kang, "Dissolution and ionization of sodium superoxide in sodium–oxygen batteries," *Nature communications*, vol. 7, p. 10670, 2016.

[44] Y.-C. Lu and Y. Shao-Horn, "Probing the reaction kinetics of the charge reactions of nonaqueous Li–O_2 batteries," *The journal of physical chemistry letters*, vol. 4, no. 1, pp. 93–99, 2012.

[45] G. Cong, W. Wang, N.-C. Lai, Z. Liang, and Y.-C. Lu, "A high-rate and long-life organic–oxygen battery," *Nature materials*, vol. 18, no. 4, p. 390, 2019.

[46] X. Gao, Z. P. Jovanov, Y. Chen, L. R. Johnson, and P. G. Bruce, "Phenol-catalyzed discharge in the aprotic lithium-oxygen battery," *Angewandte Chemie*, vol. 129, no. 23, pp. 6639–6643, 2017.

[47] C. Li, O. Fontaine, S. A. Freunberger, L. Johnson, S. Grugeon, S. Laruelle, P. G. Bruce, and M. Armand, "Aprotic Li–O_2 battery: influence of complexing agents on oxygen reduction in an aprotic solvent," *The Journal of Physical Chemistry C*, vol. 118, no. 7, pp. 3393–3401, 2014.

[48] S. Das, J. Højberg, K. B. Knudsen, R. Younesi, P. Johansson, P. Norby, and T. Vegge, "Instability of ionic liquid-based electrolytes in Li–O_2 batteries," *The Journal of Physical Chemistry C*, vol. 119, no. 32, pp. 18 084–18 090, 2015.

[49] M. Piana, J. Wandt, S. Meini, I. Buchberger, N. Tsiouvaras, and H. A. Gasteiger, "Stability of a pyrrolidinium-based ionic liquid in Li-O_2 cells," *Journal of The Electrochemical Society*, vol. 161, no. 14, pp. A1992–A2001, 2014.

[50] K. U. Schwenke, M. Metzger, T. Restle, M. Piana, and H. A. Gasteiger, "The influence of water and protons on Li_2O_2 crystal growth in aprotic Li-O_2 cells," *Journal of The Electrochemical Society*, vol. 162, no. 4, pp. A573–A584, 2015.

[51] D. G. Kwabi, T. P. Batcho, S. Feng, L. Giordano, C. V. Thompson, and Y. Shao-Horn, "The effect of water on discharge product growth and chemistry in Li–O_2 batteries," *Physical Chemistry Chemical Physics*, vol. 18, no. 36, pp. 24 944–24 953, 2016.

[52] J. Lu, Y. J. Lee, X. Luo, K. C. Lau, M. Asadi, H.-H. Wang, S. Brombosz, J. Wen, D. Zhai, Z. Chen *et al.*, "A lithium–oxygen battery based on lithium superoxide," *Nature*, vol. 529, no. 7586, p. 377, 2016.

[53] I. Landa-Medrano, R. Pinedo, X. Bi, I. Ruiz de Larramendi, L. Lezama, J. Janek, K. Amine, J. Lu, and T. Rojo, "New insights into the instability of discharge products in Na–O_2 batteries," *ACS applied materials & interfaces*, vol. 8, no. 31, pp. 20 120–20 127, 2016.

[54] R. Black, A. Shyamsunder, P. Adeli, D. Kundu, G. K. Murphy, and L. F. Nazar, "The nature and impact of side reactions in glyme-based sodium–oxygen batteries," *ChemSusChem*, vol. 9, no. 14, pp. 1795–1803, 2016.

[55] T. Liu, G. Kim, M. T. Casford, and C. P. Grey, "Mechanistic insights into the challenges of cycling a nonaqueous Na–O$_2$ battery," *The journal of physical chemistry letters*, vol. 7, no. 23, pp. 4841–4846, 2016.

[56] S. Y. Sayed, K. P. Yao, D. G. Kwabi, T. P. Batcho, C. V. Amanchukwu, S. Feng, C. V. Thompson, and Y. Shao-Horn, "Revealing instability and irreversibility in nonaqueous sodium–O$_2$ battery chemistry," *Chemical Communications*, vol. 52, no. 62, pp. 9691–9694, 2016.

[57] Y. Wang, Z. Liang, Q. Zou, G. Cong, and Y.-C. Lu, "Mechanistic insights into catalyst-assisted nonaqueous oxygen evolution reaction in lithium–oxygen batteries," *The Journal of Physical Chemistry C*, vol. 120, no. 12, pp. 6459–6466, 2016.

Deactivation of singlet oxygen by physical quencher effect

Water will never quench your thirst for knowledge.

Anthony T. Hincks

Contents

Figures

Introduction

Oxides are a prominent research subject as new cathode materials for non-aqueous alkali battery technologies, either as transition-metal oxides intercalation materials or as direct alkaline oxide in metal–O$_2$ batteries[2-7]. Beside their promises for higher energy storage, oxide based cathodes suffer from side reactions and their interfacial reactivity is the key for increased battery lifetime. Metal-O$_2$ technologies are particularly inhibited by crippling and quick fade in capacity and efficiency which is discussed in **Side reaction Intro**. To allow these technologies to reach their full potential, side reactions origins must be understood and subdued.

The side reactions plaguing metal–O$_2$ cells have been solely ascribed to superoxide reactivity for an enduring time but superoxide presence is not sufficient to explain such extended degradations, as explained in part. **intro side reactivity**. We have shown in the previous chapters **the two previous chapters** that singlet oxygen is currently an inevitable source of side reactions at all stage of cycling in Na and Li cells. ^{1}O$_2$ high reactivity was shown to correlate with common side product amount in metal–air batteries whose accumulation increases overpotential and reduces cell cyclability in part. **Singlet oxygen, Electrode, discharge products**. Singlet oxygen reactivity is moreover not confined to metal–air chemistry as it forms from parasitic products and transition metal oxide oxidations, as defined in part. **singlet oxygen prodution**. Find protection to ^{1}O$_2$ is thus of main importance to achieve long term cycling in alkaline non–aqueous based batteries.

O$_2$ quenchers can bring the answer to the ^{1}O$_2$ mitigation question. Chemical trap as DMA, decribed in the previous chapters (**site the two previous character**), can react preferentially with ^{1}O$_2$ and prevent further side reactions by forming its endoperoxide[8]. To sustain the extend lifetime requires for a battery, very high concentration of chemical trap would have to be used which would consequently form a high amount of inactive species in the electrolytes. Since the use of chemical trap is unrealistic in batteries, physical quenchers that deexcite ^{1}O$_2$ to ^{3}O$_2$ without consumption of additives, as schemed in fig. 4.1, appears well indicated. Efficient quenchers need, yet, to sustain the aggressive conditions found in metal-O$_2$ batteries.
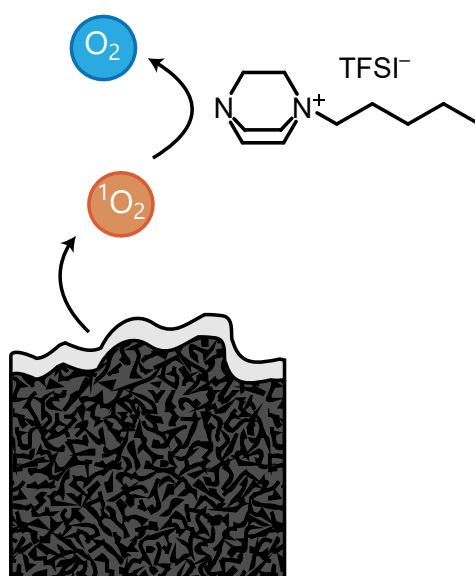
Figure 4.1: **Illustration of the quenching process by PeDTFSI in electrochemical cell.**

We present here PeDTFSI, a ionic liquid formed by monoalkylating the known quencher DABCO[8–10], as a efficient quencher in metal–O$_2$ batteries. PeDTFSI ~~presents increased oxidative stability due to its ionic properties compared to~~ DABCO. We show that the higher solubility of DABCOnium in glymes, a common solvent in metal–O$_2$ batteries, counterbalances reduced molar efficiency arising form its increased oxidation potential[9,11]. To do so, we followed the consumption of DMA in the presence of ^{1}O$_2$ by UV–vis spectrometry. The DMA consumption rate will be decreased by competitive ^{1}O$_2$ deactivation pathways, i.e. physical quenching. Quenchers as additives in Li–O$_2$ electrolytes result in reduced parasitic products and increased reaction yield during both discharge and charge. Besides providing a ^{1}O$_2$ ~~mitigation mean~~ in batteries, this study established clearly ^{1}O$_2$ as a main degradation source in metal–O$_2$ cells considering the influence of quenchers on parasitic reactions.

4.1 ~~Singlet oxygen physical quencher~~

~~Natural~~ process ~~brings~~ substantial answer to the $^1O_2$ mitigation issue in electrochemical devices. Singlet oxygen is found in biological systems that use O_2 ~~as an~~ energy storage[11,12]. Natural systems evolved to counteract negative effects of this harmful chemical. Amongst possible solutions, the most currents are chemical trapping and physical quenching agents, such as tocopheroles and carotenes[11,12]. Chemist has synthesised molecules with similar effect, e.g. the previously discussed DMA that traps $^1O_2$ by forming its endoperoxide[13,14]. This traps, yet, directly react at high rates with $^1O_2$ to form innocuous species. Their consumption render chemical traps inadequate in battery technologies where a high number of cycles needs to be sustained.

Physically deactivating $^1O_2$ to its ground state ($^3O_2$) is preferred since the quencher is not consumed and no new inactive products accumulate. Several radiationless physical quenching mechanisms can convert $^1O_2$ ~~energy excess~~ into heat[11,13]. They are namely, in increasing reaction ~~pace~~ order, electronic-to-vibrational energy transfer (e.g. $^1O_2$ quenching by solvents), charge transfer induced quenching (e.g. tertiary aliphatic amines), and electronic energy transfer (unsuitable for electrochemical systems, e.g. carotenes in biologic systems)[11]. The fastest quenching mechanism suitable for electrochemical systems hence proceeds via a charge transfer (CT) mechanism. In CT mechanism, the quencher (Q) and $^1O_2$ form a singlet encounter complex ($^1(Q^1O_2)_{EC}$), followed by a singlet charge transfer complex formation ($^1(Q^1O_2)_{CT}$), in which electronic charge is partially transferred to the oxygen. Energy is then released during the intersystem crossing (isc) to the triplet ground state complex ($^1(Q^3O_2)_{CT}$), which dissociates to Q and $^3O_2$[11,15], as described in eq. 4.1.

$$Q + {}^1O_2 \rightleftharpoons {}^1(Q^1O_2)_{EC} \rightleftharpoons {}^1(Q^1O_2)_{CT} \xrightarrow{\text{isc}} {}^3(Q^3O_2)_{CT} \rightleftharpoons Q + {}^3O_2 \qquad (4.1)$$
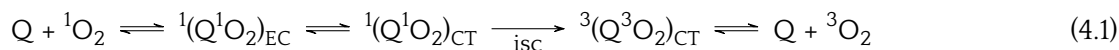
Charge transfer quenching is favoured in the case of electron-rich quenchers, such as amines. 1,4-diazabicyclo [2.2.2]octane (DABCO, fig. 4.2(a)) has been suggested for $^1O_2$ quenching as early as 1968 and was shown to be effective in aprotic media[8–10]. Amines have been widely investigated and it was found that the partial charge transfer causes the quenching efficiency to correlate logarithmically with the ionization potential and hence oxidation potential[11,15]. The quenching efficiency by CT mechanism drops by a factor of ~10^4 per volt of ~~the~~ oxidation potential for amines. The well known quenchers DABCO and LiN_3 are oxidized at ~3.6 V_{Li/Li^+}[9–11,16], whereas ~4.2 V_{Li/Li^+} are typically required to recharge Li-O2 cells[17–19]. The other non-aqueous metal–air batteries present a lower overpotential during charge and so the oxidative stability of the quencher should be fixed for Li-O_2 chemistry[7][20][21][22]. Another challenge in batteries is the reduced quenching activity due to cation interactions with strongly Lewis basic amines[11]. To be suitable ~~in~~ metal–air battery conditions, an amine quencher should then have lower Lewis basicity, raised oxidation stability (to around 4.2 V_{Li/Li^+}), be chemically stable, counterbalance the inevitably lower molar quenching efficiency by high solubility in the solvent media and ultimately be compatible with a lithium metal anode. Herein we show that monoalkylating the diamine DABCO to its onium salt (here 1-pentyl-1,4-diazabicyclo[2.2.2]octan-1-ium TFSI or PeDTFSI, presented in fig. 4.2b) achieve all these goals.

a)   b)
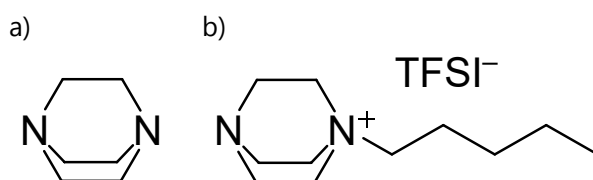
Figure 4.2: **Structure of the used $^1O_2$ quenchers.** (a) DABCO (1,4–diazabicyclo[2.2.2]octane), (b) PeDTFSI (1–pentyl–1,4–diazabicyclo[2.2.2]octan–1–ium TFSI).

4.2 Quencher adapted to lithium air batteries

According to a literature procedure detailed in **Annexes synsthese**, a pentyl DABCOnium (PeDTFSI) species counterbalanced by a bis(trifluoromethanesulfonyl)imide (TFSI⁻) anion was synthesized[23]. PeDTFSI is an ionic liquid with a melting point of 43 °C (PeDTFSI characterization is detailed in **Annexes NMR + ATG**) and is widely miscible with glymes, a common metal–air battery electrolyte, fulfilling the high solubility requirement. Concerning the low Lewis basicity criterion, its donor number (DN) was determined to be 12.5 kcal·mol⁻¹ by ^{23}Na-NMR shift as depicted in **Annexes Na NMR**. The commonly used TEGDME has a similar Lewis basicity with a DN of 12, which is much lower than other common solvents as DMSO (DN=30) or tertiary amines as triethylamine (DN=61) and 1,2-diaminoethane (DN=55), as expressed in **Annexes table Na NMR**[24]. We verified the chemical stability of DABCO and PeDTFSI in presence of superoxide, peroxide and $^1O_2$ by ^{1}H-NMR spectroscopy to assess their usability in metal-air batteries. The procedure is further described in **Annexes protocol stability** and the resulting ^{1}H-NMR are illustrated in fig. 4.3 for PeDTFSI and **Annexes NMR stability DABCO** for DABCO.
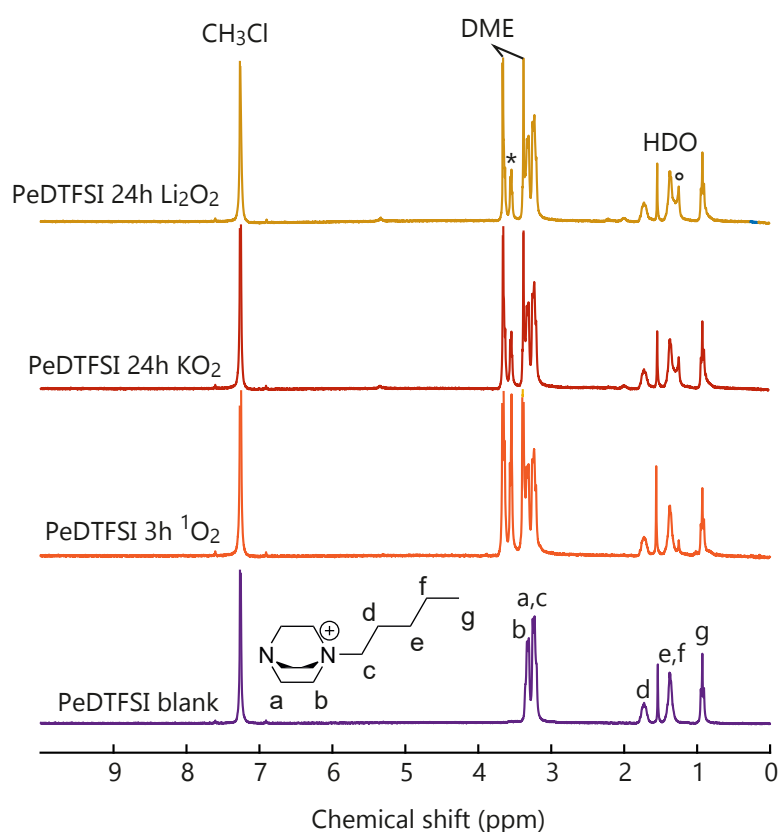
Figure 4.3: **Stability PeDTFSI study in contact with $^1O_2$, KO$_2$, and Li$_2$O$_2$ by ^{1}H-NMR in CDCl$_3$.** The ^{1}H-NMR spectra characterize PeDTFSI (in purple), PeDTFSI after 3h contact with $^1O_2$ (in orange), PeDTFSI after 24h contact with solvated KO$_2$ (in red), and PeDTFSI after 24h contact with Li$_2$O$_2$ (in yellow). The * denotes a residue from DME evaporation, which amounts to a content of 1 ppm in the DME; the ° denotes H from grease. $^1O_2$ was produced photochemically, according to a previously described method[8] and further described in **Annexes**, by dint of 1 μM *meso*-tetra(4-fluorophenyl9tetrabenzoporphyrin (Pd$_4$F) and illumination at 643 nm.

Cyclic voltammetry was used to determine the electrochemical stability window of the quenchers, as shown in fig. 4.4. Monoalkylating DABCO diminishes the tertiary amine moiety

electronegative character and raises its oxidation onset by approximately 0.6 V. The oxidation stability increase from ∼3.6 V_{Li/Li^+} for DABCO to ∼4.2 V_{Li/Li^+} for PeDTFSI, hence sufficiently high for Li–O$_2$ cells. Onset of reduction is in either case around 0.5 V_{Li/Li^+} permitting its use for every O$_2$ cathodes [7,20–22,25]. Regarding lithium metal anode, a symmetrical Li/Li cells with an TEGDME electrolyte composed of 1 M LiTFSI and 380 mM PeDTFSI could sustain 5 hours plating/deplating at 131 μA with low overpotentials upon cycling, as pictured in **Annexes Lithium**. Since recent researches advocate for additives unstable with lithium metal as mediators, the use of additives might require anyway the use of solid sate separator [26].

a)
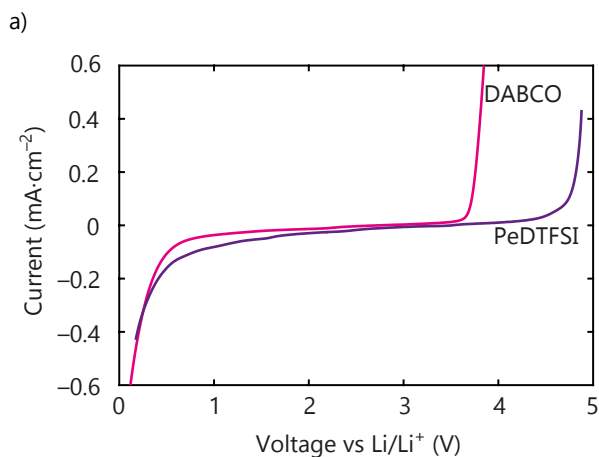
Figure 4.4: **Cyclic voltammetry of DABCO (in light purple) and PeDTFSI (in dark purple).** The cyclic voltammetries were performed on a glassy carbon disk electrode in a TEGDME electrolyte containing 0.1 M LiTFSI and 2 mM of the quencher at a scan rate of 50 mV·s^{-1}.

To verify the PeDTFSI quenching efficiency despite its higher oxidation potential, we monitored the disappearance rate of the ^{1}O$_2$ trap DMA in presence of quenchers during continuous photochemical ^{1}O$_2$ generation by UV-vis [13,27] which is further detailed in **Annexes** and depicted in 4.5. Like in part. **Quenching Imidazolium** and detailed in **Annexes**, a slower DMA decay rate in quencher presence, due to competitive reactions, is taken as a token of the quencher activity. ^{1}O$_2$ was generated photochemically at a constant rate by illuminating O$_2$ saturated TEGDME containing 1 μM Pd4F photosensitizer [8][27][28], 80 μM DMA and either the tested quencher or no additives. In order to compare the different rates, the ^{1}O$_2$ production should be constant. The quencher should hence not deactivate the excited triplet state of the sensitizer itself, responsible for the conversion of ^{3}O$_2$ into ^{1}O$_2$, effect described in part. **Singlet oxygen production singlet**. By measuring the excited sensitizer lifetime, described in **Annexes Stern Volmer Need to ask Stefan for the concentration in sensitizer and compare to the value from Borisov**, we verified the negligible influence of the studied quenchers compared to quenching by molecular oxygen and thus on the ^{1}O$_2$ generation rate.

a)

b)
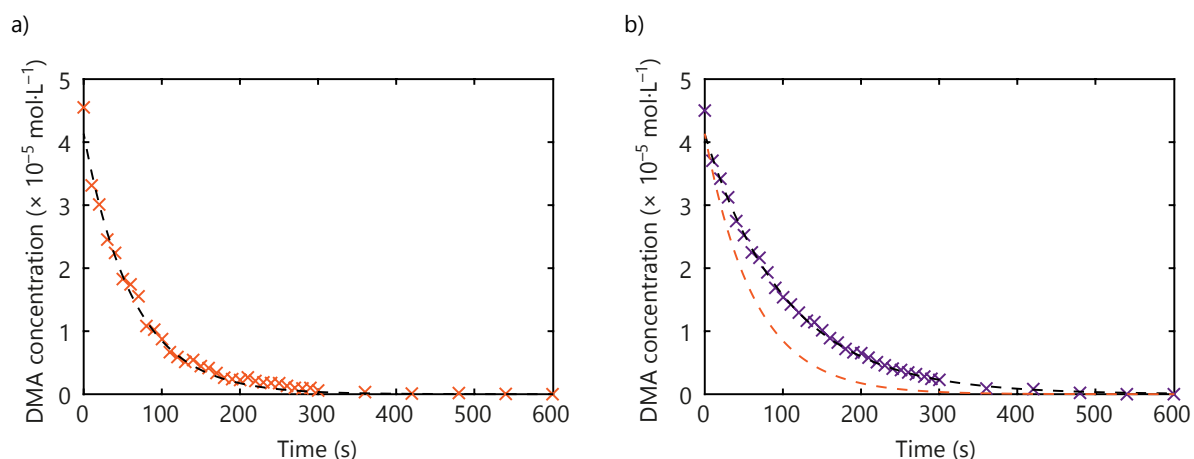
Figure 4.5: **DMA decay over time in presence of photochemically produced $^1O_2$ with or without DABCO.** (a) DMA consumption without quencher (in orange) and the first-order kinetic fit (in black) (b) DMA in presence of 40 μM DABCO (in purple), the first-order kinetic fit (in black) and the DMA without quencher fitted (in orange). The electrolytes used are based one 40 μM DMA and 1 μM Pd_4F in O2 saturated TEGDME illuminated at 643 nm, as described more lengthy in **Annexes**. The dashed lines are the exponential fit of DMA consumption.

a)

b)
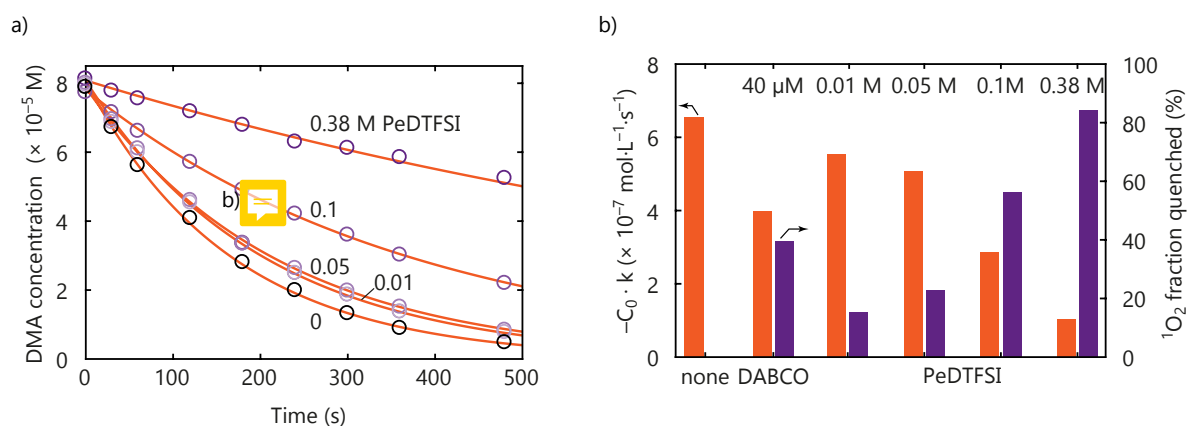
Figure 4.6: **Comparison of quenching efficiency and influence of quencher concentration.** (a) DMA concentration evolution over time in presence of photochemically produced $^1O_2$ with or without PeDTFSI at various concentrations to determine quenching efficiency. The electrolytes used are based on 80 μM DMA, the noted concentration of PeDTFSI and 1 μM Pd_4F in O2 saturated TEGDME illuminated at 643 nm, as described more lengthy in **Annexes**. The lines are the exponential fit of DMA consumption. (b) Quenching efficiency expressed as DMA decay kinetics and $^1O_2$ fraction quenched for 40 μM DABCO and various PeDTFSI concentrations.

The obtain DMA concentration decays show a clear correlation with the PeDTFSI concentration used as additives in fig. 4.6(a), verifying that higher concentrations allow to circumvent the lower activity of PeDTFSI. The DMA decay can be fitted by a pseudo first-order reaction kinetic according to eq. 4.2, considering the $^1O_2$ concentration as constantly replenished to the same level[13]; Examples of fitted decays can be found in fig. 4.5. The obtained rate at t_0 can then be compared to characterized the quenching efficiency and the $^1O_2$ fraction quenched represented by the ratio between the rate of DMA alone and in quencher presence at a given concentration, presented in fig. 4.6(b). As expected from their respective oxidation potentials, DABCO presents a higher molar quenching efficiency with roughly halved the

DMA decay rate at only 40 μM; On the other hand, PeDTFSI concentration had to be increased to the mM range for a comparable effect. With 0.01, 0.05, 0.1, and 0.38 mM, the quenched $^1O_2$ fractions were 9, 23, 56, and 86 %, respectively. Owing to its high solubility, PeDTFSI can thus compensate its lower efficiency to achieve quenching of the vast $^1O_2$ majority.

$$C = C_0 \cdot e^{-kt} \qquad\qquad (4.2)$$

4.3   Quencher influence of side reactivity

Ultimately, a suitable quencher needs to effectively decrease the amount of $^1O_2$ related parasitic chemistry in metal-air batteries. We chose the Li–O_2 cell to demonstrate the impact of PeDTFSI since amongst Li–, Na–, and K–O2 cells, Li–O_2 present the highest $^1O_2$ production rate and shows the most severe side reactions as depicted in **side reactions intro** and **singlet oxygen production**. The deviation form the theoretical yield was measured by pressure monitoring assuming that the large majority of released gas is oxygen[17][29][30], reactions products (Li$_2O_2$ and carbonates) characterized by a combination of UV–Vis and MS and $^1O_2$ production by the ratio DMA/DMA-O_2 obtained by HPLC after electrolyte extraction. The methods are further described in **Annexes and method singlet**. Li–O_2 cells were constructed as specified in **Annexes DABCO cells** with carbon black/PTFE cathodes and TEGDME electrolytes containing 1 M LiTFSI, 30 mM DMA and either no quencher, 60 mM DABCO, or 60, 120, and 380 mM PeDTFSI.

4.3.1   Discharge

Considering first the $^1O_2$ consumption yield, cells discharged at 100 mA·g$_c^{-1}$ up to 1000 mAh·g$_c^{-1}$ present a light deviation within 2% of the ideal value of 2 e$^-$/O_2 with a slight improvement in presence of a quencher in fig. 4.7(a), in accord with other reports[17,20,27,29,31]. In a similar fashion, Li$_2O_2$ yields, shown in fig. 4.7(b), stay unfazed by the presence of quenchers at ∼95%. The presence of quenchers additives is not expected to change significantly the reaction mechanism of the cell and hence influence importantly the Li$_2O_2$ or e$^-$/O_2 yield during discharge. Deactivating already formed $^1O_2$ should solely influence the side product amount and $^1O_2$ traped by DMA in solution. Consequently, the amount of unquenched $^1O_2$ directly correlates with the quantity of carbonaceous side products formed in fig. 4.7(b). The presence of 60 mM DABCO additives cuts down both the singlet oxygen trapped in solution and the side products by roughly 4. The same concentration of PeDTFSI reduce the side products only by half, as a result of its lower molar quenching efficiency. With 380 mM PeDTFSI, however, the side products were cut to 14% of the value without quencher whether a smaller amount than for 60 mM DABCO. PeDTFSI hence effectively reduces $^1O_2$ related parasitic chemistry on discharge by dint of its high solubility.

a)

b)
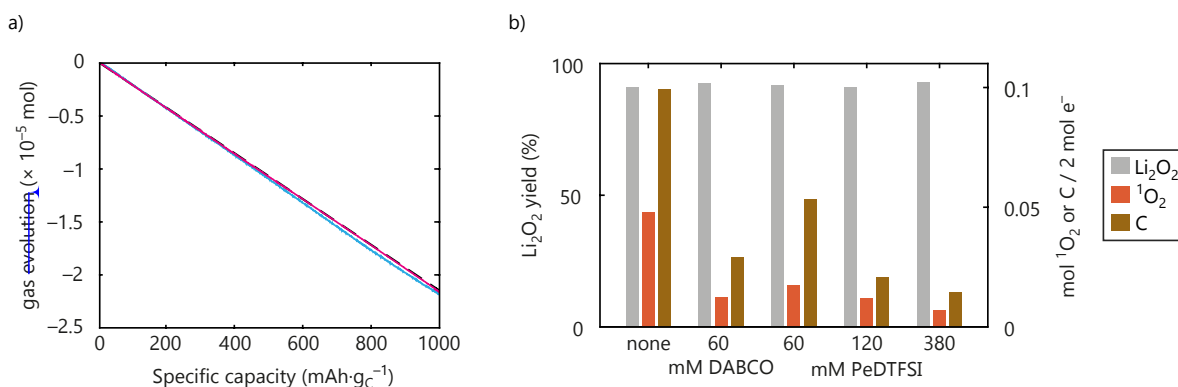
Figure 4.7: **Quencher influence on Li–O$_2$ cell discharges.** (a) Gas evolution during a Li–O$_2$ cell discharge with a carbon black cathode and LFP counter electrode discharged at 100 mA·g$_c$$^{-1}$ to 1000 mAh·g$_c$$^{-1}$ in a TEGDME electrolyte containing 1 M LiTFSI, 30 mM DMA and either no quencher (blue) or 0.38 M PeDTFSI (purple). The dashed line represent the theoretical yield of 2 e$^-$/O$_2$. The method is detailed in **Annexes**. (b) O$_2$, ^{1}O$_2$, peroxide and carbonates production during discharge of the Li–O$_2$ cells with or without quenchers. The cells are composed of a carbon black cathode and LFP counter electrode in a TEGDME electrolyte containing 1 M LiTFSI and the mentioned quencher concentration and discharged at 100 mA·g$_c$$^{-1}$ to 1000 mAh·g$_c$$^{-1}$. The method is detailed in **Annexes**.

4.3.2 Charge

Turning to cell recharge, we assessed the effect of a quencher on the gas evolution rate measured by the pressure in the cell headspace. As DABCO has already been shown to reduce ^{1}O$_2$ related parasitic chemistry on charge within the limited oxidative stability of 3.6 V$_{Li/Li^+}$ [8], focus will be given to quencher-free cell and a 380 mm PeDTFSI containing cell. Cells were first discharged in the same conditions than the discharge study and then recharged at 100 mA·g$_c$$^{-1}$ to a cut–off voltage of 4.6 V$_{Li/Li^+}$ and depicted in fig. 4.8(a)-(b).

a)

b)

c)

d)
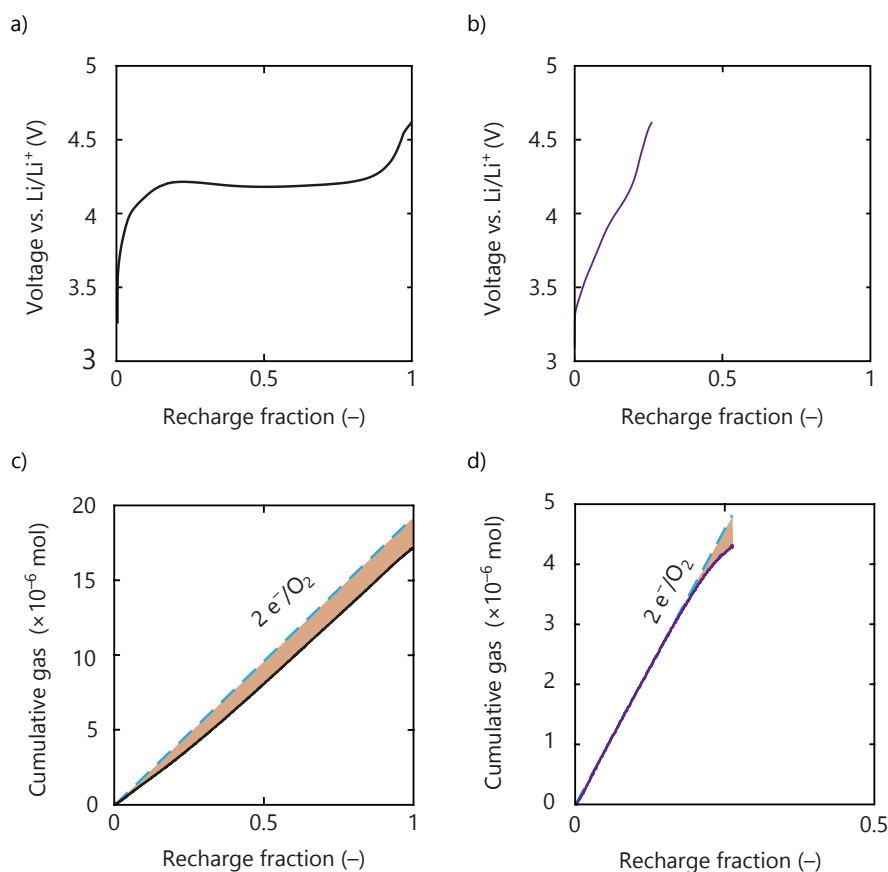
Figure 4.8: **Quencher influence on Li–O$_2$ cell charges.** The O$_2$ saturated TEGDME elecrolytes used are composed of 1 M LiTFSI on the first column ((a)–(c)) and an additional 0.38 M PeDTFSI on the second column ((b)-(d)). (a)-(b) Voltage profiles during recharge with a carbon black cathode and LFP counter electrode at 100 mA·g$_c^{-1}$ to a cut–off voltage of 4.6 V$_{Li/Li^+}$ after a discharge to 1000 mAh·g$_c^{-1}$. (c)-(d) Gas evolution during a Li-O$_2$ cell charge of the aforementioned cells (in black without quencher and in purple with 0.38 M PeDTSFI). The blue dashed line represent the theoretical 2 e$^-$/O$_2$ and the orange area represent the parasitic reactions. The method is detailed in **Annexes**.

For the quencher-free cell in fig. 4.8(a)–(c), the voltage rises within a few percents of the recharge capacity towards to a plateau at ~4.2 V$_{Li/Li^+}$ before it further rises steeply close to the end of recharge. The gas evolution remains, from the onset of charge, significantly below the theoretical value of 2 e$^-$/O$_2$, as previously observed in literature[17,20,29]. This deviation indicate e$^-$ extraction from side products, i.e. Li$_2$CO$_3$[10], and possible reaction of released O$_2$ species with cell components rather than evolving as O$_2$, as ^{1}O$_2$ evolution described in part. **singlet direct oxidation** and **singlet carbonates**. In contrast, the cell with PeDTFSI evolves O$_2$ at the ideal rate of 2 e$^-$/O$_2$ up to approximately 4.2 V$_{Li/Li^+}$, namely its oxidation stability threshold; ~~Upon~~ this voltage, part of the e$^-$ exchanged are due to PeDTFSI oxidation. A 2 e$^-$/O$_2$ reaction yield establishes that all the electrons are extracted from Li$_2$O$_2$ rather than partly from side products and any ^{1}O$_2$ formed is quenched to ^{3}O$_2$ in order to be detected in the headspace. ^{1}O$_2$ being evolved from the onset of charge in Li-O$_2$ cells from dispropor-tionation[8,27], ^{1}O$_2$ suppression can only arise via PeDTFSI quenching since the quencher is not expected to change the charging mechanism. It should be noted that charge capacity at cut–off with the electrolyte containing 380 mM PeDTFSI corresponds to only 23% of the formed Li$_2$O$_2$ during discharges, which balances with the 77% left measured by Li$_2$O$_2$ titration after recharge.

4.3.3 Consequences

The addition of quenchers ~~additives~~ results in a substantial decrease in side products formation both ~~in~~ discharge and charge. The quencher effectiveness to reduce parasitic reaction established clearly $^1O_2$ as ~~one of~~ the major degradation pathways in metal–air batteries. A reduction to 14% of the original carbonate formation ~~in~~ Li–O_2 cell discharge with high quencher concentration show that disproportionation ~~might arise as a culprit~~ for 86% of the cell degradation during discharge, accentuating the importance of disproportionation mechanism ~~developed~~ in the ch. **chapter disp**. Quenching disproportionation reaction can explain the slightly improved e^-/O_2 yield as the $^1O_2$ release by disproportion is recovered in the headspace as $^3O_2$ instead of reacting with cell component. As the $^1O_2$ formation rate is accelerated with the charge overpotential[8], quencher use is evermore important during Li–O_2 charge.

During Li–O_2 cell charge without quencher, the quickly increasing voltage is partly related to increasingly difficult electron transfer as the Li_2O_2 content decrease and mainly to increasing oxidation potential caused by formed parasitic products[32–35]. Considering the case with quenchers, the near theoretical yield through most of the recharge indicates that rising voltage is not caused by side–product formation. Together with the much lower amounts of side products at the end of discharge, the continued $^1O_2$ elimination on charge also avoids more side products forming on recharging. This is reflected in the slower overpotential rise compared to the quencher–free cell. Accounting for the 77% Li_2O_2 left in at the electrode vicinity at the charge end with PeDTFSI, rising voltage can be related to increasingly difficult electron transport from the electrode surface to remote Li_2O_2 and subsequent loss of contact as charging proceeds. PeDTFSI is amphoteric, Lewis basic at the tertiary N atom and Lewis acidic at the quaternary N atom, which could possibly solubilize the LiO_2 intermediate and favour the solution discharge pathway. Difficulties in recharging cells with additives favouring the solution mechanism are already recognized[5,36–38].

The advantages of quencher ~~additives~~ ~~is~~ not limited to Li–O_2 air batteries but to all battery chemistry ~~presenting~~ $^1O_2$ formation. Na–O_2 disproportionation at rest, accompanied by $^1O_2$ release, is responsible for ~~high~~ cell degradation, as demonstrated in part. **singlet disp + disp paper consequences**. Quencher ~~additives~~ should be able to reduce this effect. PeDTFSi presented here is only a first attempt~~ed~~ to adapt singlet oxygen quencher to battery chemistries. Singlet oxygen evolution from layered transition metal oxide at high potential would require~~s~~ an improved oxidative stability[39,40]. Nevertheless our study assess the importance of singlet oxygen reactivity in non–aqueous batteries and its mitigation through quencher ~~additives~~.

Conclusion

In conclusion, $^1O_2$ is ~~partly~~ responsible for side reactions and requires adequate mitigation ~~means~~ in non-aqueous alkali batteries. Physical quenching appears as a good solution to the $^1O_2$ production in batteries, permitting deactivation to its ground state before side reactions ~~debut.~~ We show that PeDTFSI, the monoalkylated form of the diamine 1,4-diazabicyclo[2.2.2]octane (DABCO), is an efficient $^1O_2$ quencher with sufficient voltage and chemical stability. Quaternizing one of the nitrogen atoms raises the oxidation stability of the remaining tertiary nitrogen from 3.6 V_{Li/Li^+} to approximately 4.2 V_{Li/Li^+}. Despite the lower molar efficiency of PeDTFSI, its high miscibility with glymes permits an effective $^1O_2$ quenching at high concentration.

We demonstrate the efficiency of PeDTFSI with Li–O_2 cathodes, where the quencher greatly reduces the parasitic chemistry. PeDTFSI influence on parasitic chemistries settles the importance of $^1O_2$ related parasitic chemistry in metal-O_2 batteries and the influence of side products on the Li-O_2 cell overpotential during charge. On a wider perspective, partly quaternizing diamines ~~are~~ suitable to tune the oxidation potential of $^1O_2$ quenchers. $^1O_2$ is also known to evolve from layered transition-metal cathodes and upon oxidizing Li_2CO_3, a common impurity of cathode materials. Quenchers stable under high voltage are hence relevant to control $^1O_2$ related interfacial reactivity and long-term cyclability of many currently studied cathodes. As transition-metal cathodes can ~~produced~~ singlet oxygen at higher potential than 4.2 V_{Li/Li^+}[39], alternative quencher might arise in the future. Nevertheless, this study presents a first definition of quencher potential in oxide based cathodes and their design.

Enhanced solution pathway mechanism in Li–O_2 increases the discharge capacity but also leads to difficulties to ~~reached~~ full recharge. Complete oxidation of the Li_2O_2 formed during discharge could not be achieved with PeDTFSI addition. Such cells are now recognized to require oxidation mediators for full charge[5]. As mediators change the mechanism of the reaction, singlet oxygen production via mediators ought to be studied more ~~in~~ details.

Bibliography

[1] Y. K. Petit, C. Leypold, N. Mahne, E. Mourad, L. Schafzahl, C. Slugovc, S. M. Borisov, and S. A. Freunberger, "DABCOnium: An Efficient and High-Voltage Stable Singlet Oxygen Quencher for Metal–O_2 Cells," *Angewandte Chemie International Edition*, vol. 58, no. 20, pp. 6535–6539, 2019.

[2] Q. Liu, Z. Hu, M. Chen, C. Zou, H. Jin, S. Wang, S.-L. Chou, and S.-X. Dou, "Recent progress of layered transition metal oxide cathodes for sodium-ion batteries," *Small*, p. 1805381, 2019.

[3] P. Rozier and J. M. Tarascon, "Li-rich layered oxide cathodes for next-generation li-ion batteries: chances and challenges," *Journal of The Electrochemical Society*, vol. 162, no. 14, pp. A2490–A2499, 2015.

[4] H. Kim, D.-H. Seo, A. Urban, J. Lee, D.-H. Kwon, S.-H. Bo, T. Shi, J. K. Papp, B. D. McCloskey, and G. Ceder, "Stoichiometric layered potassium transition metal oxide for rechargeable potassium batteries," *Chemistry of Materials*, vol. 30, no. 18, pp. 6532–6539, 2018.

[5] D. Aurbach, B. D. McCloskey, L. F. Nazar, and P. G. Bruce, "Advances in understanding mechanisms underpinning lithium–air batteries," *Nature Energy*, vol. 1, no. 9, p. 16128, 2016.

[6] P. Hartmann, C. L. Bender, M. Vraar, A. K. Dürr, A. Garsuch, J. Janek, and P. Adelhelm, "A rechargeable room-temperature sodium superoxide (NaO_2) battery," *Nature materials*, vol. 12, no. 3, p. 228, 2013.

[7] G. Cong, W. Wang, N.-C. Lai, Z. Liang, and Y.-C. Lu, "A high-rate and long-life organic–oxygen battery," *Nature materials*, vol. 18, no. 4, p. 390, 2019.

[8] N. Mahne, B. Schafzahl, C. Leypold, M. Leypold, S. Grumm, A. Leitgeb, G. A. Strohmeier, M. Wilkening, O. Fontaine, D. Kramer *et al.*, "Singlet oxygen generation as a major cause for parasitic reactions during cycling of aprotic lithium–oxygen batteries," *Nature Energy*, vol. 2, no. 5, p. 17036, 2017.

[9] C. Ouannes and T. Wilson, "Quenching of singlet oxygen by tertiary aliphatic amines. Effect of DABCO (1, 4-diazabicyclo [2.2.2] octane)," *Journal of the American Chemical Society*, vol. 90, no. 23, pp. 6527–6528, 1968.

[10] N. Mahne, S. E. Renfrew, B. D. McCloskey, and S. A. Freunberger, "Electrochemical oxidation of lithium carbonate generates singlet oxygen," *Angewandte Chemie International Edition*, vol. 57, no. 19, pp. 5529–5533, 2018.

[11] C. Schweitzer and R. Schmidt, "Physical mechanisms of generation and deactivation of singlet oxygen," *Chemical reviews*, vol. 103, no. 5, pp. 1685–1758, 2003.

[12] P. R. Ogilby, "Singlet oxygen: there is indeed something new under the sun," *Chemical Society Reviews*, vol. 39, no. 8, pp. 3181–3209, 2010.

[13] F. Wilkinson, W. P. Helman, and A. B. Ross, "Rate constants for the decay and reactions of the lowest electronically excited singlet state of molecular oxygen in solution. an expanded and revised compilation," *Journal of Physical and Chemical Reference Data*, vol. 24, no. 2, pp. 663–677, 1995.

[14] A. Gomes, E. Fernandes, and J. L. Lima, "Fluorescence probes used for detection of reactive oxygen species," *Journal of biochemical and biophysical methods*, vol. 65, no. 2-3, pp. 45–80, 2005.

[15] A. P. Darmanyan, W. S. Jenks, and P. Jardon, "Charge-transfer quenching of singlet oxygen O2 ($^1\Delta_g$) by amines and aromatic hydrocarbons," *The Journal of Physical Chemistry A*, vol. 102, no. 38, pp. 7420–7426, 1998.

[16] D. Shanmukaraj, S. Grugeon, S. Laruelle, G. Douglade, J.-M. Tarascon, and M. Armand, "Sacrificial salts: Compensating the initial charge irreversibility in lithium batteries," *Electrochemistry Communications*, vol. 12, no. 10, pp. 1344–1347, 2010.

[17] B. D. McCloskey, D. Bethune, R. Shelby, T. Mori, R. Scheffler, A. Speidel, M. Sherwood, and A. Luntz, "Limitations in rechargeability of Li-O_2 batteries and possible origins," *The journal of physical chemistry letters*, vol. 3, no. 20, pp. 3043–3047, 2012.

[18] Y.-C. Lu, B. M. Gallant, D. G. Kwabi, J. R. Harding, R. R. Mitchell, M. S. Whittingham, and Y. Shao-Horn, "Lithium–oxygen batteries: bridging mechanistic understanding and battery performance," *Energy & Environmental Science*, vol. 6, no. 3, pp. 750–768, 2013.

[19] B. D. Adams, R. Black, Z. Williams, R. Fernandes, M. Cuisinier, E. J. Berg, P. Novak, G. K. Murphy, and L. F. Nazar, "Towards a stable organic electrolyte for the lithium oxygen battery," *Advanced Energy Materials*, vol. 5, no. 1, p. 1400867, 2015.

[20] B. D. McCloskey, J. M. Garcia, and A. C. Luntz, "Chemical and electrochemical differences in nonaqueous Li-O_2 and Na-O_2 batteries," *The journal of physical chemistry letters*, vol. 5, no. 7, pp. 1230–1235, 2014.

[21] C. L. Bender, P. Hartmann, M. Vraar, P. Adelhelm, and J. Janek, "On the thermodynamics, the role of the carbon cathode, and the cycle life of the sodium superoxide (NaO$_2$) battery," *Advanced Energy Materials*, vol. 4, no. 12, p. 1301863, 2014.

[22] X. Ren and Y. Wu, "A low-overpotential potassium–oxygen battery based on potassium superoxide," *Journal of the American Chemical Society*, vol. 135, no. 8, pp. 2923–2926, 2013.

[23] M. Yoshizawa-Fujita, K. Johansson, P. Newman, D. R. MacFarlane, and M. Forsyth, "Novel lewis-base ionic liquids replacing typical anions," *Tetrahedron letters*, vol. 47, no. 16, pp. 2755–2758, 2006.

[24] V. Gutmann, "Solvent effects on the reactivities of organometallic compounds," *Coordination Chemistry Reviews*, vol. 18, no. 2, pp. 225–255, 1976.

[25] Z. Peng, S. A. Freunberger, Y. Chen, and P. G. Bruce, "A reversible and higher-rate Li-O_2 battery," *Science*, vol. 337, no. 6094, pp. 563–566, 2012.

[26] B. J. Bergner, M. R. Busche, R. Pinedo, B. B. Berkes, D. Schroöder, and J. Janek, "How to improve capacity and cycling stability for next generation Li–O_2 batteries: approach with a solid electrolyte and elevated redox mediator concentrations," *ACS applied materials & interfaces*, vol. 8, no. 12, pp. 7756–7765, 2016.

[27] E. Mourad, Y. K. Petit, R. Spezia, A. Samojlov, F. F. Summa, C. Prehal, C. Leypold, N. Mahne, C. Slugovc, O. Fontaine *et al.*, "Singlet oxygen from cation driven superoxide disproportionation and consequences for aprotic metal–O_2 batteries," *Energy & Environmental Science*, vol. 12, no. 8, pp. 2559–2568, 2019.

[28] S. Borisov, G. Nuss, W. Haas, R. Saf, M. Schmuck, and I. Klimant, "New NIR-emitting complexes of platinum (II) and palladium (II) with fluorinated benzoporphyrins," *Journal of Photochemistry and Photobiology A: Chemistry*, vol. 201, no. 2-3, pp. 128–135, 2009.

[29] B. D. McCloskey, A. Valery, A. C. Luntz, S. R. Gowda, G. M. Wallraff, J. M. Garcia, T. Mori, and L. E. Krupp, "Combining accurate O_2 and Li_2O_2 assays to separate discharge and charge stability limitations in nonaqueous Li–O2 batteries," *The journal of physical chemistry letters*, vol. 4, no. 17, pp. 2989–2993, 2013.

[30] B. D. McCloskey, D. S. Bethune, R. M. Shelby, G. Girishkumar, and A. C. Luntz, "Solvents' critical role in nonaqueous lithium–oxygen battery electrochemistry," *The Journal of Physical Chemistry Letters*, vol. 2, no. 10, pp. 1161–1166, 2011.

[31] N. B. Aetukuri, B. D. McCloskey, J. M. García, L. E. Krupp, V. Viswanathan, and A. C. Luntz, "Solvating additives drive solution-mediated electrochemistry and enhance toroid growth in non-aqueous Li–O_2 batteries," *Nature chemistry*, vol. 7, no. 1, p. 50, 2015.

[32] B. D. McCloskey, R. Scheffler, A. Speidel, G. Girishkumar, and A. C. Luntz, "On the mechanism of nonaqueous Li–O_2 electrochemistry on C and its kinetic overpotentials: some implications for Li–air batteries," *The Journal of Physical Chemistry C*, vol. 116, no. 45, pp. 23 897–23 905, 2012.

[33] B. McCloskey, A. Speidel, R. Scheffler, D. Miller, V. Viswanathan, J. Hummelshøj, J. Nørskov, and A. Luntz, "Twin problems of interfacial carbonate formation in nonaqueous Li–O_2 batteries," *The journal of physical chemistry letters*, vol. 3, no. 8, pp. 997–1001, 2012.

[34] Z. Zhao, J. Huang, and Z. Peng, "Achilles' heel of lithium–air batteries: Lithium carbonate," *Angewandte Chemie International Edition*, vol. 57, no. 15, pp. 3874–3886, 2018.

[35] J. Højberg, B. D. McCloskey, J. Hjelm, T. Vegge, K. Johansen, P. Norby, and A. C. Luntz, "An electrochemical impedance spectroscopy investigation of the overpotentials in Li–O_2 batteries," *ACS applied materials & interfaces*, vol. 7, no. 7, pp. 4039–4047, 2015.

[36] X. Gao, Y. Chen, L. Johnson, and P. G. Bruce, "Promoting solution phase discharge in Li–O_2 batteries containing weakly solvating electrolyte solutions," *Nature materials*, vol. 15, no. 8, p. 882, 2016.

[37] X. Gao, Z. P. Jovanov, Y. Chen, L. R. Johnson, and P. G. Bruce, "Phenol-catalyzed discharge in the aprotic lithium-oxygen battery," *Angewandte Chemie*, vol. 129, no. 23, pp. 6639–6643, 2017.

[38] Y. Zhang, L. Wang, X. Zhang, L. Guo, Y. Wang, and Z. Peng, "High-capacity and high-rate discharging of a coenzyme Q10-catalyzed Li–O_2 battery," *Advanced Materials*, vol. 30, no. 5, p. 1705571, 2018.

[39] J. Wandt, A. T. Freiberg, A. Ogrodnik, and H. A. Gasteiger, "Singlet oxygen evolution from layered transition metal oxide cathode materials and its implications for lithium-ion batteries," *Materials Today*, vol. 21, no. 8, pp. 825–833, 2018.

[40] S. E. Renfrew and B. D. McCloskey, "Quantification of surface oxygen depletion and solid carbonate evolution on the first cycle of $LiNi_{0.6}Mn_{0.2}Co_{0.2}O_2$ electrodes," *ACS Applied Energy Materials*, 2019.

Oxidation mediators influence on metal–air mechanisms

Each problem that I solved became a rule, which served afterwards to solve other problems.

René Descartes

Contents

Figures

Introduction

Owing to its high capacity per mass and volume, alkaline oxides provide an attractive energy storage. Unfortunately, alkali oxides are also wide-bandgap insulators, preventing efficient charge transport and storage as described in part. **discharge product**; The oxide high resistivity restricts pores filling, limits discharge capacity and causes high charging voltages even at low rates[1–8]. Deeply discharged Li-O_2 cathodes through the solution pathway are filled with large Li_2O_2 particles with several 100 nm in size[2,5,7–10]. Oxidizing them on charge is relatively easy at the charge onset for Li_2O_2 directly in contact with the porous electrode[11–13]. Li_2O_2 more remote from the electrode surface, however, loses contact as charging proceeds, effect seen with additivies as PeDTFSI in part. **charge DABCOnium**, causing rising voltage and incomplete charge. The problems caused by the insulating nature of oxide, e.g Li_2O_2, particles disconnection and parasitic chemistry are interrelated which are particularly severe on charge[1–5,7,14–23]. Parasitic reactions on discharge form side products such as carbonates, which are hard to oxidize and may release $^1O_2$ as seen in part. **Electrode + side reaction + singlet oxygen carbonate**. More of these side products form on charge with increasing rate as the charge voltage rises, self-amplifying the processes[16,17,24,25].

Since growth/dissolution of Li_2O_2 occurs at its surface, Li^+ and e^- transport into/out of the bulk particle are not required. Li_2O_2 role restriction to charge storage could be enabled by diffusion of available Li^+ and e^- at its surface through the electrolyte. Relocate the charge transport away from the peroxide circumvent moreover the issue of detached peroxide formed during discharge. The reactions could proceed away from the electrode and no discharge products would be lost. Bypassing alkali oxide for ion and electron transport may, in turn, enable high-power metal-O_2 cells. The main problem is the e^- transfer thought the electrolyte. During discharge, the charge transport can be assured by superoxide through the disproportionation process which correlates with higher discharge capacities as seen in part. **discharge intro** and ch. **disp**. Disproportionation, yet, does not permit recharge of particles formed away from the electrode and is slow or not favoured for Na-O_2 and K-O_2 cells.

Redox mediators address the charge transport between the e^- conductor and O_2 or oxide distant from the electrode in a more controlled fashion[2,4,6,15,19,20,24,26–30]. Mediators act by being reduced/oxidized at the e^- conductor, diffusing through the electrolyte and reducing O_2 or oxidizing alkali oxide at low overpotential, thereby being regenerated themselves. By switching electrode reactions to mediators reduction/oxidation, the peroxide becomes a convenient way to store charge and enable higher power batteries; The only requirements are faster reaction kinetic and mediators diffusion than the reaction through the highly resistive alkali oxides. Oxidation mediators allow, in principle, charging at nearly zero overpotential and a wide variety of mediators have been studied based on their redox potential as well as O_2 evolution efficiency in Li-O_2 cells and attempted in Na-O_2 cells[2,6,15,19,20,26–31]. As the main concern is the side products formation during charge and disconnect alkali oxides, this thesis will only focus on oxidation mediators. While numerous adapted mediators are known in literature, little is known on the actual mediated mechanisms and their relations with parasitic chemistry. Oxidation mediators may also induce side reactions, if for example the oxidized mediators can oxidized the electrolyte solvent[6,24,26,32]. Furthermore, chemical oxidation of peroxides and superoxides in non-aqueous media by e.g. chlorine or ferrocenium has been found to generate $^1O_2$, mediators may themselves contribute to its production[33–37]. The elementary steps during mediated Li_2O_2 oxidation pathways and governing factors leading to $^3O_2$ or $^1O_2$ are yet to be described. Only knowing them in detail may allow designing mediators for $^1O_2$-free Li-O_2 battery recharge.

Using the methods previously described in this thesis, we decipher in this chapter the mechanism of mediated alkali peroxide/superoxide oxidation and identify pathways that lead to $^1O_2$. In a first step, one electron mediated oxidation generates a superoxide intermediate form peroxide. The second step can either proceed via superoxide disproportionation or superoxide oxidation by mediators as depicted in fig. 5.1. $^1O_2$ is hence not suppressed by oxidation mediators as it can form by disproportionation or oxidation at potentials higher than the thermodynamic threshold discussed in ch. **singlet oxygen**. For low redox potential mediators, the $^1O_2$ amount is determined by the relative kinetics of the two pathways. We found that with commonly used mediators disproportionation can not be neglected and thus $^1O_2$ production. Once the $^1O_2$ presence is established, the stability of oxidation mediators towards $^1O_2$ needs to be appraised. By using UV-vis spectroscopy, we found mediator degradations at important rates in contact with $^1O_2$. Mediators with quenching moieties, e.g. tertiary amines presented in ch. **Quencher**, display increased robustness most likely by deexciting singlet oxygen to its triple state and are consequently desirable in an oxidation mediator. Chemical stability of mediators is also an essential parameter to ensure efficiency through long term cycling. We show that common mediators, e.g. TEMPO or Fc, do not reform their reduced from upon alkali oxide oxidation despite O_2 release. Mediators can spontaneously form highly oxidative species in the case of mediators with multiples oxidation degrees, e.g. TDPA, resulting in $^1O_2$ evolution by alkali oxide mediated oxidation. The results establish the main characteristic wished in a mediator to avoid degradation and achieve a good cyclability, i.e chemical stability, fast superoxide oxidation kinetic and good $^1O_2$ quenching efficiency.
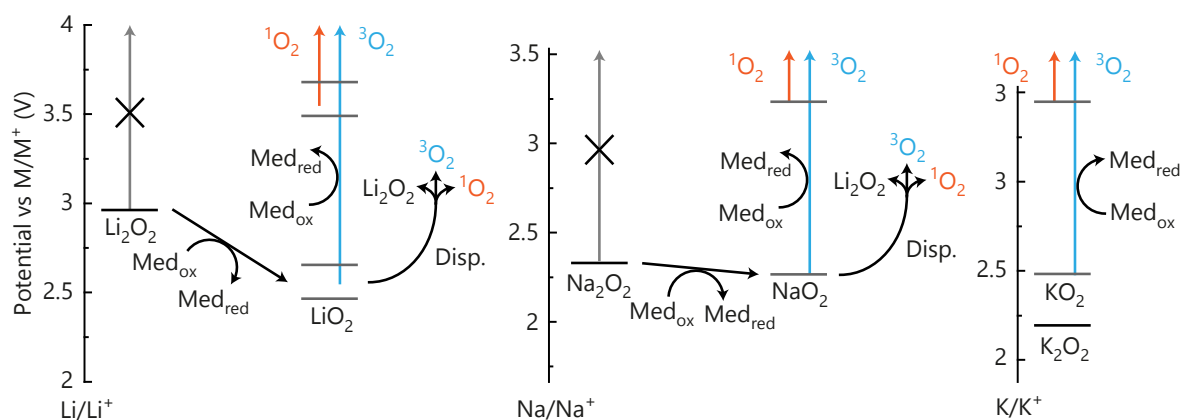
Figure 5.1: **Mediated alkali (su)peroxide oxidation mechanism.**

5.1 Oxidation mediators in metal–air batteries

The oxidation mediators are oxidized at the electrode and oxidized in turn alkali oxide giving back the reduced mediator. The oxidation mediator being solvated any peroxide surface in contact with the solution can be subject to the reaction. Notwithstanding the alkali oxide thickness or deposition geometry, the reaction potential is fixed by the mediator itself, if sufficient pristine carbon surface is present. By choosing appropriate mediators with a redox potential just above the O_2/MO_2 potential (M= Li_2, Na or K), e.g. 2.96 V_{Li/Li^+} for lithium based cells, nearly zero overpotential during charge is in principle possible. The promises of these soluble mediators in charge are tremendous for the field and numerous studied searched for appropriate mediators either organic, organometallic or halide molecules[19,26,27,38]. Commons given criteria are redox potential, fast kinetics to achieve fast charge rate, reduce the production of side products as well as stability in the Li-O_2 environment. Unless an impermeable separator is used, it needs to be compatible with the lithium metal anode. Organic mediators have most widely been investigated by dint of their wide variability[6,26].

While the exact mechanism is unknown, the reaction kinetic can be in first approximation decomposed in two steps. These are an heterogeneous oxidation of the mediators at the electrode surface (k_0) followed by the heterogeneous oxidation of Li_2O_2 by the oxidized mediators according to the overall reaction given in eq. 5.1. Due to the lack of more precise mechanistic descriptor, divergent views emerge in the literature. On one hand, apparent rate constants (k_{app}) of the overall reactions on Li_2O_2 were determined using scanning electrochemical microscopy and compared to the k_0 obtained by cyclic voltammetry on glassy carbon for a wide range of mediators with potential ranging from $\sim$3.1 to 3.85 V_{Li/Li^+}[28]. Since no clear dependence between k_0 and k_{app} appeared, it was concluded that the reaction between mediators and Li_2O_2 is an inner-sphere process and mostly governed by the sterics of the redox molecules. From the obtained k_{app}, it was calculated that even for the slowest mediators the apparent kinetics appears fast enough to sustain with a porous Li_2O_2 filled electrode a superficial current density as high as $\sim$100 mA·cm^{-2}. On the other hand, differential electrochemical mass spectrometry (DEMS) experiment showed a clear correlation between the onset potential for O_2 evolution and the mediator oxidation potential, a behaviour interpreted through an outer-sphere mechanism using the Marcus theory and Nernst law[39]. O_2 evolution was moreover found to start at low mediators concentration (e.g. 10^{-5} M for TTF).

$$2\,M^+ + Li_2O_2 \longrightarrow 2\,M + O_2 + Li^+ \qquad\qquad (5.1)$$

As the apparent rate constants seem relatively high even for the slowest mediator and taking into account the wide range of potential covered by organic molecules, the main criterion emerges as the influence on parasitic chemistry. Literature shows, yet again, discrepancies. Using mediators, online electrochemical mass spectrometry and pressure monitoring experiments showed an improved e$^-$/O_2 ratio[15][20]. Other studied showed that mediators oxidation of chemical Li_2O_2 deviate from the theoretical 2 e$^-$/O_2 ratio, instability of some mediators in presence O_2 or presence of CO_2 production by action of mediators below the Li_2CO_3 oxidation potential, all indicating side reactions[19,39].

The reactivity of some mediators could be explained by oxidation of the solvent rather than Li_2O_2, resulting in irreversibility[6][24,26,32]. A mechanistic study rationalised this effect by comparing the position of the oxidized mediator singly occupied molecular orbital to the highest occupied molecular orbital of the solvent[6]. The stability of the mediator is especially problematic due to their often organic nature, easily degradable at the contact with the lithium metal anode and potentially singlet oxygen.

5.2   Oxidation mediator mechanisms and singlet oxygen formation

The mediated alkali peroxide oxidation is commonly described by the overall reaction (eq. 5.2)[2,4,6,15,20,26–31]. The exact mechanism of mediated alkali peroxide oxidation and pathways to $^1O_2$ has to be elucidate before design $^1O_2$-free metal-O_2 battery mediators. A previous study, yet, hinted the decomposition of the oxidation reaction in two individual steps based on DEMS experiment[39]. To decipher the mechanism, we hence hypothesize that mediated oxidation may follow two possible pathways. In the first case, oxidation proceed via a direct two-electron oxidation as described in eq. 5.1. In second case, oxidation proceed by superoxide species formation (noted MO_2 or superoxide through the rest of this chapter) through a mediated one-electron step according to eq. 5.3. Once superoxide species are formed, the reaction can either continue with a second one-electron mediated oxidation described in eq. 5.4 or by disproportion as depicted in part. **disproportionation** and in eq. 5.5.

$$M_2O_2 + 2\,RM_{ox} \xrightarrow{\ k_{app}\ } 2\,M^+ + 2\,RM_{red} + 2\,O_2 \tag{5.2}$$

$$M_2O_2 + RM_{ox} \xrightarrow{\ k_1\ } M^+ + RM_{red} + MO_2 \tag{5.3}$$

$$MO_2 + RM_{ox} \xrightarrow{\ k_2\ } M^+ + RM_{red} + MO_2 \tag{5.4}$$

$$MO_2 + MO_2 \xrightarrow{\ k_{disp}\ } M_2O_2 + x\,^3O_2 + (1-x)^1O_2 \tag{5.5}$$
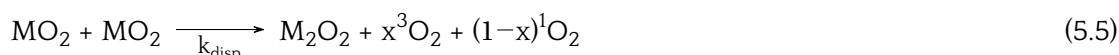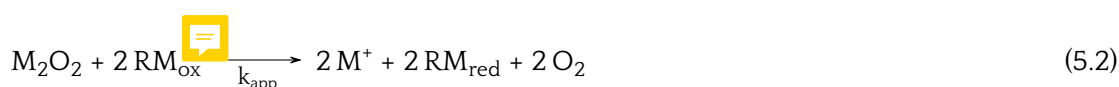
$$\tag{5.6}$$

5.2.1   Mediated oxidation pathways

Two $^1O_2$ production pathways emerge form the hypothetized elementary steps, either via disproportionation, as described in ch. **disproportionation**, or via alkali oxide oxidation above a potential threshold (e.g. 3.45 V_{Li/Li^+} for Li_2O_2 and ~3.55 V_{Li/Li^+} for MO_2 with M = Li, Na, K), as described in part. **direct oxidation**. Mediated alkali oxide oxidation could produce $^1O_2$ in accord with previous works reporting its prodcution from reaction between O_2^- and oxidized mediator with sufficiently high potentials such as Fc (3.56 V_{Li/Li^+}, measured by CV in **Annexes**)[35–37]. Using a mediator with a potential below the $^1O_2$ potential threshold (MBT, measured by CV in **Annexes**) and a mediator above (Tempo, measured by CV in **Annexes**), we performed characterization of the $^3O_2$ and $^1O_2$ released upon an excess of Li_2O_2 and KO_2 powder oxidation. The yields determination is based on a combination of MS and HPLC, similarly to part. **part disp MS** and further described in **Annexes**. KO_2 was used as stable substitue to LiO_2 due to its stability and similar redox potential, as explain in part. **part disp MS**. The mediators were chemically oxidized beforehand to avoid the presence of lithium ions in the superoxide case according to the procedure described in **Annexes**. The results are illustrated in fig. 5.2 and expressed in O_2 mol per 2 RM_{ox} for Li_2O_2 and O_2 mol per RM_{ox} for KO_2 corresponding to the theoritical yield given in eq. 5.2 and 5.4.

Change figure for the good 1O2 yield
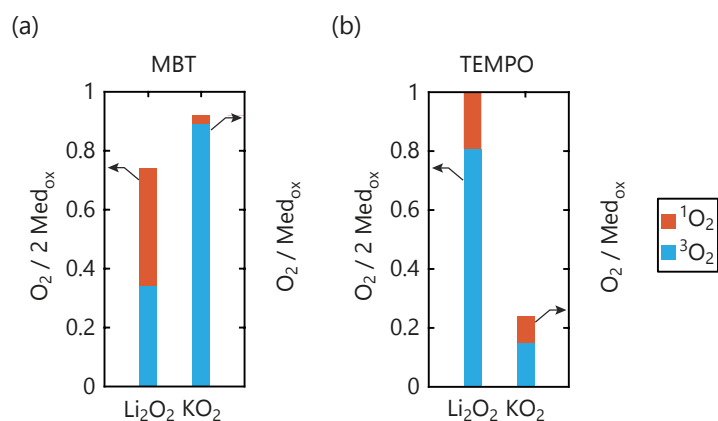
Figure 5.2: **$^3O_2$ and $^1O_2$ yield upon mediated peroxide and superoxide oxidation by MBT$^+$ and TEMPO$^+$.** $^3O_2$ and $^1O_2$ evolution obtained by addition of 1 mM (a) MBT$^+$ or (b) TEMPO$^+$ in TEGDME to an excess of Li_2O_2 or KO_2.

$^1O_2$ formation from KO_2 and Li_2O_2 oxidation with TEMPO$^+$ indicates well that singlet oxygen can be produced via mediated alkali oxide oxidation. As KO_2 does not disproportionate in absence of more Lewis acidic cations, explain in part. **disproportionation**, the important presence of $^1O_2$ can be safely associated with the superoxide oxidation. Singlet oxygen, yet, can not be produced directly by mediators below ~3.5 V_{Li/Li^+} and its presence can then be used as a proxy for disproportionation as in part. **disprop consequences**. Li_2O_2 oxidation with MBT$^+$ is accompanied by a clear release of singlet oxygen and ~~consequently~~ a negligible one with KO_2, indicating LiO_2 disproportionation even in mediator ~~presences.~~ If Li_2O_2 were oxidized by a direct two-electron process, no $^1O_2$ would be expected ~~for~~ Li_2O_2 and if singlet oxygen were produced by oxidation then it should also be produced ~~for~~ KO_2. The presence of disproportionation indicates hence a reaction in two steps as for non-mediated charge. Direct two-electron oxidation appears additionally unlikely since a trimolecular process with two mediators hitting the same surface spot at the same time would be required. Similarly, Na_2O_2 mediated oxidation occurs in two steps with superoxide as intermediate; The results are shown in **Annexes**.

5.2.2 Mediated oxidation kinetics

The use of low potential oxidation mediators hence does not prevent disproportionation and subsequent $^1O_2$ formation. Oxidation mediators could reduce the disproportionation ~~importance,~~ and ~~so~~ the $^1O_2$ yield, since ~~their~~ is competing kinetics between MO_2 disproportionation and mediated oxidation. To separate the influence of each kinetics , we measured the rate of the overall reaction between the mediators and Li_2O_2 (eq. 5.2, k_{app}), the rate of the superoxide oxidation (eq. 5.4, k_2) and the disproportionation rate (eq. 5.5, k_{disp}) for a wide range of mediators (TDPA, MBT, TMPD, DMPZ, Fc, I_2 [6,28,30,32]) covering potential from 3.09 to 3.63 V_{Li/Li^+} which are determined in **Appendix**.

Mediators were found to be all UV–vis active and their oxidation reduction rates were measured using their absorbance evolution starting at a known initial concentration. The oxidized mediator solutions were ~~exposed to~~ an excess of Li_2O_2 (k_{app}) or KO_2 (k_2) in pellet shapes with known surface area under agitation, exemplified by DMPZ in fig. 5.3. The concentration decays overtime were then fitted and the rate at the ~~initial time~~ used to calculate the ~~kinetic reaction~~ according to a pseudo first-order reaction in first approximation. The initial rate was used to neglected side reaction influences (e.g. by $^1O_2$ action or disproportionation

as Li^+ will be released upon Li_2O_2 oxidation). The mediators were oxidized chemically to avoid Li^+ ~~presence~~ and ~~subsequential~~ disproportionation of KO_2, as described in ch. **Disp**. The methods and the results are detailed in **Annexes**. Measurements via UV-vis ~~present the convenience~~ to detect possible side reactions not reforming the mediator ~~reduced forms~~ and probe the reactions on the surface as a whole compared to previous studies performed by scanning electrochemical microscopy[28]. The disproportionation rate (k_{disp}) was measured by pressure monitoring in a closed vessel after injection of 0.5 M LiTFSI TEGDME electrolytes onto KO_2 pellets under similar condition than for the mediator kinetic experiments. The pressure evolution was then fitted by a second-order ~~kinetic~~ reaction represented by the eq. 5.5, 5.7, 5.8 and 5.9 and illustrated in fig. 5.4. It can be noted that the obtained rates are minimal rates as the production of $^1O_2$ could not be detected by means of pressure measurements. We showed previously in ch. **disp** that weak Lewis acid highly influences the disproportionation reaction and increased the $^1O_2$ production. Oxidized mediators are weakly Lewis acidic and their possible influences on disproportionation were modelled by measuring disproportionation in presence of a 0.5 M LiTFSI/0.5 M TBATFSI mixture in TEGDME. The presence of TBA^+ results in a more than 2.5 fold disproportionation rate increase.
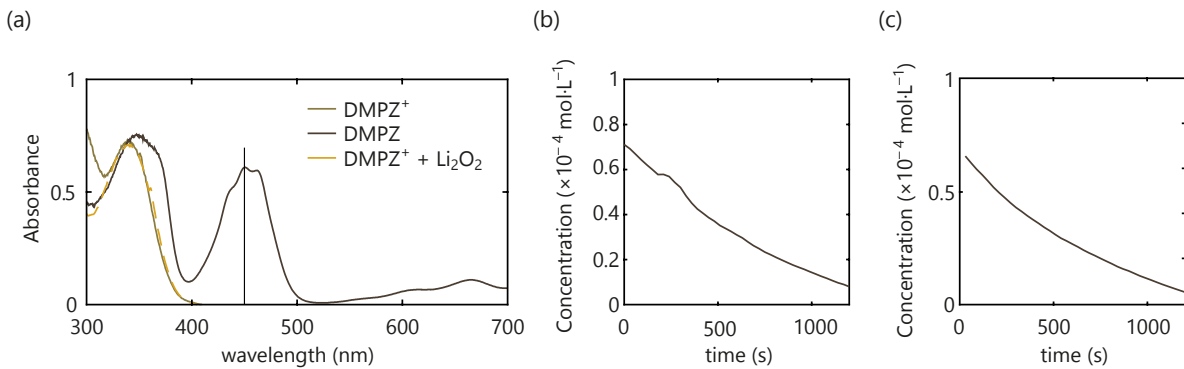
Figure 5.3: **DMPZ mediated oxidation rate obtained by UV-vis.** (a) UV-Vis spectra of DMPZ (brown), $DMPZ^+$ (light brown) and $DMPZ^+$ after reaction on Li_2O_2 (yellow). The black line denotes the wavelength used for kinetic measurement (450 nm). (b)-(c) $DMPZ^+$ concentration over time in contact with (b) KO_2 or (c) Li_2O_2 pellets

Verifier equation

$$-\frac{dC}{dt} = k \cdot C^2 \tag{5.7}$$

with C the concentration ($mol \cdot L^{-1}$); t, the time (s) and k, the kinetic constant ($mol^{-1} \cdot L \cdot s^{-1}$).

$$\frac{1}{C} - \frac{1}{C_0} = k \cdot t \qquad \frac{1}{(P_f - P_0) - (P - P_0)} - \frac{1}{P_f - P_0} = k \cdot t \tag{5.8}$$

with $C_0 = P_f - P_0$ and $C = (P_f - P_0) - (P - P_0)$; P_0 is the initial pressure (Pa), P_f is the final pressure (Pa); Assuming the temperature and the volume constant.

$$P - P_0 = \frac{((P_f - P_0)^2 \cdot k \cdot t)}{((P_f - P_0) \cdot k \cdot t + 1)} \tag{5.9}$$
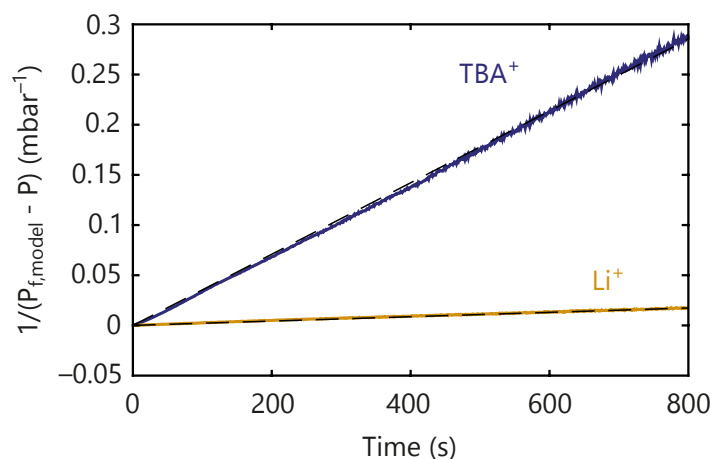
Figure 5.4: **Pressure evolution during KO$_2$ disproportionation in presence of Li$^+$ or Li$^+$/TBA$^+$ TEGDME electrolytes.** Electrolytes contained either 0.5 M LiTFSI (yellow) or 0.5 M LiTFSI and 0.5 M TBATFSI (purple). The fit obtained by eq. 5.9 are given in black dotted line.

The overall reaction rate between the oxidized mediator and Li$_2$O$_2$ is composed of several elementary step which have been elucidated in the previous part. **mechanism**. First, the reaction proceed via a one-electron oxidation according to eq. 5.3 (k$_1$), followed by either a second one electron oxidation or disproportionation. Areal mediated oxidation rate must be recalculated by assuming a mediator concentration ($v = k \cdot C_{mediator}$), here 10 mM, to be be compared to the areal disproportionation rate (v_{disp}) at the solid superoxide surface.. The initial disproportionation rate could then be compared to the mediator kinetics in fig. 5.5; The range of v_{disp} values between pure Li$^+$ and Li$^+$/TBA$^+$ allows to determine the dominant kinetic and hence the major O$_2$ evolution pathway from superoxide in presence of a specific mediator. The k$_{app}$ kinetics values obtained appears moreover similar to the ones obtained by SECM in the literature as shown in **Annexes**[28].

(a)   (b)
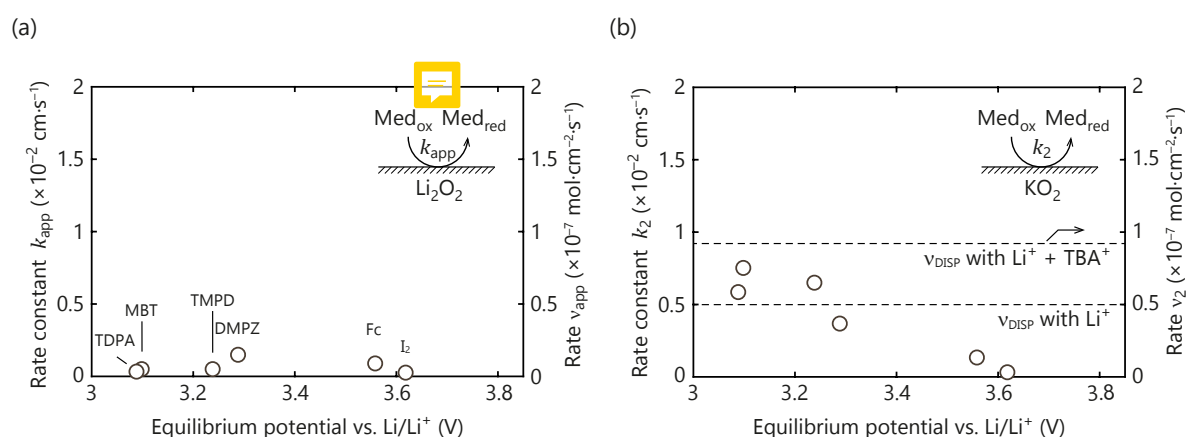
Figure 5.5: **Kinetics of mediated (su)peroxide oxidation and superoxide disproportionation.** Kinetic constants k (left axis) and rates v assuming a 10 mM concentration (right axis) in TEGDME for the reaction between oxidized mediators and the Li$_2$O$_2$ surface (a) and the KO$_2$ surface (b) obtained by UV-vis. Superoxide disproportionation rate in presence of 0.5 M LiTFSI or 0.5 M LiTFSI and 0.5 M TBATFSI is indicated by dashed line in (b).

Remove equilibrium on the botttom axis

O$_2$ evolution is clearly dominated by disproportionation for mediators with redox poten-

tial above 3.5 V_{Li/Li^+}. For high potential oxidation mediators, the disproportionation rate in pure Li^+ electrolyte appears more than 3 times faster than mediated superoxide oxidation for a 10 mM concentration. The results are more nuanced for lower redox potential with mediated superoxide oxidation rates similar or slightly higher to disproportionation in pure Li^+ electrolyte. The disproportionation in the presence of TBA^+ as a model of soft lewis acid, yet, stays faster than the mediated oxidation. Disproportionation, similarly ~~than for~~ non-mediated cell, ~~is~~ at least one of the main ~~reaction~~ pathways ~~which is known~~ to ~~yield~~ $^1O_2$, especially in presence of weak Lewis acids as oxidized mediators. The second step kinetic, ~~whether~~ it ~~be~~ oxidation or disproportionation, appears much faster than the overall reaction rate on Li_2O_2. The ~~reaction~~ rate limiting step is thus the first electron oxidation to form superoxide from peroxide.

5.2.3   Consequences

The presence of singlet oxygen permits to reveal~~s~~ the oxidation reaction mechanism which is ~~resumed~~ in fig. 5.1. $^1O_2$ formation below 3.4 V_{Li/Li^+} from Li_2O_2 oxidation indicates dispro-portionation ~~mechanism~~ and hence superoxide ~~formation.~~ Direct two–electron oxidation of Li_2O_2 or Na_2O_2, as described more ~~in~~ detail~~s~~ in **Annexes**, may ~~be~~ thus excluded. The super-oxide formation is moreover the rate limiting step of the reaction and should be optimized to allow fast reaction kinetic. By superoxide, we do not imply any particular species as it may, for example, be a Li–deficient solid solution $Li_{2-x}O_2$ phase or dissolved $LiO_{2(sol)}$ which ~~are~~ proposed for non–mediated peroxide oxidation[1,3,9,21,22].

After superoxide formation, O_2 can subsequently evolve through two competing pathway, a second mediated oxidation or disproportionation. $^1O_2$ presence has been shown to result in important degradation in metal–air batteries in previous chapters (ch.**singlet oxygen, Dabco**). Mediated metal–air cells are no stranger to $^1O_2$ existence. Singlet oxygen can be formed by superoxide oxidation above ~3.55 V_{Li/Li^+} ~~notwithstanding~~ direct or mediated ~~reaction.~~ High potential mediator shows ~~important lack~~ of $^3O_2$ release, especially in contact with KO_2. In this case, the absence of disproportionation impose all the reaction pass by the oxidation pathways, thus $^1O_2$ production, despite the lower kinetic of high potential mediators.

Disproportionation yields $^1O_2$, especially in presence of weak Lewis acids as discussed in ch. **Disp**. ~~Mediated $^1O_2$ free cells could theoretical be possible as it would not be induced by superoxide oxidation with low redox potential mediators~~. The mediators should, yet, present a ~~kinetic~~ sufficiently high ~~with O_2^-~~ ~~to prevent consequent~~ disproportionation. For the wide range of mediators tested here, disproportionation ~~and so~~ $^1O_2$ are inevitable as its kinetic is at least comparable to the mediator ones. Efforts should hence be direct towards designing mediators with fast superoxide oxidation kinetic and low redox potential to reduce the $^1O_2$ yield during charge.

5.3 Singlet oxygen reactivity of oxidation mediators

Among possible oxidation mediators, organic molecules have received special attention due to their variety and tunable oxidation potential via synthesis within the same chemical class[20]. Their organic natures, yet, make them susceptible to degradation by singlet oxygen, formed at all stage of cycling as discussed in ch. **ch. singlet oxygen**. Singlet oxygen is know for being dienophile and mediators possessing double bonds ~~should~~ be particularly sensitive to its presence, e.g. DMPZ, TTF, MPT or TMPD[6,19,28]. The presence of oxidation mediators does not prevent $^1O_2$ ~~presence~~ as explain in the previous part. **previous part**. Since Li_2O_2 oxidation proceed via superoxide formation, singlet oxygen can be formed by disproportion-ation even with low redox potential mediator. The reactivity of organic oxidation mediators towards $^1O_2$ needs to be assessed to ensure efficient effect during extended cycling and understand mechanism favouring their stability.

Redox mediators may be reactive not only with $^1O_2$ but potentially to other oxygenated species present in metal–air battery chemistry i.e, O_2, O_2^- and peroxide. We thus investigated the stability of some redox mediators towards these species. Among possibly reactive media-tors, tetrathiafulvalene (TTF) and dimethylphenazine (DMPZ) were selected ~~and schematized~~ in fig. 5.6. Both TTF and DMPZ present good oxidative stability towards TEGDME, a common solvent in metal–air batteries[6]. TTF was also chosen for historical reason, being one of the mediators proposed[19], and DMPZ due to its low redox potential[6]. TTF and DMPZ also ~~present~~ different heteroatoms that may influence their stability, sulfur or azote respectively. As singlet oxygen is a known electrophile[40], we investigated the stability of both the ~~media-tor~~ reduced and oxidized states to ~~verify the oxidation influence~~ on their reactivity[40].

Resize TTF

(a)   (b)
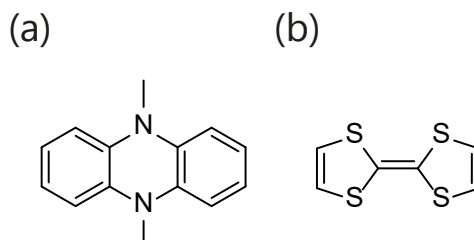
Figure 5.6: **Structure of the studied mediators.** (a) DMPZ (b) TTF.

5.3.1 Oxidation mediators in the reduced state

To determine the mediator stability, ^{1}H-NMR spectra in DMSO-d_6 were recorded for each mediator after 24 hours in presence of the oxygen~~ated~~ species as described in **Annexes**. By comparing with the pure substance ^{1}H-NMR in fig 5.7, neither dissolved O_2, dissolved O_2^- or Li_2O_2 reacts perceptibly with the studied mediators as previously reported in the case of DMPZ and O_2[6].

(a)

(b)
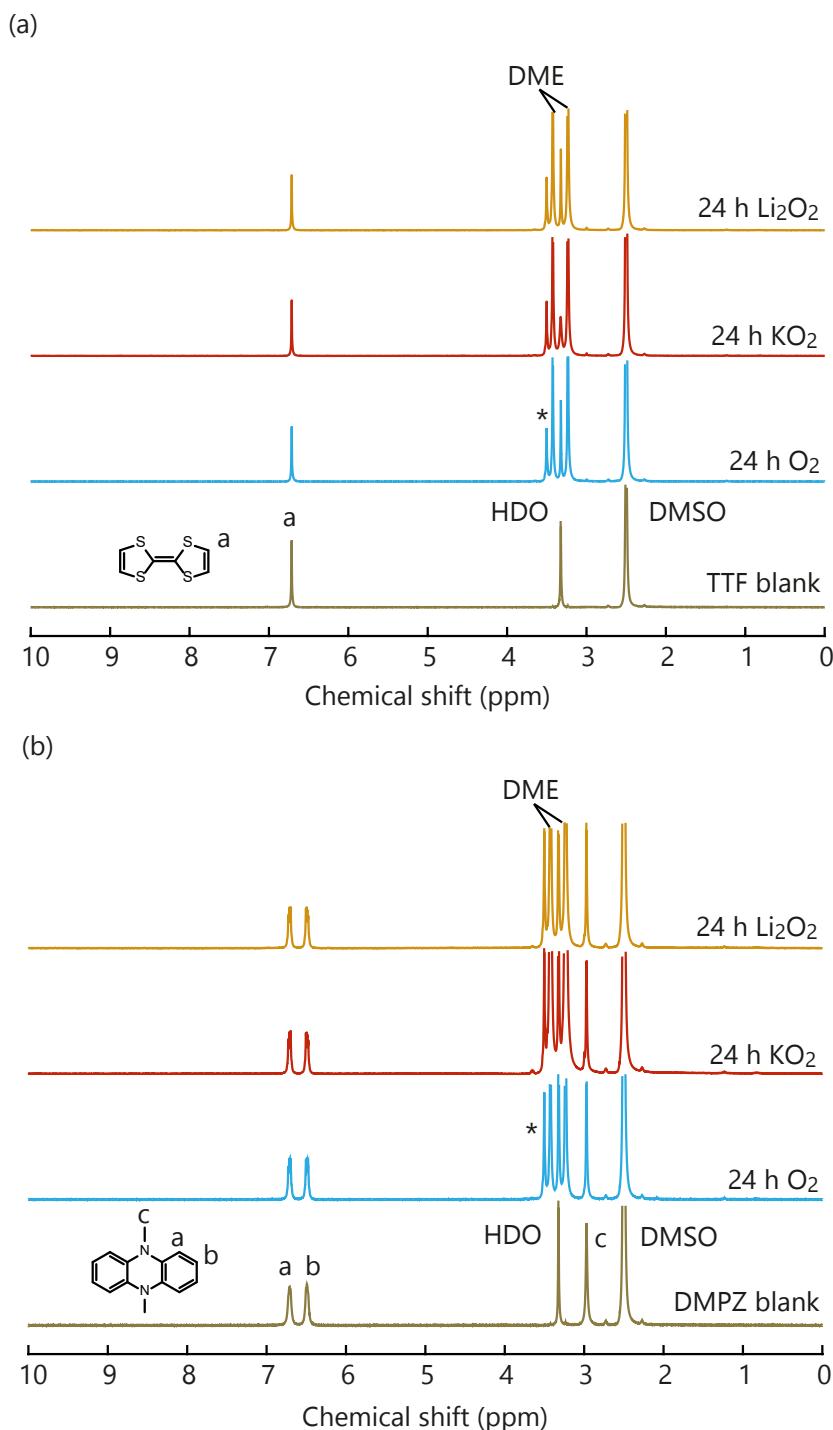
Figure 5.7: **Stability of DMPZ and TTF in contact with O_2, KO_2 and Li_2O_2 by ^{1}H-NMR in DMSO-d_6.** (a) ^{1}H-NMR spectra for DMPZ and (b) TTF. The DMSO peak is taken as internal reference for quantitative comparison of spectra. The * denotes a residue from DME evaporation, which amounts to a content of 1 ppm in the DME.

As other oxygen species do not appears to react with the mediators, we investigate their stability against photochemically produced $^1O_2$ by dint of Pd_4F and illumination at 643 nm, as described in part. **singlet oxygen production** and more in details in **Annexes**. ^{1}H-NMR analyses of the solutions DMSO-d_6 were conducted after 3 hours illumination and show the mediator disappearances in fig. 5.8. In the TTF case, the reactivity is clearly represented by the apparition of new peaks in the NMR spectrum; These new peaks indicate the formation

of 1,3-dithiol-2-one, schemed in insert of fig. 5.8, in accord with a mechanism proposed in literature[41]. Concerning the DMPZ, the NMR peaks intensities decreased by ~40% according to the calculated integrals. The absence of new peaks may indicate that DMPZ decomposition ultimately forms inorganic products or evolve as gases. Nevertheless, the ^{1}H–NMR spectra unequivocally show organic mediators reaction with $^1O_2$ despite its stability with other oxygenated species.
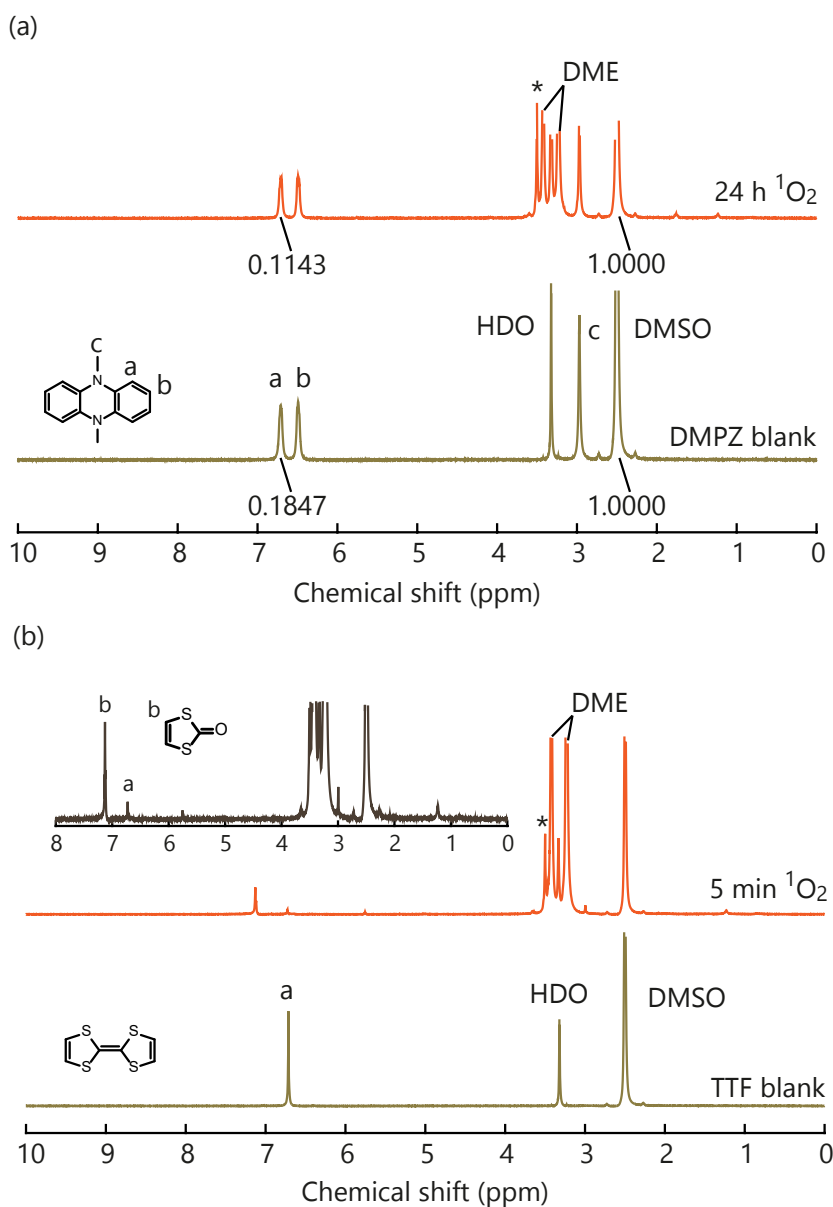
Figure 5.8: **Stability of DMPZ and TTF in contact with $^1O_2$ by ^{1}H-NMR.** (a) ^{1}H–NMR spectra for DMPZ after 24 hour exposure and (b) TTF after 24 hour exposure 5 min exposure. The insert of (b) gives the 1,3-dithiol-2-one ^{1}H-NMR for comparison as a possible decomposition products. The integrals are given for the peak (a) in (a). The DMSO peak is taken as internal reference for quantitative comparison of spectra. The * denotes a residue from DME evaporation, which amounts to a content of 1 ppm in the DME.

The DMPZ and TTF evolutions were monitored in situ by UV-vis in presence of photochemically generated $^1O_2$. A mediator concentration of 60 μM in TEGDME has been determined as a suitable concentration for UV-vis spectroscopy measurement beforehand

and ~~will be~~ used through the rest of this study if not mentioned otherwise. The main absorbance peaks of each mediator were found to decrease over time accompanied by the appearance of new peaks, indicating side products formation with $^1O_2$, as illustrated in fig. 5.9(a)-(c). TTF is much more reactive than DMPZ with a noticeable reaction in a few seconds where DMPZ necessitate a few hours. To illustrate clearly the different reactions rate, the evolution of the main absorbances peaks denoting either the disappearance of the mediators or the appearance of side products are given over $^1O_2$ exposure time in fig. 5.9(b)-(d). TTF shows high reaction rate and fully decompose over approximately 30 s, revealed by the peaks evolution end. DMPZ is more robust and presents a decay of approximately one-thirds after 3 hours; the peak indicating side products stays stable after a bit more than 30 minutes, indicating formation of species UV-vis inactive or gases in accord with the ^{1}H-NMR spectra. Although reactivity with O_2, O_2^-, or Li_2O_2, over extended time cannot be completely dismissed, the mediators' reactivity with $^1O_2$ seems much more problematic especially considering the possible presence of singlet oxygen at all stage of cycling.

(a)

(b)

(c)

(d)
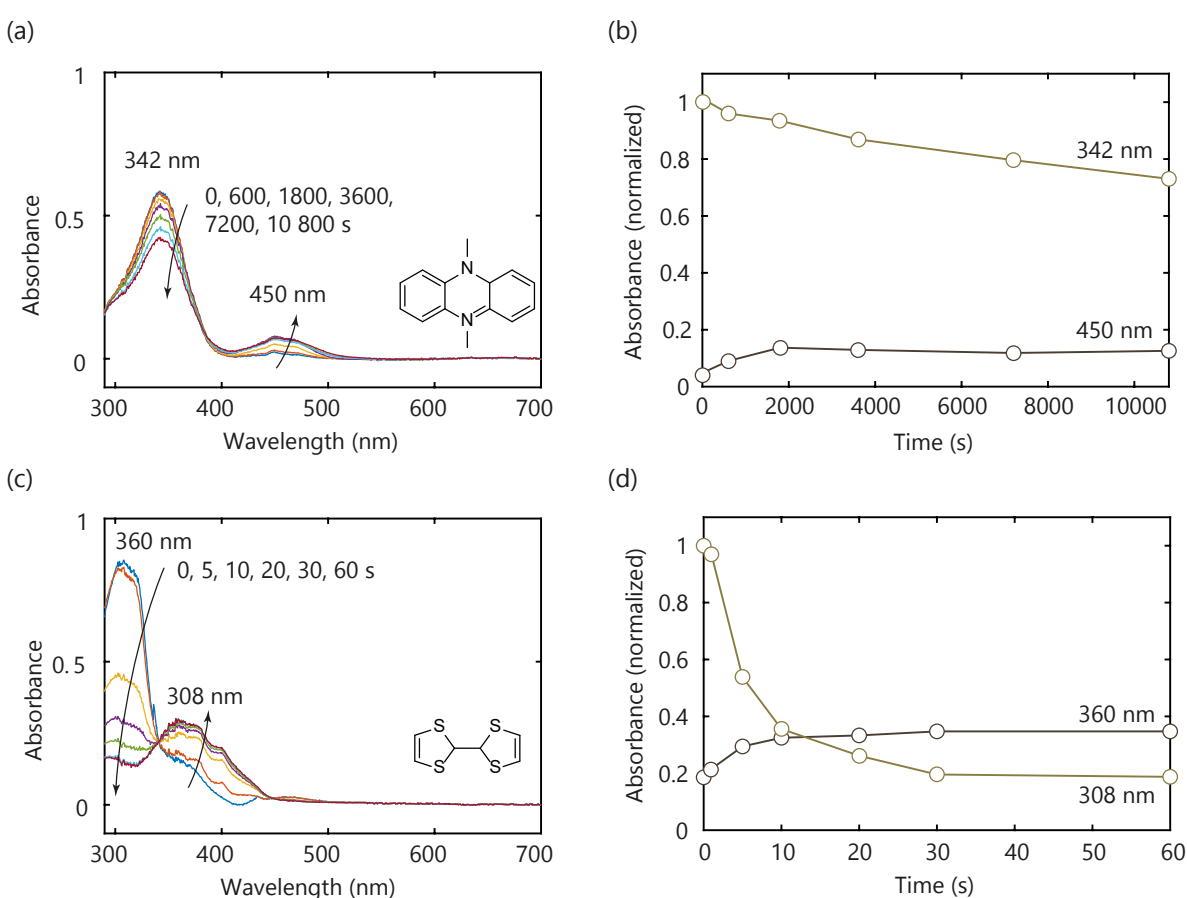
Figure 5.9: **Evolution of DMPZ and TTF in contact with $^1O_2$ over time by UV–vis.** (a)-(c) UV-Vis spectra of DMPZ (a) and TTF (c) in 0.1 M LiTFSI/TEGDME electrolyte upon $^1O_2$ exposure after substraction of the sensitizer signal. (b)-(d) Absorbance evolution over time normalized to the initial value upon exposure to $^1O_2$ for (b) DMPZ and (d) TTF at the mentioned wavelength.

5.3.2   Oxidation mediators in the oxidized state

Since $^1O_2$ reactivities associated to "ene" or "diene" reaction [42–45], the lower electronegativity of the oxidized mediators might results in increased stability. To verify this assumption, the ~~mediator~~ oxidized forms were exposed to $_1O_2$ similarly to the previous paragraph and their evolutions followed by UV-vis, ~~which are~~ depicted in fig. 5.10(a)-(c); The details about the

electrochemical oxidation procedure can be found in **Annexes**. Both oxidized mediators present degradation albeit at slower rates than their reduced forms.
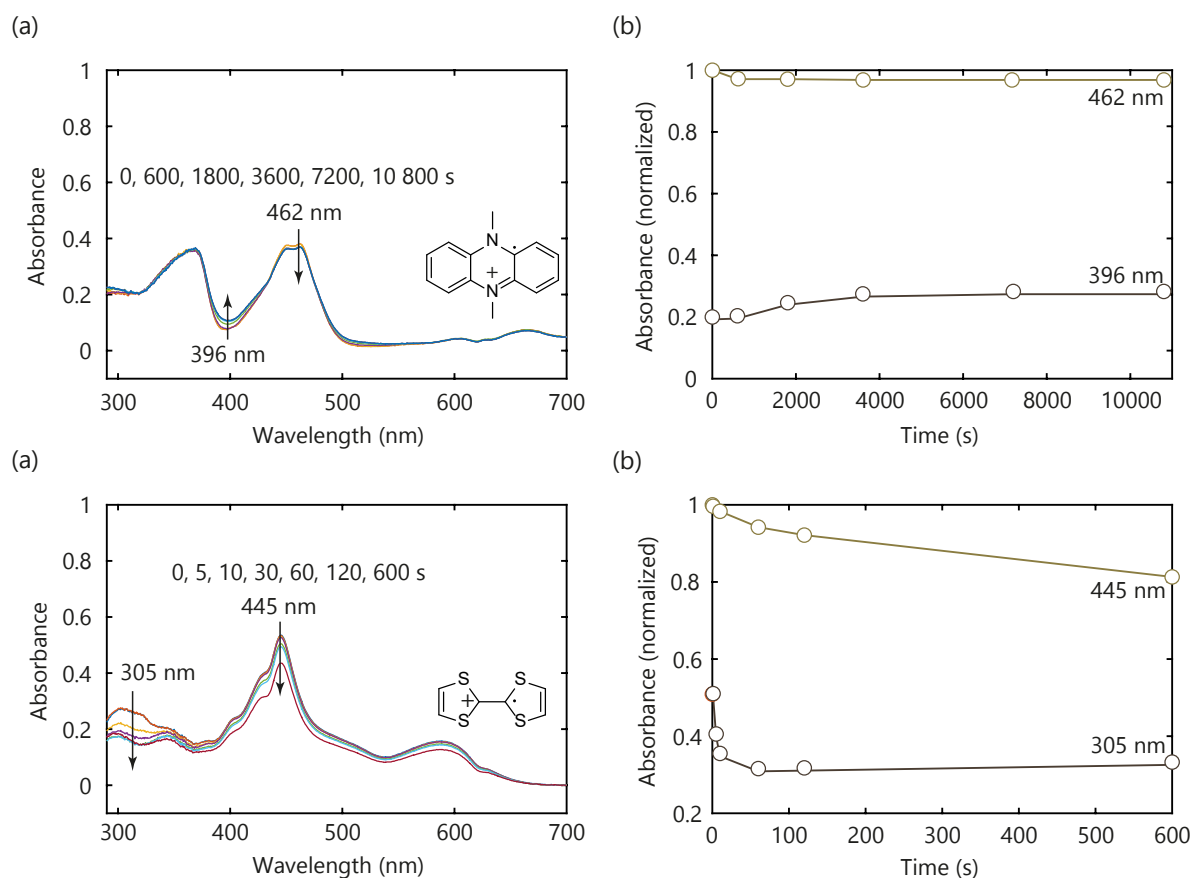
Figure 5.10: **Evolution of DMPZ$^+$ and TTF$^+$ in contact with $^1O_2$ over time by UV-vis.** (a)–(c) UV-Vis spectra of DMPZ$^+$ (a) and TTF$^+$ (c) in 0.1 M LiTFSI/TEGDME electrolyte upon $^1O_2$ exposure after substraction of the sensitizer signal. (b)–(d) Absorbance evolution over time normalized to the initial value upon exposure to $^1O_2$ for (b) DMPZ$^+$ and (d) TTF$^+$ at the mentioned wavelength.

DMPZ$^+$ shows a decrease of the 450 nm peak and increasing absorbance between 400 and 500 nm, which indicates the formation of degradation products over $^1O_2$ exposure time. Comparing now the rates of the reduced and oxidized forms from fig. 5.9(b) and fig. 5.10(b) respectively, after more than 3 hours illumination DMPZ$^+$ exhibits less than 5% degradation whereas the DMPZ only remains at 65% of its initial concentration. Likewise, TTF$^+$ is more stable than its reduced form but is still more reactive than DMPZ$^+$. TTF$^+$, yet, does not display clear degradation products peaks but rather a quick absorbance decrease in the 300 nm range and more gradual decrease through the rest of the spectrum. The spectrum evolution can nevertheless be attributed to mediator deactivation reactions. The TTF reaction rate is more complicated to extract in light of the absence of clear peak evolution. By taking the main absorbance peak at 445 nm, TTF$^+$ has reacted up to approximately one-third of its initial concentration within 10 minutes; For comparison, TTF was fully decomposed after ∼30 s and is in other words roughly 150 times more reactive.

5.3.3 Consequence

Singlet oxygen is the main danger to organic mediators in metal–air batteries. Mediator reactivity with O_2, O_2^- and O_2^{2-} is comparatively smaller, if present at all. This high reactivity arise from the presence of double bond and oxidable heteroatoms as sulfur[42–46]. The electrophile preference of $^1O_2$ protects the mediator oxidized states compared to its reduced state. Even though oxidized mediators are more robust to $^1O_2$, oxidation mediators are designed to occurs in their reduced forms during most of the cycling and the mediators as a whole would still be subject to severe deactivation in presence of $^1O_2$. As presented in ch. **dabco**, singlet oxygen is one of the main sources of side reactivity in metal–air batteries and this is hence applicable to the organic additives in presence. Design of new mediators should aim to reduce $^1O_2$ driven reactivity and present increased stability. We can draw conclusions from the different reaction rate between the TTF/TTF$^+$ and the DMPZ/DMPZ$^+$ couples. TTF/TTF$^+$ react much faster than their respective DMPZ counterparts. Mediators, as DMPZ or TDPA, may quench $^1O_2$ similarly to DABCO by dint of tertiary amines moieties and low oxidation potential[6,19,28]; The quenching mechanism of tertiary amines by charge transfer is described in part. **DABCO mechanism**. Singlet oxygen quenching might explain the different reactivity between DMPZ and TTF and its effect will be described more in-depth in the following chapter. Quenching characters is nonetheless desirable in a mediator since it would enhance its stability towards $^1O_2$. By tuning the quenching efficiency even more robust mediators could be theoretically synthesized.

Despite its higher stability, DMPZ still reacts at non-negligible rate with $^1O_2$ and might not be sufficiently stable for long term cycling in Li-O_2 batteries. The necessity of $^1O_2$ mitigation is hence still in order even for mediated metal–air cells. A combination of oxidation mediators with adapted physical quenchers, as PeDTFSI described in ch. **Quencher**, can still be required to achieve long-time cycling and avoid $^1O_2$ related degradation. Even if mediators decrease the required oxidation potential threshold for effective quenchers, increase in potential were still observed after cycling in mediated cells due to the inevitable formation of carbonate after some cycles. Using quencher stable through the all electrochemical window used in metal–air cells allows thus to prevent possible quencher degradation upon extensive cycling.

5.4   Oxidation mediators chemical stability

Organic mediator instability towards the highly reactive $^1O_2$ has been assessed in the previous part. The chemical stability of mediators is, yet, another important criterion for concrete usability in metal-O_2 cells. Fc^+ is for example known to be unstable in presence of $^3O_2$[47]. If mediators are chemically unstable, cell deterioration could be accelerated by inactive species build-up and possible further side reactions. Oxidized mediator UV-vis signal evolution allows to verify the reformation of its reduced form once brought in contact with peroxide or superoxide as described in part. **Mechanism mediator**. The mediator chemical instability towards oxygenated species can hence be easily verified and assesses efficient metal-O_2 mediator design.

5.4.1   Stability toward alkali oxide

Among the tested mediators, Fc and TEMPO showed non-exponential decrease accompanied by the absence of reduced mediators peaks appearance hinting to the presence of side reactions. To verify their stabilities, the mentioned oxidized mediators were exposed to an excess of KO_2 or Li_2O_2 powder over 12 hours under agitation in Ar atmosphere and analysed by UV-vis. The resultant spectra are showed in fig. 5.11. Both mediators do not reform their reduced state upon prolonged contact but new peaks emerge characterizing side products formation. Consumption of the Fc^+ mediators and oxygen release can be shown by UV-vis spectroscopy and mass spectroscopy as described in part. **mechanism oxidation mediators** and illustrated in **Annexes** and fig. 5.11. Side products are, yet, formed during the alkali oxide oxidation rather than the mediator reduced form despite apparent reactivity. The spectral features of TEMPO and $TEMPO^+$ in conjunction with the side product forming upon exposing $TEMPO^+$ to Li_2O_2 and KO_2 did not allow for reliable kinetics measurements using UV-Vis. Mass spectrometry measurement in fig. 5.11 insert shows, however, clear O_2 production upon reaction with $TEMPO^+$ despite absence of TEMPO reformation. The chemical stability of the mediator ought hence to be tested beforehand as they could appear active but are actually consumed during the reaction; Their uses would result in degradation product accumulation and impossibility to sustain a high number of cycling.
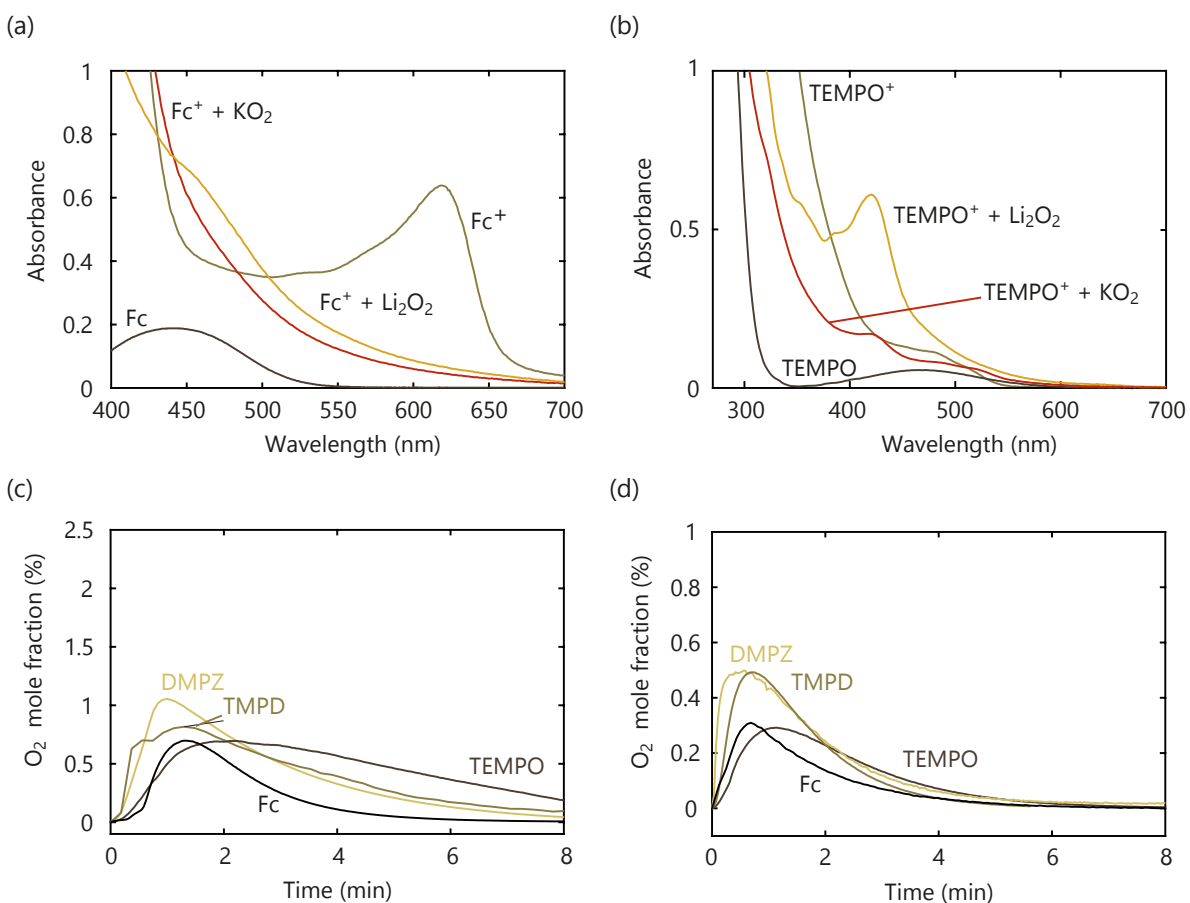
Figure 5.11: **Fc$^+$ and TEMPO$^+$ reactivity towards Li$_2$O$_2$ and KO$_2$.** UV-Vis spectra in 0.1 M LiTFSI TEGDME of 1 mM Fc, 1 mM Fc$^+$BF$_4^-$ or 1 mM Fc$^+$BF$_4^-$ after stirring for 12 h under Ar with an excess of Li$_2$O$_2$ or KO$_2$ powder, respectively, followed by filtering. (b) UV-Vis spectra in 0.1 M LiTFSI TEGDME of 5 mM TEMPO, 5 mM TEMPO$^+$BF$_4^-$ or 5 mM TEMPO$^+$BF$_4^-$ after stirring for 12 h under Ar with an excess of Li$_2$O$_2$ or KO$_2$ powder, respectively, followed by filtering. (c)-(d) ^{3}O$_2$ evolution over time by MS upon mixing an excess of (c) Li$_2$O$_2$ or (d)KO$_2$ powder with 1 mM of the indicated oxidized mediators in TEGDME. For Li$_2$O$_2$ the electrolyte contained 0.1 M LiTFSI.

5.4.2 Oxidation state stability

TDPA presents also peculiar characteristics. TDPA induced O$_2$ evolution characterized by MS and HPLC, as described in part. **mechanism mediator** and **Annexes**, shows important ^{3}O$_2$ deficiency and non-negligible ^{1}O$_2$ production for both Li$_2$O$_2$ and KO$_2$ oxidation which is illustrated in fig. 5.12. Considering the TDPA low redox potential of 3.09 V$_{Li/Li^+}$ and presence of potentially quenching amine moieties, only a small proportion of singlet oxygen should be formed with peroxide and none with superoxide in absence of disproportionation.
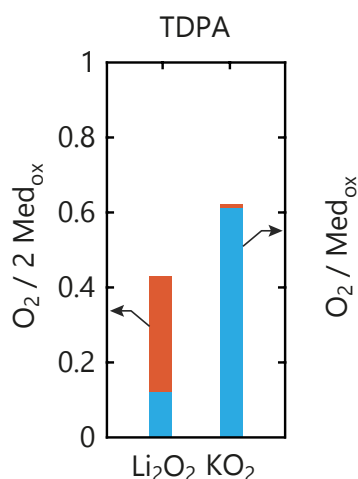
Figure 5.12: **$^3O_2$ and $^1O_2$ yield upon mediated peroxide and superoxide oxidation by TDPA$^+$.** $^3O_2$ and $^1O_2$ evolution obtained by addition of 1 mM TDPA$^+$ in TEGDME to an excess of Li_2O_2 or KO_2.

We hence hypothesized spontaneous formation of TDPA^{2+}. TDPA$^+$/TDPA^{2+} couple has a redox potential of **find a CV** and could yield $^1O_2$ by alkali oxide oxidation ~~being~~ beyond the potential threshold given in **singlet and mechanism mediator**. To demonstrate this assumption, TDPA$^+$ was produced electrochemically at a potential just sufficient for TDPA oxidation (3.15 V_{Li/Li^+} or $E^0_{TDPA/TDPA^+}$ + 60 mV), but well below the TDPA$^+$ oxidation potential, to half the capacity of the TDPA/TDPA$^+$ couple on glassy carbon in a 0.1 M LiTFSI dimethoxyethane electrolyte. The resulting solution was separated by thin–layer chromatography (TLC) on a Al_2O_3 plate with ethyl acetate/ethanol (1/1) as eluent. The TLC plate, show~~ed~~ in fig. 5.13(a), exhibits three different species after separation. The three differently coloured spots were separately analysed by UV–Vis spectroscopy and compared with simulated spectra of TDPA, TDPA$^+$ and TDPA^{2+} in fig. 5.13(b)–(c). The DFT calculations are given in **Annexes**. One of the species ~~present~~ the characteristic absorbance peaks associated ~~to~~ the modelled TDPA^{2+} whereas the others ~~one~~ correspond ~~well to~~ TDPA and TDPA$^+$. The UV–vis spectra hence confirm the spontaneous formation of TDPA^{2+} from a mixture of TDPA, TDPA$^+$ and LiTFSI in glyme. The results highlight that mediators with a redox couple below 3.5 V_{Li/Li^+} can still produce singlet oxygen by alkali oxide oxidation if highly oxidizing further oxidation steps exists and forms spontaneously. Newly designed mediators should hence be carefully tested to verify their chemical stabilities, e.g. by testing $^1O_2$ presence after KO_2 oxidation in absence of disproportionation.
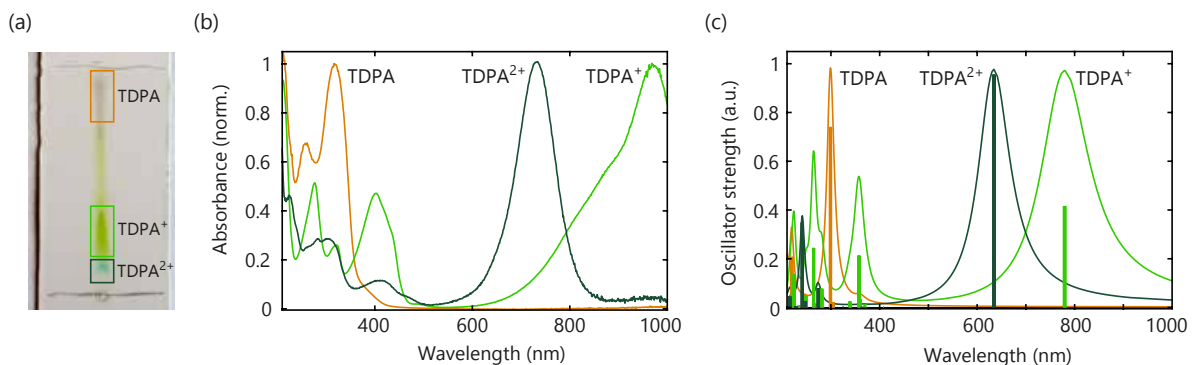
Figure 5.13: **TPDA⁺ stability and spontaneous formation of highly oxidizing TPDA²⁺** (a) Thin-layer chromatogram (TLC) of a partially oxidized TDPA solution under O_2, showing spontaneous occurrence of TPDA²⁺ in a TDPA/TDPA⁺ solution. (b) Respective UV-Vis spectra of the framed spots in (a) after dissolving them in methanol and are normalized to the most intense peak. (c) Simulated UV-Vis spectra of TDPA, TDPA⁺, and TPDA²⁺ according to **Annexes**. The stems show non-normalized oscillator strengths whereas the envelopes are normalized to the most intense peaks.

Conclusion

In conclusion, oxidation mediators hold the colossal promise of low overpotential recharge at fast rates and have been intensely studied ~~in its~~ own right. Disconnecting the electronic and ionic transport~~s~~ from the insulting alkali oxide allows to remove one of the charge overpotential ~~reason.~~ Oxidation mediators ~~set~~ the charge potential to their own avoiding theoretically the crippling side product formation and decomposition. Mediators have yet to show a clear reduction of side product formation. Despite the wide range of mediators tested in metal-O_2, mechanistic descriptors of the reaction were lacking to provide efficient design rules and achieve truly efficient ~~mediators. If they~~ were previous attempt to describe the mediat~~or~~ mechanism, kinetic influence or stability, we could show clearly the presence of competing reaction steps within the mediated oxidation process and the importance of the mediator stability, especially towards singlet oxygen already identified as a main sources of degradation in non-mediated cells.

Using $^1O_2$ presence as a disproportionation ~~marker~~ below the thermodynamic threshold for $^1O_2$ ~~induced by~~ alkali oxidation, we showed ~~the decomposition of~~ the mediated oxidation in different elementary steps. The first one is a one electron extraction forming superoxide species. Once formed, the superoxide can either be oxidized via another one electron step or disproportionate as described for non-mediated cells. This result is of high importance considering $^1O_2$. Disproportionation ~~is known to~~ yield $^1O_2$, especially in presence of weak Lewis acids as oxidized mediators. Mediators below the $^1O_2$ potential threshold are hence not immune to its production during charge. The relative importance of the two pathways is dictated by the competition of their respective kinetics. High superoxide ~~mediated~~ oxidation ~~rate~~ could allow to by-pass the disproportion reaction and ~~so~~ $^1O_2$ ~~for~~ mediators with low redox potential. Our results show, however, that current mediators do not present sufficiently high kinetic to ~~neglected~~ disproportionation. The second electron extraction or disproportionation are, yet, not the rate limiting steps. With high reaction rates in mind, mediators should also ~~present~~ high reaction kinetic with peroxide. The mediation kinetics are hence of prime importance, not only for fast reaction kinetic, but also for the parasitic chemistry.

Since oxidation mediators do not prevent the $^1O_2$ presence, we assess their reactivity with this very aggressive species. The majority of the proposed mediators are organic molecules owing to their wide variety and adaptability through adapted synthesis. $^1O_2$ is, however, a known electrophile and react~~s at high rates~~ with double bonds. DMPZ and TTF, taken as typical examples of mediators, showed clear reactivity with $^1O_2$ at ~~important~~ rates. The oxidized forms of the mediators present increased stability due to their s~~ofter Lewis acid characters~~ but still noticeably react albeit at slower rates. DMPZ is markedly more resistant to $^1O_2$ contact than TTF. This robustness can be ascribed to the presence of tertiary amines moieties that are known to physically quench $^1O_2$ to its ground state. The mediator l~~ow redox potential~~ ~~should ensure~~ high molar efficiency as described in ch. **quencher**. The presence of quenching moieties is hence desirable in oxidation mediators to increase their stability in long term cycling since the presence of singlet oxygen appears currently inevitable. The addition of an external quencher, e.g. PeDTFSI. can act as a safeguard and prevent deactivation of the mediators and unwanted accumulation of side products in the cell.

The oxidation mediator chemical stability should moreover not be overlooked. Fc and TEMPO showed important degradation in contact with alkali oxide. Despite irreversibly, the aforementioned mediators react with alkali oxide, release O_2 and could appear as efficient. Their action would nevertheless be constrained to a few cycles as they would be consumed

over time. The chemical stability of mediator with several oxidation degrees can also be questioned. TDPA$^+$ in a Li$^+$ electrolyte was shown to form spontaneous the high redox potential TDAP^{2+}. TDAP^{2+} then can induce $^1O_2$ formation from alkali oxide oxidation as its potential is above the thermodynamic threshold. Determination of the mediator chemical stability is then a prerequisite before its use in a metal–O$_2$ cell. The conclusions drawn here from the reaction mechanism could be further used to provide design rules for future oxidation mediators.

Bibliography

[1] Y.-C. Lu, B. M. Gallant, D. G. Kwabi, J. R. Harding, R. R. Mitchell, M. S. Whittingham, and Y. Shao-Horn, "Lithium–oxygen batteries: bridging mechanistic understanding and battery performance," *Energy & Environmental Science*, vol. 6, no. 3, pp. 750–768, 2013.

[2] D. Aurbach, B. D. McCloskey, L. F. Nazar, and P. G. Bruce, "Advances in understanding mechanisms underpinning lithium–air batteries," *Nature Energy*, vol. 1, no. 9, p. 16128, 2016.

[3] Y. Wang, N.-C. Lai, Y.-R. Lu, Y. Zhou, C.-L. Dong, and Y.-C. Lu, "A solvent-controlled oxidation mechanism of Li_2O_2 in lithium-oxygen Batteries," *Joule*, vol. 2, no. 11, pp. 2364–2380, 2018.

[4] Y. Ko, H. Park, B. Kim, J. S. Kim, and K. Kang, "Redox mediators: A solution for advanced lithium–oxygen batteries," *Trends in Chemistry*, 2019.

[5] X. Gao, Y. Chen, L. Johnson, and P. G. Bruce, "Promoting solution phase discharge in Li–O_2 batteries containing weakly solvating electrolyte solutions," *Nature materials*, vol. 15, no. 8, p. 882, 2016.

[6] H.-D. Lim, B. Lee, Y. Zheng, J. Hong, J. Kim, H. Gwon, Y. Ko, M. Lee, K. Cho, and K. Kang, "Rational design of redox mediators for advanced Li–O_2 batteries," *Nature Energy*, vol. 1, no. 6, p. 16066, 2016.

[7] N. B. Aetukuri, B. D. McCloskey, J. M. García, L. E. Krupp, V. Viswanathan, and A. C. Luntz, "Solvating additives drive solution-mediated electrochemistry and enhance toroid growth in non-aqueous Li–O_2 batteries," *Nature chemistry*, vol. 7, no. 1, p. 50, 2015.

[8] T. Liu, J. T. Frith, G. Kim, R. N. Kerber, N. Dubouis, Y. Shao, Z. Liu, P. C. Magusin, M. T. Casford, N. Garcia-Araez, and C. P. Grey, "The effect of water on quinone redox mediators in nonaqueous Li-O_2 batteries," *Journal of the American Chemical Society*, vol. 140, no. 4, pp. 1428–1437, 2018.

[9] S. Ganapathy, B. D. Adams, G. Stenou, M. S. Anastasaki, K. Goubitz, X.-F. Miao, L. F. Nazar, and M. Wagemaker, "Nature of Li_2O_2 oxidation in a Li–O_2 battery revealed by operando X-ray diffraction," *Journal of the American Chemical Society*, vol. 136, no. 46, pp. 16 335–16 344, 2014.

[10] D. G. Kwabi, M. Tuodziecki, N. Pour, D. M. Itkis, C. V. Thompson, and Y. Shao-Horn, "Controlling solution-mediated reaction mechanisms of oxygen reduction using potential and solvent for aprotic lithium–oxygen batteries," *The journal of physical chemistry letters*, vol. 7, no. 7, pp. 1204–1212, 2016.

[11] B. D. McCloskey, R. Scheffler, A. Speidel, G. Girishkumar, and A. C. Luntz, "On the mechanism of nonaqueous Li–O_2 electrochemistry on C and its kinetic overpotentials: some implications for Li–air batteries," *The Journal of Physical Chemistry C*, vol. 116, no. 45, pp. 23 897–23 905, 2012.

[12] V. Viswanathan, J. Nørskov, A. Speidel, R. Scheffler, S. Gowda, and A. Luntz, "Li–O_2 kinetic overpotentials: Tafel plots from experiment and first-principles theory," *The journal of physical chemistry letters*, vol. 4, no. 4, pp. 556–560, 2013.

[13] Y. Chen, S. A. Freunberger, Z. Peng, F. Bardé, and P. G. Bruce, "Li–O_2 battery with a dimethylformamide electrolyte," *Journal of the American Chemical Society*, vol. 134, no. 18, pp. 7952–7957, 2012.

[14] J. W. Choi and D. Aurbach, "Promise and reality of post-lithium-ion batteries with high energy densities," *Nature Reviews Materials*, vol. 1, no. 4, p. 16013, 2016.

[15] Z. Liang and Y.-C. Lu, "Critical role of redox mediator in suppressing charging instabilities of lithium–oxygen batteries," *Journal of the American Chemical Society*, vol. 138, no. 24, pp. 7574–7583, 2016.

[16] B. McCloskey, A. Speidel, R. Scheffler, D. Miller, V. Viswanathan, J. Hummelshøj, J. Nørskov, and A. Luntz, "Twin problems of interfacial carbonate formation in nonaqueous Li–O$_2$ batteries," *The journal of physical chemistry letters*, vol. 3, no. 8, pp. 997–1001, 2012.

[17] B. D. McCloskey, D. Bethune, R. Shelby, T. Mori, R. Scheffler, A. Speidel, M. Sherwood, and A. Luntz, "Limitations in rechargeability of Li–O$_2$ batteries and possible origins," *The journal of physical chemistry letters*, vol. 3, no. 20, pp. 3043–3047, 2012.

[18] T. Liu, G. Kim, M. T. Casford, and C. P. Grey, "Mechanistic insights into the challenges of cycling a nonaqueous Na–O$_2$ battery," *The journal of physical chemistry letters*, vol. 7, no. 23, pp. 4841–4846, 2016.

[19] Y. Chen, S. A. Freunberger, Z. Peng, O. Fontaine, and P. G. Bruce, "Charging a Li–O$_2$ battery using a redox mediator," *Nature chemistry*, vol. 5, no. 6, p. 489, 2013.

[20] B. J. Bergner, A. Schürmann, K. Peppler, A. Garsuch, and J. Janek, "TEMPO: a mobile catalyst for rechargeable Li–O$_2$ batteries," *Journal of the American Chemical Society*, vol. 136, no. 42, pp. 15 054–15 064, 2014.

[21] Y.-C. Lu and Y. Shao-Horn, "Probing the reaction kinetics of the charge reactions of nonaqueous Li–O$_2$ batteries," *The journal of physical chemistry letters*, vol. 4, no. 1, pp. 93–99, 2012.

[22] S. Kang, Y. Mo, S. P. Ong, and G. Ceder, "A facile mechanism for recharging Li2O2 in Li–O$_2$ batteries," *Chemistry of Materials*, vol. 25, no. 16, pp. 3328–3336, 2013.

[23] J. Wang, Y. Zhang, L. Guo, E. Wang, and Z. Peng, "Identifying reactive sites and transport limitations of oxygen reactions in aprotic lithium-o2 batteries at the stage of sudden death," *Angewandte Chemie International Edition*, vol. 55, no. 17, pp. 5201–5205, 2016.

[24] C. M. Burke, R. Black, I. R. Kochetkov, V. Giordani, D. Addison, L. F. Nazar, and B. D. McCloskey, "Implications of 4 e⁻ oxygen reduction via iodide redox mediation in Li–O2 batteries," *ACS Energy Letters*, vol. 1, no. 4, pp. 747–756, 2016.

[25] M. M. Ottakam Thotiyl, S. A. Freunberger, Z. Peng, and P. G. Bruce, "The carbon electrode in nonaqueous Li–O$_2$ cells," *Journal of the American Chemical Society*, vol. 135, no. 1, pp. 494–500, 2012.

[26] J.-B. Park, S. H. Lee, H.-G. Jung, D. Aurbach, and Y.-K. Sun, "Redox mediators for Li–O$_2$ batteries: status and perspectives," *Advanced Materials*, vol. 30, no. 1, p. 1704162, 2018.

[27] V. Pande and V. Viswanathan, "Criteria and considerations for the selection of redox mediators in nonaqueous Li–O$_2$ batteries," *ACS Energy Letters*, vol. 2, no. 1, pp. 60–63, 2016.

[28] Y. Chen, X. Gao, L. R. Johnson, and P. G. Bruce, "Kinetics of lithium peroxide oxidation by redox mediators and consequences for the lithium–oxygen cell," *Nature communications*, vol. 9, no. 1, p. 767, 2018.

[29] X. Gao, Y. Chen, L. R. Johnson, Z. P. Jovanov, and P. G. Bruce, "A rechargeable lithium–oxygen battery with dual mediators stabilizing the carbon cathode," *Nature Energy*, vol. 2, no. 9, p. 17118, 2017.

[30] D. Kundu, R. Black, B. Adams, and L. F. Nazar, "A highly active low voltage redox mediator for enhanced rechargeability of lithium–oxygen batteries," *ACS central science*, vol. 1, no. 9, pp. 510–515, 2015.

[31] I. Landa-Medrano, I. Lozano, N. Ortiz-Vitoriano, I. R. de Larramendi, and T. Rojo, "Redox mediators: a shuttle to efficacy in metal–O_2 batteries," *Journal of Materials Chemistry A*, vol. 7, no. 15, pp. 8746–8764, 2019.

[32] G. Leverick, M. Tuodziecki, R. Tatara, F. Bardé, and Y. Shao-Horn, "Solvent-Dependent Oxidizing Power of LiI Redox Couples for Li-O_2 Batteries," *Joule*, vol. 3, no. 4, pp. 1106–1126, 2019.

[33] Q. Li, F. Chen, W. Zhao, M. Xu, B. Fang, Y. Zhang, L. Duo, Y. Jin, and F. Sang, "A spectroscopic study on singlet oxygen production from different reaction paths using solid inorganic peroxides as starting materials," *Bulletin of the Korean Chemical Society*, vol. 28, no. 10, pp. 1656–1660, 2007.

[34] ——, "Singlet oxygen production in the reaction of potassium superoxide with chlorine," *Chemistry letters*, vol. 36, no. 4, pp. 496–497, 2007.

[35] E. A. Mayeda and A. J. Bard, "Production of singlet oxygen in electrogenerated radical ion electron transfer reactions," *Journal of the American Chemical Society*, vol. 95, no. 19, pp. 6223–6226, 1973.

[36] S. Senthil Kumar and A. J. Bard, "Background Emission of Electrogenerated Chemiluminescence during Oxidation of Tri-n-propylamine from the Dimeric $^1\Delta_g$ State of O_2," *Analytical chemistry*, vol. 85, no. 1, pp. 292–295, 2012.

[37] W. Ando, Y. Kabe, S. Kobayashi, C. Takyu, A. Yamagishi, and H. Inaba, "Formation of sulfinyl oxide and singlet oxygen in the reaction of thianthrene cation radical and superoxide ion," *Journal of the American Chemical Society*, vol. 102, no. 13, pp. 4526–4528, 1980.

[38] B. D. McCloskey and D. Addison, "A viewpoint on heterogeneous electrocatalysis and redox mediation in nonaqueous Li-O_2 batteries," 2016.

[39] P. Bawol, P. Reinsberg, C. Bondue, A. Abd-El-Latif, P. Königshoven, and H. Baltruschat, "A new thin layer cell for battery related DEMS-experiments: the activity of redox mediators in the Li–O_2 cell," *Physical Chemistry Chemical Physics*, vol. 20, no. 33, pp. 21 447–21 456, 2018.

[40] I. Saito, T. Matsuura, and K. Inoue, "Formation of superoxide ion via one-electron transfer from electron donors to singlet oxygen," *Journal of the American Chemical Society*, vol. 105, no. 10, pp. 3200–3206, 1983.

[41] X. Zhang, F. Lin, and C. S. Foote, "Sensitized photooxygenation of 6-heteroatom-substituted fulvenes: Primary products and their chemical transformations," *The Journal of Organic Chemistry*, vol. 60, no. 5, pp. 1333–1338, 1995.

[42] D. Min and J. Boff, "Chemistry and reaction of singlet oxygen in foods," *Comprehensive reviews in food science and food safety*, vol. 1, no. 2, pp. 58–72, 2002.

[43] H. H. Wasserman and J. L. Ives, "Singlet oxygen in organic synthesis," *Tetrahedron*, vol. 37, no. 10, pp. 1825–1852, 1981.

[44] P. D. Bartlett, G. D. Mendenhall, and A. P. Schaap, "Competitive modes of reaction of singlet oxygen," *Annals of the New York Academy of Sciences*, vol. 171, no. 1, pp. 79–88, 1970.

[45] A. A. Frimer, "The reaction of singlet oxygen with olefins: the question of mechanism," *Chemical Reviews*, vol. 79, no. 5, pp. 359–387, 1979.

[46] E. Clennan and A. Pace, "Advances in singlet oxygen chemistry," *TETRAHEDRON*, vol. 61, pp. 6665–6691, 10 2005.

[47] J. Hurvois and C. Moinet, "Reactivity of ferrocenium cations with molecular oxygen in polar organic solvents: decomposition, redox reactions and stabilization," *Journal of Organometallic Chemistry*, vol. 690, no. 7, pp. 1829–1839, 2005.

Efficient oxidation mediator design for $^1O_2$ suppression

In the middle of every difficulty lies opportunity
Albert Einstein

Contents

Figures

Introduction

Oxidation mediators is a promising approach to reduce metal–air cells overpotential and to permit fast reaction rates during charge[1–4]. Oxidation mediators, yet, do not prevent the highly reactive $^1O_2$ singlet oxygen presence. Alkali peroxide oxidation was shown to proceed through two consecutive steps. The first and rate limiting step is a one-electron oxidation produce superoxide species that can either disproportionate or be further oxidized. $^1O_2$ can hence either be produced via disproportionation or by oxidation at high overpotential (e.g. ~3.55 V_{Li/Li^+} for O_2^-). $^1O_2$ was shown previously in ch. **singlet oxygen, quencher** to be a main degradation pathway in metal–air batteries. Its presence is especially problematic since the widely studied organic mediators quickly react with $^1O_2$, leading to ~~its~~ deactivation and accumulation of side products. The mediators chemical stability might furthermore be problematic as its reduced state is not necessarily reformed after reaction ~~on~~ peroxide or superoxide.

Oxidation mediator optimization is hence of main interest to achieve efficient mediation. Refined mediators still augur reduced side reactions and fast charge rate. To do so, a mediator should have fast reaction rate on both peroxide and superoxide. The former one allowing fast reaction rate, being the slowest step, where the latter could reduce disproportionation ~~proportion.~~ The disproportionation and superoxide oxidation rates are competing for ~~the~~ O_2 release; A fast enough oxidation would result in ~~negligible~~ disproportionation and $^1O_2$ yield. Oxidation mediators with $^1O_2$ quenching moieties showed moreover increase stability and could guarantee low cell degradation in presence of a small disproportionation proportion. In addition, chemical stability against peroxide, superoxide and $^3O_2$ of newly proposed mediators should be insured before any further long term cyclability claims.

Considering the aforementioned observation, design rules can be drawn for efficient mediators, i.e. a high chemical stability, a high quenching efficiency, a redox potential lower than the $^1O_2$ thermodynamic threshold and a high oxidation rate on peroxide and superoxide. We ~~proposed~~ in this chapter ~~to study~~ more in-depth the influence and underlying mechanism of these parameters using a wide range of mediators as well as a newly proposed class of mediators represented in fig. 6.1, bi-cyclic ~~secondary~~ amines (BP). ~~Bi-cyclic secondary amines~~ present the advantages to have an easily tunable redox potential, which we will show the kinetic to depend on, and quenching moieties[5]. The reasons and mechanisms of efficient mediation will hence be deciphered, allowing oxidation mediators to progress further and possibly unlock $^1O_2$ free fast charge in metal–O_2 technologies.
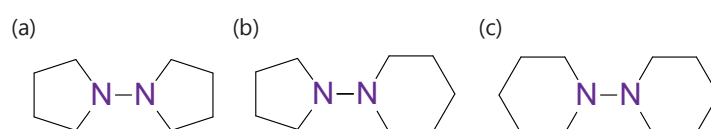
Figure 6.1: **Structure of ~~bi-cyclic secondary amines~~ proposed as oxidation mediators.** (a) 1,1'–bipyrrolidine (BP55), (b) 1-(pyrrolidin-1-yl)piperidine (BP56) and (c) 1,1'–bipiperidine (BP66). The quenching moieties are highlighted in purple.

To do so, we first determined the redox potential of several members of the ~~bi-cyclic secondary amines~~ class proposed as mediators as well as their chemical stability after prolonged contact with KO_2, Li_2O_2 and $^3O_2$. After ensuring sufficient stability, the BP mediator reaction rates with O_2^- and O_2^{2-} were measured by UV-vis as described in the previous chapter. The 1,1'–bipyrrolidine (BP55) mediator was revealed to have an unusually high reaction kinetics and could greatly reduce disproportionation occurrence. To assess the efficiency of ~~bi-cyclic~~

secondary amines mediators and verify our design rules, we measured $^3O_2$ and $^1O_2$ yield for a wide range of mediators by MS and HPLC by the method depicted in ch. **previous one**. We were able to correlate the mediator redox potential to the superoxide reaction kinetic using Marcus theory. Accordingly, the reaction kinetic decreases ~~for~~ high potential and ~~hence possess~~ a maximum that should be aimed by future oxidation mediator. Maximizing the mediator reaction allows to reduced $^1O_2$ evolution. Bi-cyclic secondary amines have moreover ~~quenching~~ tertiary amine groups[5]; Presence of quenching moieties ~~reduces~~ $^1O_2$ ~~presence~~ during mediated oxidation and we show that the quenching efficiency depends on the mediators potential and its chemical nature, as already discussed in part. **Quencher**. Finally the ~~mediator efficiencies can be shown through~~ Sankey diagrams of relative rates, ~~resuming~~ the kinetic rate and $^3O_2/^1O_2$ evolution yield. BP55 demonstrate the feasibility and draw the path to efficient oxidation mediator and reduction of $^1O_2$ ~~presence~~ during metal-O_2 cell charges at high rate.

6.1   ~~Bi-cyclic secondary amines~~ as oxidation mediator

Oxidation mediator reactivity described in the previous chapter ~~imposes~~ new ~~criterion~~ concerning its efficiency. We hence ~~proposed~~ a new class of mediators, bi-cyclic secondary amines, ~~to study~~ more in-depth the mechanism implication for mediators that could provide $^1O_2$ free charge. Bi-cyclic secondary amines present the advantage to have easily tunable redox potentials in order to optimize the mediated oxidation kinetic and tertiary amines quenching moieties. The redox potential of the molecules is fixed by the ~~number of carbon in their cycles~~. Different Bi-cyclic secondary amines were hence synthesized and select for their redox potentials of interest in the context of mediators in metal-air batteries. Before further characterizations of the mediator influences on the efficiency, we assessed their chemical stabilities and reaction kinetics to compare them to known mediators and disproportionation rate.

6.1.1   Potential characteristic

To test bi-cyclic secondary amines as mediators, synthesis methods were first developed and can be found in **Annexes**. As the cycle size can be easily tuned, bi-cyclic secondary amines can present a wide range of redox potential. Mediator redox potentials were determined by cyclic voltametries of a 2 mM mediator in 0.1 M LiTFSI TEGDME electrolyte at a scan rate of 100 mV$\cdot$s^{-1} on a glassy carbon disc electrode and depicted in fig. 6.2. 1,1'-bipyrrolidine (BP55), 1-(pyrrolidin-1-yl)piperidine (BP56) and 1,1'-bipiperidine (BP66) were selected with potential of 3.2 V_{Li/Li^+}, 3.46 V_{Li/Li^+}, 3.76 V_{Li/Li^+} respectively. These three mediators cover a similar potential range than commonly proposed mediators presented in part. **kinetic**. BP55 has a potential below the $^1O_2$ formation potential which is close to the one of TMPD (3.24 V_{Li/Li^+}) and DMPZ (3.29 V_{Li/Li^+}). BP56 potential is situated close to the thermodynamic threshold for $^1O_2$ (~3.55 V_{Li/Li^+}) and to mediators with a reduced reaction kinetics as Fc, determined in part. **kinetics previous chapter**. Finally, BP66 has the same potential ~~than~~ TEMPO and ~~can be used to characterize~~ mediator with high potentials that would produce large $^1O_2$ amount by mediated oxidation.

(a)   (b)   (c)
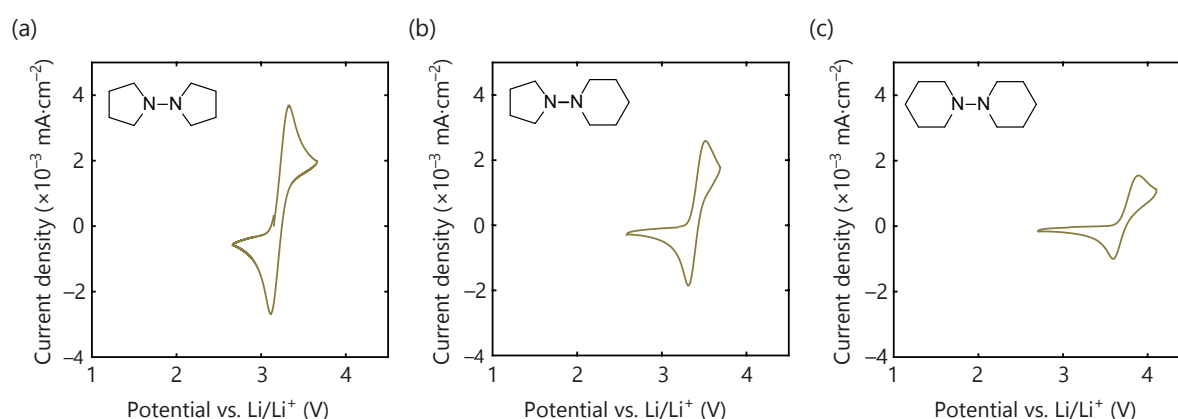
Figure 6.2: **Cyclic voltammetry of bi-cyclic secondary amines proposed as oxidation mediators.** The cyclic voltammograms were measured as 2 mM of (a) BP55 (b) BP56 or (c) BP66 in 0.1 M LiTFSI in TEGDME at a scan rate of 100 mV$\cdot$s^{-1} at a glassy carbon disc electrode.

    Put in appendix

Given their potentials, the selected ~~amines~~ can be used to ~~verify~~ the presence of a two step mediation with sodium peroxide (2.87, 3.13, 3.43 V_{Na/Na^+}, respectively for BP55, BP56 and

BP66). Considering their respective potentials, ~~concerted~~ two–electron Na_2O_2 oxidation has a $^1O_2$ threshold of 2.82 V_{Na/Na^+}, whereas the one for NaO_2 oxidation is at 3.25 V_{Na/Na^+} as shown in part. **singlet disp**. Considering the slow disproportionation rate in presence of Na^+, ~~consequent~~ singlet oxygen production is only to be expected by direct oxidation. A direct tow electron oxidation should hence produce $^1O_2$ below 3.25 V_{Na/Na^+} while a two step reaction would only yield $^1O_2$ above. we ~~characterized~~ $^3O_2$ and $^1O_2$ production upon Na_2O_2/NaO_2 mediated oxidation according to the protocol in **Annexes** and plotted in fig. 6.3.
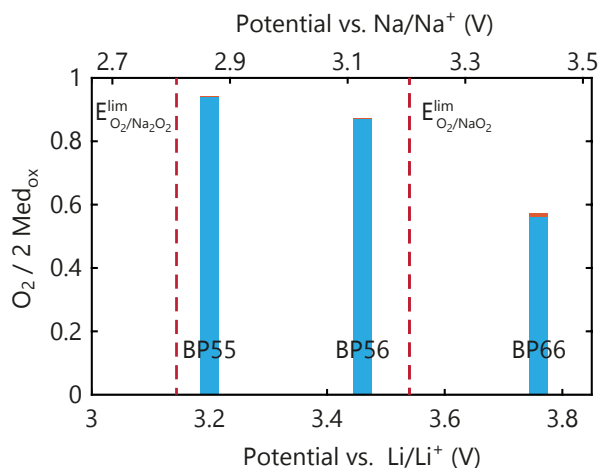
Figure 6.3: **$^3O_2$ and $^1O_2$ yield upon mediated peroxide and superoxide oxidation by BP55, BP56 and BP66.** $^3O_2$ and $^1O_2$ evolution obtained by addition of 1 mM oxidized mediators in TEGDME to an excess of Na_2O_2. The red dashed line indicates the thermodynamic thresholds for 1O2 evolution from Na_2O_2 and NaO_2 oxidation.

Sodium peroxide oxidation by both BP55, BP56, situated below 3.25 V_{Na/Na^+}, resulted in negligible $^1O_2$ amount and $^3O_2$ ~~superior to~~ ~85%. In ~~contrary~~ BP66 oxidation results present a significant lack of $^3O_2$ (~55%) and presence of $^1O_2$. $^1O_2$ appearance only above the superoxide thermodynamic threshold indicates a two step mechanism with the formation of superoxide species similarly to Li_2O_2 oxidation. The $^1O_2$ occurrence pattern advocates for superoxides formation via sequential one–electron transfers rather than direct two–electron reaction, notwithstanding the alkali peroxide nature albeit with different disproportionation rate. The design rules suggested in the main text are hence applicable to all non-aqueous metal–air chemistries.

6.1.2 Chemical stability

Once bi–cyclic secondary amines of significance were chosen, their chemical stabilities in contact with dissolved O_2, O_2^- and O_2^{2-} needed to be ~~appraised~~ Chemical stability is necessary to provide long term cyclability and verify that the determined reactions rates are only related to the oxidation reactions. We recorded ^1H–NMR spectra of BP55, BP56 and BP66 in CH_3CN–d3 after synthesis or after a 24 hour immersion in O_2 saturated electrolyte. $BP55^+$, $BP56^+$ and $BP66^+$ oxidized chemically, according to **Annexes**, were bring in contact with an excess of KO_2 or Li_2O_2 for a 12 hours period and subsequently analysed by ^1H–NMR to certify the reformation of their reduced forms rather than producing side products. The spectra of the mediators in similar concentrations can be found in fig. 6.4. The mediators show sufficient chemical stability excepted BP55 in the presence of dissolved molecular oxygen. If BP55 is thus not compatible with an actual metal–O_2 cell, it can still be used to

discuss mediators mechanism as the performed measurements involve much shorter times than 24 hours, after which BP55 is still detected albeit in a lower amount. This ~~assumption~~ was verified by UV–vis experiments where the oxidized bi–cyclic secondary amines in the mM range **Ask if Stefan knows the exact concentration used** spectra were measured before and after reaction with excess KO_2 or Li_2O_2 during 12 hours and compared to the reduced form ~~spectra.~~ The BP forms back their reduced forms after alkali oxide oxidation in similar concentration as illustrated in fig. 6.5, indicating that in the time range studied BP55 is stable enough. The other mediator UV–vis studies are given in **Annexes**.
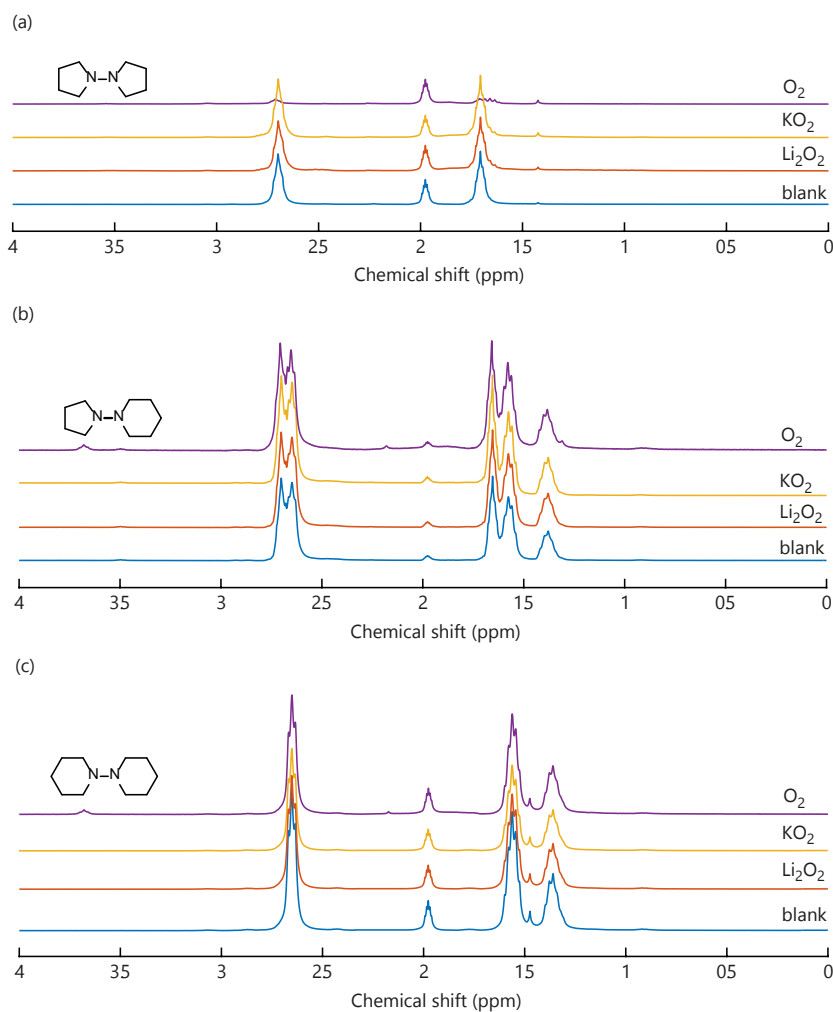
Figure 6.4: **Stability of BP mediators in contact with O_2, KO_2 and Li_2O_2 by ^{1}H–NMR.** NMR spectra of the reduced mediator as synthesized (labelled blank) or ~~kept in~~ contact with O_2 for 24 hours and of oxidized mediator after having been in contact with Li_2O_2 or KO_2 for (a) BP55, (b) BP56 and (c) BP66. Oxidized mediators ~~was~~ dissolved in CH_3CN–d3, ~~stirring~~ the solution with several mg KO_2 or Li_2O_2 for 12 hours and ~~filtering~~ before the measurement.
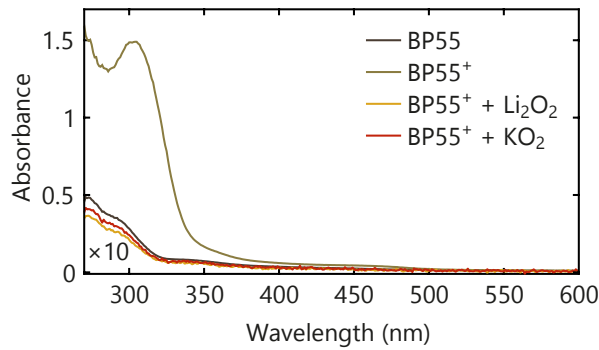
Figure 6.5: **BP55$^+$ conversion upon contact with Li$_2$O$_2$ or KO$_2$.** UV–vis spectra of BP55, BP55$^+$ and BP55$^+$ after contact with Li$_2$O$_2$ or KO$_2$ for 12 hours.

6.1.3 Oxidation kinetic

Owing to their sufficient stabilities, BP mediators can be used to ~~detect a~~ correlation between mediators redox potentials and oxidation kinetics since they are based on similar chemical motifs. Large mediator kinetic on superoxide is of prime importance to avoid $^1O_2$ during charge by ~~reducing~~ disproportionation ~~occurrence.~~ Fast reaction with peroxide is also desirable to enable fast charge ~~overall~~ rate. Determining the underlying parameters of mediated charge kinetic may hence allow $^1O_2$ free and fast paced rate. The reactions rates on both Li$_2$O$_2$ and KO$_2$ have been determined by UV–vis spectroscopy according to the method described in ch.**previous chapter** and **Annexes**. The concentrations used are in a similar range ~~than~~ during the chemical stability UV–vis experiment assuring negligible side reactions. The reaction rates were then fitted by a first–order reaction rate to obtain the kinetic rate constant and compared to the previously obtained kinetics in ch. **previous chapter**. The kinetic rates for 10 mM ~~of~~ mediators and kinetic rate constants obtained are depicted in fig. 6.6.
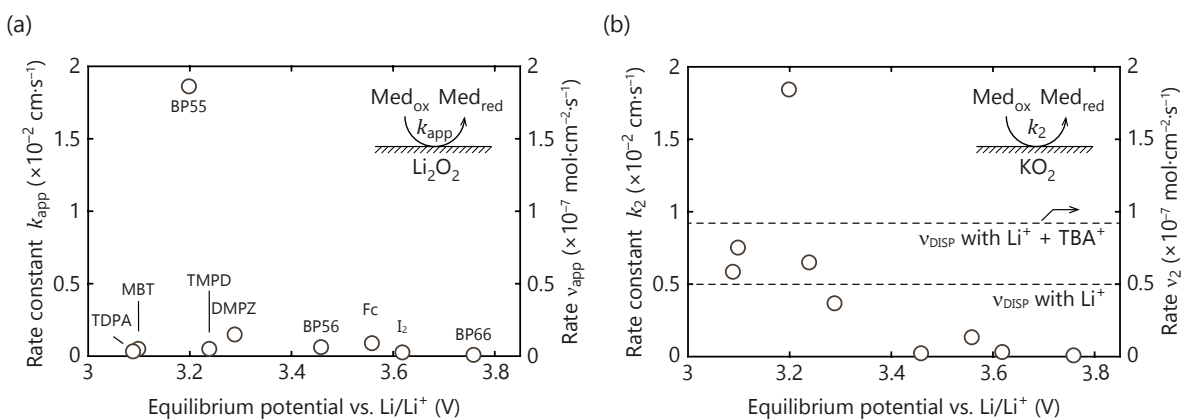
Figure 6.6: **Kinetics of mediated (su)peroxide oxidation ~~comprising~~ BP mediators and superoxide disproportionation.** Kinetic constants k (left axis) and rates v assuming a 10 mM concentration (right axis) in TEGDME for the reaction between oxidized mediators and the Li$_2$O$_2$ surface (a) and the KO$_2$ surface (b) obtained by UV–vis. Superoxide disproportionation rate in presence of 0.5 M LiTFSI or 0.5 M LiTFSI and 0.5 M TBATFSI is indicated by dashed line in (b).

The mediator kinetics show a clear dependency ~~with~~ their redox potentials. As previously observed, ~~mediators with high redox potential (> 3.4 V~~$_{Li/Li^+}$ ~~present a slow kinetic. The~~ kinetics of ~~low redox potential~~ mediators, ~~yet, increase with the potential;~~ It results in ~~the apparition of~~

a ~~peak with the~~ maximum rate at ~3.2 V_{Li/Li^+}, represented by BP55, ~~before decrease at higher redox potential~~. The evolution of the kinetic is thus rather surprisingly not proportional to the potential. The kinetics obtained ~~by~~ BP55 present remarkable characteristics. The mediated oxidation kinetics on Li_2O_2 and KO_2 are similar which indicates very fast overall reaction, roughly five times faster than the second fastest DMPZ. Maximized mediator~~s~~ kinetic should hence be able to increase tremendously the charging rate in metal–O_2 batteries. The superoxide reaction kinetics is moreover almost ~~2 times faster than~~ disproportionation in the presence of TBA^+ ions. By optimizing oxidation mediator designs, it is thus possible to outspeed disproportionation rate and reduce $^1O_2$ occurrence.

6.2 Design of efficient oxidation mediators

Oxidation mediators have mostly been studied for their low redox potentials, stabilities with the electrolyte or chemical natures[6–8]. We showed in the ch. **previous chapter** that oxidation mediator should, in addition to being chemically stable, present high stability towards $^1O_2$ and reaction kinetic towards superoxide to allows long term cyclability. The mediator oxidation kinetics appears to be govern by their redox potential but not in a linear fashion. The origin of this dependency needs to be understood to design fast and efficient mediators in metal air-batteries. Mediators quenching abilities seems correlated with the O_2 robustness and must be rationalized. Only clarifying these effects can provide efficient oxidation mediator design rules and is hence a prime interest for future mediators and metal–air batteries development.

6.2.1 Kinetic and Marcus Theory

Oxidation mediator kinetics relationship with their redox potentials has been attempted previously by scanning electrochemical microscopy but no clear correlation was determined and the reaction was defined as inner sphere process that only depends on the mediator chemical natures[8]. BP mediator kinetics, given in part. **kinetic with BP**, yet, present a clear potential dependency despite similar chemical natures. DEMS study found, on the contrary, a dependency of the oxidation reaction onset, and hence the kinetic, with the mediator redox potentials. The trend was shown to follow an outer-sphere mechanism according to Marcus theory[9]. As Marcus theory predicts a kinetic maximum, its parameters would provide a guideline to achieve fast mediated oxidation rate and reduce disproportionation importance. The UV-vis measured kinetics can be decomposed in two specific zones. At first, an increased potential provides an increase kinetic (below ~ 3.2 V_{Li/Li^+}). Further increased potentials, in other terms the reaction driving force, produce the inverse trend with a progressive decrease of the electron transfer rate. Such counterintuitive behaviour is predicted for homogeneous electron transfer by the Marcus theory and termed the "inverted region"[10,11]. Marcus theory based kinetic exhibits an exponential character similar to an Arrehnius law but with a quadratic dependency with the reaction driving force according to eq. 6.1.

$$k_{ET} = Z_{el} \cdot exp(\frac{-\Delta G^\ddagger}{R \cdot T}) = Z_{el} \cdot exp(\frac{-(\lambda + \Delta G^O)^2}{4 \cdot \lambda \cdot R \cdot T}) \tag{6.1}$$

with k_{ET}, the electron transfer constant kinetic (cm·s^{-1}); Z_{el}, the collision factor (cm·s^{-1}); $\Delta G^\ddagger$, the activation free energy (J·mol^{-1}); ΔG^O, the Gibbs free energy (J·mol^{-1}); λ, the total reorganization energy (J·mol^{-1}); R, the ideal gas constant (J·K^{-1}·mol^{-1}) and T, the temperature (K). The activation free energy is hence given by $\Delta G^\ddagger = \frac{-(\lambda + \Delta G^O)^2}{4 \cdot \lambda}$ where ΔG^O is the driving force and λ represents the energy required to change the nuclear configurations of reactants and solvent to produce the product states[10,11].

(a)

(b)
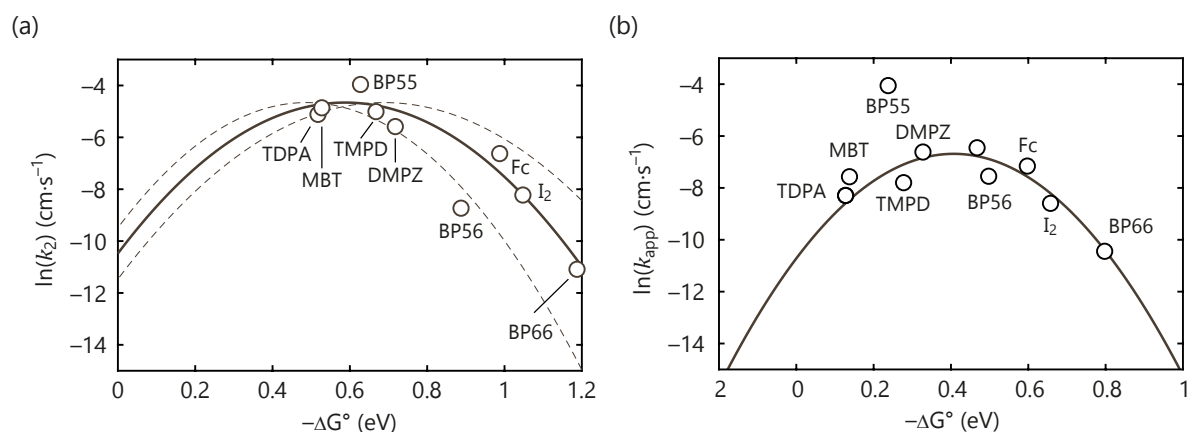
Figure 6.7: **(Su)peroxide oxidation kinetics relationship with Gibbs free energy.** (a) Dependency of k_2 and ΔG^O and associated fit according to eq. 6.1 resulting in Z_{el} = 9.5·10⁻³ cm·s⁻¹ and λ = 0.58 eV. The dashed parabolas are obtained for $\lambda \pm 0.1$ eV. (b) Dependency of k_{app} and ΔG^O and associated fit according to eq. 6.1 resulting in Z_{el} = 1.2·10⁻³ cm·s⁻¹ and λ = 0.41 eV.

Marcus theory for electron transfer described in eq. 6.1 is usually only valid for homogeneous reactions and does not apply to redox molecules reacting at metallic conductors [10,12]. Alkali oxides are however wide band-gap insulators and may justify this formalism. Considering Z_{el} as a constant in our experiments as first approximation, we could adequately fits the measured superoxide oxidation kinetic (k_2) as a function of the driving force($-\Delta G^0=(E^0_{med}-E^0_{O_2/Li_2O_2})$·F) in fig. 6.7(a). Similarly, the overall reaction (k_{app}) also follows the same trend, albeit with larger deviations in fig. 6.7(b); This deviation originates from k_{app} beind a compound rate of three elementary steps, namely the first one-electron oxidation, the second one and the superoxide disproportionation **But here there was no lithium salt?**. The use of Marcus theory ~~formalism~~ is thus justified, especially considering that the found is in a similar range than previous studies on heterogeneous electron transfer (9.5·10⁻³ and 1.2·10⁻³ cm·s⁻¹ for respectively k_2 and k_{app})[13–15] **I do not understand why Marcus can not be applied for heterogeneous transfer where you have a paper with Olivier on this subject**. Marcus theory implication gives ~~a~~ guideline ~~in~~ the choice of the redox mediator. The electron transfer efficiency maximum is achieved for λ = $-\Delta G^O$ according eq. 6.1 which correspond to a barrier-less electron transfer as ($\Delta G^\ddagger$ = 0) as illustrated in fig. 6.8; The other cases result in ~~decreased~~ kinetics and the ~~apparition~~ of the inverted region, Z_{el} and λ provide mechanistic tools to maximize the reaction kinetics and avoid $^1O_2$ production.
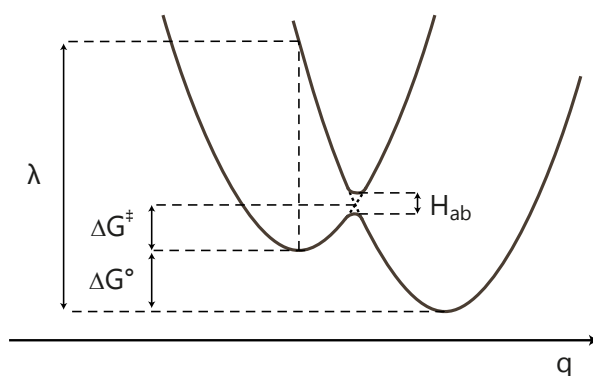
Figure 6.8: **Scheme of donor–acceptor orbitals and Marcus theory parameters.**

The total reorganization energy is the sum of all reorganisation energies during the reac-

tion which can be ~~decomposed between~~ reorganisation in the solid phase ($\lambda_{M_2O_2}/\lambda_{MO_2}$) and the redox mediator ~~one~~ ($\lambda_{mediator}$). Each reorganization energy depends ~~themselves~~ on inner and outer parameters. The outer energy (λ_{ext}) is attributed to the reorganization of the solvent shell whereas the inner energy (λ_i) represent the energy ~~provided~~ to change the reactant oxidation ~~degree~~[10,11]. λ is hence composed of four ~~components~~ for alkali oxide ~~mediated~~ oxidation, according to eq. 6.2 in the case of superoxide. The reorganisation during mediated oxidation can be further~~more~~ ~~break~~ down. Electron transfer involves firstly the oxide bond breaking λ_{i,MO_2}, followed by the solvation of M^+ and O_2 in the liquid phase λ_{o,MO_2}. The outer reorganization energy of the superoxide can then be described as $\lambda_{o,MO_2} = \lambda_{M^+,sol} + \lambda_{O_2,sol}$.

$$\lambda = \lambda_{i,MO_2} + \lambda_{o,MO_2} + \lambda_{i,mediator} + \lambda_{o,mediator} \tag{6.2}$$

A critical consequence of the Marcus behaviour is that all redox mediators ~~present~~ the same kinetic maximum corresponding to a λ of 0.58 eV for superoxide (i.e. $E^0_{med} \sim 3.2\ V_{Li/Li^+}$) ~~notwithstanding~~ their chemical nature. λ is thus ~~set~~ by the oxide reorganisation energy which ~~prevails on~~ the mediator contributions. From an energetic point of view, the ~~pre~~dominance of λ_{MO_2} results from higher ~~required~~ energy to break the oxide bond and solvate M^+ and O_2 than for the mediator ~~oxidation~~ per ~~say~~. Mediators with similar redox potential as TDPA and MBT or Fc and I_2 yield comparable kinetics despite ~~important~~ chemical differences supporting this assumption. ~~As little~~ mediator reorganization energies appear to be, they could account for small deviations that we modelled by fitting with $\lambda = \lambda_{maximum} \pm 0.1$ eV which enclose ~~al~~most ~~completely~~ the obtained kinetic.

The mediator reorganization energy is not of prime importance at first but still influence the kinetic albeit in smaller range. The mediated oxidation kinetic depends thus mostly on its potential rather than the chemical ~~structure~~ of the molecule and its solvation. The electrolyte should be ~~choiced~~ to influence the M^+ and O_2 solvation as described in part. **discharge** and the solvent was shown to have an influence on the Li_2O_2 oxidation onset potential and hypothetized to facilitate mediated oxidation[16,17]. Further deviations might arise from Z_{el} modulation between different mediators ~~, as for~~ BP55 enhanced kinetic compared to the Marcus theory ~~prevision~~ with a constant collision factor. Z_{el} is influenced by complex physico–chemical properties such as donor–acceptor coupling, i.e. the diabatic character of the electron tranfer, and was deemed out of this study ~~scope~~[11,18,19]. Overall, our first approximation of Marcus theory to mediated alkali oxide oxidation predicts maximum kinetics around 3.2 V_{Li/Li^+} that should be aimed by future oxidation mediators. Kinetic could be even maximized with proper tuning of the overall reorganisation energy or the collision factor.

6.2.2 Importance of mediator quenching efficiency

The relationship between kinetic and oxidation mediator nature being resolve, the remaining question is the influence of the mediator on $^1O_2$ production. We hence characterized $^3O_2$ and $^1O_2$ releases upon peroxide and superoxide ~~mediated~~ oxidation for the same wide range of mediator used for kinetic determinations in part. **previous part** by a combination of MS and HPLC as in part. **MS previous chapter**. The results are depicted in fig. 6.9 scaled to the theoritical ~~oxidation~~ yield.

change MBT KO2

(a)

(b)
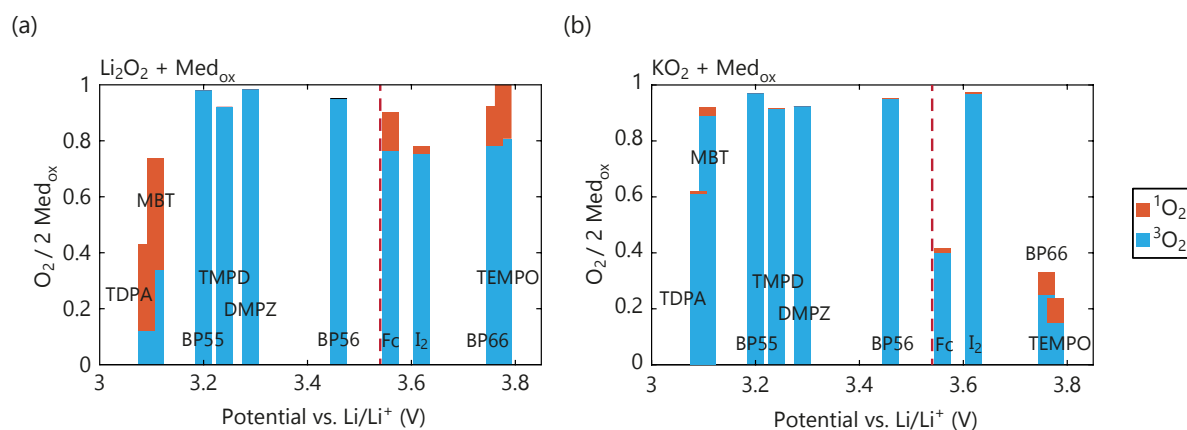
Figure 6.9: **$^3O_2$ and $^1O_2$ yield upon mediated peroxide and superoxide oxidation for a wide selection of mediators.** $^3O_2$ and $^1O_2$ evolution obtained by addition of 1 mM oxidized mediators in TEGDME to an excess of (a) Li_2O_2 or (b) KO_2. The bars are positioned according to the redox potential of the respective mediators. The red dashed line indicates the thermodynamic thresholds for $_1O_2$ evolution from LiO_2 oxidation.

Considering first the mediators with potential above ~3.5 V_{Li/Li^+}, an ~~important~~ lack of $^3O_2$ evolution can be noticed accompanied with $^1O_2$ for both peroxide and superoxide oxidation. This confirms $^1O_2$ generation by mediated alkali oxide oxidation above the $^1O_2$ potential in addition ~~of~~ disproportionation. Similarly, TDPA$^+$, that can form~~ed~~ spontaneously TDPA$_2^+$ which as a redox potential above ~3.5 V_{Li/Li^+} as shown in part. **previous chapter**. TDPA^{2+} results in $^1O_2$ production ~~on~~ superoxide in absence of disproportionation. I$_2$ shows, yet, improved efficiency in absence of disproportionation during superoxide oxidation whereas the others ~~present a degraded~~ yield. Both I$_2$ and I$^-$ are molecules known for their $^1O_2$ quenching efficiency by dint of heavy-atom colliders effect[20-22]. The quenching character of I$^-$/I$_2$ might explain the observed difference as $^1O_2$ can only be formed in the vicinity of the iodide by mediated oxidation followed by a potential $^1O_2$ quenching whereas disproportionation would dominate in presence of Li$^+$ ions.

Using mediators below ~3.5 V_{Li/Li^+} can only lead to $^1O_2$ evolution through disproportionation. As described for MBT in part. **previous chapter**, only negligible $^1O_2$ amount is produced upon KO$_2$ oxidation, hence in absence of disproportionation. Li$_2$O$_2$ oxidation, yet, yields different behaviour between MBT and BP55, TMPD, DMPZ or BP56. The low $^1O_2$ amount during peroxide oxidation compared to MBT can be explained by reduced disproportionation proportion ~~for~~ the fast kinetic BP55. The other mediators, however, possess similar or lower kinetics than MBT. We do not exclude possible undetected side reaction or influence of the MBT$^-$/MBT couples on disproportionation. The quenching proprieties of the mediators can additionally be the origin of deviations as for the I$^-$/I$_2$ couples.

To compare the $^1O_2$ quenching efficiency of different mediators, the quenching rate constants can be used. We either determined the rate constants using the UV-vis spectroscopy protocol already discussed in part. **quencher** and **Annexes** in the case of DMPZ or TDPA or from literature [5,20,21,23]. To take in account the influence of electrolyte, the quenching rate of DABCO was used as a reference in first approximation, being a well known and studied quencher. The rate were then converted to the theoritical MeCN rate using this reference **Ask Excel to Stefan for Appendix + citation for DABCO**. The resulting quenching rates are given ~~in~~ function of the mediator redox potentials in fig. 6.10. The line with a slope of 10^4/V is added as a guide since the quenching efficiency depends on the ~~molecule~~ oxidation potential for charge transfer mechanism, as discussed in part. **quencher** and observed for the BP

mediators. The quenching efficiency may nevertheless significantly differ between chemical classes[22,24].
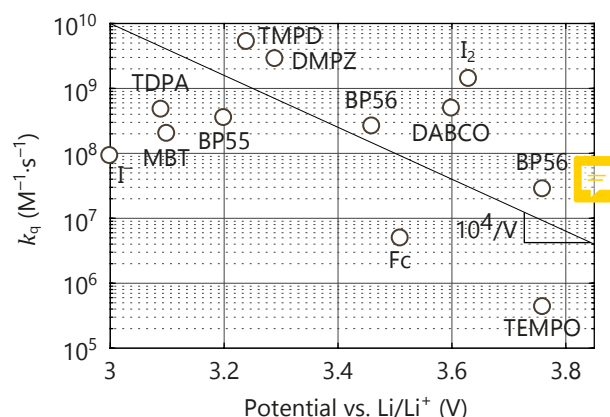
Figure 6.10: **$^1O_2$ quenching rate constants of mediators in function of their redox potential in CH$_3$CN.**

I_2 presents indeed a highly improved quenching rate constant compared to the other high potential mediator which ~~can be~~ partly responsible for the higher $^3O_2$ yield. DMPZ ~~presents~~ one of the best $^1O_2$ quenching efficiency ~~and~~ consequently an ~~improved $^1O_2$ stability~~, as verified in part. **mediator with singlet:** This high quenching ability is accompanied by negligible amount $^1O_2$ release and high $^3O_2$ yield during alkali oxide oxidation. The search for mediator ~~improved~~ stability with $^1O_2$ advocates for low potential mediators and the occurrence of quenching moieties on the molecule as tertiary amines. The $^1O_2$ quenching rates of future mediators ought thus to be determine to ~~quantify the mediator reactivity with $^1O_2$~~.

6.2.3   Consequence for oxidation mediator

$^1O_2$ ~~have a~~ crucial consequences on metal–air parasitic chemistry. To achieve~~d~~ ~~mediated~~ $^1O_2$ free cells, the main parameters to optimize are the mediator kinetics and quenching efficiencies. The oxidation kinetic is mostly govern by the mediator potential with an optimum $\sim$3.2 V_{Li/Li^+} according to the Marcus theory. The maximum kinetic could be more refined through complex physico-chemical parameters. ~~If~~ the mediator redox potential influences the quenching abilities as shown for the BP mediators, the chemical nature of the mediator is also of prime importance. The chemical class of the mediator should hence be selected to provide an efficient $^1O_2$ quenching ~~rather than~~ alkali oxide oxidation efficiency. Sankey diagrams reveal themselves as a helpful representation~~s~~ of these complex~~es~~ interactions, given for BP55, DMPZ and BP66 in fig. 6.11 as example for a low and high redox potential mediator. The diagrams for the other studied mediators are given in **Annexes**
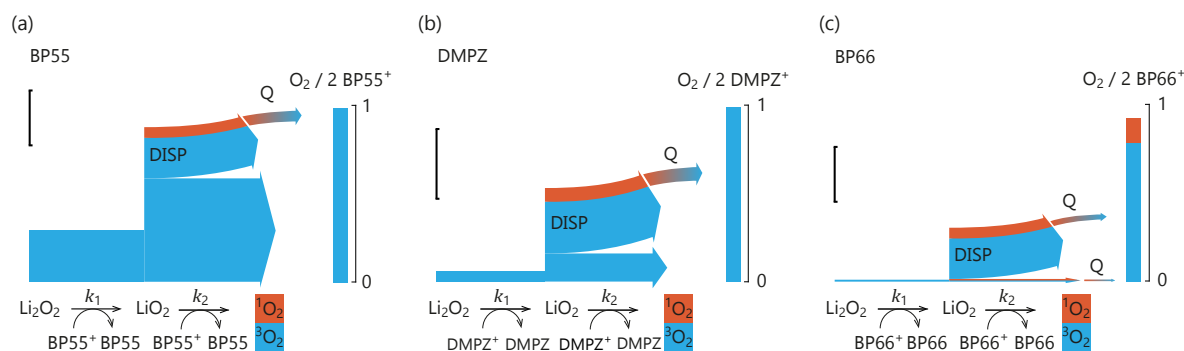
Figure 6.11: **Sankey plots of relative rates during mediated Li_2O_2 oxidation.** The width of the arrows is proportional to the rate assuming 10 mM of (a) $BP55^+$ (B) $DMPZ^+$ and (c) $BP66^+$. The vertical scale bar corresponds to 1×10^{-7} mol·cm^{-2}·s^{-1}. $^1O_2$ quenching by the RM is denoted by Q. The $^3O_2$ and $^1O_2$ yields per 2 equivalent oxidized mediators are given at the right of each panel.

In our ~~proposed~~ Sankey diagrams, the width of the arrows are proportional to the individual step ~~rates~~ and the bar graph at the right ~~end~~ shows the shares of $^3O_2$ and $^1O_2$ obtained. The diagrams allow ~~to compare~~ easily the different step ~~rates~~ for a mediator and between ~~each~~ mediators. The quenching influence can be seen via the bar graph and lower $^1O_2$ amount than expected. To approximate the first one-electron transfer kinetic (k_1) which can not be directly measured, the relationship between the different reaction steps must first be discussed. A strongly dominant disproportionation rate leads to negligible second one-electron transfer, as ~~for~~ high potential mediators (illustrated by the BP66 in fig. 6.11(c)). In this case, the overall mediator consumption observed by k_{app} is overwhelmingly due to the first electron transfer and can be approximate as k_1. As the second one-electron transfer rate is getting closer to disproportionation rate for low potential mediator, e.g. DMPZ in fig. 6.11(b), the second one-electron reaction is non negligible any more and some mediator will be consumed during the second ~~reaction step~~. We approximated k_1 in this case by k_{app} as disproportionation is still dominant and the overall reaction rate is much smaller than k_2. This indicates that k_1 is largely slower than the other two process and so susceptible to a smaller absolute error. BP55 presents the exception ~~of~~ a faster second electron reaction rate than the disproportionation ~~one~~ in fig. 6.11(c). The obtained k_2 is moreover similar to k_{app} ~~to~~ the overall reaction. In the extreme case, disproportionation would be negligible. The overall consumption rate would hence ~~be~~ only be composed of the two one electron step, as second e$^-$ transfer will immediately follow the first one. k_{app} can then be equally divided between k_1 and k_2 in this case. We chose to represent BP55 as this extreme case with $k_1 = k_{app}/2$. In reality, as disproportionation is not negligible even for this mediator, k_1 might be ~~superior to~~ the one ~~represented~~ which is the lower range of the first electron transfer kinetic. For all mediators nevertheless, the combined disproportionation and second electron transfer is faster than the first one which indicates the first electron extraction ~~as~~ the rate limiting step of mediated peroxide oxidation.

~~The theoretical~~ proportion of disproportionation compared to k_2 can be visualized with Sankey diagrams and be related to the amount of singlet oxygen. It arise from the BP55 diagram that fast second electron transfer may suppress, but cannot fully eliminate $^1O_2$ production. The absence of significant $^1O_2$ detection or $^3O_2$ ~~lack~~ for BP55 or DMPZ ~~on~~ Li_2O_2 suggests that the mediators' ability to quench $^1O_2$ is a requirement for future mediators. Sankey diagram could then be used to compare future mediator kinetics and O_2 yields. We proposed hence as ~~criterion~~ for efficient mediator design, in addition ~~of~~ chemical stability, ~~a~~ maximized kinetic using the Marcus theory and a maximized $^1O_2$ quenching efficiency via the chemical nature of the mediators. As shown by the BP55 results, only abide ~~by theses~~

rules may allow a fast reaction rate, minimized $^1O_2$ occurrence and as finality improved metal–O_2 charge.

Conclusion

To conclude, we ~~previously demonstrated~~ the mechanism of mediated alkali peroxide and superoxide oxidation which ~~possibly leads to~~ $^1O_2$ generation. Highly reactive $^1O_2$ should be avoided ~~at all cost~~ to achieve long term cyclability. $^1O_2$ evolution can ~~proceed via~~ mediated oxidation above a potential threshold of ~3.5 V_{Li/Li^+} and thus high redox potential mediator are to be ~~prevented.~~ As the mediated oxidation is composed of a two step oxidation, the ~~formation of~~ superoxide ~~convey~~ disproportionation and subsequent $^1O_2$ production. Only high mediated oxidation rates could decrease disproportionation ~~proportion~~ and ~~should~~ be aimed.

We could show that the oxidation rates go through a maximum at ~3.2 V_{Li/Li^+} and decrease at higher potential. Such behaviour is described by Marcus inverted region which predicts a quadratic dependency of the kinetic with the reaction driving force. A kinetics trend following Marcus theory has serious consequences. We could ~~derived~~ that the mediator chemical nature is of second importance ~~in front of~~ its redox potential; The overall reorganisation energy is ~~then~~ dominated by the oxide reorganisation which should be studied more deeply to optimize the reaction kinetic. Small deviation nevertheless can be ascribed to the chemical nature of the mediator and complex physico–chemical parameters, as the donor–acceptor coupling, that could be further optimized in future oxidation mediators. The maximum kinetic obtained was sufficiently high to overcome the disproportionation rate and hence reduce ~~efficiently~~ the $^1O_2$ production. The reaction rates on peroxide and superoxide were moreover similar with BP55. This indicates that the overall reaction rate can also be optimize as the peroxide rate is significantly slower for the other mediators.

Using Sankey diagrams, disproportionation appears as an inevitable process which can only be diminished by high superoxide reaction kinetic. The presence of quenching moieties appears thus very desirable for oxidation mediators. The highest $^3O_2$ yields were observed with mediators incorporating a quenching moieties as tertiary amines. The quenching efficiency ~~present a deterioration with~~ the mediator potential and depends highly on the mediator chemical ~~class.~~ If the chemical nature of the mediator does not influence greatly the reaction kinetics, this one should be chosen to provide an efficient $^1O_2$ quenching. We showed in the previous chapter that quenching moieties furthermore confers a higher resistivity to oxidation mediator deactivation induced by $^1O_2$.

The design rules drawn from the ~~uses of bi-cyclic secondary amines~~ as oxidation mediator can be resumed first as high chemical stability towards peroxide, superoxide and molecular oxygen. Second, the mediator should have optimized oxidation kinetic ~~through the use of~~ Marcus theory ~~parameters and aim for an oxidation potential in the vicinity of 3.2 V_{Li/Li^+}.~~ Finally, the oxidation mediator chemical nature should be chosen to provide a high quenching activity. Bi-cyclic secondary amines provide a new class of oxidation mediators easily tunable through organic chemistry ~~that~~ could be further optimize according to these design rules to achieve truly efficient metal-O_2 charge mediation.

Bibliography

[1] J.-B. Park, S. H. Lee, H.-G. Jung, D. Aurbach, and Y.-K. Sun, "Redox mediators for Li–O$_2$ batteries: status and perspectives," *Advanced Materials*, vol. 30, no. 1, p. 1704162, 2018.

[2] Y. Chen, S. A. Freunberger, Z. Peng, O. Fontaine, and P. G. Bruce, "Charging a Li–O$_2$ battery using a redox mediator," *Nature chemistry*, vol. 5, no. 6, p. 489, 2013.

[3] B. D. McCloskey and D. Addison, "A viewpoint on heterogeneous electrocatalysis and redox mediation in nonaqueous Li–O$_2$ batteries," 2016.

[4] V. Pande and V. Viswanathan, "Criteria and considerations for the selection of redox mediators in nonaqueous Li–O$_2$ batteries," *ACS Energy Letters*, vol. 2, no. 1, pp. 60–63, 2016.

[5] E. L. Clennan, L. Noe, E. Szneler, and T. Wen, "Hydrazines: new charge-transfer physical quenchers of singlet oxygen," *Journal of the American Chemical Society*, vol. 112, no. 13, pp. 5080–5085, 1990.

[6] D. Kundu, R. Black, B. Adams, and L. F. Nazar, "A highly active low voltage redox mediator for enhanced rechargeability of lithium–oxygen batteries," *ACS central science*, vol. 1, no. 9, pp. 510–515, 2015.

[7] S. Kang, Y. Mo, S. P. Ong, and G. Ceder, "A facile mechanism for recharging Li$_2$O$_2$ in Li–O$_2$ batteries," *Chemistry of Materials*, vol. 25, no. 16, pp. 3328–3336, 2013.

[8] Y. Chen, X. Gao, L. R. Johnson, and P. G. Bruce, "Kinetics of lithium peroxide oxidation by redox mediators and consequences for the lithium–oxygen cell," *Nature communications*, vol. 9, no. 1, p. 767, 2018.

[9] P. Bawol, P. Reinsberg, C. Bondue, A. Abd-El-Latif, P. Königshoven, and H. Baltruschat, "A new thin layer cell for battery related DEMS-experiments: the activity of redox mediators in the Li–O$_2$ cell," *Physical Chemistry Chemical Physics*, vol. 20, no. 33, pp. 21 447–21 456, 2018.

[10] R. A. Marcus, "Electron transfer reactions in chemistry. Theory and experiment," *Reviews of Modern Physics*, vol. 65, no. 3, p. 599, 1993.

[11] J.-M. Savéant, *Elements of molecular and biomolecular electrochemistry: an electrochemical approach to electron transfer chemistry.* John Wiley & Sons, 2006, vol. 13.

[12] M. C. Henstridge, E. Laborda, N. V. Rees, and R. G. Compton, "Marcus–Hush–Chidsey theory of electron transfer applied to voltammetry: A review," *Electrochimica Acta*, vol. 84, pp. 12–20, 2012.

[13] R. Marcus, "Electron transfer at electrodes and in solution: comparison of theory and experiment," *Electrochimica Acta*, vol. 13, no. 5, pp. 995–1004, 1968.

[14] J.-M. Savéant, "Evidence for concerted pathways in ion-pairing coupled electron transfers," *Journal of the American Chemical Society*, vol. 130, no. 14, pp. 4732–4741, 2008.

[15] W. R. Fawcett and M. Opallo, "On the differences in the magnitude of the observed solvent effect in the kinetics of simple heterogeneous electron transfer reactions," *Journal of Electroanalytical Chemistry*, vol. 349, no. 1-2, pp. 273–284, 1993.

[16] G. Leverick, M. Tuodziecki, R. Tatara, F. Bardé, and Y. Shao-Horn, "Solvent-Dependent Oxidizing Power of LiI Redox Couples for Li-O$_2$ Batteries," *Joule*, vol. 3, no. 4, pp. 1106–1126, 2019.

[17] A. Nakanishi, M. L. Thomas, H.-M. Kwon, Y. Kobayashi, R. Tatara, K. Ueno, K. Dokko, and M. Watanabe, "Electrolyte composition in Li/O$_2$ batteries with LiI redox mediators: solvation effects on redox potentials and implications for redox shuttling," *The Journal of Physical Chemistry C*, vol. 122, no. 3, pp. 1522–1534, 2018.

[18] S. W. Feldberg and N. Sutin, "Distance dependence of heterogeneous electron transfer through the nonadiabatic and adiabatic regimes," *Chemical physics*, vol. 324, no. 1, pp. 216–225, 2006.

[19] W. R. Fawcett, *Liquids, solutions, and interfaces: from classical macroscopic descriptions to modern microscopic details*. Oxford University Press, 2004.

[20] F. Wilkinson and A. Farmilo, "The mechanism of quenching of singlet oxygen O$_2$*($^1\Delta_g$) by molecular iodine," *Journal of Photochemistry*, vol. 25, no. 2-4, pp. 153–160, 1984.

[21] I. Rosenthal and A. Frimer, "The quenching effect of iodide ion on singlet oxygen," *Photochemistry and photobiology*, vol. 23, no. 3, pp. 209–211, 1976.

[22] C. Schweitzer and R. Schmidt, "Physical mechanisms of generation and deactivation of singlet oxygen," *Chemical reviews*, vol. 103, no. 5, pp. 1685–1758, 2003.

[23] F. Wilkinson, W. P. Helman, and A. B. Ross, "Rate constants for the decay and reactions of the lowest electronically excited singlet state of molecular oxygen in solution. An expanded and revised compilation," *Journal of Physical and Chemical Reference Data*, vol. 24, no. 2, pp. 663–677, 1995.

[24] A. P. Darmanyan, W. S. Jenks, and P. Jardon, "Charge-transfer quenching of singlet oxygen O$_2$ ($^1\Delta_g$) by amines and aromatic hydrocarbons," *The Journal of Physical Chemistry A*, vol. 102, no. 38, pp. 7420–7426, 1998.